STRUCTURAL STUDIES OF SHIKIMATE AND FATTY ACID BIOSYNTHESIS PATHWAY'S ENZYMES

Ph.D. THESIS

by

VIJAY KUMAR

DEPARTMENT OF BIOTECHNOLOGY
INDIAN INSTITUTE OF TECHNOLOGY ROORKEE
ROORKEE-247 667 (INDIA)
MARCH, 2018

भारतीय प्रौद्योगिकी संस्थान रुड़की
INDIAN INSTITUTE OF TECHNOLOGY ROORKEE

STRUCTURAL STUDIES OF SHIKIMATE AND FATTY ACID BIOSYNTHESIS PATHWAY'S ENZYMES

A THESIS

Submitted in partial fulfilment of the

Requirements for the award of the degree

of

DOCTOR OF PHILOSOPHY

in

BIOTECHNOLOGY

by

VIJAY KUMAR

DEPARTMENT OF BIOTECHNOLOGY
INDIAN INSTITUTE OF TECHNOLOGY ROORKEE
ROORKEE-247 667 (INDIA)
MARCH, 2018

भारतीय प्रौद्योगिकी संस्थान रुड़की
INDIAN INSTITUTE OF TECHNOLOGY ROORKEE

©INDIAN INSTITUTE OF TECHNOLOGY ROORKEE, ROORKEE-2018
ALL RIGHTS RESERVED

भारतीय प्रौद्योगिकी संस्थान रुड़की
INDIAN INSTITUTE OF TECHNOLOGY ROORKEE

INDIAN INSTITUTE OF TECHNOLOGY ROORKEE ROORKEE

CANDIDATE’S DECLARATION

I hereby certify that the work which is being presented in the thesis entitled “**STRUCTURAL STUDIES OF SHIKIMATE AND FATTY ACID BIOSYNTHESIS PATHWAY’S ENZYMES**’’ in partial fulfilment of the requirements for the award of the Degree of Doctor of Philosophy and submitted in the Department of Biotechnology of the Indian Institute of Technology Roorkee, Roorkee is an authentic record of my own work carried out during a period from January 2013 to March 2018 under the supervision of Dr. Pravindra Kumar, Associate Professor, Department of Biotechnology, Indian Institute of Technology Roorkee, Roorkee.

The matter presented in this thesis has not been submitted by me for the award of any other degree of this or any other institution.

Signature of the Candidate

This is to certify that the above statement made by the candidate is correct to the best of our knowledge.

Signature of Supervisor (s)

The Ph.D Viva-Voce Examination of Vijay Kumar, Research Scholar has been held on ……………………

Chairman, SRC

Signature of External Examiner

This is to certify that the student has made all the corrections in the thesis.

Signature of Supervisor (s)

Head of the Department

Dated:____________

भारतीय प्रौद्योगिकी संस्थान रुड़की
INDIAN INSTITUTE OF TECHNOLOGY ROORKEE

ABSTRACT

Infectious diseases are the leading cause of death all over the world, with substantial contributions from microbial infections to this high rate of mortality. The traditional approaches to control bacterial infections were identified, and primarily derived from other microorganisms. These approaches mainly depend upon the disruption of the microbial growth cycle by inhibiting the synthesis, and association of the essential components of bacterial processes like cell wall synthesis, DNA replication, and protein synthesis. Although these methods and compounds were highly effective, but they have created substantial stress on target microorganism, and subsequently during the course of evolution, these bacterial pathogens rapidly selected for resistant subpopulations. The emergence of drug resistance in bacterial pathogens is pressing concerns in health sector all over the world. Antibiotic resistance in microbes is the outcome of innate genetics and physiology, which are vertically transmitted through species, and the outstanding ability of bacteria to perform the horizontal transfer of genetic material across species and genera.

Since the bacterial pathogens have developed the resistance against the antibiotics, which targeted the essential pathways like cell wall synthesis, DNA (or RNA) replication, protein synthesis, and folate biosynthesis pathways it has become more important to discover antibacterial agents targeting other vital pathways or processes of bacteria. Other important pathways of bacteria that have been validated for drug development are shikimate pathway, fatty acid biosynthesis, lipid polysaccharide synthesis, cell division, two-component regulatory system, and bacterial efflux pumps.

The current study focuses on the two such essential pathways, including shikimate pathway and fatty acid biosynthesis pathway. The thesis encompasses the biochemical, biophysical and structural characterization of three proteins, including chorismate mutase like domain of DAHPS from *Bacillus subtilis*, and β-hydroxyacyl-acyl carrier protein dehydratase and Malonyl-CoA: acyl carrier protein transacylase from drug-resistant pathogen *Moraxella catarrhalis*. More importantly, new inhibitors against these three proteins have been discovered and characterized using biochemical, biophysical, and *in silico* based approaches.

Shikimate pathway is responsible for the synthesis of chorismate that serves as the substrate for aromatic amino acids, folate and ubiquinone biosynthesis pathways. The first enzyme of shikimate pathway, 3-deoxy-D-arabino-heptulosonate-7-phosphate-synthase (DAHPS) catalyzes the aldol-condensation of D-erythrose-4-phosphate (E4P) and phosphoenolpyruvate (PEP) to form 3-deoxy-D-arabino-heptulosonate-7-phosphate (DAHP). In this study, we have determined the crystal structure of chorismate mutase type II in complex with chlorogenic acid from *Bacillus subtilis* (BsCM_2) at 1.8 Å resolution. The structure provides the insight into the mode of binding of the inhibitor with enzyme and active site plasticity via the flexibility of active site loop L1'. Molecular dynamic simulation results showed that helix H2' undergoes uncoiling at the first turn and increases the mobility of loop L1'. Residues Arg45, Phe46, Arg52 and Lys76 show flexibility in side chain orientation, which may play an important role in DAHPS activity regulation by the formation of domain-domain interface. Biochemical characterization has shown that this domain has residual activity with k_{cat} of 0.78 S^{-1} which is much lesser that the other reported chorismate mutases or AroH classes of CMs. Chlorogenic acid has shown the competitive mode of inhibition for BsCM_2 enzyme with K_i of 0.34 ± 0.07 mM. Additionally, the binding study showed that chlorogenic acid binds to *Bs*CM_2 with more affinity than chorismate. The chlorogenic acid's minimum inhibitory concentration against *B. subtilis* was calculated to 30 ± 5µg/ml. In the era of prevalent antibiotic resistance among pathogenic bacteria, these findings may lead to explore the possibility of validating the chlorogenic acid as an inhibitor of chorismate mutase, type II enzyme.

Fatty acid biosynthesis is an essential pathway in the metabolism of microbes and most under-exploited for the development of antibacterial agents. In this study, we have characterized two important drug targets; β-hydroxyacyl-acyl carrier protein dehydratase (FabZ) and Malonyl-CoA:acyl carrier protein transacylase (FabD) from Type II FAS pathway. FabZ is an essential component of type II fatty acid biosynthesis and performs the dehydration of β-hydroxyacyl-ACP to trans-2-acyl-ACP in the elongation cycle of the FAS II pathway. FabZ is ubiquitously expressed and has uniform distribution, which makes FabZ an excellent target for developing novel drugs against pathogenic bacteria. We focused on the biochemical and biophysical characterization of FabZ from drug-resistant pathogen *Moraxella*

catarrhalis (McFabZ). More importantly, we have identified and characterized new inhibitors against McFabZ using biochemical, biophysical and *in silico* based studies. We have identified three isoflavones (daidzein, biochanin A and genistein) as novel inhibitors against McFabZ. Mode of inhibition of these compounds is competitive with IC_{50} values lie in the range of 6.85 µM to 27.7 µM. Conformational changes observed in the secondary and tertiary structure marked by a decrease in the helical and the sheet content in McFabZ structure upon inhibitors binding. In addition, thermodynamic data suggest that biochanin A has a strong binding affinity for McFabZ as compared to daidzein and genistein. Molecular docking studies have revealed that these inhibitors are interacting with the active site of McFabZ and making contacts with catalytic and substrate binding tunnel residues. These biochemical and biophysical findings lead to the identification of chemical scaffolds, which can lead to broad-spectrum antimicrobial drugs targeted against FabZ, and modification to existing FabZ inhibitors to improve affinity and potency.

The next part of the study will focus on Malonyl-CoA:acyl carrier protein transacylase (FabD), which is an attractive target for developing broad-spectrum antibiotics. It performs initiation reaction to form malonyl-ACP, which is a key building block in fatty acid biosynthesis. In this study, we have characterized the FabD from drug-resistant pathogen *Moraxella catarrhalis* (McFabD). More importantly, we have shown the kinetic inhibition and binding of McFabD with three new compounds from the class of aporphine alkaloids. ITC based binding studies have shown that apomorphine is binding to McFabD with a stronger affinity (K_D = 4.87 µM) as compared to boldine (K_D = 7.19 µM) and magnoflorine (K_D = 11.7 µM). The possible mechanism of fluorescence quenching is found to be static with K_q values higher than 10^{10}, which was associated with the ground state complex formation of aporphine alkaloids with McFabD. Conformational changes observed in the secondary and tertiary structure marked by the loss of helical content during the course of interactions. Molecular docking based studies have predicted the binding mode of aporphine alkaloids and it is found that these compounds are interacting in a similar fashion as known inhibitor corytuberine is interacting with McFabD. The analysis of docking poses has revealed that His 210, Leu102, Gln19, Ser101 and Arg126 are critical residues which may play important role in binding of these alkaloids to McFabD. The growth inhibition assay has shown that apomorphine has better MIC value (4-8 µg/ml) against *Moraxella catarrhalis* as compared to boldine and

magnoflorine. Therefore, this study suggests that aporphine alkaloids can act as antibacterial agents and possible target of these compounds could be FabD enzyme from the FAS II pathway, and apomorphine scaffold will be more suitable among these compounds for the development of antibacterial agents.

In the last part of the study, we tried to develop the multi-targeted inhibitor of FAS II pathway. In this study, we reported the 1,4-Naphthoquinone as dual inhibitors of two enzymes, FabD and FabZ of *Moraxella catarrhalis*. The biochemical inhibition assay has shown that NPQ has inhibited both FabZ and FabD with IC_{50} of 26.67 µM and 23.18 µM respectively. Mode of inhibition of NPQ against both enzymes was found to be non-competitive inhibition. Conformational changes marked by the loss of helical content were observed using CD based studies. Fluorescence quenching based binding studies have shown that NPQ has ≈7x more binding affinity for FabZ as compared to FabD enzyme which is in agreement with binding affinities determined using ITC based assay. In both cases, binding reactions were exothermic in nature driven by ethlapy change ($\Delta H<0$). Molecular docking has predicted the binding poses of NPQ, and found that NPQ is interacting with active site key residues of both proteins. Additionally, we have checked the inhibitory action of aporphine alkaloids on FabZ, and BLD has inhibited FabZ with IC_{50} of 20.56 µM as compared to MNG (IC_{50} = 41.88 µM) and AMF (IC_{50} = 76.56 µM). Therefore, this study suggests that single inhibitor can be developed to target these key enzymes of FAS II pathway.

Dedicated to my beloved parents

ACKNOWLDGEMENTS

The work presented in this thesis would not have been possible without my close association with many people. I take this opportunity to extend my sincere gratitude and appreciation to all those who made this Ph.D thesis possible. First and foremost, I would like to thank God for all the opportunities he has presented to me. I have prayed many times for an experiment to work, and He has answered every prayer.

Secondly, I would like to extend my sincere gratitude to my research guide Dr. Pravindra Kumar for introducing me to this exciting field of science and for his dedicated help, advice, inspiration, encouragement and continuous support, throughout my Ph.D. His guidance and suggestions were indeed of great help not only in my PhD work, as well as in various other aspects of life. I take this opportunity to express my sincere gratitude to him for providing me all the support and freedom I enjoyed during my tenure. Thank you for providing a vigorous and creative research environment to train in; for giving me so much independence in exploring different directions in my project and for teaching me that learning science is in many ways like learning how to play an instrument; you need to practice the parts that you’re bad at until you get better. This and so many other lessons will stay with me wherever I go.

I would like to express my gratitude to Prof. R. Prasad internal member, my research committee. His helpful discussions and support have played an important role in the quality of my research and its successful completion. I would like to thank Dr. R. K. Peddinti, for the valuable input he has provided for my research project as an external member of my research committee.

I would like to take this opportunity to thank Prof. Partha Roy, the chairperson of my research committee, for his valuable advices and suggestions throughout my studies. I wish to thank Dr. A. K. Sharma Head, Department of Biotechnology, for providing necessary facilities, support, and cooperation in the Department. He is very supportive and always keen to help students in any matter.

I would like to thank many elite faculties in the Department of Biotechnology, IIT Roorkee for being great teachers and scientists, who are always

assessable to students. Particularly, I would like to express my sincere gratitude to Dr. Shailly Tomar for her concern, guidance and all the discussions and valuable suggestions in molecular biology and biochemistry at various stages of my work.

I express my gratitude to Dr. Ramesh Chandra and Dr. Harsh Chauhan for their encouragement, constant enthusiasm and guidance. I would like to express me thanks to Prof. T. C Bhalla, HPU Shimla, and Dr. Navneet Batra, GGDSD College Chandigarh. These are the two people in my life who encouraged me to do research and inspired me to pursue the carrier in this field.

I wish to thank department and their staff for providing me access to their facilities. A special word of gratefulness to Mr. Jain, Mr. Ved Pal Saini, Mr. Charan Singh and other staff members who have gone out of the way to help me with several official matters.

I would like to thanks my seniors especially Dr. Shivendra Pratap, Dr. Aditya Dev, Dr. Shashi Bhatia, Dr. Vijay Kumar and Dr. Manju Narwal for their continuous support throughout the period. They always helped me and guided me right through the journey. Special thanks to Dr. Shivendra Pratap for his help, support and guidance, he provided as elder brother and always with me in my ups and down. Besides these, I would like to thank other seniors of department especially Dr. Umesh, Dr. Prabhat, Dr. Lambadi, Dr. Pradeep, Dr. Vivekanad Kar, Dr. Tapas Bhattacharya and Dr. Naresh. Special thanks to Dr. Naresh Kumar for his help and support. He shares special bond with me as we both have done masters from same university. He always provided me moral support and motivation.

I would like to thank my lab members and colleagues, Anchal, Madhusudhan, Neha, Neetu, Jai, Poonam, Ishaan, Vikram, Pooja, and Monika. Special thanks to Madhusudhan RaoK and Anchal Sharma for their kind support and help. I always used to share ideas and research with these peoples. They always helped me and provide the wonderful environment in the lab to carry out the work. I would like to thank other lab members from our collaborative labs specially Harvijay, Anjali, Benazir, Dr. Rajesh, Rajat, Dr. Ravi Saini, Pranav, Gunjan, Atin Sharma, Tamoghna, and Dr. Sidharath. Special thanks to Harvijay Singh for being my colleague and friend. We always share a good bond and he always helped me in my professional as well as in personal life.

I would like to thank Somesh, Shashank, Amol, Jacky, Sandeep, Ragvendra, Bhandendra, Tara Chand, Viswhjeet, Akash, Rakesh, Yogesh, Sunil and Swapaneel for their support and time spent together. Most of the time in the IIT Roorkee I have spent these peoples and they always helped me. Special thanks to Somesh Banerjee for his support and being a nice friend. I always admired and endorsed him for his simple, calm and composed nature. I would like to thank Shashank Saini and Amol Sarkate for their support and help. My friendship with these three people (Somesh, Amol and Shashank) is the one of the best things happened in IIT Roorkee. We four have spent most of the times together and always supported each other. I will always cherish this friendship and hope it will remain like that.

I would like to thank other my college friends especially Vikram Thakur, Vimal Bhutani, Abhishek Rathore, Vishal Tiwari, Mukesh Garg, Vishal Ahuja, Swati Sharma, Kaamini Chauhan, Kavita Sharma, Alka Saini and Stanzil for their moral support and motivation. I would like to thank my childhood friends namely Sumeet Sharma, Dr. Tammana Sharma, Dr. Neel Kamal and Vijay Thakur. These peoples always helped me and always inspired and encouraged me. Furthermore, I would like to thank my dearest friend Sucheta Verma, who gave me hearty support whenever I depressed. I am lucky to have a friend like her. She always encouraged me and always supported me in my bad phase. Her unconditional and spiritual support was also indispensable to sustain me to complete this thesis.

I would like to thank my other friends from IITR who have been a source of moral support to me and have extended their helping hands without fail. I would also like to thank all my seniors and juniors from Department of Biotechnology for all the love that they have showered upon me. I could not have asked for more than what I got from them. Further, I wish to express my gratitude to all the collaborators of this project and co-authors of my manuscripts for their great assistance and skillful comments that greatly contributed to the improvement of this work.

Finally, I want to acknowledge the people who mean a lot to me, my parents, Mumma and Papa, for showing faith in me and giving me the liberty to choose what I desired. I salute you all for the selfless love, care, pain, and sacrifice you did to shape my life. I would never be able to pay back the love and affection showered upon by my parents. I would like to express my gratitude to my loving elder sister Anita Sharma and Brother-in-law Jai Sharma for their love, moral support and motivation during the entire life.

(Vijay Kumar)

TABLE OF CONTENTS

Abstract I

Dedication V

Acknowledgement VII

List of publications

XVII

List of Figures XIX

List of tables XXIII

List of Abbreviations XXV

Chapter 1 Introduction and review of literature 1

- 1.1 Antibiotics- Historical overview 3
- 1.2 Mechanism of action of known classes of antibiotics 4
- 1.2.1 Bacterial cell wall biosynthesis inhibitors 4
- 1.2.2 Protein synthesis inhibitors 5
- 1.2.3 Inhibition of DNA replication 6
- 1.2.4 Folate biosynthesis inhibitors 6
- 1.3 Emergence of Antibiotic Resistance 6
    - 1.3.1 Drugs efflux 7
    - 1.3.2 Modification of antibiotics 7
    - 1.3.3 Modification of antibiotic target 8
- 1.4 Combating drug resistance in bacteria 9
- 1.5 Shikimate pathway 11
    - 1.5.1 The Enzymes of the main trunk 13
        - 1.5.1.1 Deoxy-D-Arabino-Heptulosonate 7-Phosphate Synthase (DAHPS) 13
        - 1.5.1.2 Dehydroquinate Synthase (DHQS) 15
        - 1.5.1.3 Dehydroquinate dehydratase (DHQD) 15
        - 1.5.1.4 Shikimate dehydrogenase (SDH) 16
        - 1.5.1.5 Shikimate kinase (SK) 17
        - 1.5.1.6 5-Enolpyruvylshikimate 3-phosphate synthase (EPSPS) 18
        - 1.5.1.7 Chorismate synthase (CS) 19
- 1.6 Fatty acid biosynthesis pathway 21
    - 1.6.1 The FAS II pathway in *E.coli* 22

1.6.2 Inhibiting bacterial fatty acid biosynthesis pathway (FAS II) 23
    1.6.2.1 Enzymes involved in the initiation modules 24
    1.6.2.2 Enzymes involved in the condensation of elongation products 25
    1.6.2.3 Enzymes involved in reduction (Reductases) 25
    1.6.2.4 Dehydratases and isomerases 25
    1.6.2.5 Targeting acyl carrier protein (ACP) and CoA 26

1.7 Natural products as continuing source of drugs 26
    1.7.1 Prediction of macromolecular targets for natural products 27
1.8 Outline of the Research work 28

Chapter 2 Biochemical and Structural characterization of Chorismate mutase like domain of DAHP synthase from *Bacillus subtilis* 31
2.1 Introduction 33
2.2 Materials and methods 35
    2.2.1 Materials 35
    2.2.2 Methods 36
        2.2.2.1 Protein expression and purification 36
        2.2.2.2 Crystallization and data collection 37
        2.2.2.3 Structure solution and refinement 38
        2.2.2.4 Molecular dynamics 30
        2.2.2.5 Molecular docking 40
        2.2.2.6 BsCM_2 activity assay 41
        2.2.2.7 Isothermal titration calorimetry based studies 41
        2.2.2.8 Minimum inhibitory concentration (MIC) 42
2.3 Results 42
    2.3.1 Overall structure of BsCM_2 42
    2.3.2 Dimeric structure 43
    2.3.3 Active site and interaction with inhibitor 44
    2.3.4 Comparison with monofunctional B. subtilis AroH class of chorismate mutase 45
    2.3.5 Comparison of BsCM_2-CGA with EcCM (catalytically active CM type 2) 46
    2.3.6 Comparison of BsCM_2-CGA with LmCM (regulatory CM type 2) 47
    2.3.7 Comparison of BsCM_2 with CM domain of GspDAH7PS 48
    2.3.8 Molecular dynamics simulation 49

2.3.9 Chlorogenic acid's interaction with monofunctional CM (BsAroH) 51
2.3.10 BsCM_2 assay and activity 51
2.3.11 Isothermal titration calorimetry 53
2.3.12 Minimum inhibitory concentration 54
2.4 Discussion 55
2.4.1 Helices H1-H2 connecting Loop L1 flexibility 56
2.4.2 Regulation mechanism 58
2.5 Conclusion and future prospects 60

Chapter 3 Biochemical, Biophysical and Structural characterization of FabZ from *Moraxella catarrhalis* 61
3.1 Introduction 63
3.2 Materials and methods 65
3.2.1 Materials 65
3.2.2 Methods 66
3.2.2.1 Cloning of *M. catarrhalis* FabZ gene (McFabZ) 66
3.2.2.2 Protein expression and purification 66
3.2.2.3 Biochemical characterization 67
3.2.2.4 Effect of pH and temperature on McFabZ activity 67
3.2.2.5 Kinetic inhibition studies 67
3.2.2.6 CD based studies 68
3.2.2.7 Molecular modeling 69
3.2.2.8 Intrinsic fluorescence spectroscopy 69
3.2.2.9 Binding studies using ITC 70
3.2.2.10 Molecular docking 70
3.2.2.11 Molecular Dynamics (MD) Simulations 71
3.2.2.12 MIC determination 71
3.3 Results 72
3.3.1 Purification and oligomeric characterization of McFabZ in solution 72
3.3.2 Biochemical properties of McFabZ 75
3.3.3 Effect of pH and temperature on McFabZ activity 75
3.3.4 Kinetic inhibition studies 76
3.3.5 Circular dichroism studies 78
3.3.5.1 Effect of substrate 79
3.3.5.2 Effect of pH and temperature 80
3.3.5.3 Effect of different inhibitors 81
3.3.6 Molecular modeling 84

3.3.6.1 Overall structure and comparison 85
3.3.6.2 Active site analysis 89
3.3.7 Intrinsic fluorescence measurements 90
3.3.8 Thermodynamic analysis of binding of inhibitors to McFabZ 92
3.3.9 Molecular docking studies 94
3.3.9.1 Biochanin A docking study 94
3.3.9.2 Genistein docking study 95
3.3.9.3 Daidzein docking study 96
3.3.9.4 Juglone docking study 96
3.3.10 Molecular dynamics based simulation studies 98
3.3.11 Antibacterial activity assay 99
3.4 Discussion 99
3.4.1 Biochemical and stability aspects of McFabZ 100
3.4.2 Inhibition mechanism and Structure activity relationship 101
3.5 Conclusion 105
3.6 Future prospects 105

Chapter 4 Biochemical, Biophysical and Structural characterization of FabD from *Moraxella catarrhalis* 107
4.1 Introduction 109
4.2 Experimental 111
4.2.1 Materials 111
4.2.2 Methods 111
4.2.2.1 Cloning of McFabD gene from *M. catarrhalis* 111
4.2.2.2 Expression and purification of McFabD 112
4.2.2.3 Oligomeric characterization of McFabD 112
4.2.2.4 Biochemical characterization of McFabD 113
4.2.2.5 Kinetic inhibition studies 113
4.2.2.6 CD studies 114
4.2.2.7 Fluorescence spectroscopy 114
4.2.2.8 UV-Visible spectroscopy 115
4.2.2.9 Binding studies using Isothermal titration calorimetry based assays 115
4.2.2.10 Molecular modeling 116
4.2.2.11 Molecular docking 116
4.2.2.12 MIC determination 116
4.3 Results 117
4.3.1. Purification and oligomeric characterization of McFabD 117
4.3.2 Kinetic characterization and inhibition studies 118

4.3.3 CD based studies 120
4.3.3.1 Effect of substrate 122
4.3.3.2 Effect of pH and temperature 122
4.3.3.3 Effect of different ligands 123
4.3.4 Fluorescence analysis 126
4.3.4.1 Quenching mechanism 127
4.3.4.2 Binding equilibrium analysis 128
4.3.5 UV-Visible spectroscopic studies 129
4.3.6 ITC based studies 130
4.3.7 Molecular modeling 132
4.3.7.1 Sequence and phylogenetic analysis 134
4.3.8 Molecular docking 136
4.3.9 Growth inhibition assay 138
4.4 Discussion 138
4.5 Conclusion 144
4.6 Future prospects 144

Chapter 5 Identification and characterization of dual inhibitors against FabD and FabZ using biochemical, biophysical and *in silico* approaches 145
5.1 Introduction 147
5.2 1,4- Napthoquinone as multi-targeted dual inhibitor of FAS II pathway 149
5.2.1 Materials and methods 149
5.2.1.1 Materials 149
5.2.1.2 Methods 149
5.2.1.2.1 Expression and Purification of McFabZ 149
5.2.1.2.2 Expression and purification of McFabD 149
5.2.1.2.3 McFabZ inhibition assay 150
5.2.1.2.4 McFabD inhibition assay 150
5.2.1.2.5 CD based studies 150
5.2.1.2.6 Fluorescence quenching based binding studies 151
5.2.1.2.7 Binding studies using ITC 151
5.2.1.2.8 Molecular docking 151
5.2.1.2.9 Growth inhibition assay 152
5.2.2 Results 152
5.2.2.1 Kinetic inhibition of McFabZ and McFabD 152
5.2.2.2 Monitoring changes in secondary and tertiary structures upon the binding of NPQ 153
5.2.2.2.1 Monitoring structural changes in McFabD 154

5.2.2.2.2 Monitoring structural changes in McFabZ 155
5.2.2.3 Binding studies using Fluorescence quenching 155
5.2.2.4 Thermodynamic studies of Binding interactions 157
5.2.2.5 Predicting binding modes using molecular docking based studies 159
5.2.2.5.1 McFabZ-NPQ docking study 160
5.2.2.5.2 McFabD-NPQ docking study 161
5.2.3 Discussion 162
5.3 Characterization of aporphine alkaloids as inhibitors of McFabZ 164
5.3.1 Kinetic inhibition of McFabZ by aporphine alkaloids 164
5.3.2 Binding studies using Fluorescence bases quenching 164
5.3.3 Molecular docking studies 167
5.4 Conclusion and future prospects 168

BIBLIOGRAPHY 169

List of publications/published/communicated

[1] **V. Kumar**, A. Sharma, S. Pratap, P. Kumar, Characterization of isoflavonoids as inhibitors of β-hydroxyacyl-acyl carrier protein dehydratase (FabZ) from Moraxella catarrhalis: Kinetics, spectroscopic, thermodynamics and in silico studies, Biochim. Biophys. Acta - Gen. Subj. 1862 (2017) 726–744.

[2] **V. Kumar**, A. Sharma, S. Pratap, P. Kumar, Biophysical and in silico interaction studies of aporphine alkaloids with Malonyl-CoA: ACP transacylase (FabD) from drug resistant Moraxella catarrhalis, Biochimie. 149(2018) 18-33.

[3] S. Pratap, A. Dev, **V. Kumar,** R. Yadav, M. Narwal, S. Tomar, P. Kumar, Structure of Chorismate Mutase-like Domain of DAHPS from Bacillus subtilis Complexed with Novel Inhibitor Reveals Conformational Plasticity of Active Site, Sci. Rep. 7 (2017) 1–15.

[4] A. Sharma, **V. Kumar,** A. Chatrath, A. Dev, R. Prasad, A.K. Sharma, S. Tomar, P. Kumar, In vitro metal catalyzed oxidative stress in DAH7PS: Methionine modification leads to structure destabilization and induce amorphous aggregation, Int. J. Biol. Macromol. 106 (2018) 1089–1106.

[5] **V. Kumar**, A. Sharma, S. Pratap, P. Kumar, Biochemical and biophysical characterization of 1,4-Naphthoquinone as a dual inhibitor of two key enzymes of type II fatty acid biosynthesis from Moraxella catarrhalis, Biochim. Biophys. Acta – Proteins and Proteomics (Communicated).

[6] A. Sharma, **V. Kumar**, S. Pratap, P. Kumar, The inhibitory and binding studies of methyl-sulfone hydroxamate based inhibitors against LpxC from drug-resistant Moraxella catarrhalis using biophysical, biochemical and in silico approaches, Spectrochimica Acta Part A: Molecular and Biomolecular Spectroscopy (Communicated).

Book Chapter

Vijay Kumar, Ilu Kumari and Pravindra Kumar (2016). Phthalates Biodegradation. Environmental Pollution: Biodegradation and Bioremediation II.Studium Press LLC, USA.

Conference/ Poster presentation

Vijay K and Pravindra K. (2014) MAP Kinnase 4 as Therapeutic drug target in *Leishmania donovani"*at Indo-US International conference on "Recent Advances on Structural Biology and Drug Design" on 9-11 October, 2014.

List of Figures

1.1 The pipeline of antibiotic discovery 4

1.2 The schematic representation of the major pathways targeted by commonly used antibiotics. 5

1.3 Emergence of drug resistant in bacteria 8

1.4 The overview of drug discovery process 11

1.5 The shikimate pathway 12

1.6 Reaction catalyzed by the DAHP synthase (DAHPS) enzyme 13

1.7 Reaction catalyzed by the DHQS enzyme 15

1.8 Reaction catalyzed by the DHQD enzyme 16

1.9 The reaction catalyzed by the shikimate dehydrogenase (SDH) enzyme 17

1.10 The reaction catalyzed by the shikimate kinase enzyme 18

1.11 The reaction catalyzed by EPSPS enzyme 19

1.12 The reaction catalyzed by chorismate synthase (CS) enzyme 20

1.13 The schematic representation of Type II FAS pathway 23

2.1 Purification of BsCM_2 enzyme 37

2.2 BsCM_2 crystallization and X-ray diffraction 38

2.3 Ribbon diagram of BsCM_2 complexd with chlorogenic acid 44

2.4 Active site architechture (A) and interaction of BsCm_2 with chlorogenic acid (B) and citrate (C) 46

2.5 Multiple sequence alignment of BsCM_2 with related homologs 47

2.6 Molecular dynamics simulation results of *Bs*CM_2-CGA 50

2.7 Molecular docking and biochemical characterization of BsCM_2 52

2.8 Kinetic inhibition of BsCM_2 with chlorogenic acid. 53

2.9 ITC titration data describing the binding of chorismate (A), citrate (B) and chlorogenic acid (C) to *Bs*CM_2 54

2.10 Flexibility of loop L1 57

2.11 The proposed model for the regulation of DAHPS activity by the CM2 domain 59

3.1 The chemical structure of compounds used in this study 68

3.2 Molecular cloning of McFabZ gene 72

3.3 Purification of McFabZ 73

3.4 Oligomeric characterization of McFabZ 74

3.5 Biochemical characterization of McFabZ 75
3.6 Effect of pH and temperature on the activity of McFabZ 76
3.7 Kinetic analysis of inhibition mechanism of biochanin A (A), daidzein (B), genistein (C) and juglone (D) 78
3.8 The CD spectra of McFabZ at different conditions 79
3.9 Melting curve of McFabZ 81
3.10 The far-UV CD spectra of McFabZ in the presence of different inhibitors 82
3.11 The near-UV CD spectra of McFabZ in presence of different inhibitors 83
3.12 Structure of McFabZ 86
3.13 Structure based sequence alignment of FabZ 87
3.14 Phylogenetic analysis of McFabZ 88
3.15 Overall structural similarities of McFabZ with related homologs 89
3.16 Active site analysis 90
3.17 Intrinsic fluorescence spectra of McFabZ in presence of different ligands. 91
3.18 ITC studies of inhibitors binding 92,93
3.19 Molecular docking based studies 95,97
3.20 MD simulation 99
3.21 Thermodynamic signatures of binding 102
4.1 Chemical structures of aporphine alkaloids 113
4.2 Molecular cloning of McFabD gene 117
4.3 Purification and oligomeric state characterization of McFabD 118
4.4 Kinetic characterization of McFabD 119
4.5 Analysis of the mode of inhibition of aporphine alkaloids 120
4.6 Circular dichroism based studies 121
4.7 Melting curve of McFabD 123
4.8 Effect of (A) Boldine, (B) Apomorphine, (C) Magnoflorine and (D) Iodoacetamide upon Far-UV CD spectra of McFabD 124
4.9 The near-UV CD spectra of McFabD in presence of (A) Boldine, (B) Aporphine, (C) Magnoflorine and (D) Iodoacetamide 125
4.10 McFabD fluorescence quenching studies 126
4.11 Stern-Volmer plots of McFabD quenching studies with apomorphine (A), boldine (B) and magnoflorine (C) 127
4.12 Fluorescence quenching of malonyl-CoA and iodoacedamide 129

4.13 UV-Visible spectra of McFabD under native conditions and in the presence of different ligands 130
4.14 ITC based binding assays 131,132
4.15 Predicted 3D model (A) and binding pocket of McFabD (B) 134
4.16 Multiple sequence alignment 135
4.17 Phylogenetic analysis of McFabD gene 135
4.18 Molecular docking based studies 137
4.19 Thermodynamic signatures of Binding 140
4.20 Structural comparison of binding poses 142
4.21 Molecular docking of known inhibitor corytuberine (A) and juglone (B) with McFabD 143
5.1 Kinetic inhibition of McFabZ and McFabD by NPQ 153
5.2 The far-UV and near-UV CD spectra of McFabD and McFabZ upon the binding of NPQ 154
5.3 Fluorescence emission spectra of McFabZ (A) and McFabD (B) in presence of NPQ 156
5.4 Stern-Volmer plots and fluorescence quenching based binding studies 157
5.5 Binding studies using ITC based assay 159
5.6 Docking studies of McFabZ and mcFabD with NPQ 161
5.7 Kinetic inhibition of McFabZ by aporphine alkaloids 165
5.8 Fluorescence emsisson spectra of McFabZ in presence of AMF (A), BLD (B) and MNG (C) 166
5.9 Fluorescence based binding studies of AMF (A), BLD (B) and MNG (C) with McFabZ 166
5.10 Molecular docking of McFabZ with AMF (A), BLD (B) and MNG (C) 168

भारतीय प्रौद्योगिकी संस्थान रुड़की
INDIAN INSTITUTE OF TECHNOLOGY ROORKEE

List of Tables

2.1 Summary of data collection, structure refinement, and validation statistics 39
2.2 Comparison of kinetic parameters of BsCM_2 with other reported CMs 52
2.3 Binding parameters of *Bs*CM_2 with chorismate, citrate, and chlorogenic acid using ITC 53
3.1 Inhibitory activities of myricetin, epicatechin gallate, genistein, biochanin A, daidzein, juglone, emodin and quercetin against McFabZ 77
3.2 Predicted Secondary Structures* of McFabZ in presence of substrate (crotonyl- CoA) and different inhibitors 83
3.3 Assessment of predicted 3D model of McFabZ 85
3.4 Thermodynamic parameters determined using ITC based assays 94
3.5 Binding energy and Binding constant calculated via auto dock 98
3.6 Minimum inhibitory concentration (MIC) values of inhibitors tested against *M. catarrhalis, B. subtilis and Pseudomonas sp.* 99
4.1 Inhibitory activities of aporphine alkaloids against McFabD 119
4.2 The quenching constants of McFabD interactions with different ligands determined by Stern-Volmer plots 128
4.3 Binding constant and number of binding sites 129
4.4 Thermodynamic parameters 132
4.5 The quality assessment of predicted 3D model of McFabD 133
4.6 Binding parameters of different ligands determined using Autodock 136
4.7 Predicted binding interactions of McFaBD with different ligands 138
5.1 Kinetic inhibition parameters of NPQ against McFabD and McFabZ 153
5.2 The quenching constants of McFabD interactions with different ligands determined by Stern-Volmer plots 156
5.3 Thermodynamic parameters of binding of NPQ with McFabZ and McFabD 158
5.4 Binding parameters and predicted binding interactions 160
5.5 Docking results summary 167

LIST OF ABBREVIATIONS

Ala	Alanine
DHFR	dihydrofolate reductase
DHPS	dihyropteroate synthase
MRSA	methicillin resistant *S. aureus*
PEP	phosphoenol pyruvate
E4P	Erythrose-4-phosphate
DAHPS	Deoxy-D-Arabino Heptulosonate 7-Phosphate Synthase
DHQS	Dehydroquinate Synthase
DHQD	Dehydroquinate dehydratase
SDH	Shikimate dehydrogenase
SK	Shikimate kinase
EPSPS	5-Enolpyruvylshikimate 3-phosphate synthase
CS	Chorismate synthase
FAS	Fatty acid synthesis
ACP	Acyl carrier protein
ACC	Acyl Co-A carboxylase
FabD or MCAT	Malonyl-CoA: ACP transacylase
FabH	β- ketoacyl-ACP synthase III
FabG	β-ketoacyl-ACP reductase
FabZ or FabA	β-hydroxyacyl-ACP dehydratase
FabI	enoyl-ACP reductase
FabB or FabF	β-ketoacyl-ACP synthase I or II
BsCM_2	Chorismate mutase type II from *Bacillis subtilis*
ITC	Isothermal titration calorimetry
K_m	Michaelis–Menten constant
k_{cat}	Catalytic turnover number
CD	Circular dichroism
IC$_{50}$	The half maximal inhibitory

	concentration
K_D	Thermodynamic equllibrium dissociation constant
N	Number of binding sites
CGA	Chlorogenic acid
IPTG	Isopropyl-β-D- thiogalactoside
PBS	Phosphate buffer saline
RMSD	Root mean square deviation
MD	Molecular dynamics
RMSF	Root mean square fluctuation
TSA	Transition state analogue
K_i	Kinetic inhibition constant
MIC	Minimum inhibitory concentration
MRW	Mean residue weight
DMSO	Dimethyl sulfoxide
VMD	Visual molecular dynamics
Cfu	Colony forming units
PAINS	Pan assay interference compounds
MRE	Mean residue ellipticity
T_M	The melting temperature
PDB	Protein data bank
AMF	Apormorphine
MNG	Magnoflorine
BLD	Boldine
DTT	Dithiothretol
TCEP	Tris(2-carboxyethyl)phosphine
$\Delta\varepsilon$	Molar ellipticity
IDA	Iodoacetamide
NPQ	1,4-napthoquinone

भारतीय प्रौद्योगिकी संस्थान रुड़की
INDIAN INSTITUTE OF TECHNOLOGY ROORKEE

Chapter 1

Introduction and Review of Literature

INDIAN INSTITUTE OF TECHNOLOGY ROORKEE

Chapter 1

1. Introduction

1.1 Antibiotics- Historical overview

Selman Waksman, one of the reputed investigators in the field of bacteriology coined the term “antibiotic” and defined it as the substance that has ability to kill bacteria[1,2]. Earlier this term was used to define a molecule which can be bacteriostatic or bactericidal, however in todays world this definition has been changed and expanded – it applies to natural as well as synthetic products which have antibacterial, antifungal, and antiparasitic activities[1].

The discovery of penicillin in 1928 by Alexander Fleming was one the greatest achievement of humankind[3,4]. The active compound found in penicillin was identified, isolated, and produced in large scale, thanks to Howard Florey and Ernst Boris Chain[5] for their outstanding work, for which they received Nobel Prize in 1945 along with Sir Alexander Fleming. After the discovery of penicillin, some untreatable diseases like *Streptococcus* and *Chlamydial* infections become treatable with the introduction of penicillin.

The discovery of antibiotics started a new era in the treatment of infectious diseases and become the backbone of modern medicine with golden era of antibiotic drug development from 1940-1960’s. However, excessive unchecked usage of antibiotics for many decades have rendered the worlds supply of new antibiotics severely deteriorated. Regular use of antibiotics has created substantial stress on target microorganism, and subsequently during the course of evolution these bacterial pathogens rapidly selected for resistant subpopulations[6].

The emergence of drug resistance in bacterial pathogens is pressing concerns in health sector all over the world and led to the post antibiotic era, where from the last decades very few new scaffolds have been discovered creating a huge discovery void in the field of antibiotic discovery (Figure 1.1). Drug-resistant pathogens are responsible for approximately 24 000 deaths in the United States and 26 000 deaths in Europe per annum, and this number is much higher in developing countries. Based upon the world bank data, the mortality rate due to crude infectious diseases in India is 420 per 100 000 persons[7,8].

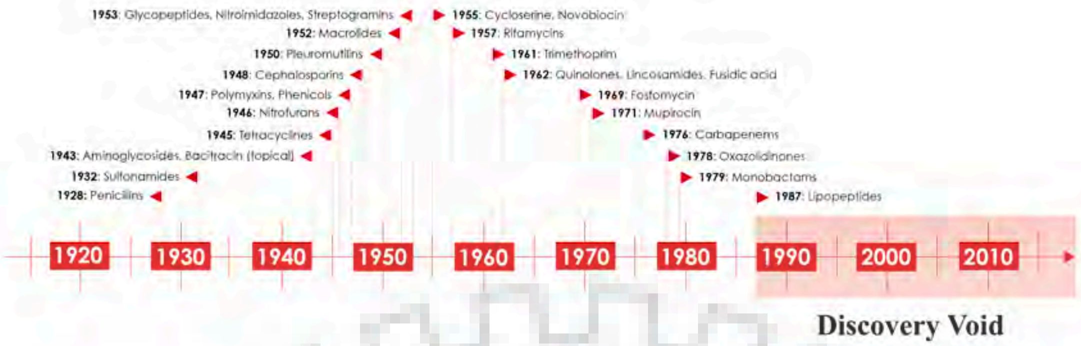

Figure 1.1 The pipeline of antibiotic discovery. Adopted from Gwynn et al[9].

1.2 Mechanism of action of known classes of antibiotics

The most commonly used antibiotics act upon the three primary targets with in the bacteria, and each class has different mode of action (Figure 1.2). These targets include inhibition of protein synthesis, cell wall biosynthesis and DNA or RNA replication enzymes (DNA polymerase or RNA polymerase) [6,8,10]. Brief overview of mode of action of these antibiotics are given as follows:

1.2.1 Bacterial cell wall biosynthesis inhibitors

The β-lactams based antibiotics like penicillin and cephalosporins, which interfere with the crosslinking step of peptidoglycan synthesis which is the precursor of bacterial cell wall and vital for its survival. These compounds act as a suicide inactivator of transpeptidase enzyme, which performs the transpeptidation reaction. The four membered β -lactam rings in these compounds are attacked by serine hydroxyl and forming a acyl intermediate, which is slow to hydrolyze further halts the synthesis of cell wall, and therefore weakens the replicating cells. Others antibiotics, which attack on transpeptidase enzyme but with different mode of actions are vancomycin and glycopeptides. These drugs bind to the terminal D-Ala-D-Ala peptidyl tail through strong hydrogen bonding and inhibiting the cell wall construction from proceeding.

1.2.2 Protein synthesis inhibitors

There are several classes of antibiotics, which inhibit protein synthesis specifically acting upon different components of the bacterial ribosome. These include natural products derived macrolides like erythromycin which acts by binding to 50S larger subunit in polypeptide exit tunnel. Others are synthetically derived like oxazolidinones (linezolid), which bind to 50S subunit. Another natural products derived antibiotic class tetracyclines bind to smaller 30S subunit in acceptor site (A-site), where it blocks the attachment of charged aminoacyl tRNA which further prevents the introduction of new amino acids.

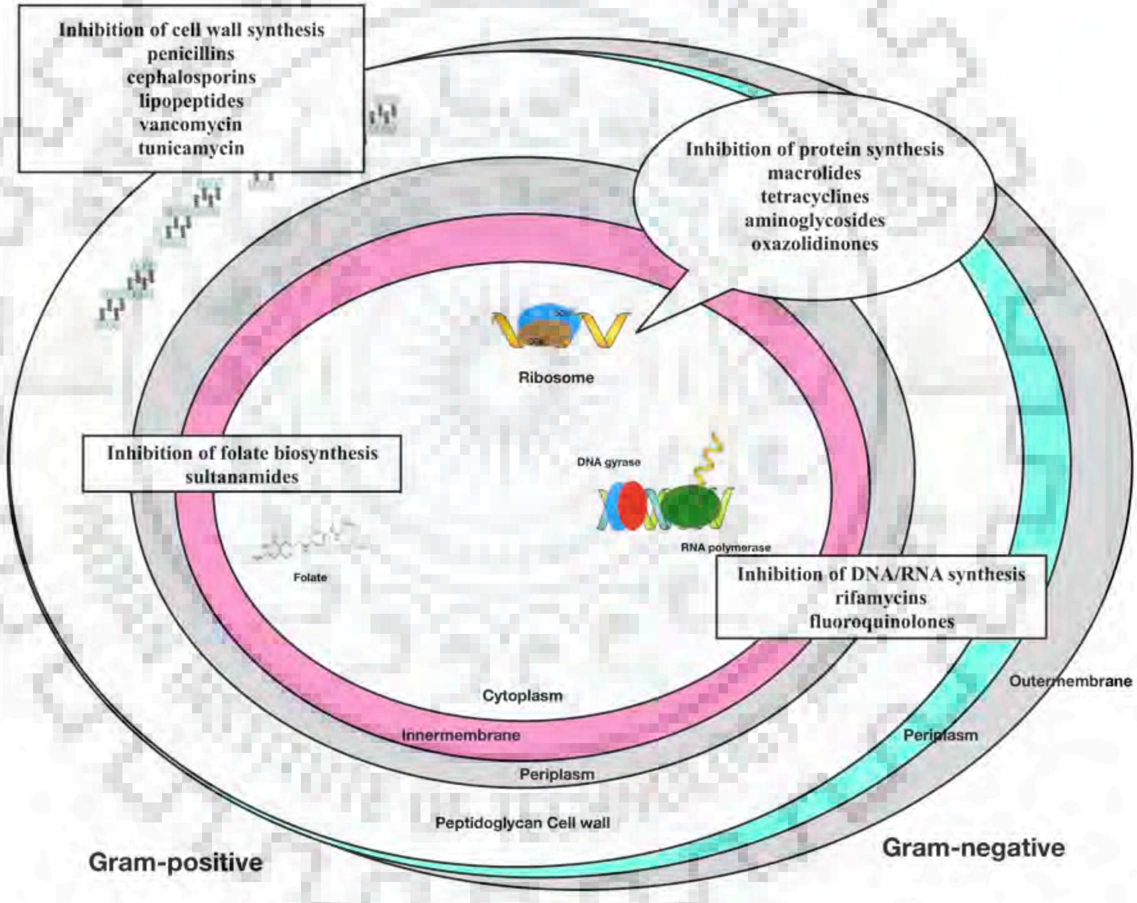
Inhibition of cell wall synthesis
penicillins
cephalosporins
lipopeptides
vancomycin
tunicamycin
Inhibition of protein synthesis
macrolides
tetracyclines
aminoglycosides
oxazolidinones
Ribosome
Inhibition of folate biosynthesis
sultanamides
DNA gyrase
RNA polymerase
Folate
Inhibition of DNA/RNA synthesis
rifamycins
fluoroquinolones
Outermembrane
Periplasm
Cytoplasm
Innermembrane
Periplasm
Peptidoglycan Cell wall
Gram-positive
Gram-negative

Figure 1.2 The schematic representation of the major pathways targeted by commonly used antibiotics.

1.2.3 Inhibition of DNA replication

The third major target of antibiotics is DNA replication and its repair mechanisms. Most of antibiotics in this category are synthetically derived class of quinolones, including ciprofloxacin, which targets DNA gyrase specifically DNA topoisomerase II. These gyrases play important role in relieving the torsional stress in the replicating supercoils by making cuts in both strands of DNA. These quinolones bind to the cleavage sites of these enzymes, and thus preventing the further repair to system[11].

1.2.4 Folate biosynthesis inhibitors

Another class of antibiotics includes sulfa drugs (sulfonamides) like sulfamethizole, which targets the folate biosynthesis in the bacterial system. These classes of drugs are the structural mimics of p- aminobenzoic acid, an important precursor in the synthesis of folate. This pathway synthesize the important precursors required for maintaining the necessary cellular functions, and also contains an essential node dihydrofolate reductase (DHFR) which has been shared between prokaryotes and eukaryotes. The DHFR is important target for anticancer drugs (methotrexate) and for antibacterials (trimethoprim). The dihyropteroate synthase (DHPS) is the primary target of sulfa drugs, which act synergistically with DHFR inhibitors[12].

1.3 Emergence of Antibiotic Resistance

Although targeting many essential pathways, antibiotics have lost their efficacy due to the emergence of resistance mechanisms among various pathogens. It is postulated that antibiotics are evolved as arsenals to biological combat between bacteria which means resistance among pathogens has been developing for millennia. Because, as per the “survival of the fittest”, methods to resist the antibiotic induced death in microbes are passed to the next generation through cell division further ensuring the multiplication of resistant bacteria with evolutionary advantages. Additionally, the resistant mechanisms among pathogens are also shared through horizontal gene transfer. Although these resistance mechanisms are quite diverse across the bacterial species, but can be grouped based upon the general similarities. Particularly, microbes have evolved three different mechanisms to resist antibiotics, including the decreasing the penetration of drug via limiting the permeability and efflux pumps, modifying the binding target by mutations, and degradation of antibiotic itself (Figure 1.3). Also, as the targeted pathways are critical for bacterial survival, there is a substantial selection pressure, which drives the spread of resistance[11,13,14]. Brief overview of resistance mechanism relevant to each class of antibiotics among pathogens has been addressed in the following sections.

1.3.1 Drugs efflux

The porins present in the outer membrane of bacteria are responsible for the entry of antibiotics into the cell. The reduced expression of porins or mutations in the porins genes leads to the reduction of the antibiotics entry into the cell rendering them lesser effective. Apart from this, bacteria also possess multidrug efflux pumps, which are responsible for the active transport of antibiotics out of the bacterial cells. These pumps found in both gram-positive gram-negative bacteria and exhibit variable level of substrate scope and specificity. The first identified efflux pump was tetracycline pump critical for providing resistance to tetracycline in bacteria. Some of the pumps have properties to remove various substrates from the cell making these factors important for developing multidrug resistance. These are classified in the five major families with difference in the structure, source of energy, specificity to substrates, and species distribution [15,16].

1.3.2 Modification of antibiotics

Another mechanism of resistance in microbes is either degradation of antibiotic by enzymes or inactivation in such a fashion that it cannot bind to its own target. The method mainly depends upon the chemical modification or transformation of antibiotics to destroy their inherent bioactivity. Enzymes, which are responsible for the degradation of these antibiotics, are present in several bacteria. Different variants of β-lactamases are encoded in the bacteria, and each of these variants can degrade various β-lactam based antibiotics. Bacteria resistant to all kind of β-lactam antibiotics have been emerged and new classes of β-lactamases have been discovered in pathogenic microbes like *Klebsiella pneumoniae*, *E.coli*, *Pseudomonas aeruginosa*, etc. Additionally, there are various known enzymes that can transfer different chemical groups (phosphate, nucleotidyl, acyl, etc.) to the antibiotics making them lesser effective with reduced affinity to their respective targets. The amino-glycoside based antibiotics are known to be modified by acetyltransferases, nucleotidyltransferases, as well as phosphotransferases [17].

1.3.3 Modification of antibiotic target

The third mechanism that confers resistance to antibiotics in bacteria is the modifications or mutations in the binding sites of the antibiotic targets. Although only those mutations that lead to the decreased drug binding without compromising the activity of protein are favored. Well-known examples are the methylation of ribosomes to inhibit binding of ribosomes targeting antibiotics and mutation in the rpoB gene encoding the β- subunit of RNA polymerase providing resistance to *M. tuberculosis* against rifampicin. In the first case, the methylation provides the stearic hindrance or blockage, which results in the clash of highly substituted backbone of macrolide-based antibiotics.

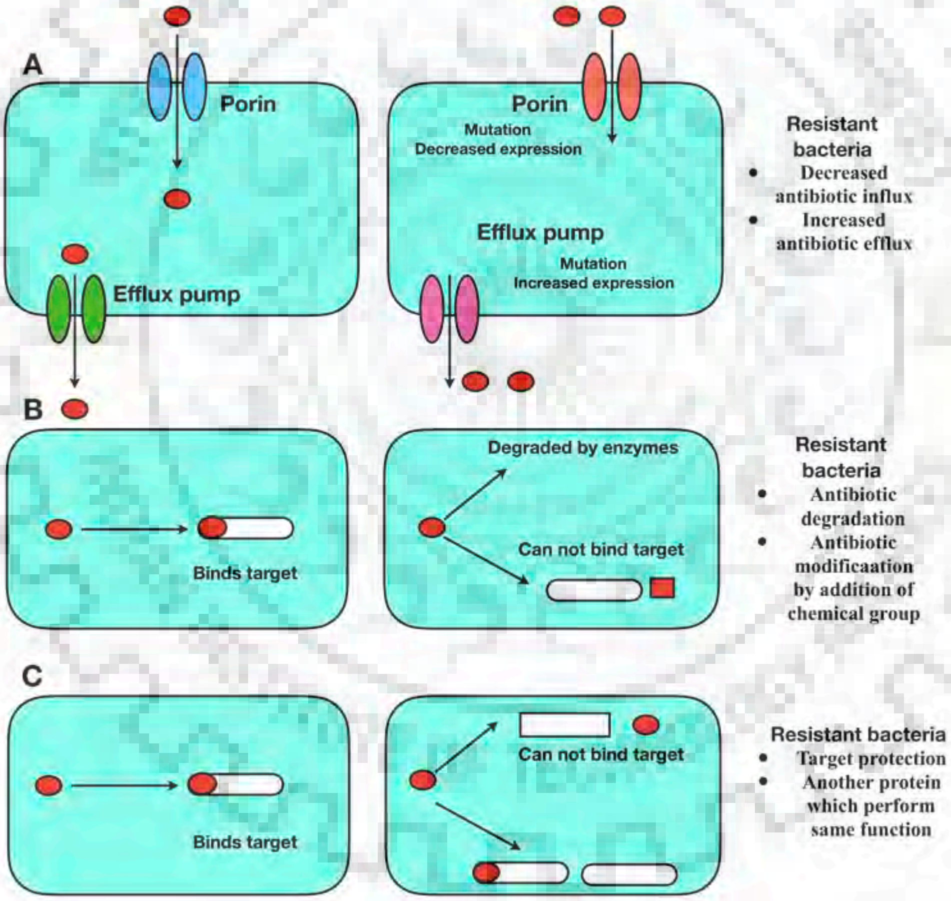
A
Porin
Efflux pump
Porin
Mutation
Decreased expression
Efflux pump
Mutation
Increased expression
Resistant bacteria
• Decreased antibiotic influx
• Increased antibiotic efflux
B
Binds target
Degraded by enzymes
Can not bind target
Resistant bacteria
• Antibiotic degradation
• Antibiotic modificaation by addition of chemical group
C
Binds target
Can not bind target
Resistant bacteria
• Target protection
• Another protein which perform same function

Figure 1.3 Emergence of drug resistance in bacteria. The three main ways in which bacteria acquired resistance to antibiotics are changes in the efflux of drugs, modification of antibiotics and modification of the antibiotic target.

In another case, a single point mutation is responsible for reducing the affinity of rifampicin while allowing the bacteria to operate normally with maintained RNA polymerase functions. Also, bacterial genome can acquire a gene, which encodes the homologue of a drug target that does not bind to the respective drug. In this case, the most studied example is methicillin resistant *S. aureus* (MRSA), where this bacterium possesses a similar type of penicillin binding protein (PBP2a) in addition to genome encoded PBP. Therefore, β -lactam based drugs will inhibit PBP but cell can carry out cell wall synthesis as homologue protein PBP2a will be resistant to the action of β-lactam antibiotics [8,18,19].

1.4 Combating drug resistance in bacteria

The antimicrobial drug resistance is the one of the important challenges in the management of the diseases caused by infectious pathogens. This is the issue that has impact in all kind of infections caused by different microbes (viruses, parasites, fungi or bacteria). However it’s the manifestation of the multi-drug resistance in the bacteria that has resulted in the pressing concern in modern medicine[20,21]. The most celebrated golden era of antibiotics had led to the discovery of several vital antibiotics but the last decade has produced very few possible drug candidates. This has set the alarming concerns in the world as its becoming challenging to treat the drug resistant pathogens. The list of drug resistant pathogens is increasing and most commonly classified as ESKAPE pathogens, which include *Enterococcus faecium, Staphylococcus aureus, Klebsiella pneumoniae, Acinetobacter baumanii, Pseudomonas aeruginosa*, and *Enterobacter* species. These are classified as ‘ESKAPE’ because of capability of these pathogens to effectively escape the effects of antibiotics [22,23]. In order to address this issue, we need the collaborations of many disciplines, innovations in the identification of new scaffolds and complementing antibacterial strategies. Combating drug-resistant needs: (a) a comprehensive understanding of drug resistance at molecular level, its evolution and dissemination across different species; (b) new chemical scaffold with potential antimicrobial properties to fill the classical antibiotic pipeline; (c) innovative strategies to modify the currently used antibiotics to increase their life or discovering new approaches to control the growth of microbial pathogen[20,24–30].

As the bacterial pathogens have developed the resistance against the antibiotics which targeted the essential pathways like cell wall synthesis, DNA (or RNA) replication, protein synthesis, and folate biosynthesis pathways[6,8,10,31] it has become more important to discover antibacterial agents targeting other vital pathways or processes of bacteria. Other important pathways of bacteria that have been validated for drug development are shikimate pathway, fatty acid biosynthesis, lipid polysaccharide synthesis, cell division, two-component regulatory system, and bacterial efflux pumps [32–42]. In the past, most common approach to discover antibiotics was the mining of environmental microbes for their metabolites, and screening and testing against pathogens. The compounds, which have shown antibacterial effects, were considered to be the putative drug candidate with lesser information deciphering their mode of action. However, now a days target based approach can be followed for the development of new drugs with the advancement in the genome sequencing techniques[20,35,43–49].

A typical drug discovery process starts form the identification of drug target followed by the target validation using various biochemical or gene knockout based studies. Drug target should be essential for the survival of the pathogen. Once the target is validated, hit identification and lead discovery process will start, where inhibitors are screened based upon biochemical based high-throughput assays or structure based screening. After this step, lead optimization followed by the selection of candidate compound for clinical development [50–54]. A pictorial presentation of drug discovery process has been shown in Figure 1.4.

The present study focuses on the two essential pathways from bacteria, including shikimate pathway and fatty acid biosynthesis pathway. The thesis encompasses the biochemical, biophysical and structural characterization of three proteins, including chorismate mutase like domain of DAHPS from *Bacillus subtilis*, and β-hydroxyacyl acyl carrier protein dehydratase (FabZ) and Malonyl-CoA: ACP transacylase (FabD), from drug-resistant gram-negative pathogen *Moraxella catarrhalis*. More importantly, new inhibitors against these three proteins have been discovered and characterized using biochemical, biophysical, and *In silico* based approaches.

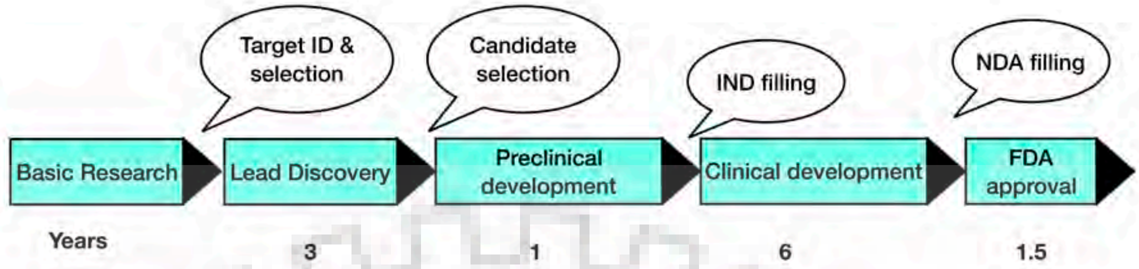

Figure 1.4 The overview of drug discovery process. Drug discovery process from target ID and validation through to filing of a compound and the approximate timescale for these processes. FDA, Food and Drug Administration; IND, Investigational New Drug; NDA, New Drug Application.

1.5 Shikimate pathway

The shikimate pathway, being an important pathway in the metabolism of plants, fungi, bacteria, and apicomplexian parasites, links the metabolism of carbohydrates with the synthesis of aromatic amino acids. Since this pathway is absent in animals, enzymes of this pathway are considered as attractive targets for the development of drugs and herbicides. The pathway involved the seven metabolic steps where primary metabolites phosphoenol pyruvate (PEP) and erythrose 4-phosphate (E4P) are converted into chorismic acid, which is the key precursor of aromatic amino acids and various secondary metabolites. The structural and functional characterization of the enzymes of this pathway is important to understand the regulation of biosynthesis of aromatic amino acids as well as for the development of drugs against bacteria or parasites. The glyphosate is the known herbicide to inhibit the bacterial growth in vitro via inhibiting the penultimate step of the shikimate pathway[55–58]. The schematic representation of the seven metabolic steps of this pathway has been shown in Figure 1.5.

The metabolic enzymes of this pathway were first discovered through studies on bacteria, mainly *E.coli* and *Salmonella typhimurium*. Although substrates, products and intermediates of the pathway are identical in prokaryotes and eukaryotes but sometimes major differences are found in primary sequence level and some of the properties of enzymes of prokaryotes and eukaryotes[59]. A brief overview of the seven enzymes of shikimate pathway and reaction catalyzed by respective enzymes have been given as follows:

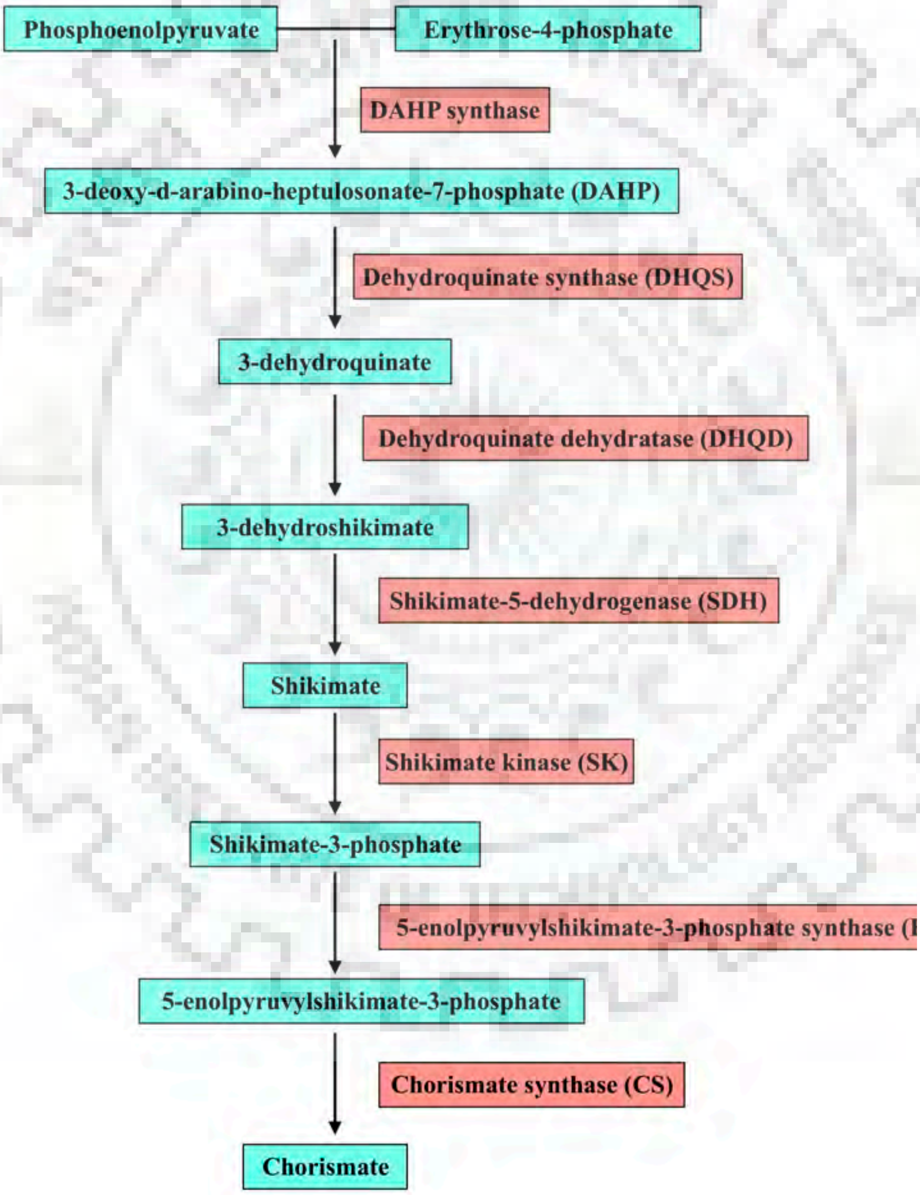
Phosphoenolpyruvate
Erythrose-4-phosphate
DAHP synthase
3-deoxy-d-arabino-heptulosonate-7-phosphate (DAHP)
Dehydroquinate synthase (DHQS)
3-dehydroquinate
Dehydroquinate dehydratase (DHQD)
3-dehydroshikimate
Shikimate-5-dehydrogenase (SDH)
Shikimate
Shikimate kinase (SK)
Shikimate-3-phosphate
5-enolpyruvylshikimate-3-phosphate synthase (
5-enolpyruvylshikimate-3-phosphate
Chorismate synthase (CS)
Chorismate

Figure 1.5 The Shikimate pathway. The seven key enzymes of shikimate pathway and reactions performed by them.

1.5.1 The Enzymes of the main trunk

1.5.1.1 Deoxy-D-Arabino-Heptulosonate 7-Phosphate Synthase (DAHP synthase)

The first committed step towards the biosynthesis of aromatic amino acids is performed by DAHP synthase (EC 2.5.1.54). It catalyzes the aldol condensation of PEP and E4P to form 3-deoxy-D-*arabino*-heptulosonate 7-phosphate (DAHP) and inorganic phosphate (Figure 1.6). This enzyme is first purified from *E. coli* at the level of electrophoretic homogeneity and most intensively studied. In most of the microbes including *E.coli* this enzyme exists in three isozymes each regulated by feedback inhibition from one of the aromatic amino acids (Phe, Tyr or Trp)[57,60,61]. Phe regulated DAHPS is the major form of the enzyme exists around 80% of the microbes while Tyr and Trp regulated DAHPS are less abundant constitutes around 20% and 1% respectively. All these isozymes require divalent cations for their activity with most efficient in presence of Mn^{2+} ions followed by Fe^{2+}, Co^{2+}, Cu^{2+}, Ni^{2+} and Zn^{2+}. At sequence level these isozymes share 41% identity with each other[62].

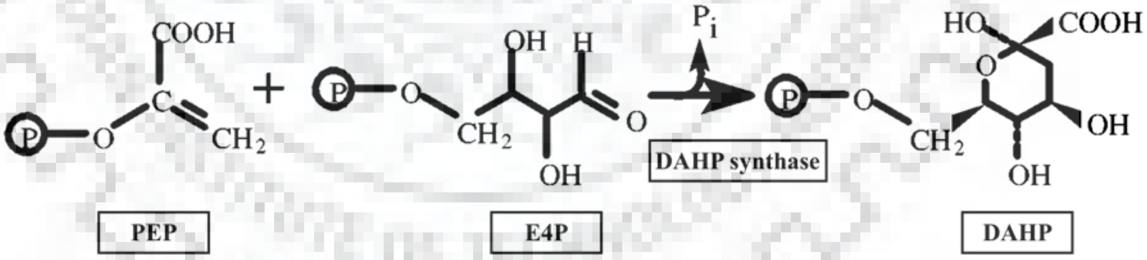

Figure 1.6 Reaction catalyzed by the DAHP synthase (DAHPS) enzyme.

The DAHPS has been classified into two types Type I and Type II, which mainly differs in the sequence length. Type I are relatively smaller in sequence length (~270 residues) and contains only DAHP synthase domain while Type II are longer in sequence length (~ 350 residues) and contains additional segment at N or C terminus[61]. These two types of DAHP synthases share less than 10 % sequence identity and have substantial differences in the quaternary structures. Although if we look at the monomeric level their fold, arrangement of amino acids, and interaction with substrate (PEP) and divalent ions, are highly conserved in these two types of DAHP synthases[60,63]. Type II enzymes are primary associated with plants and microbes while type I are mainly found in bacteria[61]. The reaction mechanism of DAHP synthase involves the nucleophilic attack of water molecule on PEP (C2 position) followed by the addition C3 of PEP to C1 of arabinose-5-phoshphate. The metals ion plays a important role in activating the enzyme through structural organization of the active site and arranging the key active sites residues in a suitable position for water activation and further activating the water molecule for nucleophlic attack[64].

Structural features of DAHP synthase

The crystal structures of DAHP synthase have been reported from bacteria as well as from eukaryotic organisms. Most of the structures deposited in PDB databases are from bacteria including *Mycobacterium tuberculosis*, *E.coli*, *Thermotoga martium, Listeria monocytogenes*, *Geobacillus*, and *Pyrococcus*. In eukaryotes, major fractions of structures deposited were from *Saccharomyces cerevisiae* [60]. The first crystal structure of DAHP synthase was determined from *E.coli* in complex with PEP and divalent Pb^{2+} [65]. Each subunit has a typical tim barrel fold $(\beta/\alpha)_{8,}$ which is characteristic to this family of enzymes. The active site of this enzyme is mainly dominated by the positively charged residues and located at the C-terminal end. The secondary structure elements that involved in the formation of active site in *E.coli* DAHPS were beta strands- β2, β5, β8, and β-α loops. The substrate PEP and metal ion were positioned at the active site and interacting with Arg92, Lys97, Cys61, His268, Ala164, Arg165, Lys186, Asp326, Arg324, and Glu302 residues. The sequence comparison has shown that these residues were found to be conserved in known DAHPS structures with exception in type II DAHPS from *M. tuberculosis* where Lys97 is conserved. There is also a variation in two types of DAHPS with respect to phosphate binding motif. In type I DAHPS this motif is RxxxxKPRS/T where as in type II DAHPS there is insertion of two amino acids in the same motif (RxxxxxxKPRS/T). This motif plays an important role in the binding of E4P for the condensation reaction with PEP. Regulation of DAHP synthase in microbes were accomplished either by any metabolite intermediate or by feedback inhibition by end products of the pathway or by repression at the transcription level[61].

1.5.1.2 Dehydroquinate Synthase (DHQS)

The second step in the shikimate pathway is catalyzed by 3-Dehydroquinate Synthase (EC 4.2.3.4) enzyme. This is a NAD dependent metalloenzyme that performs the five-step transformation of 3-deoxy-D-arabino-heptulosonate-7- phosphate (DAHP) to dehydroquinate (Figure 1.7). DHQS has been characterized from prokaryotes and eukaryotes with significant variations found at structural level. In bacteria, this enzyme is encoded by the single gene (AROB) and exists as a monofunctional enzyme while in eukaryotes it exists as multifunctional polypeptide (encoded by AROM gene), which catalyzes the five enzymatic reactions starting from step 2 to step 7 of the shikimate pathway i.e. conversion of DAHP to chorismate[66]. DHQS is an oxido-reductase enzyme where five sequential reactions were performed at the single active site. Reaction mechanism involves alcohol oxidation, elimination of phosphate group, reduction of carbonyl, ring opening and intramolecular condensation of aldol moiety. NAD^+ mediated oxidation of alcohol is carried out at C5 of the DAHP led to the formation of NADH which is further used in the reduction of ketone/carbonyl intermediate at C5 of DAHP followed by the spontaneous opening and cyclization of the ring. Co^{2+} and Zn^{2+} are the divalent cations required for the activity of microbial DHQS[67].

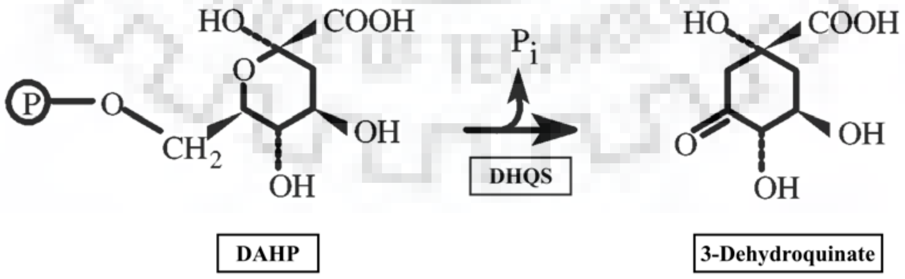

Figure 1.7 Reaction catalyzed by the DHQS enzyme. This enzyme requires NAD for its activity.

The first 3D structure of DHQS was determined from fungus *Asperegillus nidulans* (PDB: 1DQS) and monomeric unit of multifunctional polypeptide composed of N – terminal (α/β) domain and C- terminal α - helical domain[68]. The activity of this enzyme is solely associated with the N- terminal domain, which consists of seven stranded β-sheets, containing a βαβ unit and αβαβαβ unit. The secondary structures elements of the N- terminal domain fold to form Rossmann fold which is reported to bind with NAD cofactor. The crystal structures of DHQS were also reported from *Helicobacter pylori*, *Staphylococcus aureus*, *Thermus thermophilus*, and *Vibrio cholerae*. It has been reported that plants DHQS are more related to bacetrial DHQS as compared to fungus DHQS.

1.5.1.3 Dehydroquinate dehydratase (DHQD)

The third step in the shikimate pathway is catalyzed by dehydroquinate dehydratase (EC 4.2.1.10) enzyme, which belongs to the family of lyases and cleaves carbon-oxygen bonds. It performs the dehydration of substrate 3-dehydroquinate and lead to the synthesis of 3-dehydroshikimate (Figure 1.8). Reaction performed by this enzyme is common to two metabolic pathways – the biosynthetic shikimate pathway and catabolic quinate pathway. Shikimate pathway leads to the formation of chorismate, which is essential for aromatic amino acids synthesis, while quinate is used as carbon source for the synthesis of paracatechuate[69]. The first 3D structure of DHQD was reported in 1999 from *M. tuberculosis* (PDB: 2DHQ). This enzyme is important because it exists as bifunctional form (DHQD-SDH) in plants and is useful to understand the channeling of dehydroshikimate from DHQD to the active site of SDH.

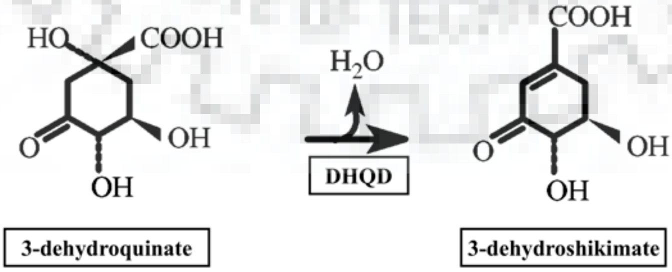

Figure 1.8 Reaction catalyzed by the DHQD enzyme.

Structurally, DHQD protein has TIM barrel fold, which consists of alternating α/β secondary structure elements and is characteristic to the dehydratase family. There are two classes of DHQD enzymes (type I and type II) with major differences found in primary sequences and 3D structures. Type I is found in plants, fungi and some of the bacterial species while type II are limited to bacteria and fungi only[70].

1.5.1.4 Shikimate dehydrogenase (SDH)

Shikimate dehydrogenase (EC 1.1.1.25) is the fourth enzyme of shikimate pathway and catalyzes the reduction of substrate 3- dehydroshikimate using NADPH to form the shikimate as product (Figure 1.9). It belongs to the family of oxidoreductases. Based upon the biochemical characterization and phylogeny, SDH has been classified into three different classes AroE (SDH), YdiB (shikimate/quinate dehydrogenase) and SDH-L (SDH-like). AroE type is broadly distributed as NADP dependent SDH that is only active in shikimate pathway. YdiB is NAD(H) or NADP(H) dependent dehydrogenases are present in both quinate metabolism and shikimate pathway.

The crystal structures of SDH have been reported from different organisms, including *E.coli*, *Helicobacter*, *Haemophillus*, *Corneybacterium*, *Thermus thermophillus* and *Arabidopsis thaliana*.

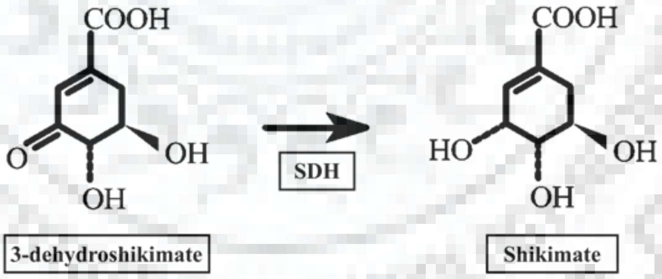

Figure 1.9 The recation catalyzed by the shikimate dehydrogenase (SDH) enzyme.

In *E. coli*, 3D structure has revealed that there is the presence of two structural domains- one is catalytic domain while another is NADPH binding domain. The catalytic domain has distinct α/β fold involving six stranded β-sheets surrounded by α-helices, while NADPH binding C-terminal domain forms Rossmann fold similar to other NADPH binding dehydrogenases[60,71].

1.5.1.5 Shikimate kinase (SK)

The conversion of shikimate to shikimate-3-phospahte is catalyzed by the shikimate kinase (EC 2.7.1.71) using ATP as cosubstrate (Figure 1.10). This enzymes exists in two isoforms in *E. Coli* (Type I & Type II). Type II isoenzyme has higher affinity (100 fold more) for shikimate as compared to type I, and therefore plays a main role in the catalysis reaction in shikimate pathway. The two isoforms share 45% sequence homolgy and have type A Walker motif for the binding of ATP or GTP. The crystal structures of SK were mainly reported from bacteria with one structure came from eukaryotes (*Arabidopisis thaliana*).

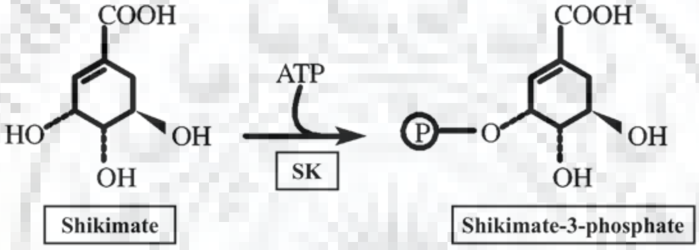

Figure 1.10 The reaction catalyzed by the shikimate kinase enzyme.

Among bacteria, structures are known from *M. tuberculosis*, *E. coli* and *Erwinia chrysanthemi*. Shikimate kinase belongs to the family of NMP kinase despit having low sequence identity. Both isoforms (type I & type II) have similar structurral fold conatning five stranded parallel β-sheets surrounded by eight α- helices. Similar to NMP kinase family, SK is also composed of three domains including core domain, LID and shikimate binding domain[72].

1.5.1.6 5-Enolpyruvylshikimate 3-phosphate synthase (EPSPS)

The penultimate step towards the biosynthesis of aromatic amino acids in higher plants, bacteria and fungi is catalyzed by 5-Enolpyruvylshikimate 3-phosphate synthase a carboxyvinyl transferase (Figure 1.11). It performs the condensation reaction of PEP with shikimate-3-phosphate to form 5-enolpyruvyl-3- shikimate phosphate and inorganic phosphate (Pi). This enzyme along with MurA (involved in bacterial cell wall synthesis) exists in monomeric form among the class of enolpyruvyl transfeases. EPSPS and MurA have share unique structures with two globular domains made up of β- sheets and α-helices comprised of three copies of βαβαββ folding units which further forms an overall structural fold with inverse α/β barrel. The active site is sandwiched between the two globular domains linked by two strands and during the substrate-product conversion these strands behave like a hinge to bring these two domains closer to each other allowing the conformational changes.

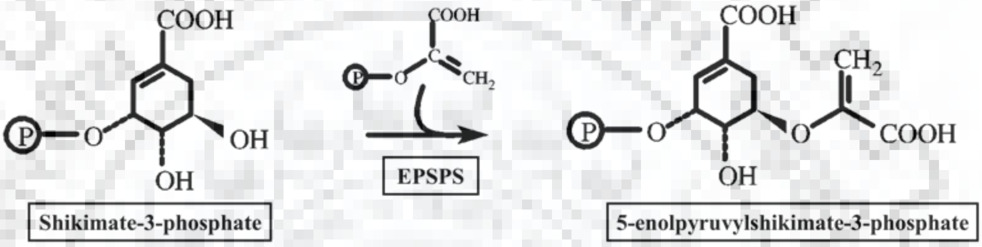

Figure 1.11 The reaction catalyzed by EPSPS enzyme.

Being an essential enzyme of the pathway, it's not surprising that numerous studies have been performed to characterize the EPSPS to understand its mechanism and structure. MurA, a homologue of this enzyme is considered as potent target for naturally existing fosfomycin antibiotic. The glyphosate, a potent inhibitor of the plant EPSP synthase is considered to be one of the most effective herbicide in the field of agriculture, and has revolutionized the agricultural field for the development of glyphosate resistant plants. Additionally, same compound is also known to inhibit the EPSPS enzyme in several pathogenic parasites, including *Plasmodium falciparum*, *Taxoplasma* and *Cryptosporidium*. The majority of the crystal structures of EPSP synthase has been reported from *E. coli*. Schonbrunn et al determined the crystal structure of this enzyme in two states: first one is in complexed with S3P and glyphosate in the active site (PDB: 1G6S), and the second one is complexed with S3P, phosphate ion and formate (PDB: 1G6T). In both of these structures, the two globular domains of the enzyme come closer and forming the active site in the inner cleft rendering the induced fit mechanism of substrate binding to EPSPS active site[73].

1.5.1.7 Chorismate synthase (CS)

The last step in the shikimate pathway is catalyzed by chorismate synthase (EC 4.2.3.5) which involves the trans-1,4 elimination of a phosphate group from 5-enolpyruvylshikimate-3-phosphate (EPSP) to form chorismate (Figure 1.12). Chorismate is an essential precursor for the synthesis of aromatic metabolites including aromatic amino acids, Coenzyme Q, folate, vitamin K and E, plastoquinones and entrobactin. CS is the only enzyme to perform such kind of transformation in biological systems and therefore considered as unique enzyme. This enzyme requires a reduced FMN for its activity, however transformation of EPSP into chorismate does not involve any kind of redox change[74].

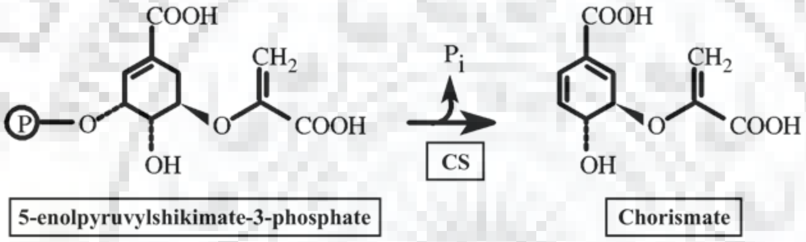

Figure 1.12 The reaction catalyzed by chorismate synthase (CS) enzyme.

Based upon the functionality, chorismate synthase has been classified into two types, monofunctional and bi-functional. In plants and eubacteria, it possesses only trans-elimination activity, thus constitute its monofucntional form. However in fungi (*Neurospora* and *Saccharomyces*), it has additional NADPH: FMN oxidoreductase activity along with trans-elimination activity, therefore it exists as bifucntional form. In *Bacillus subtilis* another kind of CS exists where it forms heterotrimeric complex with flavin reductase and DHS. The crystal structure of CS has been reported from *Streptococcus pneumoniae, Helicobacter pylori, Mycobacterium tuberculosis* and *Aquiflex aelicus*. In *S. pneumonia*, it has tetrameric structure formed by the dimer of dimers. The single monomeric subunit comprises of single large domain surrounded by loops and distinct stretches of α- helices and β-sheets[60].

1.6 Fatty acid biosynthesis pathway

Fatty acids are the essential metabolites synthesized by the efficient, complex and important biosynthetic machinery. Fatty acids are produced in the nature for many purposes including for biological scaffolds like cell wall and cell membranes, key elements for the synthesis of essential metabolites like biotin or lipoic acid, and for energy storage in the form of triglycerides [75]. The biogenesis of cell membranes is important phenomenon in microbial physiology. The survival of bacteria depends upon the homeostasis of the cell membranes and specifically depends upon the ability of bacteria to adjust their lipid content to acclimatize in different environments[76]. The major and essential component of the bacterial cell membrane is lipid bilayer composed of phospholipids. The majority of the phospholipids in the bacterial world are glycerolipids consists of two fatty acid chains. The viscosity of the cell membrane depends upon the composition of phospholipids, which further govern the many vital membrane associated functions like transport of different molecules across the membrane and protein-protein interactions. As the fatty acids play an important role in the membrane architecture, the fatty acid biosynthesis considered as attractive pathway for the development of new antibacterial agents.

In nature, the fatty acid synthesis (FAS) pathway has evolved into two different types, type I (FAS I) and type II (FAS II). Type I exists in mammals, fungi, and mycobacteria, where all the reactions are catalyzed by the active sites situated at the same polypeptide chain. In this case single multifunctional protein carries all the proteins as distinct domains. While type II system exists in bacteria, protozoa and plants, where a collection of separate enzymes catalyzed the each reaction[77–79]. Although both the systems catalyze the similar reactions, but the difference in their structural organization provide us an opportunity to target FAS II pathway in pathogenic bacteria without exerting toxic effects to human host. The difference in the subcellular organization of the different components of the FAS II pathway as compared to FAS I and predominance of FAS II system in bacteria, makes FAS II pathway as an attractive target for the development of antibacterial agents. Also, the higher level of conservation in most of the enzymes of FAS II systems holds the possibility of developing broad-spectrum antibiotics[80]. The gene knockout and knockdown experiments have validated this pathway, and shown that this pathway is important for the survival of bacterial cell[78,81,82]. Additionally, this pathway is further validated as drug target by the use of triclosan and isoniazid, which target the enzymes from the bacterial FAS II pathway.

The fatty acid biosynthesis pathway (FAS II) has been extensively studied in *E.coli* system and provides the detailed information about the underlying mechanism of each reaction[83,84]. The reactions of the FAS II pathway in *E. coli* have been shown in Figure 1.13. The each of the enzymes exists in soluble form and encoded by the unique separate genes. Although this pathway (FAS II) is conserved in bacteria, but subtle differences have been observed in different organisms.

1.6.1 The FAS II pathway in E. coli

That FAS II pathway in *E. coli* is divided into two parts. First part of the pathway involves the enzymes, which constitute the initiation module (Figure 1.13).

The first step in the synthesis of fatty acid is catalyzed by the acetyl coenzyme A (CoA) carboxylase (ACC), which performs the carboxylation of acetyl-CoA to yield malonyl-CoA. AAC requires biotin as cofactor to catalyze this reaction. Acetyl-CoA carboxylase is a multi-subunit protein, and to perform the carboxylation reaction overall coordination of four gene products (AccA, AccB, AccC and AccD) is requited [85–87]. Next reaction of this module is the transfer of malonyl moiety to the sulfhydryl group of acyl carrier protein (ACP), which acts as transport machinery and carried the product of each reactions of elongation step [88]. FabD (malonyl-CoA: ACP transacylase) catalyzes this reaction through transthioesterification. Next reaction in this module is the condensation of malonyl-ACP with acetyl-CoA to form the β-ketoacyl-ACP, catalyzed by the β-ketoacyl-ACP synthase III (FabH) enzyme [89].

The second part of the FAS II pathway is the elongation module (Figure 1.13) where β-keoacyl-ACP formed by the reaction of FabH enters the elongation cycle, and progressively elongated by the two carbon units after each cycle via the activities of four enzymes.

The next step is the NADPH dependent reduction of the β-keoacyl-ACP to give β-hydroxyacyl-ACP by ubiquitously expressed FabG (β-ketoacyl-ACP reductase) enzyme [91]. The next step is catalyzed by β-hydroxyacyl-ACP dehydratase (FabA or FabZ), which involves the dehydration of β-hydroxyacyl-ACP to form trans-2-enoyl-ACP [92]. The next step is the NADH dependent reduction of enoyl-ACP by enoyl-ACP reductase (FabI) to complete the cycle. There are two other isoforms of this enzyme exists in bacteria including FabK and FabL. FabK is found in gram-positive bacteria and has additional cofactor in the form of flavin.

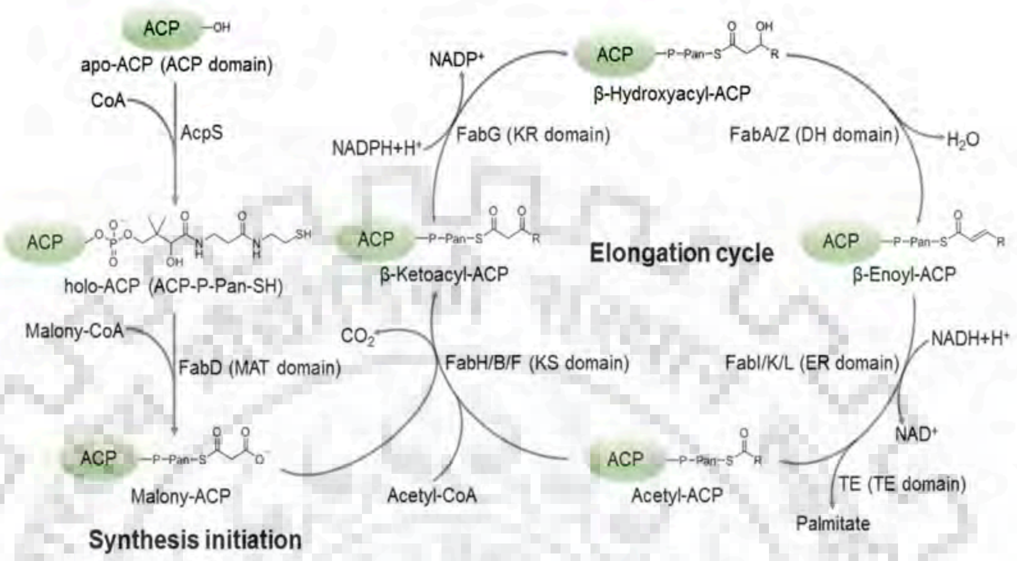
ACP
apo-ACP (ACP domain)
CoA
AcpS
ACP
holo-ACP (ACP-P-Pan-SH)
Malony-CoA
FabD (MAT domain)
ACP
Malony-ACP
Synthesis initiation
NADP⁺
NADPH+H⁺
FabG (KR domain)
ACP
β-Hydroxyacyl-ACP
FabA/Z (DH domain)
H₂O
ACP
β-Ketoacyl-ACP
Elongation cycle
ACP
β-Enoyl-ACP
CO₂
FabH/B/F (KS domain)
FabI/K/L (ER domain)
NADH+H⁺
NAD⁺
Acetyl-CoA
ACP
Acetyl-ACP
TE (TE domain)
Palmitate

Figure 1.13 The schematic representation of Type II FAS pathway.

The pathway is divided into two parts, initiation module and elongation module. In the initiation stage, apo from of ACP is converted into the holo form by attaching the 4-phosphopantethine moiety. The FabD (MCAT) uses the ACP as one of the substrate and transfers the malonyl group from malonyl-CoA to form the malonyl-ACP. The elongation modules perform four catalytic reactions catalyzed by FabH/B/F, FabG, FabZ/A, and FabI/K/L respectively. After each elongation cycle 2-carbon units have been added to fatty acid chain, and fatty acid chain either re-enters to elongation cycles fro further extension or released from ACP by thioesterase (TE) enzyme. Adopted from Zhang et al[90].

The subsequent rounds involve the condensation of the acyl-ACPs (products of the elongation cycle) with malonyl-ACP by the condensing enzyme known as β-ketoacyl-ACP synthase I or II (FabB or FabF). These enzymes increase the length of growing acyl chains by two carbon units per cycle. Finally, fatty acid is cleaved by the thioesterases from ACP once the chain length reaches to sufficient length (16-18 carbons) [83].

1.6.2 Inhibiting bacterial fatty acid biosynthesis pathway (FAS II)

The fatty acid biosynthesis pathway is validated target for the development of antibacterial drugs. Structural differences in the two types of FAS systems (Type I and

II) allow the identification of inhibitors molecules that specifically target the bacterial system. The most of the enzymes of FAS II pathway are vital for the survival of the bacteria and in principle become the attractive targets for developing antibacterial drugs. Additionally, high-resolution three-dimensional structures of all the enzyme components of the pathway also facilitate the structure based drug design[93,94]. Brief overview of the each component and their suitability as target for drug discovery has been addressed in the following sections.

1.6.2.1 Enzymes involved in the initiation modules

The first committed step in the FAS II pathway is catalyzed by acetyl-CoA carboxylase (ACC). Being a committed, regulated and rate limiting step in the pathway, this reaction is considered as good and potential chemotherapeutic target. The ACC is a multifunctional complex composed of four subunits as AccA (Carboxytransferase subunit), AccB (Biotin carboxyl carrier protein), AccC (Biotin carboxylase) and AccD (Carboxytransferase subunit). This complex in bacteria is found to be highly conserved and structurally different from the mammalian counterpart, rendering it a potential broad-spectrum drug target [94]. Naturals compounds like moiramide B known to inhibit the growth of bacteria by targeting AccAD complex. The plants also possess bacteria like ACC complex and being targeted for the development of herbicides. The consistent efforts have been made for developing ACC inhibitors against bacteria [95]. Malonyl-CoA: ACP transacylase (FabD or MCAT) catalyzes the transfer of malonyl group to ACP forming malonyl-ACP. This enzyme is essential enzyme and only single isoform of fabD is known in nature. Gene knock out studies on temperature sensitive mutants have revealed the importance of this protein for the functionality of the FAS II pathway. All these features suggest the suitability of FabD as excellent drug target for developing antibiotics. Also, a natural compound corytuberine has bee reported to inhibit the FabD from *Helicobacter pyroli* with IC_{50} of 33.1 µM in uncompetitive manner [96,97]. FabH performs the condensation reaction, which is also the one of rate limiting step in FAS II pathway. This makes the FabH potential targets for antibiotic development. The most of the inhibitors of FabH have been developed against *Streptococcus pneumoniae*. However, it has been reported that there is wide differences in the effectiveness of the inhibitors of SpFabH against EcFabH and HiFabH (*H. influenza*)[98].

1.6.2.2 Enzymes involved in the condensation of elongation products

FabB/FabF catalyzes the condensation of the elongation products and play main role in the regulation of FAS II pathway. Naturals products are reported to inhibit this step of fatty acid biosynthesis, clearly makes these enzymes as desirable drug targets. Cerulenin was the first known inhibitor of FabB/FabF enzymes, and it covalently modifies the cysteine residue of the active site[99]. Binding sites of these natural inhibitors are not known, but as these inhibitors have hydrophobic structures it might possible they can bind to acyl chain pocket (hydrophobic) of the enzymes. Another natural compound known to inhibit these condensing enzymes is thiolactomycin, and it binds to the site that is occupied by malonyl-ACP. Also, as these condensing enzymes catalyze similar kind of reactions and have similar mechanism, its also possible single inhibitor can inhibit both classes of condensing enzymes [94,95].

1.6.2.3 Enzymes involved in the reduction (Reductases)

In the elongation cycles, there are two reduction reactions catalyzed by FabG and FabI respectively. There are four characterized isoforms of enoyl-ACP reductases (FabI, FabK, FabV and FabL). FabI is a validated target for antibacterial therapeutics and presently some of the inhibitors of FabI are being evaluated in clinical trials. However, fabI distribution is not uniform in nature but it has been found that it is present in key pathogens like *Streptococcus*, *Mycobacterium*, *Neisseria*, *Acinetobacter*, *Enterococcus*, etc. It is the target of biocide triclosan and anti tuberculosis drug isoniazid. Because of these features, FabI has been most intensively exploited drug target from the FAS II pathway [100–102]. Another reductase of elongation cycle is FabG (beta-ketoacyl-ACP reductase). It has been found to be highly conserved which suggests that inhibitors against FabG would have broad-spectrum effects. Validation of FabG for its potential as drug target needs to be explored yet. However, some natural compounds have been reported to inhibit this enzyme[103].

1.6.2.4 Dehydratases and isomerases (FabZ and FabA)

FabA is the vital enzyme required for the synthesis of unsaturated fatty acids in many bacetria. It has dehydratase as well as isomerase activity. It is mainly present in those organism who synthesis unsaturated fatty acids. It does get much attaention as it has limited distribution in nature, which poses the limitation of its use as drug target. The most attractive target for antibacterial development in this pathway would be FabZ. This enzyme is ubiquitously expressed in Type II systems, and has uniform distribution in bacteria. All these features makes FabZ desirable and potential target for broad-spectrum drugs. Inhibitors of FabZ have been developed from various pathogens like *Plasmodium*, *Helicobacter*, *Yersinia*, *Moraxella*, etc [104–107].

1.6.2.5 Targeting Acyl carrier protein (ACP) and Co-enzymeA (CoA)

Another target that can be exploited for antibacterial drug development is ACP. This protein is released as apo form and converted into the functional form by the attachment of phosphopantetheine group by AcpS (ACP synthase) enzyme. AcpS has wide distribution among bacteria and considered as essential gene. Natural inhibitor against AcpS has been reported showing antibacterial activity against *S. aureus*[108]. Another important enzyme, which can be targeted for antibacterials development, is phosphopantetheine adenylyltransferase (PPAT). It is the most logical target as it plays important role in two pathways, including FAS II and CoA synthesis pathway. It has uniform distribution and single gene (CoaD) code for this enzyme. Inhibitors against PPAT have been reported but high quality 3D resolution structures are required for further inhibitor screening and development of inhibitors against PPAT[109].

1.7 Natural products as continuing source of drugs

Naturals products and their complicated molecular scaffolds are the source of wide range of chemoypes for the discovery of drugs and chemical probes. Naturals products normally possess the biologically useful molecular scaffolds with pharmacological features that evolved as preferred protein- ligand binding motifs. Therefore, natural products have been exploited for providing the leads compounds for medicinal chemists for drugs discovery especially for cancer and infectious diseases[110,111].

The fragment based drug discovery is the one of the alternative approach emerged from last two decades which take care of the typical drawbacks of the traditional drug discovery approaches. This approach has been benefitted by the diverse biophysical methods and ligand efficiency metrics. Fragment based drug discovery poised to optimize the small molecular compounds, which have potent biological activity into lead candidates through stepwise molecule growing and linking[112].

The natural products based synthetic molecular scaffold can provide the possible and advanced solutions to resolve the bottleneck in the field of drug designing. There have been many examples where natural products inspired compounds have been optimized for lead candidates. For example deoxynybomycin based chemical compound have potent inhibitory activity against *Staphylococcus aureus* and enhanced water solubility. Infected mice when treated with this compound have shown the significantly longer life span as compared to untreated mice[113]. Most of the investigated lead candidates compounds fail to fit into the stringent criteria set by medicinal chemists for drugs leads. However, the deoxynybomycin based chemical compound has been optimized and validated as lead probe by thoroughly analyzing the physiochemical and pharmacological profiling. The success of this compound suggests that the stringent decision guidelines and rules like ‘Lipinski's rule of five’[114] or ‘rule of three’[115] may prevent the finding of new biologically relevant chemical scaffolds. In fact if we compare the data, 18-20 % of the natural products from the Natural Products Database violate the ‘rule of five’ (Also 31 % traditional Chinese Medicine Database, 10 % ChEMBL database and 15 % Drug Bank). Therefore, careful application of these guidelines is important for synthetic as well as natural compounds[116].

1.7.1 Prediction of macromolecular targets for natural products

The progress of natural products based discovery of useful molecular scaffolds and drugs is hampered by the lack of information about the molecular targets of most of the known natural compounds. Many new target prediction tools are now available which help in the identification of macromolecular target, potential drawbacks of drugs like or lead molecules and also may help in the identification of different biological activities natural compounds[117]. The contemporary virtual screening of a group of potential drug targets offers a feasible and attractive solution to know about the possible ligand-target interactions. For example, cyclooxygenase-2 and peroxisome proliferator-activated receptor, the targets of meranzin have been successfully identified using inverse molecular docking approach and this inhibitor has exhibited similar activities as rosiglitazone and indomethacin[111].

The PASS is the one of the software that can predict the numerous biological activities qualitatively from the 2D chemical structure using molecular fragment based descriptors. This software has been successfully used to predict the anti cancer activities form the naturals products isolated from the set of marine sponges[118]. The several target identification tools have been established to analyze the numerous synthetic molecules. Most of these tools exploit the different features including similarity in the chemical substructure for target based upon the information of the reference drugs with known targets, precise ligand-receptor docking poses, and knowledge of pathway and genomic sequence[119,120]. Other tools like SPiDER works in different approaches and relies on the pharmacophore topology and physiochemical properties[121].

1.8 Outline of the Research work

The emergence of drug resistance against the most commonly used antibiotics has set the alarming concerns in the health sector all over the world. It has become more important to find innovative strategies to combat drug resistant pathogens. To address this problem, pathways that have not been targeted by the traditional antibiotics become more important. In the present study, we have characterized the drug targets from such pathways, including shikimate pathway and type II FAS pathways, via biochemical, biophysical and structural based characterization. The overall aim of this study is to discover the new inhibitors with antibacterial activities against the drug resistant pathogens.

The first study described in the chapter 2, focused on the biochemical and structural characterization of chorismate mutase like domain of DAHPS of shikimate pathway from *Bacillus subtilis*. In this study, we have determined the high-resolution crystal structure of BsCM_2 domain of DAHPS in complex with new inhibitor chlorogenic acid at 1.8 Å resolution. Active site analysis and structural comparison of BsCM_2 with related homologs have been performed. Binding studies of BsCM_2 with natural substrate as well as with chlorogenic acid have been performed using ITC basesd binding assays. Biochemical characterization and inhibition assays have been studied and discussed in detail.

Chapter 3 describes the biochemical, biophysical and in silico structural characterization of FabZ from *Moraxella catarrhalis* (McFabZ). FabZ gene is cloned in pET28c vector and expressed in rosetta cell lines. McFabZ protein was purified using Ni-NTA affinity-based chromatography and oligomeric state characterization has been determined using size exclusion chromatography. The biochemical activity of McFabZ is determined using a continuous assay and kinetic parameters (K_m, V_{max}, k_{cat}, k_{cat}/K_m, etc) were determined. Biophysical characterization of McFabZ was accomplished using circular dichroism (CD) and fluorescence-based assays. Structural characterization was performed using *in silico* based approaches. More importantly, three new inhibitors from the class of isoflavones have been identified and characterized using biochemical, biophysical and *in silico* based methods. Kinetic inhibition parameters (K_i and IC_{50}) have been determined and compared with known inhibitors. Structural changes in the secondary and tertiary structure of McFabZ upon the binding of inhibitors were analyzed using CD and fluorescence based assays. Binding studies were further performed using ITC based assays. Molecular docking based studies have shown how these inhibitors are interacting with the active site of McFabZ. Molecular dynamics-based simulations were performed to evaluate the stability of best-docked inhibitor complexes. A detailed structure-activity relationship (SAR) studies were conducted and discussed in this chapter.

Chapter 4 describes the biochemical, biophysical and *in silico* characterization of FabD from drug- resistant *Moraxella catarrhalis.* FabD gene is cloned, expressed and purified. Oligomeric state characterization was performed using gel filtration chromatography. Biochemical characterization and kinetic inhibition studies were performed. Biophysical studies of FabD are carried out using CD, fluorescence and UV-visible spectroscopy based techniques. Structural characterization is carried out using homology based in silico methods. More importantly, three new inhibitors from the class of aporphine alkaloids have been identified and characterized. CD studies have shown how the secondary and tertiary structure of McFabD changes upon ligands binding. Fluorescence quenching based studies were performed to determine the binding parameters (Binding constant and N). Thermodynamic parameters (K_D, N, ΔH, $T\Delta S$ and ΔG) of binding were calculated using ITC based binding assays. Molecular docking studies were carried out to predict the binding mode and plausible interactions observed during the course of binding. Critical residues, which play an important role in binding, have been identified. Minimum inhibitory concentrations of aporphine alkaloids against *Moraxella catarrhalis* have been determined.

Chapter 5 describes the inhibitory activities of aporphine alkaloids, and naphthoquinone against McFabZ. Based upon the analysis of active sites of FabD and FabZ, it has been found that a single compound can inhibit both enzymes. In this chapter, we have shown the inhibitor actions of NPQ against FabD and FabZ enzymes. Molecular docking based studies have shown that aporphine alkaloids can also bind to McFabZ. To further validate this study, kinetic inhibition experiments against McFabZ were conducted for these alkaloids. Kinetic inhibition parameters (K_i and IC_{50}) were determined using continuous assays. Fluorescence quenching studies were further conducted to calculate the binding parameters (K_b and N). Binding parameters obtained through molecular docking (binding constant and binding energy) and fluorescence quenching for these compounds against FabZ and FabD were compared and structure-activity relationships were drawn.

Chapter 2

Biochemical and Structural characterization of Chorismate mutase like domain of DAHP synthase from *Bacillus subtilis*.

भारतीय प्रौद्योगिकी संस्थान रुड़की
INDIAN INSTITUTE OF TECHNOLOGY ROORKEE

Chapter 2

2.1 Introduction

Chorismic acid, the precursor for a wide range of aromatic compounds, including aromatic amino acids, folate, and ubiquinones, is essential for the survival of bacteria, and synthesized through the shikimate pathway[122]. The shikimate pathway is present in microorganisms, plants, and apicomplexan parasites, but is absent in higher eukaryotes. Altogether, these properties make enzymes of this pathway promising targets for the development of antibiotics, herbicides and pesticides [123,124]. The DAHP synthase enzyme catalyzes the first committed step of the pathway and it performs the aldol condensation of phosphoenolpyruvate (PEP) and D-erythrose-4-phosphate (E4P) to yield 3-deoxy-D-arabino-heptulosonate-7-phosphate (DAHP). DAHP synthase activity is regulated by feedback or allosteric based mechanisms to control the substrate input with respect to the cellular concentration of downstream reaction products [125–127]. Different organisms have evolved to regulate DAHP synthase activity through different allosteric mechanisms and associated allosteric machinery [128,129].

All structurally characterized DAHPS enzymes share a characteristic $(\beta/\alpha)_8$ TIM – barrel fold and similar active site architecture[130–133]. Initially, based on variations in amino acid sequences, DAHPS enzymes were classified into different classes, including type Iα, type Iβ and type II. With the availability of structural information, these sequence variations were attributed to different structural additions to the core catalytic barrel[131,134–137]. In *Escherichia coli*, three isoenzymes of DAHPS type Iα are present, and each isoenzyme is responsive to phenylalanine, tyrosine or tryptophan[138]. *Mycobacterium tuberculosis* DAHPS, a type II enzyme, has a synergistic mode of inhibition caused by binding of tyrosine and tryptophan or phenylalanine and tyrosine at discrete allosteric sites. Additionally, noncovalent complex formation between chorismate mutase (CM) and DAHPS in *M. tuberculosis* modifies allosteric regulatory properties of both the enzymes through molecular symbiosis[134,139]. Chorismate, a substrate of CM, inhibits DAHPS activity, which suggests that CM has a regulatory role in this complex[63]. In *Thermotoga maritima* DAHPS, a type Iβ enzyme, is regulated by an N-terminal ferredoxin-like (FL) regulatory domain. Aromatic amino acids, phenylalanine or tyrosine binds to the FL domain and cause a conformational change which restricts substrate access to the active site[126,140,141].

A DAHPS enzyme from *Listeria monocytogenes* has an N-terminal CM, type II domain (*Lm*CM), which regulates the enzyme's activity through binding of chorismate or prephenate[131]. The regulatory *Lm*CM domain is entirely helical in structure and is classified as a "Chorismate Mutase II fold" in the SCOP database[142]. The regulatory domain is connected to the DAHPS domain through a linker region. Light *et al.* have also summarized the possible mode of allosteric regulation, such as (i) domain linker mediated transmission of inhibitory conformational changes or (ii) domain-domain inhibitory interaction stabilization. Domain-domain interface interactions are mediated by polar and hydrophobic contacts between catalytic and regulatory domains. In *L. monocytogenes,* residues Phe46, Leu49, Arg52, and Lys76 of the regulatory domain participate in domain-domain interface interactions with Phe163, Asp326, and Val329 of the catalytic domain[131]. The N-terminal domain of bifunctional P-protein from *E. coli* (*Ec*CM) also has a chorismate mutase II fold [143,144]. Although, *Ec*CM shares same fold as *Lm*CM, it is a fully functional enzyme, unlike *Lm*CM.

A recently published crystal structure of DAH7PS from *Geobacillus sp.* shares a similar architecture, with an N-terminal CM domain, which is shown to be catalytically active. The full-length protein exhibits the activity of both enzymes, but interestingly, in the absence of the CM domain, the DAHPS activity is significantly increased, whereas the separated CM domain is catalytically less active. This observation clearly implies that the CM domains interacts with the DAHPS domain and possess a regulatory role in the wild-type enzyme. Furthermore, Nazmi *et al.* showed the inhibition of DAHPS domain activity in the wild-type enzyme in the presence of prephenate, the product of CM. This inhibitory activity was not observed for a separated DAHPS domain. Based on the prephenate bound DAHPS crystal structure, in addition to SAXS analysis, Nazmi *et al.* proposed that in the unbound state, the CM domain adopts a open conformation and allows the DAHPS substrate to access its active site. In contrast, binding of prephenate to the CM domain induces conformational changes resulting in a more compact closed conformation, which bring both domains close to each other. This structural rearrangement results in obstruction of the DAHPS active site, thereby inhibits its activity[145].

The N-terminal domain of DAHPS from *B. subtilis* is homologous to the AroQ class of chorismate mutase, type II [58,146]. However, *B. subtilis* also contains a monofunctional AroH class of chorismate mutase situated downstream of the shikimate pathway[147]. Chorismate mutase converts chorismic acid into prephenate, which is further converted into the aromatic amino acids tyrosine and phenylalanine. The N-terminal domain of DAHPS has minimal catalytic activity, and CM's substrate/product have been shown to inhibit the activity of the *Bs*DAHPS enzyme [148,149]. Previously, it was argued that the N-terminal domain has a regulatory function rather than a catalytic one[137,146] . Chlorogenic acid (CGA), one of the most abundant polyphenols in human diet, is the ester of caffeic acid and quince acid. CGA decreases the incidence of chemical carcinogenesis in animal models, and also inhibits bacterial growth [150,151]. However, the molecular mechanism of its anticancer and antibacterial activity is largely elusive.

In the present study, we have determined the high-resolution structure of chorismate mutase like domain of DAHPS from *Bacillus subtilis* (BsCM_2) in complex with chlorogenic acid at 1.8 Å resolution. Based on our biochemical and structural findings, we have shown that chlorogenic acid, a structural analogue of chorismic acid, is an inhibitor of chorismate mutase, type II regulatory domain (*Bs*CM_2) of DAHPS. The present study is the first report of the AroQ class of *Bs*CM_2 structures and provides insight into active site architecture and its regulatory role. Molecular dynamics simulations were performed to observe active site loop flexibility. Through structural analysis, we have provided explanations of the minimal catalytic activity of *Bs*CM_2 and other previously reported observations regarding its role in DAHPS activity regulation. This data also provides evidence to reinforce the domain-domain interface hypothesis of DAHPS regulation. More importantly, we have also determined the kinetic parameters of inhibitory activity of chlorogenic acid and its minimum inhibitory concentration against *B. subtilis*.

2.2 Materials and Methods

2.2.1 Materials

*Bacillus subtilis s*train 3256 was purchased from Microbial Type Culture Collection and Gene Bank (MTCC No.1427). All nucleic acid manipulations were performed using standard procedures [152]. All enzymes (DNA polymerase, restriction enzymes, T_4 DNA ligase, *etc.*) were purchased from New England BioLabs. Qiagen kits were used for plasmid isolation, purification, and gel extraction. *Escherichia coli* DH5α cells and *E. coli* BL21 (DE3) cells were obtained from Novagene. Primer procurement and DNA sequencing was from Eurofins (India). All other chemicals and reagents were purchased from Sigma.

2.2.2 Methods

2.2.2.1 Protein expression and purification

E. coli BL21(DE3) cells with the desired plasmid (pET28c/*Bs*CM_2) were grown in kanamycin (50 μg/ml) containing LB (Luria–Bertani) medium at 37°C. When OD_{600} of the culture reached to ~0.8, cells were induced with 0.4 mM isopropyl-β-D-thiogalactoside and kept for growth at 37°C for 4h. Cells were harvested and stored at −80°C. Cell pellets were suspended in lysis buffer (buffer A) composed of 25 mM Tris buffer (pH 7.5), 200 mM NaCl and 10 mM imidiazole (pH 7.5). Cell pellets were disrupted using high-pressure cell disrupter (Constant Systems Limited, UK), with 20 kPSI pressure in the minicell for 60s, followed by centrifugation to remove cell debris (12000 rpm, 60 min, 4°C). The clarified supernatant was loaded onto a 5 ml HisTrap Ni-NTA agarose affinity column (GE Healthcare) pre-equilibrated with buffer A, and elution was performed with a linear or step gradient of 50–250 mM imidazole in buffer A. The fractions containing the desired protein, as confirmed by SDS-PAGE, were pooled and dialyzed overnight against 2 litres of 25 mM Tris buffer (pH 7.5). The protein was further concentrated up to approximately 5 mg/ml using a 3kDa cutoff Amicon Ultra-15 concentrator (Millipore, Bedford, Massachusetts, USA). The concentrated protein sample was loaded onto a HiLoad 16/60 prep grade Superdex 75 size-exclusion chromatography column (GE Healthcare), pre-equilibrated with 25 mM Tris-HCl (pH 7.5) and 50 mM NaCl, operated by UNICORN software. The absorbance of eluted protein samples was continuously monitored spectrophotometrically at 280 nm. The purity of the major chromatogram peak collected in different fractions was further analyzed with 12 % SDS-PAGE (Figure2.1). The purified protein was concentrated up to 18 mg/ml for crystallization trials.

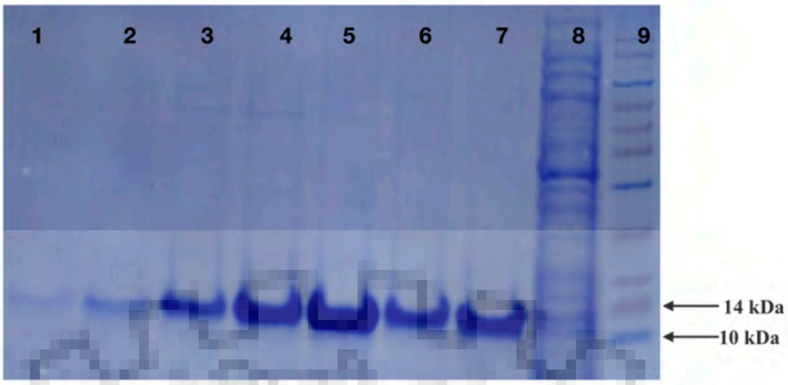

Figure 2.1 Purification of BsCM_2 enzyme.

The BsCM_2 enzyme is purified by Ni-NTA affinity based chromatography. Lane 1-5, fractions eluted by 250 mM imidiazole; Lane 6-7, fractions eluted at 100 mM imidiazole; Lane 8, Flow through; Lane 9, Protein ladder (Abcam).

2.2.2.2 Crystallization and data collection

For crystallization, a sitting drop vapor diffusion method was used in which each well was loaded with 1.0 µl of protein sample and an equal volume of the reservoir solution, equilibrated against 50 µl reservoir solutions. The initial screening for the crystallization of *Bs*CM_2 was carried out using various commercial kits from Hampton Research (Hampton Research Inc., Aliso Viejo, CA). Crystal hits were observed in conditions containing 1 M ammonium sulphate, 0.1 M potassium sodium tartrate, and 0.1 M sodium citrate pH 5.8 as the buffer at 20°C in 15 days. In order to make a complex with the substrate analogue, *Bs*CM_2 was co-crystallized with chlorogenic acid (25 mM). *Bs*CM_2 protein mixed with chlorogenic acid at a 1:1 molar ratio was incubated at 4°C for 2-4 hrs prior to crystallization.

Prior to data collection, crystals of *Bs*CM_2-chlorogenic acid (Figure 2.2A) were cryoprotected by brief soaking with well solutions containing 20% glycerol and 10% ethylene glycol, respectively. X-ray diffraction was performed at the home source, with a Bruker-Nonius Microstar H rotating-anode X-ray generator (CuK_α = 1.54 Å), at 100K temperature. Diffraction data from crystals were collected using a MAR345dtb image plate detector. Diffraction data (Figure 2.2B) were processed using the HKL2000 program[153].

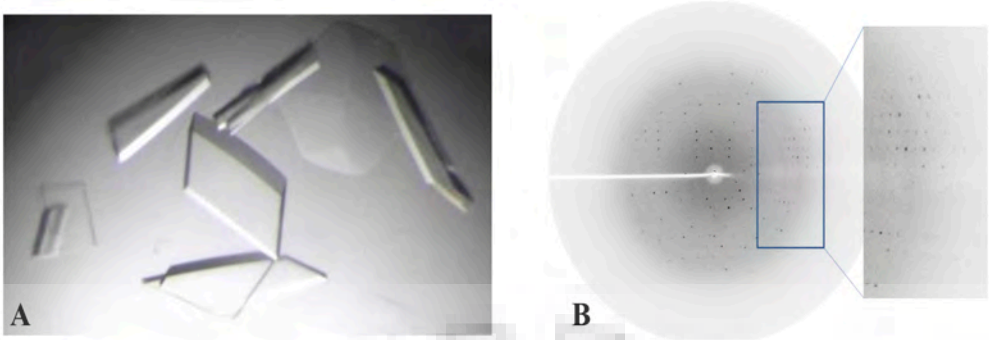

Figure 2.2. BsCM_2 crystallization and X-ray diffraction. BsCM_2 crystals in complex with chlorogenic acid (A), Diffaraction image (B).

2.2.2.3 Structure solution and refinement

Protein structures were solved and refined using PHENIX [154] and CCP4i[155] suites. MOLREP[156] was used for molecular replacement; and phenix.refine[153] and REFMAC5[157] programs were used for refinement. COOT was used for visualization of electron density maps and manual model building[158]. The *Bs*CM_2 domain shares 64% identity with N-terminal CM domain of bifunctional DAHPS from *Listeria monocytogens* (PDB ID: 3NVT). The *Lm*CM domain structure (modified 3NVT containing only residues 25-108) was used as template for initial phase determination using molecular replacement. The *Bs*CM_2-chlorogenic acid complex (*Bs*CM_2-CGA) structure was refined up to R_{work} and R_{free} values of 17.73 % and 21.52 %, respectively. Data collection, structure refinement, and validation statistics of BsCM_2-CGA is shown in Table 2.1. For structural validation, stereochemical properties of crystal structures were accessed through MolProbity[159]. PISA (Protein Interfaces, Surfaces and Assemblies) tool was used for dimer interface interactions analysis[160]. The PyMOL visualization tool was used for structural analysis and figure preparation [Schrödinger, LLC][161].

Table 2.1 Summary of data collection, structure refinement, and validation statistics.

	*Bs*CM_2-CGA
PDB ID	5GMU
Crystallographic data	
Space group	$P2_1$
Resolution	1.80
Cell dimensions	
a, b, c (Å)	35.7, 47.0, 56.8
α, β, γ (°)	90, 107.2, 90
Unique reflections (Last shell)	16372 (716)
Completeness (%) (Last shell)	98 (88)
R_{meas}[a]	0.07
R_{pim}[b]	0.04
I/σ (Last shell)	37.2 (3.76)
Multiplicity (Last shell)	3.4 (2.7)
Refinement	
No. of Residues	171
Water molecules	116
Resolution range (Å)	50.00-1.80 (1.83-1.80)
R_{work} (%)	17.73
R_{free} (%)	21.52
RMSD on bond lengths (Å)	0.016
RMSD on bond angles (Å)	1.769
Average *B*-factors (Å^2)	
ChainA	20.64
ChainB	19.32
Water atoms	40.91
Ramachandran plot (%)	
Favored	100
Outliers	0

*Statistics for the highest-resolution shell are shown in parentheses.

$^{a}R_{meas} = \sum_{hkl}\{N/(N\text{-}1)\}^{½}\sum_{i} |I_{i,hkl} - <I_{hkl}>| / \sum_{hkl}\sum_{i} |I_{i,hkl}|$

$^{b}R_{pim} = \sum_{hkl}[1/\{N_{hkl} - 1\}]^{½}\sum_{i} |I_{i,hkl} - <I_{hkl}>| / \sum_{hkl}\sum_{i} |I_{i,hkl}|$

2.2.2.4 Molecular dynamics based simulation

To study the backbone flexibility and the side chain orientation of the loop connecting helices H1-H2, the *Bs*_CM2-CGA protein structure in the chlorogenic acid bound form was simulated using Discovery Studio (Accelrys Inc., San Diago, CA, USA) suite's simulation protocol. Before the simulation, the protein structure was prepared by adding hydrogen atoms and was typed with CHARMm forcefield[162]. Typed protein was solvated with the explicit periodic boundary solvation model in an orthorhombic cell whose edges had minimum 7Å distance from protein surface. Sodium (Na^{+}) and chloride ions (Cl^{-}) were also added to the system as counter ions for neutralizing the system. Solvated protein was subjected to the molecular dynamics simulation using Standard Dynamics Cascade protocol. The protocol consists of two minimization steps along with heating, equilibrium, and production steps. Minimazation1 and minimization2 steps were performed using the steepest descent algorithm for 1000 cycles and Powell algorithm for 2000 cycles, respectively. The system was heated for 120ps from 50K to 300K temperature. Subsequently, the system was equilibrated for 100ps at 300K temperature under constant pressure conditions. Finally, 5ns production step was performed on isobaric-isothermal ensemble (NPT) at 300K temperature. The results were saved at every 5ps time interval. For the entire simulation, 2fs time step was used. The Particle Mesh Ewald (PME) method was used for handling electrostatic interactions with non-bond list radius of 14Å. SHAKE constraints were used for constraining hydrogen atoms involving bonds.

2.2.2.5 Molecular docking

To assess the plausible interactions of chlorogenic acid with the active site of monofunctional *B. subtilis* AroH class of chorismate mutase (*Bs*AroH), molecular docking was performed using AutoDock4[163]. The crystal structure of *Bs*AroH (PDB ID: 2CHT) was used for the same[164]. For docking, protein and ligand were prepared using AutoDock Tools-1.5.6. A grid centered at (51.787, 25.245, 45.348) with dimensions 40X40X40 ($Å^{3}$) and 0.375 Å spacing was used for map calculations.

Lamarchian Genetic Algorithm was used for docking. AutoGrid4 and AutoDock4 programs were executed for calculating energy maps and docking of ligands, respectively. Analysis of docking conformations was performed by converting docking conformations into *Pdbqt* files and visualizing in PyMol.

2.2.2.6 BsCM_2 activity assay

Chorismate mutase activity was measured by using the fixed-point assay, with minor modifications. The standard assay was carried out in assay buffer (50 mM Tris–HCl, pH7.5) supplemented with 2 mM chorismic acid in a final volume of 200 µl. The mixture was then incubated with shaking at 37°C for 5 min, and enzyme was further added to initiate the reaction. The reaction was terminated by the addition of 0.2 ml of 1 M HCl. The reaction mixture was left over at 37°C for 15 min, and finally terminated by the addition of 0.5 ml of 1M NaOH. The absorbance of samples were recorded at 320 nm using Agilent Carry 300 UV/Vis Spectrophotometer, to monitor the formation of phenylpyruvate. For calculations, 17500 $M^{-1}cm^{-1}$ was used as the extinction coefficient at 320 nm (ε320nm) for phenylpyruvate[165]. Blank readings were taken without the addition of enzyme to account non-enzymatic conversion of the chorismate to the prephenate.

2.2.2.7 Isothermal titration calorimetry based binding studies

ITC experiments were performed on MicroCal ITC 200 unit (GE Healthcare) operating at 298K temperature. The binding of a *Bs*CM_2 protein with its natural substrate chorismic acid, and substrate analogue chlorogenic acid were studied. Protein sample was dialyzed against Buffer I (25 mM Tris HCl, pH 7.5) and concentrated up to 8 mg/ml concentration (750µM). All solutions were degassed before use. The reference cell was filled with buffer I. The Titration reactions were performed using *Bs*CM_2 protein in ITC sample cell and ligands (Chorismate: 7.5 mM, Citrate: 10 mM and Chlorogenic acid: 2.5 mM) in a syringe with 200 rpm stirring speed and initial delay of 60s. A total of 15-20 injections were made with first one of 0.5µl and the rest of 2.0 µl each. The first injection was treated as scouting injection to calibrate the ITC200 instrument. The time interval between each injection was 150 s, and the reference cell power was set to 8 µW. ITC data were analyzed using single binding site model using Origin 7.0 software.

2.2.2.8 Minimum inhibitory concentration (MIC)

An MIC test for the chlorogenic acid on *B. subtilis* was performed using the broth micro dilution method on a 96 well microtiter plate[166]. A concentration gradient (10 µg/ml – 200 µg/ml) of chlorogenic acid was tested. A single colony of *B. subtilis* strain 3256 was used to inoculate the nutrient broth medium. Correlation between OD_{600} and microbial number was determined using serial dilution. The OD_{600} of overnight grown culture was adjusted to 1 by dilution with PBS (1x) buffer. The culture was then serially diluted from 10^{-1} to 10^{-7} and 100 µl from the last four dilutions (10^{-4} to 10^{-7}) were plated on nutrient agar plates followed by overnight incubation at 37°C. Colonies were counted and colony-forming-units (cfu) per ml of culture were calculated for each dilution. Correlation between OD_{600} and cfu per ml was then calculated. Bacterial suspensions having 1×10^{8} cfu per ml were used to inoculate 96 well microtiter plates. Chlorogenic acid was dissolved in PBS buffer (1x). 100 µl of broth solution was added to all wells. 50 µl of inhibitor solution was used in each well, except growth control (broth and inoculum) and sterility control (broth only) wells. 50 µl of bacterial suspension adjusted to 1×10^{6} cfu per ml was used, giving 5×10^{5} cfu per ml in the final inoculum. Microtiter plates were then incubated at 37°C for 16-20 h.

2.3 Results

2.3.1 Overall structure of BsCM_2

*Bs*CM_2 crystals complexed with substrate analogue chlorogenic acid (*Bs*CM_2-CGA) diffracted up to 1.8 Å resolutions. *Bs*CM_2-CGA structure contains two monomers per asymmetric unit. The *Bs*CM_2 protein has an all-helix entirely helical tertiary structure. "In the *Bs*CM_2-CGA structure, the electron density of first N-terminal residue was missing from both the chains. Additionally, residues 2,3 and 40 could not be modeled due to the absence of any interpretable electron density in chain A.

In *Bs*CM_2–CGA, the monomeric structure contains a ‘Chorismate Mutase, type II fold’, a three-helix bundle connected through the loops. In chain B, three helices H1, H2, and H3 are composed of residues 5-40, 48-60 and 68-87, respectively. Helix H2 is connected to the helices H1 and H3 by 7 residues long loops L1 and L2, respectively.

In chain A, helices H1', H2' and H3' are connected by loops L1' and L2' (Figure 2.3). The two chains are structurally very similar to each other, except for the L1 and L1' regions, with a root mean square deviation (RMSD) of 0.188. The BsCM_2-CGA structure has several residues in alternate conformations. His73 exists as alternative conformation in both the chains. In chain A, a sulphate ion, contributed by the crystallization buffer, coordinates with ND1 atoms in both conformations. The sulphate ion's O3 atom interacts with the backbone carbonyl oxygen of His73 and the OE2 side chain atom of Glu77. The O1 atom of sulphate interacts with the NZ atom of Lys76. Altogether, these results indicate that backbone of these residues is rigid and alternative conformation of protein residues allow them to interact with the solvent and the surrounding environment.

2.3.2 Dimeric structure

In *Bs*CM_2–CGA, two molecules are present in an asymmetric unit, which form a helical dimeric structure (Figure 2.3). Previously, few structures of CM_2 dimers from *E.* coli[144] and *L. monocytogens*[131] have been reported. Those structures are stabilized by cross-helical interactions between two subunits. The dimer interface and assembly analysis performed using PISA server[167] revealed that almost one third (~2260 Å^2) of each monomer's surface area was buried during dimer formation. Dimer assembly has a free energy of assembly dissociation (ΔG^{diss}) value of 31.7 kcal/mol, which suggests that the assembly is stable. The solvation free energy gain (ΔG^{int}) of the dimer is -37.7 kcal/mol. The negative ΔG^{int} value corresponds to hydrophobic interfaces. The interface interactions are dominated by hydrophobic interactions between monomers. In *Bs*CM_2, residues Leu6, Leu9, Leu16, Ile20, Leu23 and Val30 corresponding to Leu7, Leu10, Leu17, Leu21, Leu24 and Leu31 of *Ec*CM, respectively, participate in these hydrophobic interactions. In previously reported CM_2 dimer structures, helices from both the monomers arrange themselves in an antiparallel manner[131,144].

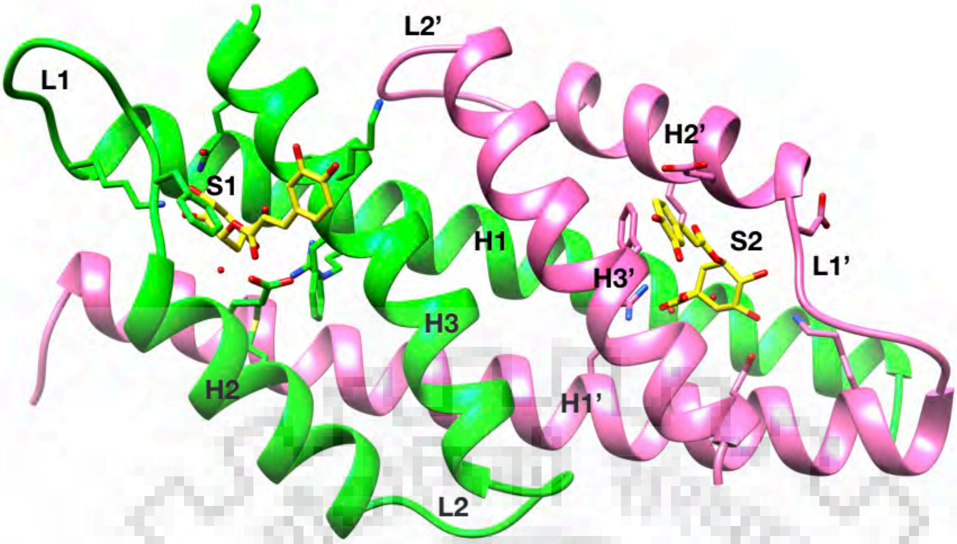

Figure 2.3 Ribbon diagram of BsCM_2 complexd with chlorogenic acid. The dimeric structure of BsCM_2 complexed with chlorogenic acid. Chain A and Chain B shown in Hot Pink and Green color respectively. CGA molecules have been shown in yellow color.

Similarly in *Bs*CM_2, antiparallel H1-H1 ‘and H3-H3’ helix pairs form the dimeric interface. These interfaces are stabilized by inter-subunit interactions involving hydrogen bonding, salt bridge formation, and hydrophobic interactions. Residues Arg10, Ala13, Asn17, Arg27, Arg50 and Thr70 from chain A form hydrogen bonds with residues Arg10, Asn17, Arg27, Arg50, Met54 and Glu84 of chain B. Residues Asp14 and Arg50 from both the subunits are involved in salt bridge formation.

2.3.3 Active site and its interaction with inhibitor

In the *Bs*CM_2-CGA structure, two active sites- S1 and S2 are located at the interface of two monomers, as shown in Figure 2.3. Residues from both the monomers contribute in each active site formations. Residues from helices H1, H2, H3, H1' and loop L1 form the S1 active site, while the S2 active site is formed by residues from the H1', H2', H3', H1 helices and the L1' loop. The active site contains charged/polar residues, which are highly conserved among all known chorismate mutases. Some hydrophobic residues, proposed to be essential for substrate binding and catalysis, are also present at the active site, but are not conserved. At active site S1, charged/polar residues Arg27, Lys38, Asp47, Arg50, Glu51, and Gln86 from chain B and Arg10 from chain A provide the electrostatic environment for the incoming ligand (substrate/inhibitor). The hydrophobic residues Ile34, Met54, Phe79, Gly82, and Leu83 are also part of the active sites (Figure 2.4A).

Chlorogenic acid, a structural analogue of the enzyme's substrate, was co-crystallized with the *Bs*CM_2 protein. Unambiguous electron density of this ligand was observed at both the active sites of the dimer. The ligand interacts with key active site residues through direct or water bridge-mediated hydrogen bonding. As shown in Figure 2.4B, at the active site, chlorogenic acid makes hydrogen bonds with the side chain of Arg27, Lys38, Gln86, and the main chain atoms of Arg45, Asp47, and Phe79 of chain B. The ligand molecule also interacts with Lys38, Arg50, and Lys80 of chain B, and Arg10 of chain A through water bridge formation. However, at another active site, along with the above interactions, the ligand forms a direct hydrogen bond with Lys80 and an additional water bridge-mediated hydrogen bond with Gln86 of chain A.

Previously, our research group has crystallized *Bs*CM_2 in native form where citrate molecules from crystallization solutions were found to interact with the active site of this enzyme. Figure 2.4C shows the interaction of *Bs*CM_2 with citrate molecules. The citrate molecule interacts with the residues Arg27, Lys38, Asp47 and Gln86 of chain A and Arg10 of adjacent chain B through hydrogen bonding (Figure 2.4C). The citrate molecule also makes additional interactions with the residues Arg27, Arg50 and Phe79 via water bridge formation. It has been previously reported that the citrate inhibits the 90-*Mt*CM protein [168].

2.3.4 Comparison with monofunctional *B. subtilis* AroH class of chorismate mutase

Monofunctional *B.subtilis* chorismate mutase (*Bs*AroH) exits as a trimer and forms a pseudo-αβ-barrel core structure via contributions of β -sheets from each monomer. A functional trimer has three active sites formed at the interface of two monomers. However, *Bs*CM_2 forms an entirely helical dimeric structure with two active site clefts are formed by the residue contributions from both monomers, as previously described.

The *Bs*AroH active site contains charged residues Arg7, Arg90, Arg116, Arg63' and polar residues Glu78, Tyr108, Lys60', Thr74', and Cys75' (prime (') represents the residue from an adjacent chain). Residues Phe57', Ala59' and Leu115 are also part of the active site[164]. The *Bs*CM_2 active site consists of similar residues.

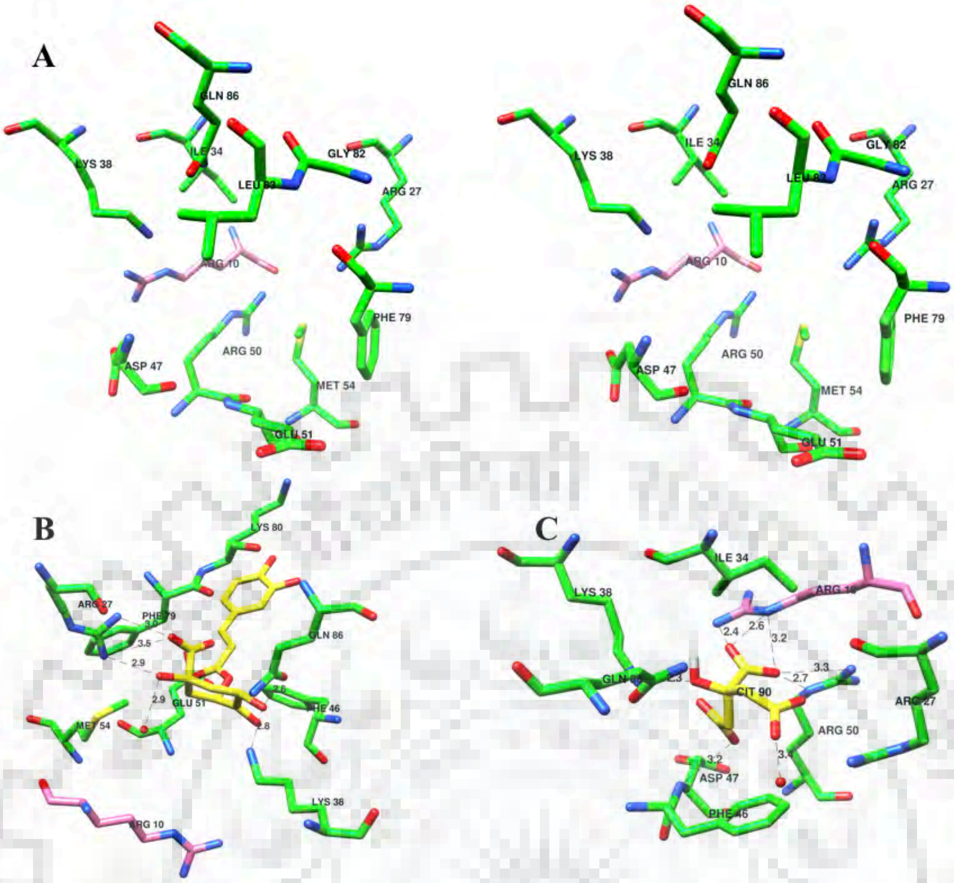
A
GLN 86
LYS 38
ILE 34
GLY 82
LEU 83
ARG 27
ARG 10
PHE 79
ARG 50
ASP 47
MET 54
GLU 51
B
LYS 80
ARG 27
PHE 79
3.5
2.9
2.9
GLU 51
2.6
GLN 86
PHE 46
MET 54
2.8
LYS 38
ARG 10
C
ILE 34
LYS 38
ARG 10
2.4
2.6
3.2
3.3
GLN 86
2.3
CIT 90
2.7
ARG 27
ARG 50
3.4
3.2
ASP 47
PHE 46

Figure 2.4 Active site architechture (A) and interaction of BsCm_2 with chlorogenic acid (B) and citrate (C). (A) Stereo images of the active site. Residues contributing from both the chains of physiological dimer form the active site. The polar residues at the active site are highly conserved in all CM_2 or CM-like domains. However, hydrophobic acid residues are not conserved. (B) Shows the interaction of chlorogenic acid with the active site residues in *Bs*CM_2-CGA structure. (C) Shows the interaction of citrate with the active site residues in the *Bs*CM_2-CIT structure. Residues from different chains are colored accordingly.

Polar residues Arg10', Arg27, Lys38, Asp47, Arg50, Glu51, and Gln86 form the active site along with hydrophobic residues Ile34, Met54, Phe79, and Gly82. The similarity of these active site residues and their chemical nature may allow the binding of similar small molecules to these enzymes.

2.3.5 Comparison of BsCM_2-CGA with EcCM (catalytically active CM type 2)

In *E. coli*, the N-terminal region of bifunctional P-protein (*Ec*CM) contains a functional ‘cChorismate mMutase II fold’[144]. Although, *Bs*CM_2 shares only 37% sequence identity with *Ec*CM, but they have a similar tertiary structure with an RMSD value of 0.815. Both the proteins’ active sites are formed by the residue contribution from both the monomers. *Bs*CM_2 contains charged residues Arg27, Lys38, Asp47, Arg50, Glu51, and Gln86 from one monomer and Arg10 from the other monomer corresponding to Arg28, Lys39, Asp48, Arg51, Glu52, and Gln88 from one monomer and Arg11 from the other monomer of *Ec*CM. Hydrophobic residues Ile34 (Val35), Met54 (Leu55), Phe79 (Ile81), and Leu83 (Val85) are also present at the active site (residues mentioned in parentheses are corresponding hydrophobic residues present in *Ec*CM). These hydrophobic residues are not conserved between these two proteins. The Ser84 residue of *Ec*CM is also mutated to Gly82 in *Bs*CM_2. In *Ec*CM, residues Ser15, Asp18, Arg47, Asp48, and Gln88 are key residues playing that play a supporting role in inhibitor binding. But in *Bs*CM_2, the corresponding residues are Asp14, Asn17, Phe46, Asp47, and Gln86. Variation in these residues may be a contributing factor towards the reduced catalytic activity of *Bs*CM_2. Previous studies of *Ec*CM have shown that mutation of residues A32, V35, I81, and V85 decreases the catalytic activity of the protein [103].

These residues may be important for substrate binding or catalytic activity of the protein. In *Bs*CM_2, the corresponding residues were different, which may result in poor substrate binding/catalysis.

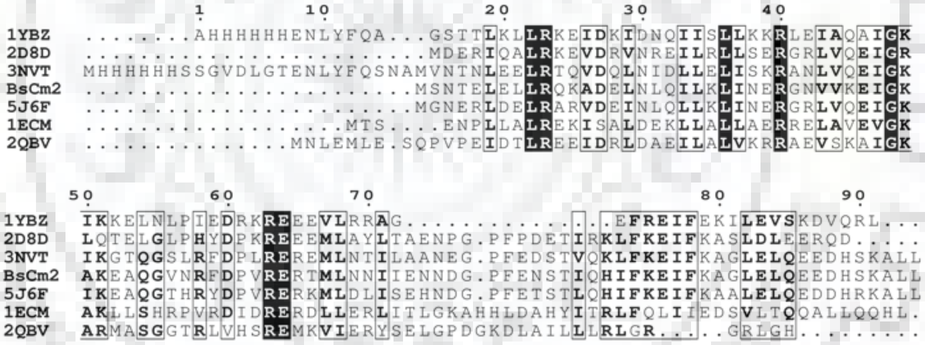
1
10
20
30
40
1YBZ ........AHHHHHHENLYFQA...GSTTLKLLRKEIDKIDNQIISLLKKRLEIAQAIGK
2D8D .........................MDERIQALRKEVDRVNREILRLLSERGRLVQEIGR
3NVT MHHHHHHSSGVDLGTENLYFQSNAMVNTNLEELRTQVDQLNIDLLELISKRANLVQEIGK
BsCm2 ........................MSNTELELLRQKADELNLQILKLINERGNVVKEIGK
5J6F ........................MGNERLDELRARVDEINLQLLKLINERGRLVQEIGK
1ECM ....MTS....ENPLLALREKISALDEKLLALLAERRELAVEVGK
2QBV ....MNLEMLE.SQPVPEIDTLREEIDRLDAEILALVKRRAEVSKAIGK
50
60
70
80
90
1YBZ IKKELNLPIEDRKREEEVLRRAG..............EFREIFEKILEVSKDVQRL...
2D8D LQTELGLPHYDPKREEEMLAYLTAENPG.PFPDETIRKLFKEIFKASLDLEERQD.....
3NVT IKGTQGSLRFDPLREREMLNTILAANEG.PFEDSTVQKLFKEIFKAGLELQEEDHSKALL
BsCm2 AKEAQGVNRFDPVRERTMLNNIIENNDG.PFENSTIQHIFKEIFKAGLELQEEDHSKALL
5J6F IKEAQGTHRYDPVRERKMLDLISEHNDG.PFETSTLQHIFKEIFKAALELQEDDHRKALL
1ECM AKLLSHRPVRDIDRERDLLERLITLGKAHHLDAHYITRLFQLIIEDSVLTQQALLQQHL.
2QBV ARMASGGTRLVHSREMKVIERYSELGPDGKDLAILLLRLGR.....GRLGH.........

Figure 2.5 Multiple sequence aligment of BsCM_2 with related homologs.

Multiple sequence alignment of *Bs*CM_2 with *Ec*CM (1ECM), *Lm*CM (3NVT), 90- *Mt*CM (2QBV), *Tt*CM (2D8D), *Gsp*CM (5J6F) and *Pyrococcus furiosus* hypothetical protein (1YBZ).

2.3.6 Comparison of BsCM_2-CGA with LmCM (regulatory CM type 2)

Overall, the folds of *Bs*CM_2 and *Lm*CM are similar with an RMSD of 0.816. In the *Lm*CM domain structure, residues 40-44 of chain A and residues 33-52 of chain B (corresponding to connecting loop L1 of helices H1-H2) were missing, which indicates the structural flexibility of the loop regions. In *Bs*CM_2-CGA, clear density for loop L1 was observed, however, residue 40 was missing from loop L1'. The binding of the substrate analogue may be responsible for stabilizing the loop. Chain A of the *Lm*CM domain was used for further structural analysis. The comparison of the loop region of *Lm*CM with chain A of *Bs*CM_2 showed a small shift in C_α atom positions of residues Arg45 (1.0 Å) and Phe46 (0.8 Å), but side chain orientations of these residues were significantly changed. However, chain B of *Bs*CM_2 showed a relatively large shift in both side chain orientations and C_α atom positions of residues Arg45 (2.1Å) and Phe46 (1.2Å) (values represent C_α position shift) in comparison to the corresponding residues of *Lm*CM. It is evident that such a significant shift in the backbone atoms, along with huge variation in side chain orientations in residues of L1 loop, confers plasticity to the enzyme's active site to accommodate different incoming ligands. The active site residues of both the proteins were similar. As *Lm*CM has been shown to possess a more regulatory role than a catalytic role [90], the similarities in structure and active site architecture suggest that *Bs*CM_2 may also have a regulatory function in the bifunctional DAHPS enzyme. Previous studies have also reported that *Bs*CM_2 may have a regulatory function [96,106].

2.3.7 Comparison of BsCM_2 with CM domain of GspDAH7PS

*Bs*CM_2 shares high sequence identity (71%) over 90 amino acids with the CM domain of *Gsp*DAH7PS. Structurally, *Bs*CM_2-CGA aligns very well with N-terminal 95 residues corresponding to CM domain of *Gsp*DAH7PS with RMSD value of 0.556 Å (5J6F)[145]. The residues demarcating the active site of both structures are highly similar with comparable side chain orientations. In both the structures, ligand (chlorogenic acid in *Bs*CM_2-CGA and prephenate in *Gsp*DAH7PS) occupies the active site with similar network of interactions. Comparison of inter-helical loop regions L1 and L2 of *Bs*CM_2-CGA with *Gsp*DAH7PS showed minimal deviation in their relative orientation with similarly extended helix H1. These observations reinforce that binding of ligand induces the conformational changes with significant rearrangement of secondary structure in *Bs*CM_2. Overall, the structure of *Bs*CM_2-CGA resembles the closed conformation observed in prephenate bound *Gsp*DAH7PS structure.

Interestingly, the structural comparison of chain A of *Bs*CM_2-CIT with CM domain of *Gsp*DAH7PS showed relatively less structural similarity with RMSD value of 0.794 Å (5J6F). The structural variations are primarily confined to inter-helical loop L1 that adopted a less compact extended conformation with shortening of helix H1. This leads to straightening of helix H2 and overall structure resembles the open form of enzyme. Together, these observations clearly indicate that binding of ligand to CM domain induces the significant conformational changes in active site loop L1.

2.3.8 Molecular dynamics simulation

As described earlier, chorismate mutase type 2 proteins have an intrinsically disordered loop region, which contributes to active site formation and may be involved in wider substrate specificity and/or regulation. Structural analysis of *Bs*CM_2 revealed a significant shift in the backbone position of L1 and L1' loop residues, as well as changes in the side chain orientation. To assess the extent of loop movement and side chain flexibility, molecular dynamics (MD) simulation studies of *Bs*CM_2 protein were performed. Discovery Studio suite’s Standard Dynamics Cascade tool was used for the simulation studies using CHARMm forcefield. For solvation, 4327 water molecules were added, along with 21 Na^+ and 11 Cl^- ions to neutralize the system. Conformations generated in a 5ns production step of simulation were used for analysis. Root mean square deviation (RMSD) of the chlorogenic acid bound *Bs*CM_2 conformations generated during production step of simulation has been found to be fluctuating around an average of 1.9 Å within a narrow range (Figure $2.6A_1$). Backbone shift was analyzed by calculation of the root mean square fluctuation (RMSF) for individual residues. A plot of RMSF values for each residue of both the chains is shown in Figure $2.6A_2$. Higher RMSF values correspond to higher flexibility of residues. For terminal residues, higher RMSF values were expected because of increased degree of freedom for these residues. From Figure $2.6A_2$, it is evident that there is a sudden increase in RMSF values of intrinsically disordered loop residues (Gln41 to Val49). The chlorogenic acid bound at the active site S1 shows a slight deviation in its position. At active site S2, chlorogenic acid maintains its position during the initial 1ns. In 1ns-2ns time intervals, the caffeic acid moiety shifts towards the loop L1' and remains intact in the same conformation for the rest of the simulation. This change in the chlorogenic acid conformation may contribute to the shift in the loop L1' backbone.

In chain A, loop L1' region residues show significant backbone deviation and side chain orientation change (Figure 2.6B). Residues Asn44, Arg45, Phe46 and Asp47 show variations during simulation. During 1ns-2ns intervals, Asn44 undergoes a large shift in backbone position and also orients its side chain parallel to the active site.

Residue Arg45 and Phe46 main chains undergo large shifts away from the active site and also cause significant changes in side chain orientations (Figure 2.6D-E). The amino acid Asp47 orients its side chain towards the active site during simulation. Unlike chain A, chain B's loop L1 region shows only slight deviation in backbone position (Figure 2.6C).

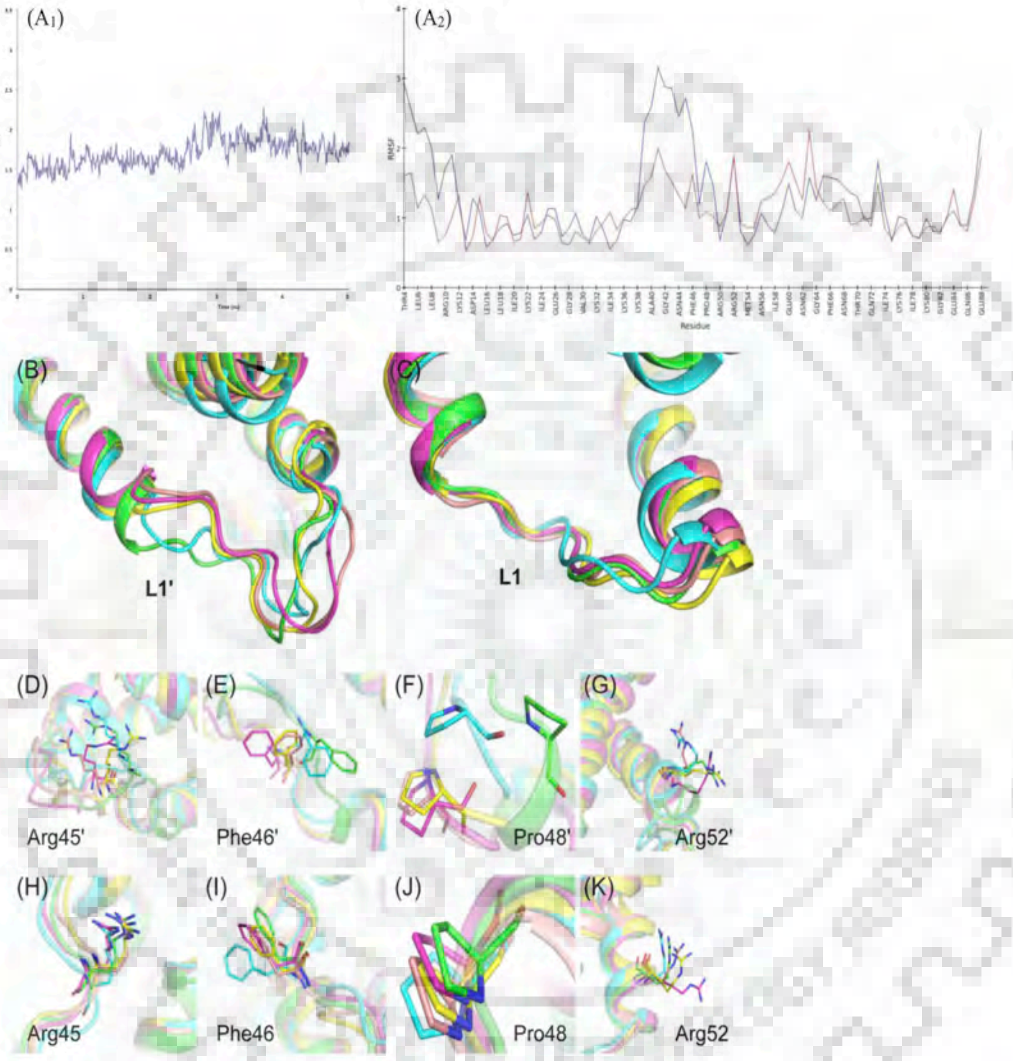

Figure 2.6 Molecular dynamics simulation results of *Bs*CM_2-CGA. (A_1) RMSD of the backbone atoms with respect to initial structure of the chlorogenic acid bound *Bs*CM_2 structure over 5-ns simulations. (A_2) Plot of RMSF values against individual residues for the conformation generated in production steps with respect to crystal structure. During a simulation backbone shift in loop L1 (B) and L1′ (C) regions were observed. In chain A, large changes were observed in side chain orientations of Arg45′ (D), Phe46′ (E), Pro48′ (F), and Arg52′ (G). However, relatively small changes were observed in chain B (H–K). Color code: Green (crystal structure), Cyan (after 1 ns), magenta (after 2 ns), yellow (after 3 ns) and brown (after 4 ns).

Arg45 and Phe46 undergo little deviation in side chain orientation, but obtain the initial orientation towards the end of the simulation (Figure 2.6H-I). For residue Asp47, main chain fluctuations were observed, but side chain orientation remained intact.

In the crystal structure, Pro48 was positioned in the first turn of helix H2'. During the simulation, helix H2' undergoes local uncoiling at the first turn (Figure 2.6B). Due to uncoiling, Pro48 and Val49 shift their backbone position away from the protein. Large deviations were observed during the initial 2ns of production step, after which Pro48 maintains a fixed position during the rest of the simulation (Figure 2.6F). Towards the end of the simulation, helix H2' continues to uncoil and increases the size of loop L1' extended to residue Glu51.

Residue Arg52 of both the chains shows a significant change in side chain orientations during the simulation (Figure 2.6G and 2.6K). In chain A, Lys76 shows the deviation in side chain orientation during 1ns-2ns time intervals, but in chain B, the corresponding residue had no significant change in orientation. *Bs*CM_2 residues Phe46, Val49, Arg52, and Lys76, corresponding to residues Phe46, Leu49, Arg52 and Lys76 of *Lm*CM, show backbone or side chain flexibility. These residues may be involved in domain-domain interface formation between the catalytic and regulatory domains of bifunctional DAHPS.

2.3.9 Chlorogenic acid's interaction with monofunctional CM (BsAroH)

To assess the plausible interaction of chlorogenic acid with the monofunctional AroH class of CM, the molecule was docked at the active site of *Bs*AroH (PDB ID: 2CHT). Similar to *Bs*CM_2, in *Bs*AroH, the chlorogenic acid's position is shifted from the transition state analogue (TSA) position. The chlorogenic acid interacts with residues Arg63, Val73, Thr74 from one chain and Arg7, Arg90, Val114, Leu115, and Arg116 from the adjacent chain (Figure 2.7A). The similarity of chlorogenic acid's interaction with both monofunctional *Bs*AroH and *Bs*CM_2 may result in similar binding to both proteins.

2.3.10 BsCM_2 enzyme assay and activity

The kinetic parameters (K_m and k_{cat}) for *Bs*CM_2 have been calculated and compared with monofunctional *Bs*AroH and chorismate mutase from other reported organisms. The catalytic turnover number, i.e. k_{cat}, was determined to 0.78 ± 0.02 S^{-1} for

*Bs*CM_2. K_m was calculated and found to be 1514 ± 175 µM. A plot of Michaelis-Menton kinetics is shown in Figure 2.7B. Both k_{cat} and K_m of *Bs*CM_2 are compared with monofunctional *Bs*AroH. k_{cat} and K_m values for *Bs*AroH are 46.0 S^{-1} and 67.0 µM, respectively[164]. As expected, the kinetic parameters clearly suggest that *Bs*CM_2 has much lesser activity than *Bs*AroH.

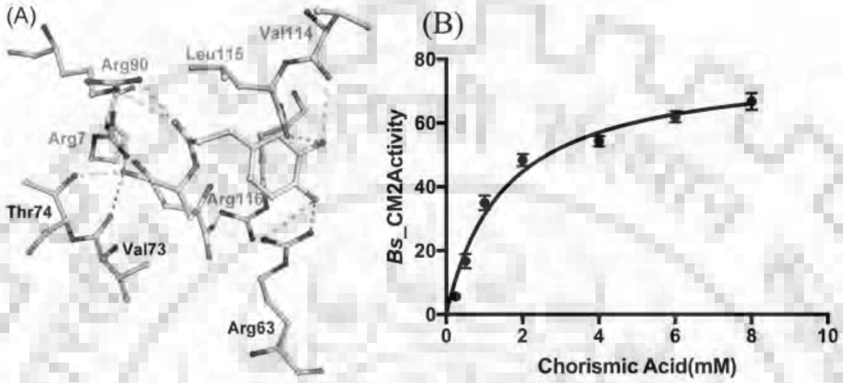

Figure 2.7 Molecular docking and biochemical characterization of BsCM_2.
(A) Interaction of CGA with BsAroH enzyme (B) Michaelis–Menten kinetic curve of BsCM_2. BsCM_2 is found to be active with K_m of 1514 ± 175 µM.

Table (2.2) Comparison of kinetic parameters of BsCM_2 with other reported CMs

Enzyme	**k_{cat} (S^{-1})**	**K_m (µM)**
BsCM_2	0.78	1514
EcCM	72	296
BsCM	47	67
MtCM	27	112

The CM activity of *Bs*CM_2 follows Michaelis–Menten kinetics, with a catalytic efficiency (k_{cat}/K_m) of 0.5×10^3 M^{-1}S^{-1}. This catalytic efficiency is three orders of magnitude lower than expected for wild-type CMs[58]. The enzyme activity of *Bs*CM_2 was also assessed in the presence of the substrate analogue, chlorogenic acid. There is a 60% reduction in activity of *Bs*CM_2 after the addition of 1.0 mM chlorogenic acid. Higher concentrations of chlorogenic acid (>4.0 mM) resulted in complete loss of *Bs*CM_2 activity. The kinetic inhibition constant (K_i) for chlorogenic acid was 0.33 ± 0.07 mM. A plot of inhibition of *Bs*CM_2 activity by chlorogenic acid has been shown in Figure 2.8A. Mode of inhibition was analyzed by plotting a double reciprocal plot shown in Figure 2.8B. From the plot it has been found that chlorogenic acid is a competitive inhibitor of BsCM_2.

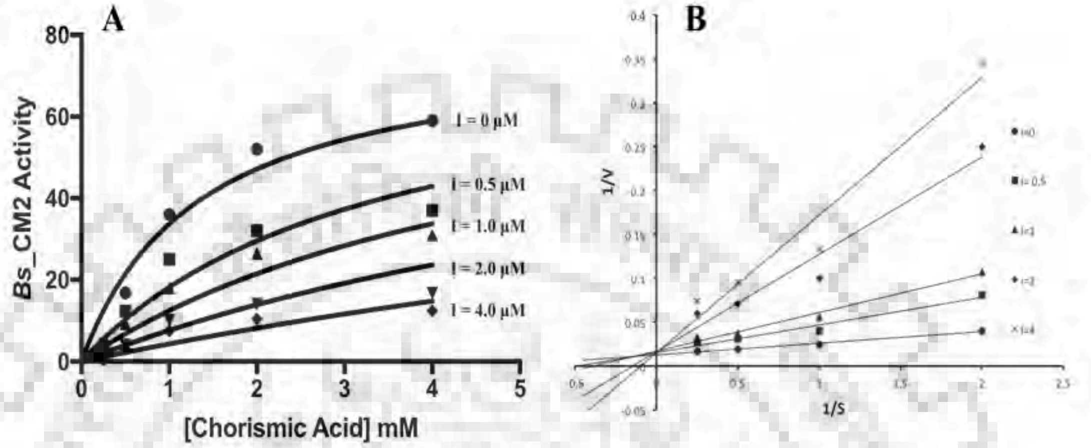

Figure 2.8 Kinetic inhibition of BsCM_2 with chlorogenic acid.

Steady state inhibition curve of BsCM_2 (A), double reciprocal plot of inhibition of BsCM_2 (B). Lines intersecting at 1/V axis clearly indicated the competitive inhibition of BsCM_2 by chlorogenic acid.

2.3.11 Isothermal titration calorimetry (ITC)

Binding of *Bs*CM_2 protein with its natural substrate chorismate was performed using ITC. Additionally, binding of *Bs*CM_2 protein with citrate and chlorogenic acid was also assessed. Thermodynamic parameters – enthalpy change (ΔH), entropy change (ΔS), Gibbs free energy change (ΔG), and equilibrium dissociation constant (K_D) have been determined. Table 2.3 shows the thermodynamic parameters of binding of ligands.

Table 2.3 Binding parameters of *Bs*CM_2 with chorismate, citrate, and chlorogenic acid using ITC.

Compound	**Enthlapy change (Joules/mol)**	**Entropy change (Joules/mol/K)**	**Free energy (Joules/mol)**	**Dissociation constant, K_D (µM)**
Chorismate	-1.397×10^5	-408	-1.8×10^3	725
Citrate	-4.291×10^4	-82.2	-18.4×10^3	602
Chlorogenic acid	-1.504×10^5	-441	-18.9×10^3	480

Reactions of these ligands with *Bs*CM_2 are spontaneous in nature as evident by negative ΔG values. Binding of these three compounds with *Bs*CM_2 is driven by enthalpy change (ΔH), which indicates that polar interactions are involved during binding. Reactions of these ligands are exothermic in nature as confirmed by the downward trend in ITC profile. The equilibrium dissociation constant for chorismate, citrate, and chlorogenic acid was calculated as 725 μM, 600 μM and 480 μM, respectively. The K_D values showed better affinity of chlorogenic acid for *Bs*CM_2 than citrate and chorismate. Figure 2.9 shows the thermogram and the fitting curve of chorismate, citrate and chlorogenic acid.

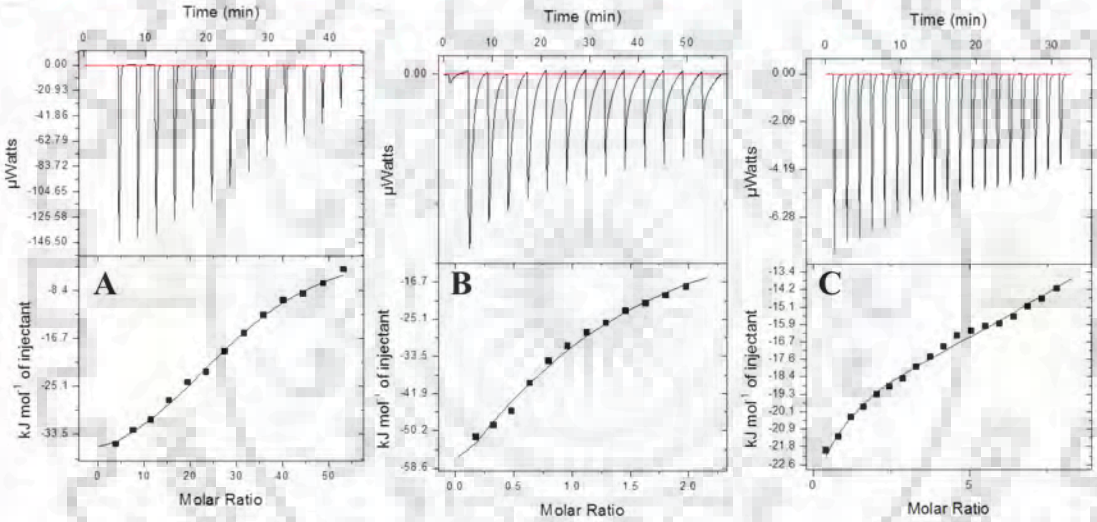

Figure 2.9 ITC titration data describing the binding of chorismate (A), citrate (B) and chlorogenic acid (C) to *Bs*CM_2. Data is fitted using single binding site model to evaluate dissociation constant (K_D). Upper part of each panel shows the thermogram (thermal power Vs time) after baseline correction, while lower part of each panel is binding isotherm (normalized heat Vs molar ratio of reactants).

2.3.12 Minimum inhibitory concentration (MIC)

The MIC test for chlorogenic acid was performed with *B. subtilis* strain 3256 using the microdilution method. The MIC value of chlorogenic acid was calculated and found to be the range of 30 ± 5 μg/ml. The moderately high MIC value may be attributed to the low affinity of chlorogenic acid for BsCM_2. It has been reported that chlorogenic acid can inhibit bacterial growth or kill bacterial cells, but the exact mechanism of its inhibitory effect is largely elusive. It has been reported that binding of either the substrate chorismic acid or the product prephenate to the regulatory domain of DAHP synthase of *B. subtilis* regulates the activity of DAHP synthase[148,149]. As described earlier, the ITC data reveals better binding of chlorogenic acid with *Bs*CM_2 in comparison to chorismic acid, it is possible that chlorogenic acid can inhibit the DAHP synthase enzyme by binding to its regulatory domain, which will further lead to inhibition of the shikimate pathway.

2.4 Discussion

During the course of evolution, nature has developed several mechanisms to regulate metabolic pathways. The molecular mechanisms involved in allosteric regulation of enzyme catalysis have been studied increasingly as more structural information on proteins become apparent. Different classes of DAHP synthases are regulated by different regulation mechanisms [84-89]. In *B. subtilis*, regulation of DAHP synthase is thought to be controlled by its N-terminal domain (*Bs*CM_2), which has residual chorismate mutase activity [105,106,108]. Herein, we have reported the crystal structures of the *Bs*CM_2 domain of DAHP synthase from *B. subtilis* in complex with chlorogenic acid. These crystal structures provide crucial information regarding the interaction of ligands with the protein and subsequent conformational changes, which may be responsible for allosteric regulation of DAHP synthase activity. Additionally, this data paves the way for rational drug design to inhibit the DAHPS activity via targeting the N-terminal chorismate mutase like domain. The active site of *Bs*CM_2 contains polar residues (Arg27, Lys38, Asp47, Arg50, Glu51, and Gln86 from one chain and Arg10 from an adjacent chain), which are highly conserved in all chorismate mutases (Figure 2.5). Additionally, the active site of *Bs*CM_2 also contains some non-conserved hydrophobic residues (Ile34, Met54, Phe79, Gly82, and Leu83) (Figure 2.4A). Analysis of *Bs*AroH and *Bs*CM_2 structures revealed that both the structures have different folds, but contain similar active site architecture. Comparison with catalytic and regulatory CM type-2 domains/proteins showed that polar residues at the active site are conserved in all the CM_2 proteins/domains. However, variations were limited to the hydrophobic residues of the active site. These residues may be responsible for differences in catalytic activity in between functional and regulatory domains.

Citrate and the chlorogenic acid both interact with the active site residues through hydrogen bonds and water bridges, as shown in Figure 2.4. Position and interactions of the citrate with the protein differ from chlorogenic acid. Chlorogenic acid forms direct hydrogen bonds with Lys38, Arg45, and Lys80, as well as Water Bridge mediated interactions with Lys38 and Lys80. However, citrate only makes a hydrogen bond with Lys38 and does not have any polar contact with Arg45 and Lys80. Additionally, Phe79 backbone atoms form direct interactions with chlorogenic acid, but form water mediated interaction with citrate. These differences in protein-ligand interactions are likely to be responsible for differences in the binding of ligands with protein as observed in ITC studies. According to ITC data, the binding of chlorogenic acid to *Bs*CM_2 is approximately 1.5X stronger than that of chorismic acid, and 1.25X stronger than that of citrate molecules.

The comparison of catalytic efficiency of *Bs*CM_2 with previously reported parameters of monofunctional *Bs*AroH suggests that the *Bs*CM_2 enzyme has three fold less catalytic efficiency than *Bs*AroH. These findings suggest that *Bs*CM_2 may have regulatory role as fusion partner with *Bs*DAHPS [105,106,108]. As per earlier reported data, chlorogenic acid is an antibacterial compound, but the mechanism of its inhibitory action is poorly understood [151]. The activity of *Bs*CM_2 enzyme was assessed in the presence of chlorogenic acid, and it was found that chlorogenic acid inhibits the *Bs*CM_2 enzyme competitively with a K_i of 0.33 ± 0.07 mM.

As both *Bs*CM_2 and *Bs*AroH share similar active site architecture, it is plausible that chlorogenic acid might also bind to the *Bs*AroH enzyme and inhibit its function. Docking studies to assess the interactions of chlorogenic acid with *Bs*AroH showed that chlorogenic acid interacts with the active site residues of the protein in a manner similar to substrate. The MIC of chlorogenic acid for a *B. subtilis* strain was found to be 30 ± 5 μg/ml. These results suggest that chlorogenic acid and its structural analogues may be developed as potential drug molecules.

2.4.1 Helices H1-H2 connecting Loop L1 flexibility

In previous studies, the *Lm*CM_2 domain structure had H1-H2 connecting loop regions disordered in both the chains, which emphasizes the flexible nature of the this loop. In *Bs*CM_2-CGA, chlorogenic acid interacts with active site loop L1 residues Arg45 and Asp47 directly and via water bridges mediated by hydrogen bonds. This extensive hydrogen-bonding network might be stabilizing loop L1. In two chains of

*Bs*CM_2-CGA structures, the position of loop region residues varies significantly relative to each other (Figure 2.10A). Between chain A and chain B, corresponding C_α atom positions of residues Gly42, Val33, Asn44, Arg45, and Phe46 deviated by 6.8, 8.9, 4.6, 1.5 and 1.1 Å, respectively. Structural comparison with other proteins with the same fold also showed the deviation in the backbone position of loop region residues (Figure 2.10B&C). The huge shift in backbone position suggests the plasticity of active site loop L1.

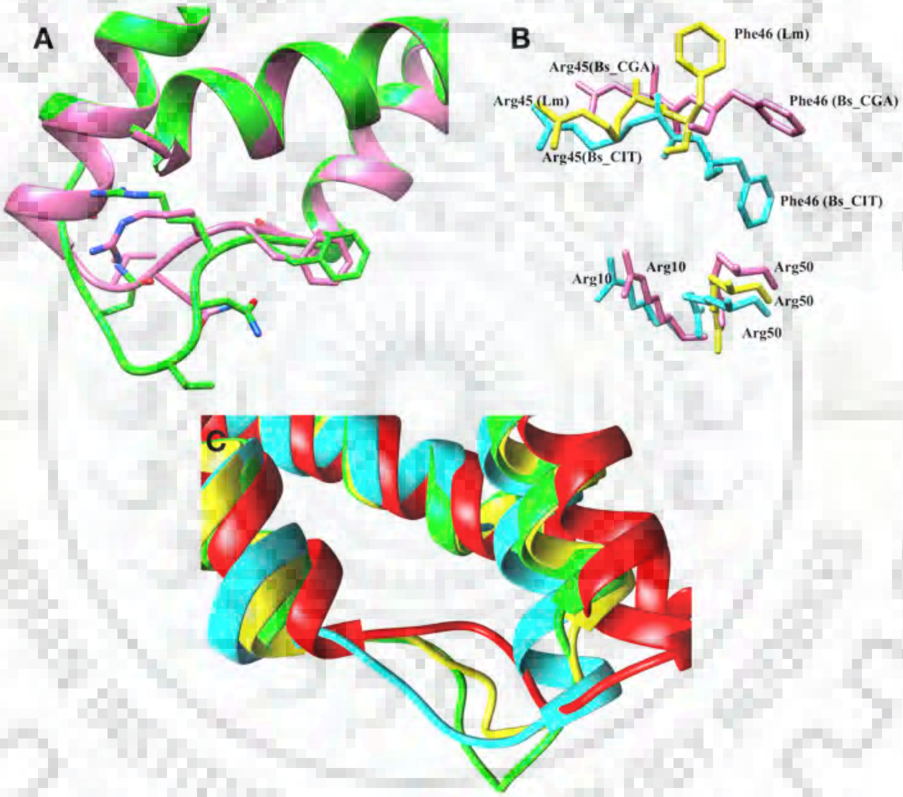

Figure 2.10 Flexibility of loop L1. In panel (A), superimposition of two chains of the *Bs*CM_2-CGA structure shows the deviation in backbone position of residues corresponding to loop L1. Panel (B) depicts the conformational flexibility of loop L1 residues Arg45 and Phe46 in different structures (parentheses are corresponding residues in *Lm*CM domain). Superimposition of *Bs*CM_2-CGA chainB (hot pink), *Bs*CM_2-CIT chainA (cyan) and *Lm*CM domain (PDB ID: 3NVT) chainA (yellow) reveals the flipping of side chains of residues. In panel (C), superimposition of CM_2 domains has shown that loop L1 exists in different conformations. This backbone deviation and side chain flipping may participate in regulation of DAHPS activity by CM_2 domains. *Bs*CM_2-CGA chainA (green), *Bs*CM_2-CIT chainB (yellow), *E. coli* P-protein’s CM domain (PDB ID: 1ECM) chainA (red) and

*Mt*CM (PDB ID: 2VKL) (cyan) were used for structural analysis to assess the conformational flexibility of loop L1.

Molecular dynamics simulations of the *Bs*CM_2-CGA structure showed deviations in backbone position and side chain orientations of loop region residues. In the *Bs*CM_2-CGA structure, loop L1' has a higher B-factor than loop L1. During simulation, large deviations were observed in the loop L1' region, but loop L1 showed only slight deviations in backbone atoms (Figure 2.6B-C). In chain A, helix H2' undergoes uncoiling at the first turn, thus increasing the size of loop region. Significant backbone movement was observed for the longer loop. This long loop region contains residues Phe46, Val49 and Arg52, which correspond to the Phe46, Leu49, and Arg52 of *Lm*CM. These residues may be involved in domain-domain interface formation along with Lys76. The residues of loop L1' contribute to the active site formation, and flexibility of these residues provide plasticity to the active site and may play an important role in the wider substrate specificity.

2.4.2 Regulation Mechanism

Previously, Light *et al.* described plausible regulatory mechanisms of DAHPS activity by the CM_2-like domain [90]. They proposed two hypotheses by which the CM_2-like domain may regulate DAHPS activity. First, domain linker mediated direct inhibitor conformation change transmission and second, domain-domain interface mediated allosteric regulation. They have also summarized the arguments against and in support of both the mechanisms.

Recently, Nazmi *et al.* provided functional and structural evidences suggesting that CM mediated regulation of DAHPS activity results from the significant inter-domain conformational changes upon binding of ligand to the CM domain [104]. These changes make the DAHPS active site inaccessible to substrate, therefore inhibiting the DAHPS activity.

From our structural and molecular dynamics simulation studies, we reinforce the hypothesis of the domain-domain interface interaction mediated DAHP synthase regulation mechanism in *B. subtilis*. Structural and molecular dynamics simulation studies revealed the flexibility of loop connecting helices H1 and H2. Structural analysis of *Lm*DAHPS and *Gsp*DAH7PS showed that a linker region connecting the two domains is highly flexible and can exist in both open and close forms [90,104]. On the basis of our crystal structures, we propose that in the absence of ligand binding in the *Bs*CM_2 active site, the inter-helical loop L1 exist in an extended form leads to the shortening of helix H1 and the linker adopts an open conformation. Upon binding of the ligand at the *Bs*CM_2 active site, the loop L1 becomes shorter and acquires a more compact form, result in longer helix H1. The change in the orientation of loop L1 leads to rearrangement of side chains of loop region residues, and linker regions adopt a closed conformation, bringing the two domains near to each other. The domain-domain interface formation may limit the access of the substrate to the DAHPS active site, inhibiting its activity. The ligands bound at the active site of *Bs*CM_2 can be its substrate, product or their analogues. Binding of any of these ligands may allow *Bs*CM_2 to form a domain-domain interface with the DAHPS domain and limit DAHPS catalytic activity (Figure 2.11).

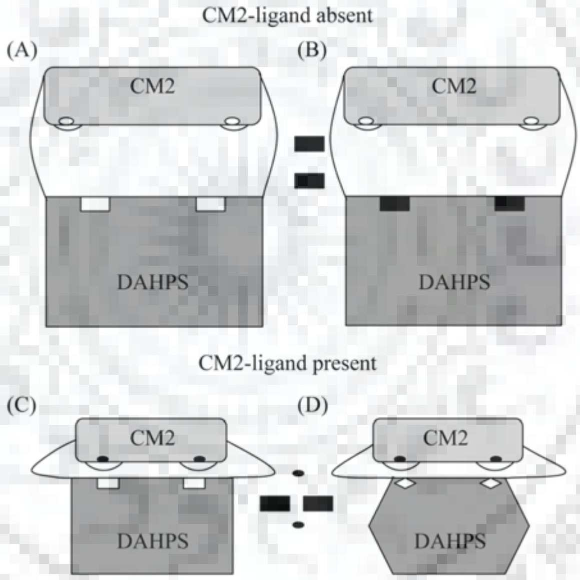

Figure 2.11 The proposed model for the regulation of DAHPS activity by the CM2 domain. Panel (A) shows the basic architecture of DAHPS-CM domain dimers in the absence of a CM2-ligand. Panel (B) shows the substrate (rectangular black box) binding at the active site of the DAHPS domain in the absence of a CM2-ligand. In panel (C), CM2-ligand (oval black box) binds at the active site of CM2, which leads to the conformational changes in linker region and loop L1, which connects helices H1-H2. The linker region adopts the kinked conformation and brings the DAHPS and CM2 domains near to each other. Loop L1 extends outward and flips side chains of loop residues. Loop L1 mediates the domain-domain interface formation between DAHPS and CM2 domains and blocks the DAHPS-substrate access to the DAHPS-active site. As shown in panel (D), the DAHPS domain undergoes conformational changes, which will hinder in the binding of substrate at the active site of this domain. For simplicity, the only dimer of DAHPS has been shown instead of the tetramer.

2.5 Conclusion and future prospects

Previously, it has also been reported that the AroH and the AroQ type chorismate mutase enzymes share the functional uniformity and similar affinity towards common substrate. Therefore, inhibitors simultaneously targeting both types of CM enzymes can be developed. Targeting two different enzymes of the same shikimate pathway with a common inhibitor may limit the availability of essential aromatic amino acids and metabolites required by pathogenic microbes, thus causing death. Also, targeting multiple enzymes using a single inhibitor/drug reduce the possibility of developing drug resistance. The crystal structures of *Bs*CM_2 complexed with chlorogenic acid, and citrate, provide insight into the mode of protein-ligand interactions. This information can be utilized for designing analogues of these ligands for potent *Bs*CM_2 inhibitor development. Additionally, inhibitory activity of CGA shound be explored against full length DAHP synthase enzyme to further validate the allosteric regulation of DAHPS through CM domain. Crystallization of full length BsDAHPS with CGA will give more insights of its regulation and inhibitory actions and to develop more potent inhibitors of DAHPS, more derivatives of CGA can be explored and analyzed.

Chapter 3

Biochemical, Biophysical and structural characterization of FabZ from *Moraxella catarrhalis*

Chapter 3

3.1 Introduction

Moraxella catarrhalis is the third most common bacterial pathogen of respiratory tract after *Streptococcus pneumoniae* and *Haemophilis infuenzae*. It is a Gram-negative diplococcus aerobic bacterium first described in 1896 [169,170]. It causes infections in upper as well as lower respiratory tracts. In hosts with immune deficiency, this bacterium can cause a variety of severe infections, including pneumonia, endocarditis, septicemia, and meningitis. The emergence of strains of this pathogen producing β-lactamase against a range of common antibiotics has generated much interest in this species. *Moraxella catarrhalis* produces two β -lactamases, BRO-1 and BRO-2 classified under class A, hydrolyze penicillin, methicillin, ampicillin, and cefaclor. β-lactamases associated with this bacterial species are unique among β-lactamases [171–173]. In the era of multidrug resistance, it has become more important to develop new approaches to combat bacterial pathogens. A combination of antibiotics is a good strategy for treatment therapy and controlling resistance[174,175]. The utmost requirement for an effective antibacterial agent is that it should target a pathogen-specific essential reaction or pathway in the infectious organism. There are a number of reasons, which makes fatty acid biosynthesis an attractive target for the development of antibacterial agents. The microbes have developed resistance against the antibiotics, which have been used for decades. This antibiotic resistance has increased the value of agents, which acts orthogonally against their targets like fatty acid synthase (FAS) because of ineffective extant resistance mechanisms. The FAS II pathway is validated as a drug target pathway via the use of successful antibacterials, isoniazid and triclosan, which target an enzyme in the bacterial FAS II pathway. There is a higher level of conservation among the different component enzymes of the FAS II pathway, which holds the possibility of developing broad-spectrum antibiotics. The difference in the subcellular organization of the components of the FAS pathway in mammals (Type I FAS) and, bacteria, parasites, and plants (Type II FAS) further validate this pathway, as effective antibacterial drugs will be target specific [80,94,96].

The central feature of the type II FAS pathway is the elongation cycle, where a fatty acid chain is extended by two carbons in each round. There are four steps in the elongation cycle and the enzymes involved as described in *Escherichia coli* are 1) Malonyl-ACP condensation with acyl- ACP, catalyzed by FabB and FabF, 2) NAD(P)H dependent reduction of keto moiety by FabG reductase, 3) FabA or FabZ perform dehydration of the β-hydroxyacyl- ACP and 4) NAD(P)H dependent reduction of trans-2-acyl-ACP by FabI or FabK reductases. After each elongation cycle, resulted acyl-ACP is increased by two carbon units, and either re-enters the cycle for further rounds of elongation or is transferred to glycerol phosphate when chain lengths reach 16-18 carbons to produce phospholipids[83,176].

Dehydratases namely FabA and FabZ, which catalyze the third step in the elongation cycle of FAS II pathway, are the focus of our study. FabA was first discovered dehydratase; perform isomerization reaction along with dehydratase activity. It isomerizes trans-2- to cis-3-decenoyl-ACP as an important step in the synthesis of unsaturated fatty acids[177,178]. However, FabA has limited distribution in nature, and found in Gram-negative bacteria, which produce unsaturated fatty acids[179]. The second dehydratase; FabZ is ubiquitously expressed in type II FAS systems and cannot carry out isomerization reaction. It performs dehydration reaction, and only dehydratase, which exists in most of the bacteria[180,181]. FabZ, being a key component of FASII pathway, is an important target for the development of new antibacterial agents. It’s not surprising that considerable attention has given for identification and biochemical characterization of FabZ. Enzymatic characterization of FabZ has been reported in *Escherichia coli*[182], *Pseudomonas aeruginosa* [92], *Plasmodium falciparum* [183,184], *Enterococcus faecalis* [181], *Yersina pestis* [106], and *Helicobacter pylori* [185]. Several crystal structures of native and inhibitor-bound FabZ from different organisms have been solved in recent years. These include structures from *Pseudomonas aeruginosa* [92] (PaFabZ), *Helicobacter pylori* [186] (HpFabZ), *Plasmodium falciparum* [104] (PfFabZ), *Burkholderia thailandensis* [187] (BtFabZ), *Neisseria meningitides* (NmFabZ)(PDB ID: 4I83), *Yersinia pestis* [145] (YpFabZ), and *Campylobacter jejuni* [188] (CjFabZ). Till now, two kinds of inhibitors are reported based upon their preferential binding sites, referred either as gate blocker or channel blocker [189]. Although enough biochemical and structural information is available for FabZ, there is a need to identify the new chemical compounds with high potency and efficacy in order to develop antibacterial agents targeting FabZ. Flavonoids are secondary metabolites synthesized by the plants in response to microbial infection. These polyphenolic compounds known to exhibit various pharmacological activities like antioxidant, antibacterial, antiviral, antidiabetic, anticancer, etc. The activities and chemical nature of these compounds are structure dependent and governed by the degree of hydroxylation, the presence of different constituents, conjugations, and degree of polymerization [190–192].

In this study, we have characterized FabZ from a drug resistant strain of *Moraxella catarrhalis* (McFabZ) biochemically and biophysically. We have identified three isoflavones (daidzein, genistein and biochanin A) as new inhibitors against bacterial FabZ. Additionally, we have also characterized other reported inhibitors of FabZ against McFabZ. Binding studies and thermodynamic characterization with inhibitors have been performed via biochemical, circular dichroism (CD), fluorescence spectroscopy and ITC based assays. Molecular modeling and docking studies have assessed the plausible interactions involved upon inhibitors binding to the McFabZ. Molecular dynamics-based simulations evaluate the stability of docked complexes. The growth inhibition assay has been performed to calculate the minimum inhibitory concentration (MIC). Therefore, the current study suggests that isoflavone and their analogues are potential antibacterial agents. Thus, comparing relative strength of new and known inhibitors against McFabZ could be helpful for the development of new chemical scaffolds against bacterial pathogens.

3.2 Materials and Methods

3.2.1 Materials

Moraxella catarrhalis strain MTCC No.445 (equivalent to ATCC 8176) was procured from the Microbial Type Culture Collection and Gene Bank (MTCC) Chandigarh. All nucleic acid manipulations were performed using standard procedures[152]. All enzymes (DNA polymerase, restriction enzymes, T4 DNA ligase, *etc.*) were purchased from New England Bio Labs. The Qiagen kits were used for plasmid isolation, purification and gel extraction. *Escherichia coli* DH5α cells and *E. coli* Rosetta cells were obtained from Novagen. Primer procurement and DNA sequencing was done from Eurofins (India). All other chemicals, inhibitors and reagents were purchased from Sigma. Media components were purchased from HiMedia (India).

3.2.2 Methods

3.2.2.1. Cloning of *M. catarrhalis* FabZ gene (McFabZ)

Based on genome sequence of *M. catarrhalis* strain RH4 (Genbank Accession No. EKF84083), two PCR primers P1 (Forward: 5'-GGCTCATATGTCTGTTTCAAACA TTGATTTTG-3') and P2 (Reverse: 5'-GAACTCGAGTCATTTGACG CCATCCAC-3') were designed. 525 bp fragment coding McFabZ gene was PCR amplified from genomic DNA of *M. catarrhalis*. The amplified product was PCR purified and digested with restriction enzymes (NdeI & XhoI) and then ligated into pET28c similar treated vector using T4 DNA ligase enzyme. Ligated product was then transformed into *E.coli* DH5α cells. Clone confirmation was done using restriction digestion and further confirmed by DNA sequencing.

3.2.2.2. Protein Expression and Purification

The pET28c-McFabZ construct was transformed in *E.coli* Rosetta cell lines and cells were cultured in LB broth media supplemented with kanamycin (50 µg/ml) and chloramphenicol (35 µg/ml) at 37 ^{0}C. After sufficient growth at OD$_{600}$ reached to 0.6 - 0.8, culture was induced with 0.5 mM IPTG concentration. The culture was then incubated at 20 ^{0}C for 16-18 hrs. Cells were harvested by centrifugation at 6000 rpm for 10 min at 4 ^{0}C and stored at -80 ^{0}C. For purification of McFabZ protein, harvested cells were suspended in buffer A (25 mM Tris HCl, pH 7.8, 200 mM NaCl, 5% glycerol, 1 mM PMSF and 10 mM imidazole). Lysozyme was added to the final concentration 0.25 mg/ml. The Cells were further disrupted using high-pressure cell disrupter. Clear supernatant was obtained by centrifuging the disrupted cells at 12000 rpm for 60 min at 4 ^{0}C in a high-speed centrifuge. His-tagged McFabZ protein was subsequently purified on a Ni–NTA agarose column using a linear gradient of buffer B (25mM Tris HCl, 200 mM NaCl, glycerol 5% and 500 mM imidazole). The fractions containing the desired protein, as confirmed by SDS-PAGE, were pooled and dialyzed overnight against 2 litres of 20 mM Tris HCl buffer (pH 7.8). The protein was further concentrated up to 5 mg/ml using a 3 kDa cutoff Amicon Ultra-15 concentrator (Millipore, Bedford, Massachusetts, USA).

3.2.2.3. Biochemical characterization

The enzymatic activity of McFabZ was determined using substrate analogue crotonyl-Co A via reported spectrophotometric assay [104]. Decrease in the absorbance at 260 nm was observed as crotonyl- CoA converted into hydroxy butyl -Co A. The standard reaction mixture consists of 10 µg McFabZ, 20 mM Tris HCl (pH 7.8), 100 mM NaCl and 100 µM crotonyl- CoA in a total volume of 200 µL. Kinetic parameters K_m, V_{max}, k_{cat} etc. have been determined by varying the substrate concentration (10 µM to 200 µM). All biochemical reactions have been performed in triplicates. The obtained data have been fitted using nonlinear regression analysis of graph pad prism software [193].

3.2.2.4. Effect of pH and temperature on McFabZ activity

The biochemical activity of McFabZ protein has been checked at different pH range (3-10). The different buffer system has been used to obtain the desired pH. Sodium citrate buffer (25 mM) for 3.0 – 5.0 pH, Tris HCl (25 mM) for 6.0 – 8.0 pH and sodium bicarbonate buffer (25 mM) for 9.0 – 10.0 pH have been used. Reaction mixture consists of buffer of different pH, 10 µg McFabZ, 100 mM NaCl and 100 µM substrate in total volume of 200µL. Temperature dependent McFabZ activity was determined from 20 ^{0}C - 80 ^{0}C.

3.2.2.5. Kinetic inhibition studies

The natural compounds, which were tested against McFabZ, include flavonoids (daidzein, genistein, biochanin A, catechin gallate, quercetin and myricetin) and reported inhibitors (juglone, emodin). The chemical structures of all the inhibitors used in the current study have been shown in Figure 3.1. All tested inhibitors were dissolved in DMSO (100%) and added to the reaction mixture with final concentration $\leq$ 1% DMSO. Dose dependent IC_{50} value has been calculated keeping substrate concentration constant (100 µM). Kinetic inhibition constant (K_i) has been calculated by varying inhibitor (10-150 µM) and substrate concentration (10-200 µM). McFabZ protein was incubated with tested inhibitor for 1 hr at 4^{0}C. Reaction was initiated by adding the substrate and then, decrease in the absorbance at 260 nm was measured spectrophotometrically.

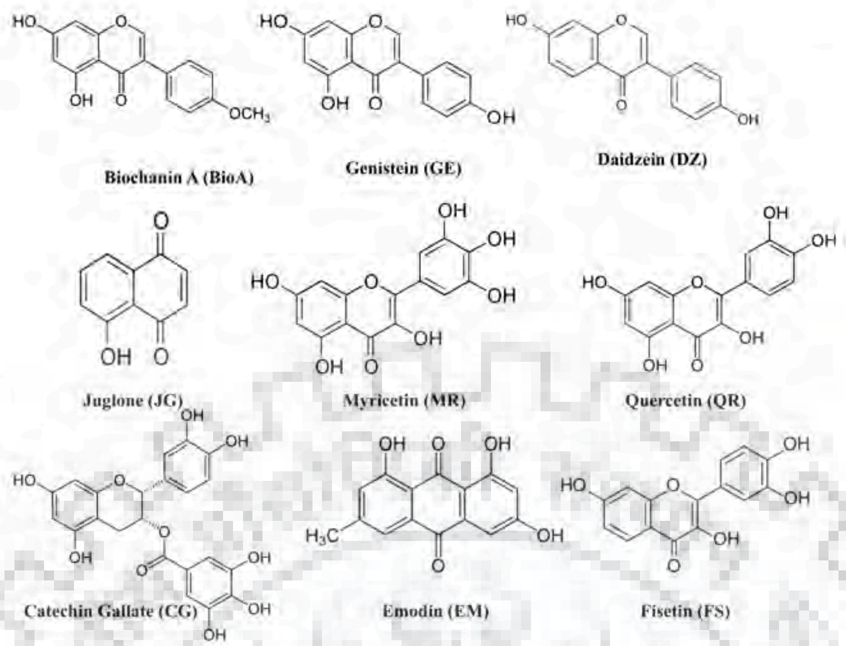

Figure 3.1 The chemical structure of compounds used in this study.

3.2.2.6. Circular Dichroism (CD) based Studies

The far-UV and the near-UV circular dichroism spectral measurements were carried out using J-Model-1500 spectrophotometer (JASCO) equipped with temperature control system. CD studies were done to observe the conformation changes in protein structure upon inhibitors binding. All CD spectra were measured at 25 ^{0}C using quartz cuvette of 0.1 cm optical path length. Protein concentration was kept to 0.2 mg/ml. Buffer C (20 mM Sodium phosphate (pH 7.8), 100 mM NaCl) was used to suspend protein and to make different dilutions of inhibitors. Effect of pH on the conformation of McFabZ protein was also determined using different buffers (citrate buffer for pH 3.0 – 5.0, and phosphate buffer for pH 6.0 – 8.0). Effect of temperature was also studied by taking thermal spectra of McFabZ protein at different temperature. Thermal spectra were recorded from 20 to 90 ^{0}C with 5 ^{0}C intervals. CD spectra for thermal denaturation was also taken at 222 nm with rate of temperature change 1 degree/min.

The melting temperature (T_M) of McFabZ is calculated by the equation (1):

$$[\theta]_t = \alpha([\theta]_F - [\theta]_U) + [\theta]_U \qquad (1)$$

T_M is the temperature where $\alpha = 0.5$, θ_t is the observed ellipticity at any temperature, θ_F is the ellipticity of the fully folded form and θ_U is the ellipticity of the unfolded form [194]. All spectra scans have been taken in triplicate and final spectra obtained by averaging them. Experimental data were corrected by subtracting the blank taken under the same conditions without protein. All the CD data analysis was done using Dichroweb online software [195]. The CD data were expressed in molar ellipticity ($\Delta\varepsilon$) in deg cm^2 $dmol^{-1}$, which is defined as per following equation:

$$\Delta\varepsilon = \frac{\theta\ (\text{mdeg}) \times 0.1 \times \text{MRW}}{P \times C \times 3298}$$

where MRW is mean residue weight (Molecular weight of protein / no. of residues - 1), P is the path length in cm, C is molar concentration of McFabZ protein and 3298 is the constant [196].

3.2.2.7. Molecular Modeling

As the crystal structure of McFabZ protein is not available, structural model of McFabZ was constructed using homology modeling. Swiss Model [197] and Modeller [198] program was used to build a model based upon homology. The most suitable template to construct a 3D model was selected based upon the sequence identity. Multiple sequence alignment was performed using T Coffee server [199]. Validation of predicted models for their stereo chemical quality and accuracy was done by PROCHECK’s analysis, ERRAT, PROVE, Verify3D (all available at http://nih-server.mbi.ucla.edu), ProQ [200,201] and ProSA [202]. The global structure match was performed using COFACTOR web server based on TM- align algorithm. TM score was then calculated to assess the structural similarity where values range from 0 to 1(TM score= 1 corresponds to perfect match, scores below 0.17 indicates randomly chosen proteins and scores above 0.5 implies for generally same fold) [203]. Structural studies were performed and model figures were generated by Chimera tool [204].

3.2.2.8. Intrinsic Fluorescence Spectroscopy

Fluorescence measurements were carried out to observe the conformational and structural changes in McFabZ upon ligand binding. All fluorescence experiments were performed at 25 ^{0}C using Horba Fluro Log Spectrofluorometer with 5 nm emission slits and cuvette of 1.0 cm path length. Final protein concentration was kept to 2.0 – 4.0 µM in 20 mM sodium phosphate buffer (pH 7.5). All inhibitors were dissolved in DMSO (100%) and added to the reaction mixture with final concentration ≤ 1% DMSO. The intrinsic fluorescence was measured by keeping excitation wavelength 290 nm. Emission spectra were collected at 100 nm/min in the range 300 nm – 500 nm, and 3 parallels scans were acquired. Spectra of blank samples were subtracted from the main spectra.

3.2.2.9. Binding Studies using ITC

Binding affinities of McFabZ with different inhibitors have been measured using Microcal ITC200 (GE Health Care). All titration reactions have been performed at 25 ^{0}C. McFabZ protein was extensively dialyzed against buffer D (20 mM Tris-HCl pH 7.8, 100 mM NaCl, 5% glycerol and 0.5 mM TCEP). As the all inhibitors were dissolved in DMSO and used in the final concentration ≤ 1% DMSO, the corresponding amount (1%) of DMSO was added to the protein solution to avoid buffer-buffer mismatch. The titration reactions were performed using McFabZ protein (50-100 µM) in ITC sample cell and ligands (1-2 mM) in a syringe with 200 rpm stirring speed and initial delay of the 60s. After an initial injection of inhibitors (0.5 µl, not used in data fitting), 15 injections (2.5µl each) were performed with 150 seconds gap between each injection and then heat changes were monitored. The reference cell power was set to 8 µW. ITC data were analyzed using single binding site model using Origin 7.0 software. The free energy change (ΔG) is calculated by the following equation (3)

$$\Delta G = \Delta H - T\Delta S \qquad (3)$$

where ΔG is the Gibbs free energy change, ΔH is enthlapy change, ΔS is entropy change and T is the temperature (298K).

3.2.2.10. Molecular Docking

To study the possible interactions of inhibitors with the active site of McFabZ, molecular docking was performed using Autodock [163] from ADT tools for the preparation of ligand and macromolecules pdbqt files. Grid maps for the docking calculations were made using 50×50×50 grid points with 0.375 Å spacing in the x, y, and z directions centered at the active site. Lamarchian Genetic Algorithm was used for docking. AutoGrid4 and AutoDock4 programs were executed for calculating energy maps and docking of ligands, respectively. Docking conformations were analyzed by converting them into *pdbqt* files and visualizing in chimera[204].

3.2.2.11. Molecular Dynamics (MD) Simulations

MD simulations were performed to further evaluate the structural and binding stability of three best-docked complexes for McFabZ (biochanin A, genistein and daidzein) for 20 ns using AMBER14 [205]. The partial atomic charges for all three ligands were computed by Gaussian 09 [206] by utilizing the Hartree− Fock (HF) method with the 6-31G(d) basis set. Further, the calculation of restricted electrostatic potential (RESP) and assignment of GAFF force field parameters was carried out by using Antechamber program [207]. Each ligand-receptor system was solvated in a 10Å orthorhombic box of TIP3P water. The whole system was neutralized by the addition of 8 Na^+ counter-ions. The protein was parameterized with the AMBER ff14SB force field. The MD simulation was performed at 7.0 pH. The bond lengths and bond angles involving hydrogen atoms were held by using a SHAKE algorithm [208]. The time step for combining the atomic equation of motion was set to 2 fs and coordinates of trajectory were recorded at 30 ps interval. The cutoff for distances of electrostatic interaction was truncated to 8 Å and particle mesh Ewald (PME) summation was used to calculate the electrostatic interaction beyond cutoff [209]. All the structures were initially minimized with the 1000 cycles of the steepest decent. Further, the minimized structures were heated from 0 to 300 K in 30 ps using Langevin thermostat followed by equilibration at constant pressure of 1 atm. At this point, a production run of 20 ns was carried out with an NPT (constant composition, pressure, and temperature) ensemble at 300 K and a pressure of 1 atm using velocity re-scale thermostat and Berendsen barostat [210]. MD trajectory analyses were performed using Visual Molecular Dynamics (VMD) [211].

3.2.2.12 Minimum Inhibitory Concentration (MIC) determination

MIC of daidzein, genistein, biochanin A and juglone against *Moraxella catarrhalis, Bacillus subtilis and Pseudomonas sp.* has been determined using a broth micro dilution method on 96 well microtiter plate [166,212]. A concentration gradient (5 μg/ml – 200 μg/ml) of inhibitors was tested. A single colony of bacterial strain was used to inoculate the nutrient broth medium. Correlation between OD_{600} and colony forming units (cfu) has been determined using serial dilution technique. Bacterial suspension having 1.0 × 10^6 cfu per ml was used to inoculate 96 well microtiter plates. The different dilutions of inhibitors were prepared in dissolved in sterile PBS buffer (1x). 100 µl of broth solution was added to all wells. 50 µl of inhibitor solution was used in each well, except growth control (broth and inoculum) and sterility control (broth only) wells. 50 µl of bacterial suspension adjusted to 1×10^6 cfu per ml has been used which gives final inoculum 5×10^5 cfu per ml. Microtiter plate was then incubated at 37 ^{0}C for 16-20 h.

3.3 Results

3.3.1. Purification and oligomeric characterization of McFabZ in solution

Based on the genomic sequence of *M. catarrhalis* strain RH4 (Genbank Accession No. EKF84083) 575 bp McFabZ gene was cloned into pET28c expression vector. The clone was confirmed by restriction digestion and later by DNA sequencing (Figure 3.2A&B).

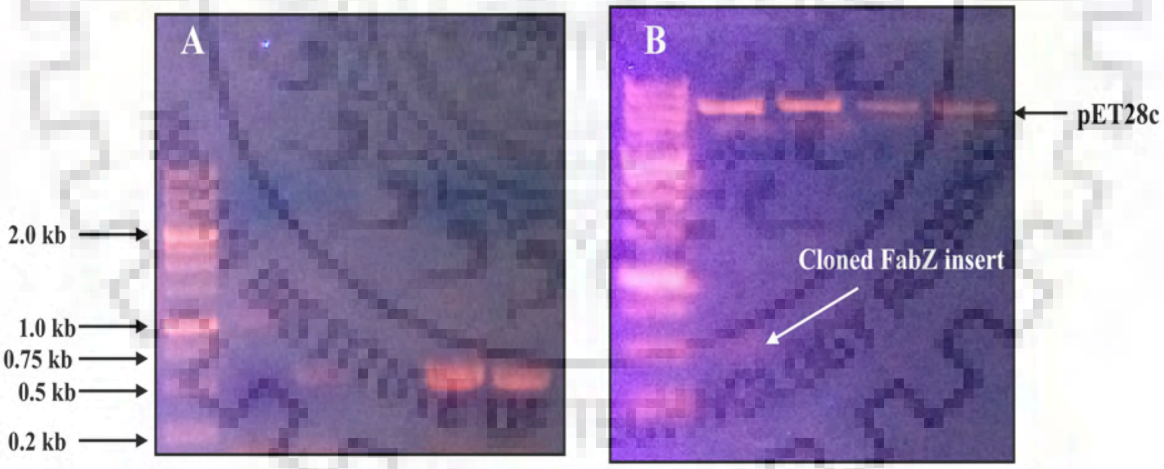

Figure 3.2 Molecular cloning of McFabZ gene. (A) PCR amplification of 575 bp McFabZ gene fragment. (B) Confirmation of clone by restriction digestion experiment.

McFabZ gene was expressed in *E. coli* Rosetta cells at 20 ^{0}C by inducing with 0.5 mM IPTG. Purification of McFabZ protein was accomplished using Ni-NTA affinity followed by size exclusion chromatography and protein purity was confirmed by SDS PAGE analysis. ≈19.25 kDa size protein was expressed and purified (Figure 3.3).

The oligomeric state of McFabZ protein in solution was determined using size exclusion chromatography, which separate proteins on the basis of size and shape. The superdex G200 column was equilibrated with five globular proteins. A McFabZ protein with concentration of 5 mg/ml was loaded into a superdex G200 column. The elution was done using buffer E (20 mm Tris HCl, pH 7.8, 100 mM NaCl and 5 % glycerol). The apparent molecular weight of McFabZ was estimated by interpolation using standard calibration curve (Figure 3.4A).

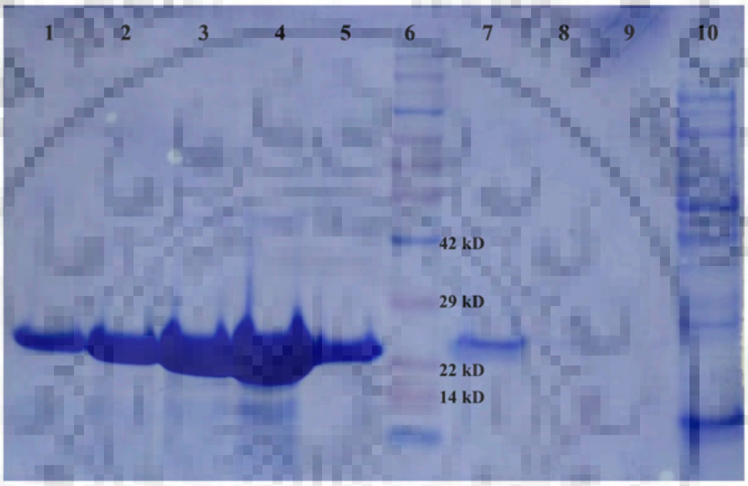

Figure 3.3 Purification of McFabZ. Lane 1-2, fractions eluted at 100 mM imidiazole; lane 3-5,7-9 fractions eluted at 250 mM imidiazole; lane 6, protein ladder (abcam); lane 10, flowthrough. ≈ 19.25 kDa size FabZ protein was purified.

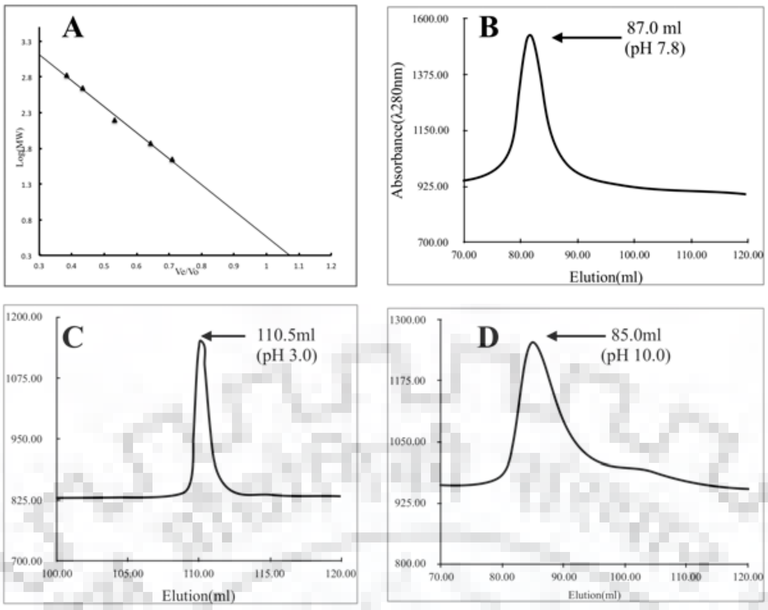

Figure 3.4 Oligomeric characterization of McFabZ. **(A)** Determination of molecular mass by size exclusion chromatography. Standard curve Log of molecular weight Versus Ve/Vo was derived from the elution profile of standard protein on Superdex 200 Gel filtration column. Ve is peak elution volume and Vo is the void volume of the column. The standards used were as follows: 1. Thyroglobulin (669 kDa) 2. Ferritin (440 kDa) 3. Aldolase (158 kDa) 4. Conalbumin (75 kDa) 5. Ovalbumin (43 kDa). **(B), (C)** and **(D)** Chromatogram of McFabZ protein observed at pH7.8, pH 3.0 and pH 10.0 respectively.

At pH 7.8, a single peak was observed at 87.0 ml elution volume, which corresponds to the size of McFabZ dimer (38.5 kDa). At lower pH (3.0) peak was shifted and McFabZ protein eluted at 110.5 ml elution volume, which is consistent with the size of the monomeric protein (19.25 kDa). At higher pH (10.0) McFabZ was eluted at 85.0 ml elution volume and peak corresponds to the size of dimer (≈40.0 kDa). Figure 3.4B-D, shows the gel filtration peaks observed at different pH. This shows that lower pH disrupts the oligomeric assembly of McFabZ. Similar pH dependent oligomeric transition has been observed in PfFabZ. In PfFabZ, transition of stable active hexameric assembly to less stable inactive dimeric assembly is triggered by low pH [183]. In McFabZ low pH triggers the transition of stable dimeric form to unstable monomeric form.

3.3.2. Biochemical properties of McFabZ

The activity of McFabZ was determined using a spectrophotometric assay in which decrease in the absorbance of crotonyl Co-A was monitored at 260 nm. Biochemical parameters (K_m, k_{cat}, V_{max}, k_{cat}/K_m) were determined. McFabZ protein was found to be active with K_m 66.98 ± 6.94 µM and V_{max} 332 ± 13.31 nmol min^{-1} mg^{-1} respectively. The k_{cat} value was determined to 1.663 ± 0.06 S^{-1}. The catalytic turnover number (k_{cat}/K_m) is determined to 2.4 x 10^4 $M^{-1}S^{-1}$.

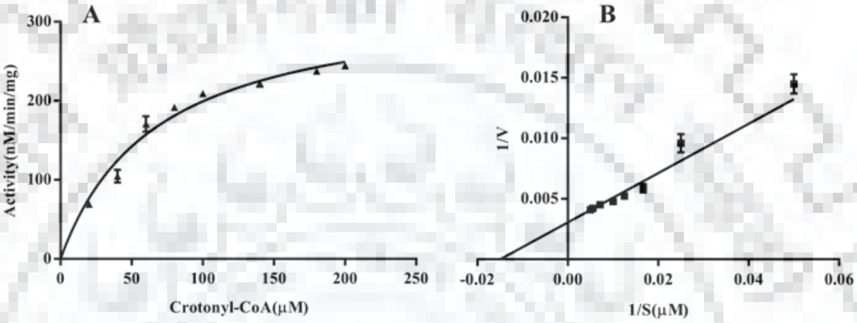

Figure 3.5 Biochemical characterization of McFabZ. **(A)** Kinetic analyses of McFabZ with crotonoyl - Co A. Initial velocities were determined with increasing concentration of substrate (Crotonoyl- CoA). **(A)** The steady state kinetic curve of McFabZ. **(B)** Double reciprocal plot. Data was analyzed using non-linear regression analysis. The K_m value was found to be 66.98 ± 6.94 µM with crotonoyl -CoA.

The enzymatic characterization of FabZ has been reported from several homologs with K_m of 61.8 µM (YpFabZ)[106], 69.7 µM (CjFabZ)[188], 82.6 µM (HpFabZ)[185] and 86.0 µM (PfFabZ)[104]. However, the reported k_{cat}/K_m values for other homologs fall between 1.57 x 10^2 $M^{-1}S^{-1}$ to 1.43 x 10^4 $M^{-1}S^{-1}$. The Michaelis Menten and double reciprocal plot of native McFabZ has shown in Figure 3.5A-B.

3.3.3. Effect of pH and temperature on McFabZ activity

The optimum pH for McFabZ activity was found to be 8.0. There is a concurrent decrease in the activity of McFabZ with pH decrease. At pH 3.0, McFabZ is found to be catalytically inactive. These results are in agreement with gel filtration data, where it has been shown that at pH 8.0 McFabZ exists as a dimer, while at low pH (3.0) it exists as a monomer. This shows that McFabZ is active in dimeric form and pH plays an important role in the transition of active to inactive form.

The optimum temperature for McFabZ activity is 25 ^{0}C. Higher temperature leads to reduction in McFabZ activity as it loses more than 50% activity at 45 ^{0}C. Effect of pH and temperature on McFabZ activity has been shown in Figure 3.6A and 3.6B respectively.

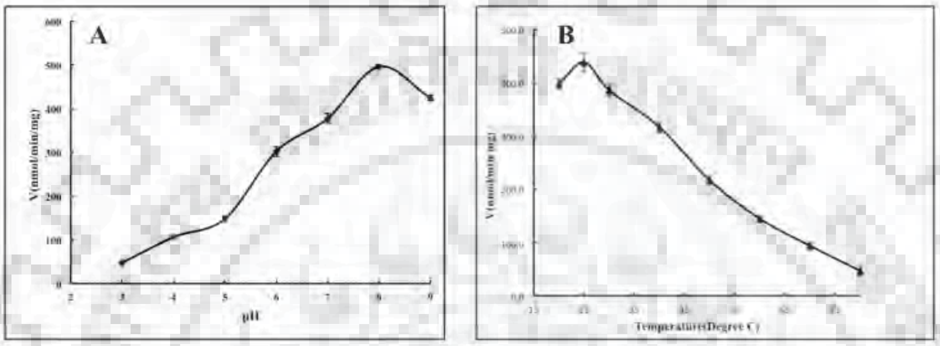

Figure 3.6 Effect of pH and temperature on the activity of McFabZ. (A) Effect of pH on the activity of McFabZ. The optimum pH of McFabZ for its biochemical activity was determined to 8.0. At lower pH, there is a drastic decrease in the activity of McFabZ. **(B)** Effect of temperature on McFabZ activity. The optimum temperature for McFabZ activity was found to be 25 ^{0}C and higher temperature leads to a reduction in the activity.

3.3.4. Kinetic Inhibition Studies

The compounds which were tested for their inhibitory action against McFabZ protein include juglone, genistein, catechin gallate, quercetin, emodin, myricetin, biochanin A and daidzein. The kinetic inhibition constant (K_i) for these compounds has been calculated using non-linear regression analysis. Table 3.1 shows the K_i and IC_{50} values of all these inhibitors. Daidzein, genistein, biochanin A and juglone have lower K_i and IC_{50} values than the other compounds tested in this study. In comparison to other inhibitors, genistein has more inhibitory activity against McFabZ with K_i value of 4.3 µM. Biochanin A, daidzein and juglone have K_i values of 16.83µM, 11.86µM and 15.48 µM respectively. IC_{50} value of genistein, daidzein, biochanin A and juglone are 6.85 µM, 7.48 µM, 29.7 µM and 32.4 µM respectively.

More importantly, inhibitors with better K_i and IC_{50} values compare to other compounds taken in consideration, were further analyzed through available filters

[213,214] to remove PAINS (pan assay interference compounds). Biochanin A, genistein and daidzein had successfully passed the filter.

Mechanism of inhibition of these inhibitors has been analyzed via plotting double reciprocal plot. Based upon the analysis of double reciprocal plot, biochaninA, daidzein and genistein were found to be competitive inhibitors of McFabZ (Figure 3.7A, 3.7B and 3.7C). The lines intersecting at 1/V axis clearly indicating the competitive type of inhibition mechanism of these three compounds for crotonoyl-CoA substrate. Mode of inhibition of juglone is found to be noncompetitive (mixed type) as shown in Figure 3.7D. Based on the biochemical findings, molecular docking of daidzein, genistein, biochaninA, juglone, catechin gallate and quercetin was performed with McFabZ.

Table 3.1 Inhibitory activities of myricetin, epicatechin gallate, genistein, biochanin A, daidzein, juglone, emodin and quercetin against McFabZ.

Compound	IC$_{50}$ (μM)	K_i (μM)
Biochanin A	29.7 ± 1.13	16.83 ± 3.59
Genistein	6.85 ± 1.14	4.3 ± 0.62
Daidzein	7.48 ± 1.07	11.83 ± 1.99
Myricetin	121.0 ± 2.01	41.1 ± 4.21
Quercetin	161.0 ± 2.78	67.0 ± 3.98
Juglone	32.4 ± 1.58	15.48 ± 3.58
Catechin gallate	417.0 ± 2.39	77.04 ± 8.91
Emodin	48.6 ± 3.56	28.4 ± 2.45

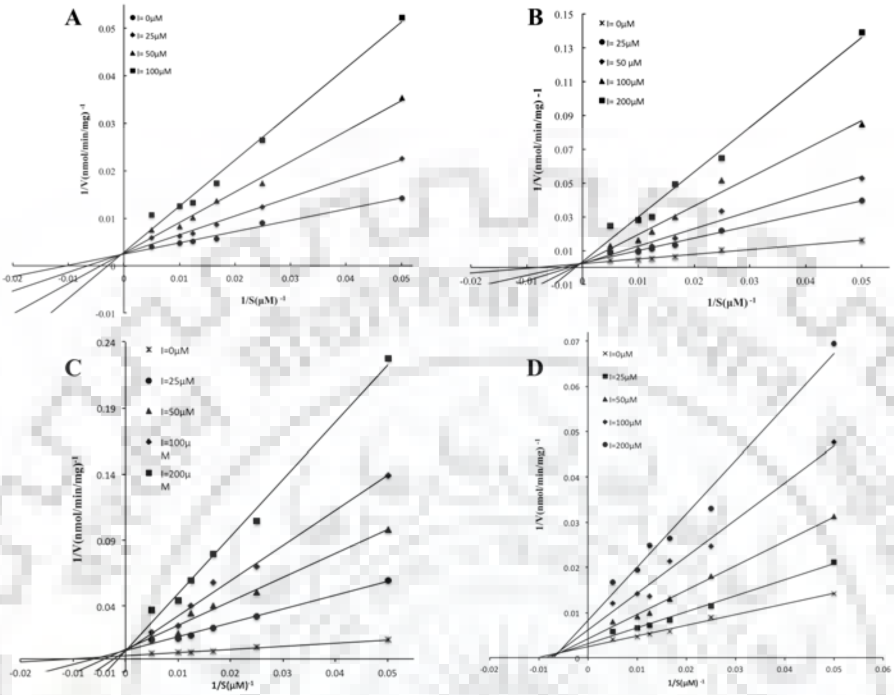

Figure 3.7 Kinetic analysis of inhibition mechanism of biochanin A (A), daidzein (B), genistein (C) and juglone (D). Four panels show the representative plot of 1/V vs 1/S at different inhibitor concentration. Lines intersecting at 1/V for daidzein, biochanin A and genistein indicate the competitive mode of inhibition with a K_i value of 11.83 ± 1.99 µM, 16.83 ± 3.59 µM and 4.3 ± 0.62 µM respectively, while juglone shows mixed type (non-competitive) of inhibition with a K_i value of 15.48 ± 3.58 µM. All reactions have been performed in triplicates and mean data have been plotted here.

3.3.5. Circular Dichroism Studies

Circular dichroism experiments were carried out to observe conformational changes in McFabZ protein upon inhibitors binding. The far-UV CD spectroscopy is widely used to observe the changes in the secondary structure of proteins, while some information related to tertiary structure can be obtained through near-UV CD spectra [215–219]. Figure 3.8A & 3.8B shows the far-UV and the near-UV CD spectra of McFabZ protein in native condition and in presence varying amount of substrate. Being a β-sheet rich protein with some α-helical content, the CD spectra of McFabZ shows characteristic negative peaks at 222 nm, 208 nm and positive peaks at 190-195 nm wavelengths. There is the presence of the single broad minimum band in the range 210-220 nm because of overlapping α-helical and β-sheets contents.

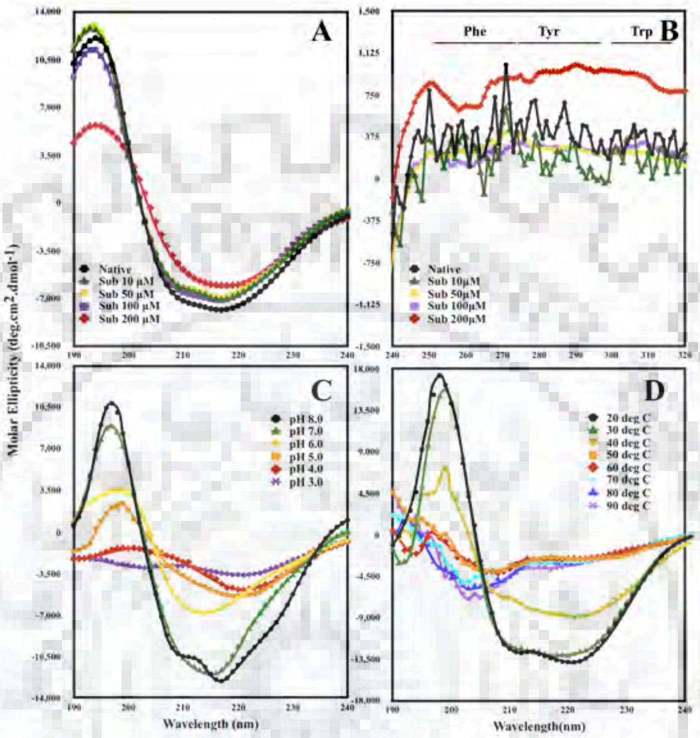

Figure 3.8 The CD spectra of McFabZ at different conditions.

(A) The far-UV and (B) near-UV CD spectra of McFabZ in native condition and in the presence of different concentration of substrate. At higher substrate concentration, changes in secondary and tertiary structure of McFabZ were observed. (C) The far-UV CD spectra of McFabZ at different pH: Conformational change observed at low pH as spectra become more distorted and unstable. (D) The Far-UV CD spectra of McFabZ at different temperature: At higher temperature McFabZ become unstable, which leads to distorted spectra. Changes in helical and sheet contents were also observed.

Percentage of secondary structure content is determined by CONTIN method using the dichroweb web server for CD data analysis [220]. For native McFabZ protein, the helical, sheet and coil content was 20.5%, 38.6%, and 16.5 %, respectively (which is in agreement with secondary structure content of McFabZ 3D model calculated by DSSP algorithm).

3.3.5.1. ***Effect of substrate*** on the far-UV CD spectra of McFabZ has been shown in Figure 3.8A. It is clearly demonstrated that increasing substrate concentration has caused a decrease in ellipticity of McFabZ enzyme. The effect on far-UV CD spectra becomes more evident at higher substrate concentrations (200 µM). A noticeable loss of alpha helices and sheet content has been observed relative to native spectra, as mentioned in Table 3.2. The near-UV CD spectra of McFabZ in presence substrate has been shown in Figure 3.8B. McFabZ protein contains 8 phenylalanine residues, 7 tyrosine residues and 1 tryptophan residue respectively. At higher substrate concentration (200 µM) substantial changes in tertiary structure of McFabZ have been observed which might be due to changes in the microenvironment of aromatic residues present in the active site and substrate binding tunnel regions. From Figure 3.8B, we have observed that there is a decrease in MRE towards negative values up to 100-µM substrate concentrations, while at a higher substrate concentration (200 µM) MRE has increased towards positive values.

3.3.5.2. Effect of pH and temperature

The far-UV CD spectra at different pH range (3.0 – 8.0) show considerable conformational change upon a gradual decrease in pH. Percentage of disorderedness has been increased as the pH decreases marked by a decrease in the helical and the sheet content. This observation is consistent with loss of McFabZ activity at similar pH. At pH 3.0, the helical and the sheet content was found to be 4.8% and 20.3% respectively. Figure 3.8C shows the effect of pH on the CD spectra of McFabZ protein. At lower pH, McFabZ became unstable and stable conformation of protein become deformed. Characteristic broad minima at 210-220 nm and maxima at 190-195 nm have been affected and the spectra become more flat in the entire region.

The melting temperature (T_M) of McFabZ has determined to 42.5 ^{0}C as per the equation mentioned in the methods. The thermal denaturation curve of McFabZ has a sigmoidal profile (Figure 3.9). Low T_M value depicts that McFabZ protein is a temperature sensitive protein. The CD spectra at different temperature intervals have been taken. From Figure 3.8D, it was observed that with increase in the temperature, the spectra of McFabZ become deformed and conformational change was observed. The Spectra become more flat and characteristic bands disappeared, which depicts the loss of secondary elements at higher temperature.

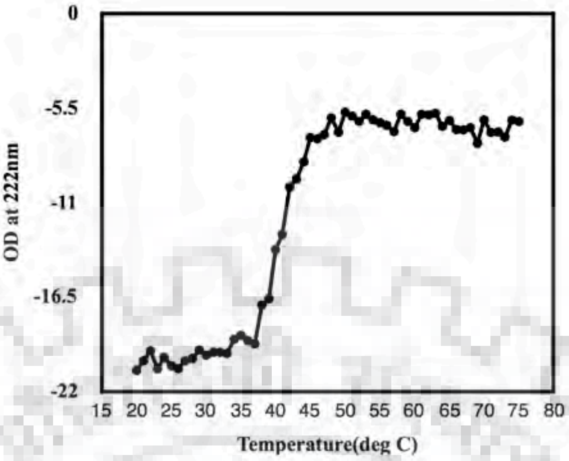

Figure 3.9 Melting curve of McFabZ.

3.3.5.3. Effect of different inhibitors

The effect of inhibitors binding on McFabZ protein was also studied. The far-UV and near- UV CD spectra of McFabZ in the presence of different concentration inhibitors are given in Figure 3.10A-3.10F and Figure 3.11A-3.11F respectively. Interestingly, the binding of inhibitors brought some striking variations in far-UV CD spectra in comparison to native FabZ spectra. Upon ligand binding, the common observation in CD spectra reveals the significant loss of helical content evident by the diminishing ellipticity at 208 nm, 222 nm and 195 nm. Also, some loss of sheets was also observed with decrease in broad minima around 210-220 nm. The composition of secondary structure content at various concentrations of ligands calculated by Dichroweb server is given in Table 3.2. The results clearly indicate that ligand binding at the active site accompanied by significant structural rearrangement of McFabZ.

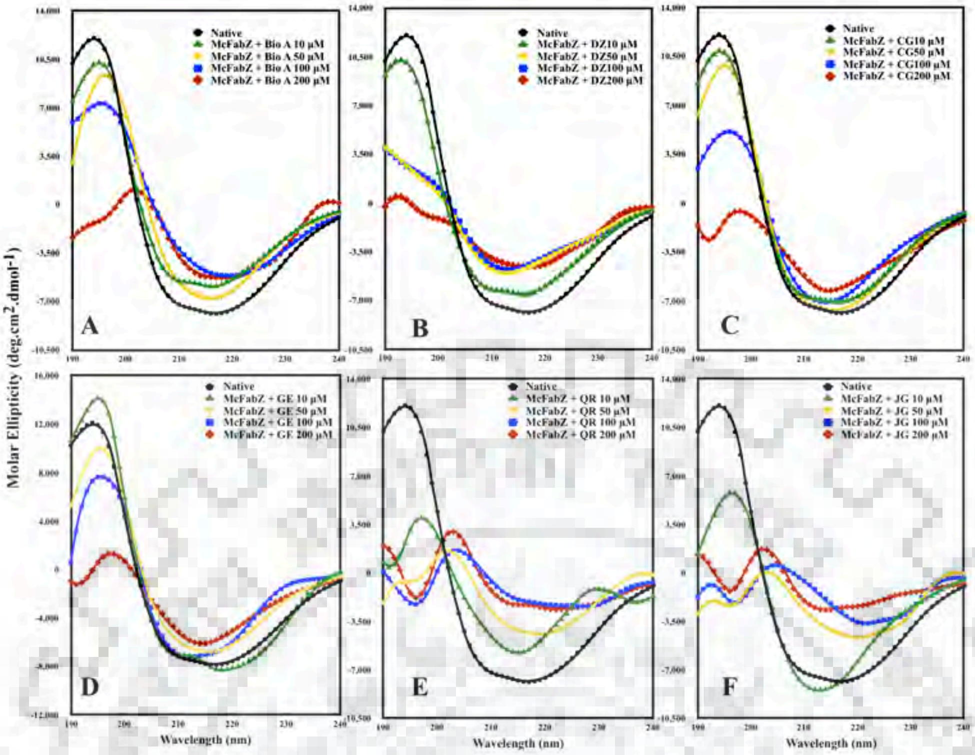

Figure 3.10 The far-UV CD spectra of McFabZ in the presence of different inhibitors. The far-UV CD Spectra were recorded at different concentration of inhibitors. Binding of these inhibitors leads to changes in the CD spectra of McFabZ. Decrease in the helical and the sheet content evident by diminished ellipticity at characteristic peaks (208 nm, 222 nm and 195 nm) were observed upon inhibitors binding.

Relative changes in the near-UV CD spectra of McFabZ in presence of different concentration of inhibitors have been shown in Figure 3.11A-3.11F. Overall, all the inhibitors binding leads to changes in tertiary structure of McFabZ protein as evident from the Figure 3.11. An increase in the ligand concentration leads to changes in near-UV spectra arises of all three aromatic amino acids (Phe, Tyr and Trp). Biochanin A and Genistein binding have produced a similar kind of effect on near-UV spectra. Daidzein has affected more Phe (255nm -270 nm) and Tyr regions (275 nm-282 nm). Catechin gallate has shown more effects in phe and trp (290 nm-305 nm) regions. Altogether we can say that a regular decrease in MRE at 280nm is observed upon inhibitors binding. Alternations in MRE towards more negative value corresponds to more flexibility of Tyrosine residues, while in case of substrate binding MRE value at 280nm increased towards positive value which corresponds to reduced flexibility of tyrosine residues. The higher substrate and inhibitor concentration leads to structural destabilization evidenced by notable loss of ellipticity in the far-UV CD spectra and changes in tertairy structure as evident in the near-UV CD spectra.

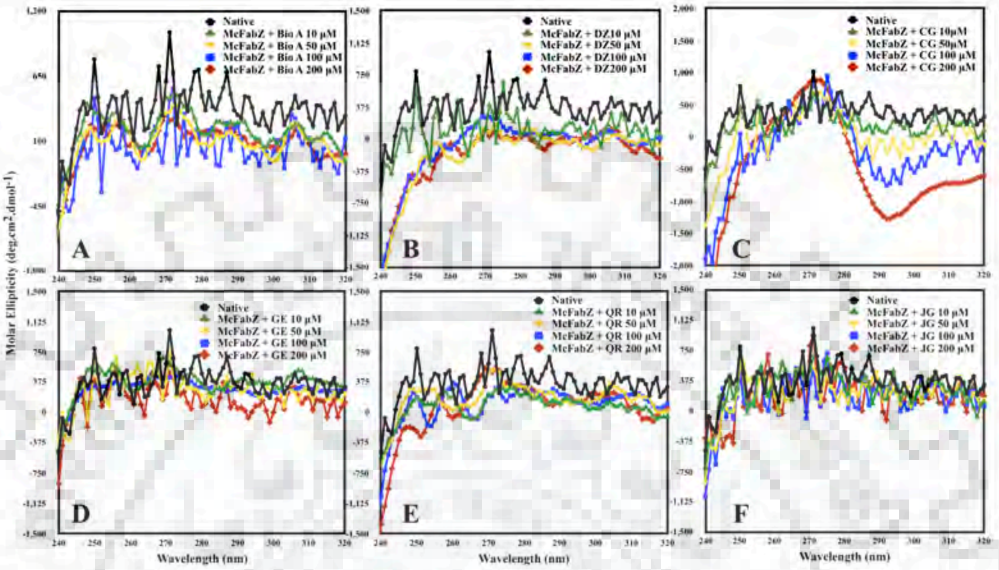

Figure 3.11 The near-UV CD spectra of McFabZ in presence of different inhibitors. The near-UV CD Spectra were recorded at different concentration of inhibitors. Binding of these inhibitors leads to changes in the tertiary structure of McFabZ.

Table 3.2 Predicted Secondary Structures* of McFabZ in presence of substrate (crotonyl-CoA) and different inhibitors.

Ligand (μM)	α-helices (%)	β- sheets (%)	Turns (%)	Random coils (%)
Crotonyl-CoA				
10	20.7	28.9	19.9	30.5
50	20.3	28.3	19.9	31.5
100	9.0	24.6	20.0	36.5
200	10.2	32.8	8.4	38.7
Biochanin A				
10	21.8	24.5	19.7	34.1
50	18.5	28.9	19.3	33.2
100	11.7	37.0	18.7	32.5
200	3.3	38.3	18.2	40.2
Genistein				
10	24.4	29.1	19.4	30.0
50	24.7	20.9	20.0	34.7
100	20.4	25.6	18.8	36.1
200	13.5	29.1	15.3	42.0

Daidzein				
10	19.3	25.9	18.7	36.2
50	14.6	24.3	17.4	43.7
100	12.4	27.3	17.5	42.9
200	12.3	22.3	18.4	48.1
Juglone				
10	21.3	23.1	19.1	36.4
50	13.9	21.0	16.5	48.5
100	11.8	18.3	14.4	40.5
200	7.8	17.4	13.9	41.9
Catechin gallate				
10	21.9	25.0	18.8	34.3
50	20.2	22.9	18.8	38.1
100	16.7	19.8	23.0	40.5
200	8.3	30.1	19.8	41.9
Quercetin				
10	13.9	31.6	16.9	37.5
50	12.0	27.7	14.8	45.5
100	15.2	24.0	13.5	47.3
200	5.4	30.1	10.2	54.4

***** The secondary structures content has been determined using CONTIN method using dichroweb server. The values shown here are the average of triplicates.

3.3.6. Molecular Modeling

The crystal structure of YpFabZ (PDB ID: 5BUX) was chosen as the best template available to build a 3D model of McFabZ (sequence identity 46.48 %) using homology modeling. Various tools have been used to validate the predicted 3D model. Table 3.3 shows the assessment of built 3D model using various validation tools. The secondary structure elements as predicted by PSIPRED [221] presented a good correlation with the built 3D model. The backbone dihedral angle analysis has been performed by the Ramachandran plot of PROCHECK [222] and results revealed that 99.8 % residues are within the allowed regions (Table 3.3). The Overall G factor of McFabZ model is -0.17 where the value >-0.5 indicates a good model [223]. Verify 3D [224] analysis of McFabZ model revealed that 92.41% of the residues had an averaged 3D-1D score >= 0.2. ERRAT [225] analysis gives the overall quality factor value 93.67, where good resolution structures always give value 95% or higher value. Z score predicted by PROSA server gives the value that lies within the range of scores normally found for native structures determined by NMR and X ray crystallography. LG score and MaxSub score predicted by ProQ server revealed the good quality of McFabZ. All of these validation tools suggested that the proposed 3-D model of McFabZ protein could be accepted with high confidence. Structural similarity analysis has been performed via global structure match using TM align algorithm. In this case

TM - scores of McFabZ model with other structural analogs were found to be more than 0.8, which explained the higher level of structural conservation between a McFabZ model with other related proteins.

Table 3.3 Assessment of predicted 3D model of McFabZ

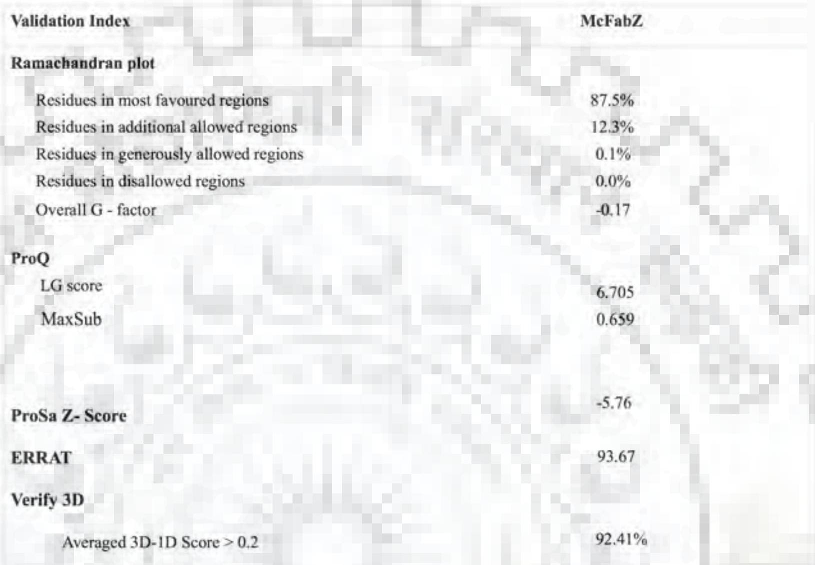

Validation Index	McFabZ
Ramachandran plot	
Residues in most favoured regions	87.5%
Residues in additional allowed regions	12.3%
Residues in generously allowed regions	0.1%
Residues in disallowed regions	0.0%
Overall G - factor	-0.17
ProQ	
LG score	6.705
MaxSub	0.659
ProSa Z- Score	-5.76
ERRAT	93.67
Verify 3D	
Averaged 3D-1D Score > 0.2	92.41%

3.3.6.1. Overall Structure and comparison

The monomeric McFabZ structure adopts typical β + α hot dog fold which is characteristic to the dehydratase family [226] where six anti parallel β sheets (β1, β2, β3, β4, β5 and β6) wrap around a central helix (α3). In addition, there is a presence of two helices α1 and α2. α1 is present at the N terminal end, while α2 is present between β2 sheet and alpha α3 helix (Figure 3.12A). The dimeric structure of McFabZ is similar to other reported FabZ structures [92,104,106].

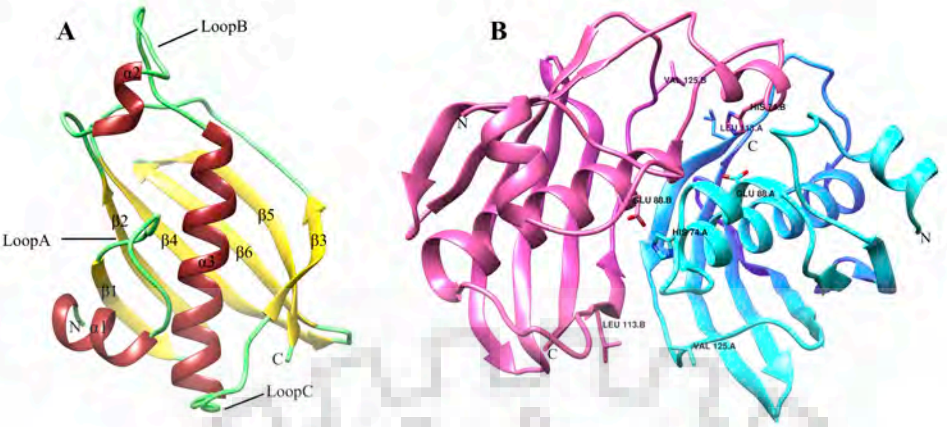

Figure 3.12 Structure of McFabZ.

(A) Ribbon diagram of McFabZ monomer with α- helices in red, β- sheets in yellow and loop regions in green. **(B)** Ribbon diagram of dimeric McFabZ with locations of two individual active sites. Key catalytic residues (His74 and Glu88*) and gatekeeper residues (Val125 and Leu113*) have been shown in stick representation.

The driving force that drives the dimeric assembly of McFabZ is hydrogen bonding between the residues from two β3 strands. The association of two monomers along the groove of β3 stands leads to the formation of 12 stranded anti parallel-extended β sheet. The central α3 helices of both monomers are oriented opposite to each other. The dimeric assembly is further stabilized by hydrophobic interaction in the central α3 helices. The substrate-binding tunnel is formed at the interface of both monomers. Therefore, each dimeric assembly harbours two active sites (Figure 3.12B).

Multiple sequence alignment (MSA) of the McFabZ protein with other model organisms has been performed using T Coffee server [40]. Figure 3.11 shows the MSA profile of McFabZ with PfFabZ (*Plasmodium falciparum*), HpFabZ (*Helicobacter pylori*), CjFabZ (*Campylobacter jejuni*), YpFabZ (*Yersinia pestis*), NmFabZ (*Nessiera meningitis*), EcFabZ (*E.coli*), PaFabZ (*Pseudomonas aeruginosa*). McFabZ share 46.4%, 47.9%, 43.3%, 46%, 53%, 43.2% sequence identity with YpFabZ, NmFabZ, HpFabZ, PfFabZ, PaFabZ and CjFabZ respectively. MSA results show that FabZ gene is quite conserved. The active site residues His and Glu are strictly conserved in all homologs. Conserved regions have been shown in blocks (Figure 3.13).

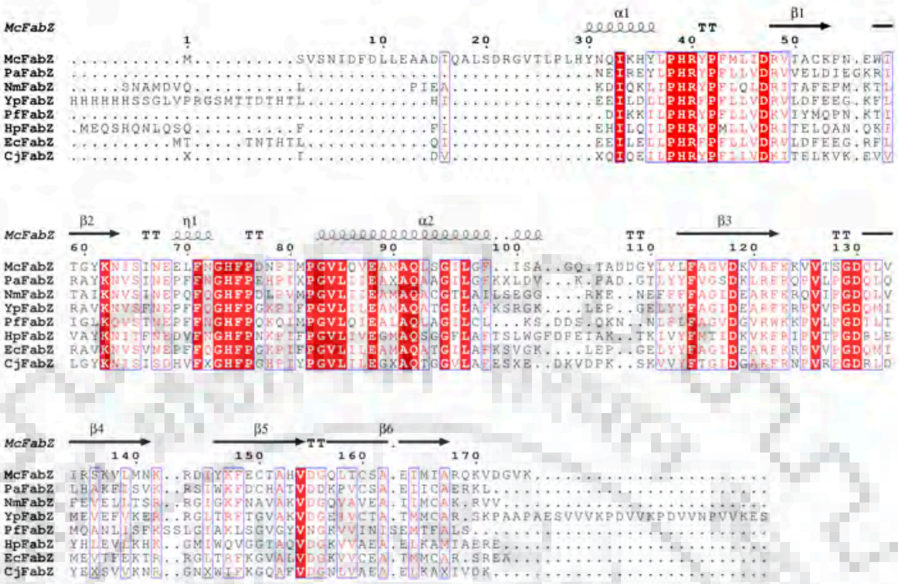
McFabZ
α1
TT
β1
β2
η1
α2
β3
β4
β5
β6
McFabZ
PaFabZ
NmFabZ
YpFabZ
PfFabZ
HpFabZ
EcFabZ
CjFabZ

Figure 3.13 Structure based sequence alignment of FabZ.

Multiple sequence alignment of McFabZ with PfFabZ, HpFabZ, CjFabZ, NmFabZ, EcFabZ, YpFabZ and PaFabZ. FabZ gene was highly conserved in all homologs. Catalytic residues (His and Glu) were strictly conserved in all homologs. Conserved regions are shown in Red blocks. The alignment was performed using ESPript 3 software.

Five key conserved motifs (PHRYPFLLXD, GHFP, PGVL, EAXAQ and PGD) were found as shown in Figure 3.11. Phylogenetic analysis has been performed using Phylogeny-PhyML online tool [227]. Figure 3.14 shows the phylogenetic tree of McFabZ with other model organisms. McFabZ gene is closely related to PaFabZ and PfFabZ gene as compared to other organisms.

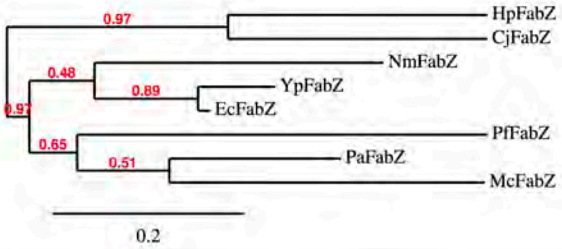

Figure 3.14 Phylogenetic analysis of McFabZ

Among these homologs, HpFabZ [186,228], PaFabZ [92], CjFabZ [188], NmFabZ [PDB: 4I83] and YpFabZ [106] have hexameric structures. PfFabZ [183,189] exists in both dimeric and hexameric forms. The hexameric assembly in these homologs is formed by the interaction of three dimers through hydrogen bonding and hydrophobic interactions. The residues which play important role in the formation of hexamer as reported in HpFabZ [186] are Tyr100, Thr49, Asp31, Lys46, Phe50, Ile14, Leu18, and Leu28. However, when these residues compared with the residues of McFabZ and PfFabZ some changes were observed. Tyr100 is replaced by Leu113 and Leu170 in McFabZ and PfFabZ respectively. Also, Thr49, Phe50, Leu18, and Leu28 residues of HpFabZ are replaced by Ser65, Ile66, Lys34, and Met44 residues in McFabZ. The variations in these residues in different bacterial species may be responsible for the existence of FabZ protein in dimeric or hexameric forms. The cartoon diagram showing the superimposition of these homologs with McFabZ structure has been shown in Figure 3.15. RMSD values varied from 0.174 (YpFabZ) to 1.83 (PaFabZ) when Cα positions of the dimeric McFabZ structure were superimposed on these homologs which suggested that overall fold of FabZ in conserved in all homologs. Substantial changes observed in loop regions (loop A, loopB and loopC) especially in loopC, where extra alpha helix is present in HpFabZ (Figure 3.15).

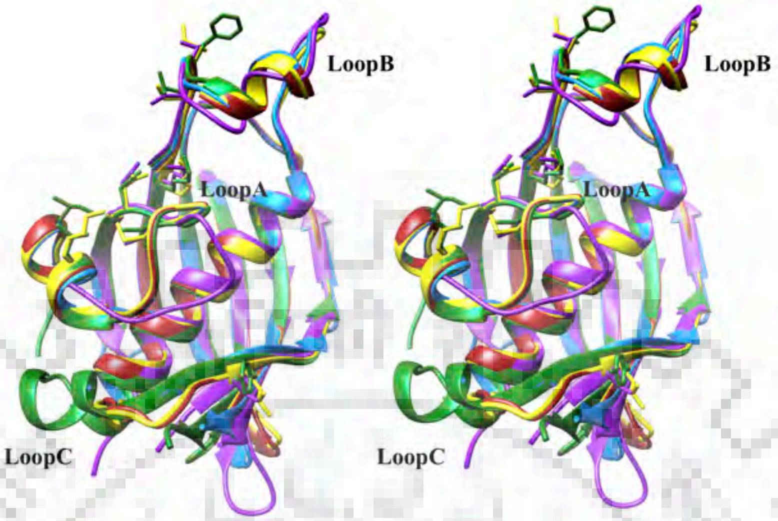

Figure 3.15 Overall structural similarities of McFabZ with related homologs.
(A) Comparative cartoon stereo diagrams of superimposition of McFabZ (yellow) with HpFabZ (green), PaFabZ (blue), PfFabZ (purple) and YpFabZ (red) structures. The key residues, which govern the oligomeric state, are shown in stick representation. The structural fold of FabZ is highly conserved in all homologs. For better presentation and comparison only monomeric structures of homologs have been superimposed.

3.3.6.2 Active Site analysis

Based on the active site analysis of other reported crystal structures, McFabZ active site was defined. The binding tunnel consists of residues His74, Phe75, Pro76, Ile80, Met81, Pro82, Gly83, Gln86, Phe122, Lys123, Lys124, Val125 and Val126 from one subunit and Leu37, His39, Glu88, Ala91, Gln92, Gly95, Phe99, Tyr110, Leu111, Tyr112, Leu113, Phe114, Ala115 and Ile166 from another subunit. These residues are mostly present in the loop region between α2 and α3, central helix α3 and β3, are well conserved. Inside the tunnel region, the conserved His74 and Glu88 residues form catalytic site. These residues are contributed by opposing monomer with His74*(* indicate residue from another dimeric subunit). His74* is coming from loop region between α2 helix and central α3 helix while Glu88 is present in α3 region on another monomer. The substrate-binding tunnel is largely dominant by the presence of hydrophobic residues except catalytic residues. Deeper into the tunnel after the catalytic site, tunnel narrows down and follows the path of α3 helix and passing through Tyr 112 and ending at Phe99 (Figure 3.16A).

Significant changes in key residues have been observed. Val125 is present at the entrance of active site on one side opposed by Leu113 on opposite side. When structurally aligned Leu113 occupies the same position as Leu170 in PfFabZ [104], while Tyr92 and Tyr100, is present in YpFabZ [106] and HpFabZ [186] respectively. Both these residues (Val125 and Leu113) are located to act as entrance gatekeeper residues. From the structural analysis of PfFabZ and HpFabZ, two separate residues have been proposed as potential exist gate residues, which either adopt an open conformation or closed conformation. For PfFabZ this residue is Phe169, which corresponds to Tyr112 of McFabZ while in case of HpFabZ this residue is Phe83, which corresponds to Phe99 of McFabZ (Figures 3.16B).

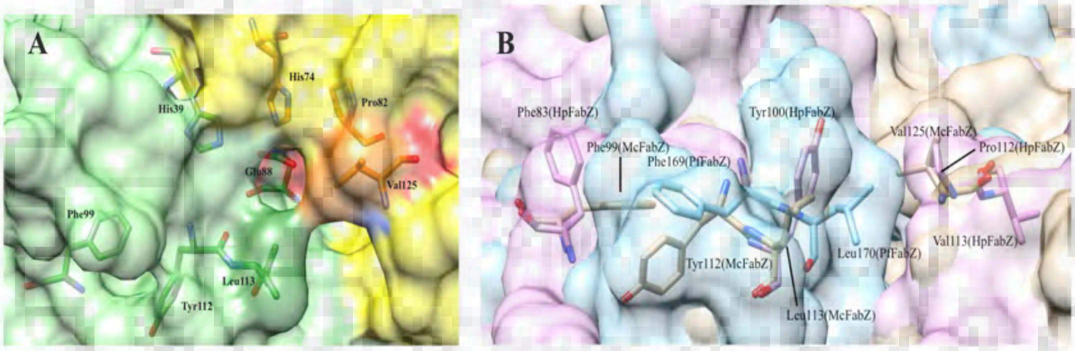

Figure 3.16 Active site analysis.

(A) Surface representation active site and entrance tunnel region McFabZ with key residues shown in stick representation. Active site residues (His74, Pro82, His39*and Glu88*), gate keeper residues (Val125 and Leu113*) and potential exist residues (Tyr112 and Phe88) have been shown in stick representation. (B) Superimposition of potential gate keeper and exist residues in different homologs.

3.3.7. Intrinsic Fluorescence Measurements

Fluorescence measurements were carried out to investigate how aromatic amino acids environment is affected upon ligand binding. Fluorescence spectroscopy is a highly sensitive technique used to observe the aromatic amino acids interactions and can provide the useful information regarding the orientation of residue of interest (buried or exposed) with in the tertiary structure of proteins [229–232]. Fluorescence spectra of native McFabZ protein showed emission at λ_{max} 351nm, which is characteristic to tryptophan. In general, fluorescence emission assigned to Trp residues buried in hydrophobic environment $\lambda_{max} < 330$ nm, while proteins with Trp residues exposed in a polar environment shows emission at $\lambda_{max} > 330$ nm. This shows that in McFabZ protein Trp residue is exposed in polar environment.

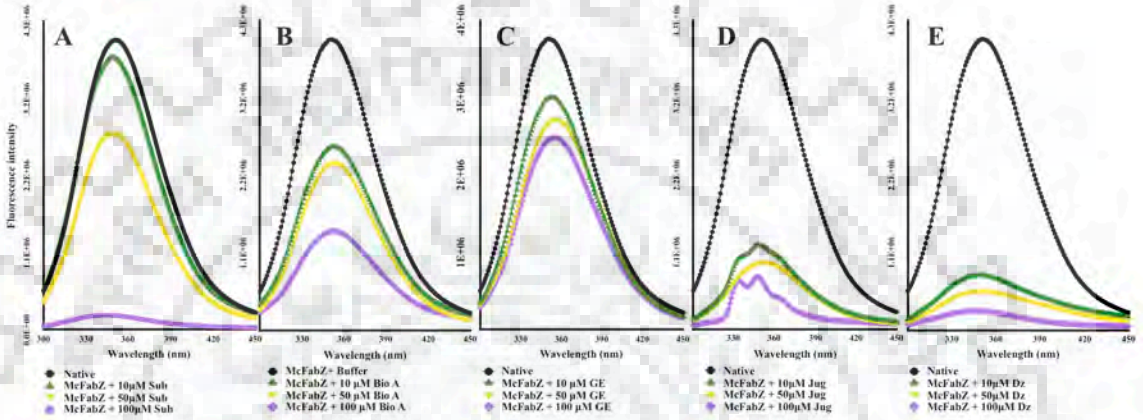

Figure 3.17 Intrinsic fluorescence spectra of McFabZ in presence of different ligands. The emission spectra of McFabZ in native condition as well as in presence of different ligands' concentrations. The changes in the emission spectra as evidenced by a loss of fluorescence intensity were observed during the ligands binding.

Figure 3.17 shows the fluorescence emission spectra of McFabZ in native condition and in presence of different ligands. In presence of crotonyl-CoA, decrease in fluorescence intensity and blue shift in emission λ_{max} was observed. λ_{max} emission shifted to 343 nm, 349 nm and 348 nm as shown in Figure 3.17A. Biochanin A and Genistein showed similar kind of effect on McFabZ fluorescence. In both cases, the fluorescence intensity decreased when compared to native spectra, while red shift is observed in λ_{max} emission (Figure 3.17B & 3.17C). In case of juglone and daidzein blue shift is observed (Figure 3.17D & 3.17E). Overall we can say that ligand binding to McFabZ protein leads to decrease in fluorescence intensity and formation of ligand-protein complexes.

3.3.8. Thermodynamic analysis of binding of inhibitors to McFabZ

The binding of McFabZ protein with different inhibitors was studied using Isothermal Titration Calorimetry (ITC). The compounds used for titration against McFabZ were genistein, biochanin A, daidzein, juglone, myricetin and quercetin. ITC data obtained was solved using one site model analysis program of Origin7. Thermodynamic parameters - Enthalpy change (ΔH), Entropy change (ΔS), Gibbs free energy (ΔG) and Equilibrium dissociation constant (K_D) have been calculated. Table 3.4 shows the thermodynamic parameters of binding.

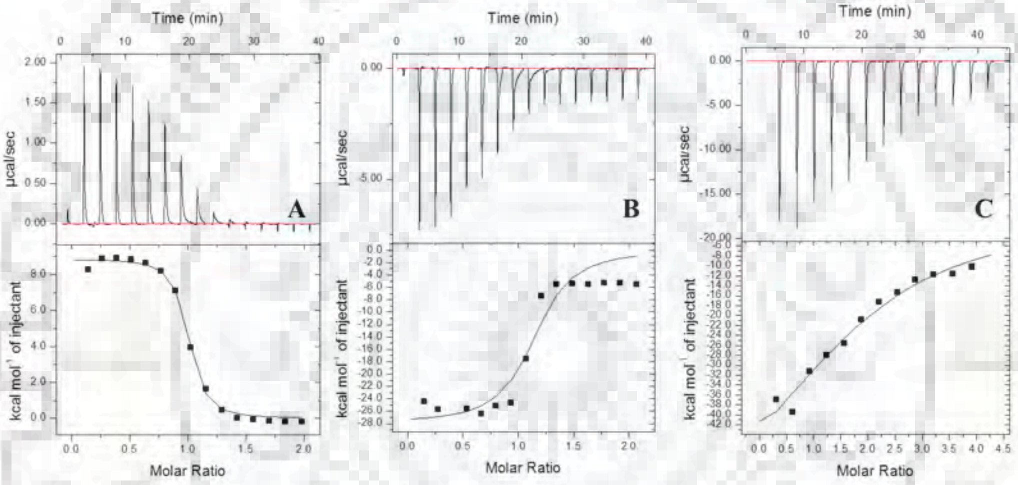

Figure 3.16. ITC studies of inhibitors binding.

ITC titration data describing the binding of biochanin A (A), daidzein (B), juglone (C), genistein (D), quercetin (E), and myricetin (F) with McFabZ. Data is fitted using one site model analysis using Origin 7.0. Upper part of each panel shows the thermogram (thermal power Vs time) after baseline correction while lower part of each panel is binding isotherm (normalized heat vs molar ratio of reactants). Binding of biochanin A to McFabZ is endothermic reaction, driven by entropy (A). Binding of daidzein (B), juglone (C), genistein (D), quercetin (E), and myricetin (F) to McFabZ is enthalpy driven exothermic reaction.

A clear 1:1 stoichiometric binding was observed in all cases except myricetin (N= 1.90 ± 0.293). Downward trends in the ITC profile (Figure 3.18) reveal an exothermic profile of the reaction, while upward trends correspond to the endothermic nature of the reaction.

Reaction of biochanin A with McFabZ is endothermic in nature while with other compounds, are exothermic in nature. Reaction of biochanin A with McFabZ is entropy driven ($\Delta S>0$) while reaction of other remaining five compounds is enthalpy driven ($\Delta H<0$).

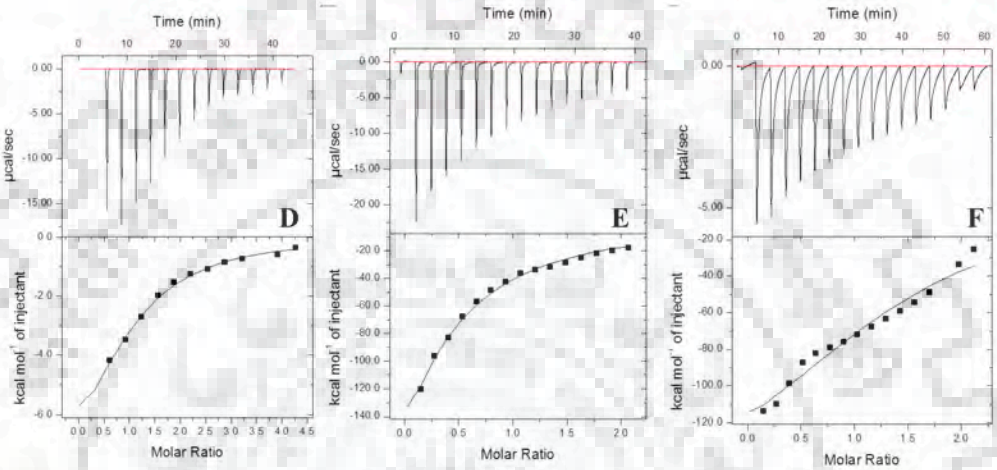

Figure 3.18 ITC studies of inhibitors binding (continued).

The Gibbs free energy for all reactions has negative value ($\Delta G<0$), which confirmed the spontaneous nature of all the reactions. The corresponding binding interactions were in micro molar (µM) range as evident from equilibrium dissociation constant (K_D) value. Daidzein, biochanin A, genistein and juglone have a K_D value of 2.47 µM, 0.5 µM, 71.0 µM and 85.0 µM respectively.

Biochanin A and daidzein have a strong binding affinity over other compounds. Biochanin A is binding 4.94x, 142x and 170x stronger than daidzein, genistein and juglone respectively. Figure 3.18 shows the thermogram and the fitting curve of biochanin A, genistein, daidzein and juglone.

Table 3.4 Thermodynamic parameters determined using ITC based assays

Compound	**Enthalpy change (cal/mol)**	**Entropy change (cal/mol/degree)**	**Free energy change (cal/mol)**	**Dissociation constant (K_D), μM**	**N (No.of binding sites)**
Genistein	-1.032×10^4	-20.4	-4.2×10^3	71.0	0.956±0.151
Biochanin A	8.868×10^3	58.6	-8.5×10^3	0.5	0.954±0.007
Juglone	-2.25×10^5	-728	-9.0×10^3	85.47	0.925±0.154
Daidzein	-2.79×10^4	-68.0	-7.64×10^3	2.5	1.12±0.0561
Quercetin	-9.95×10^4	-303.0	-9.2×10^3	143.47	1.11±0.0046
Myricetin	-6.795×10^4	-210	-5.37×10^3	122	1.90±0.293

3.3.9. Molecular docking studies

In order to study the binding mode of different inhibitors with McFabZ protein, docking calculations were performed using autodock and autogrid from ADT tools. These eight inhibitors biochanin A, genistein, juglone, epicatechin gallate, quercetin, daidzein, fisetin, and myricetin have been docked into the active site of McFabZ. Table 3.5 shows the binding energy and binding constant calculated by ADT tools.

3.3.9.1. ***Biochanin A docking Study.*** Docking analysis suggested that biochanin A adopts a binding pose spanning the tunnel interacting with key residues via hydrogen bonding and hydrophobic interactions. Gly83 and Phe114* residues are involved in hydrogen bonding with biochanin A, while residues His74, Pro82, Val125, Met81, Gly83, Glu88*, Gln92*, His39*, Gly95*, Ala91*, Phe114*, Tyr112* and Leu113* are involved in hydrophobic interaction with this inhibitor. Methoxy benzene moiety of biochanin A is buried deep inside the tunnel and interacting with Ala91* and Phe114* via hydrophobic interactions. Three hydrogen bonds are formed as follows: 1) 5- hydroxyl group of biochanin A with NH group of Phe114*. 2) 4- Oxo group with NH group of Phe114*. 3) Oxygen of pyran ring with NH of Gly83. The predicted binding energy and affinity of biochanin A is -7.49 kcal mol^{-1} and 3.24 µM respectively.

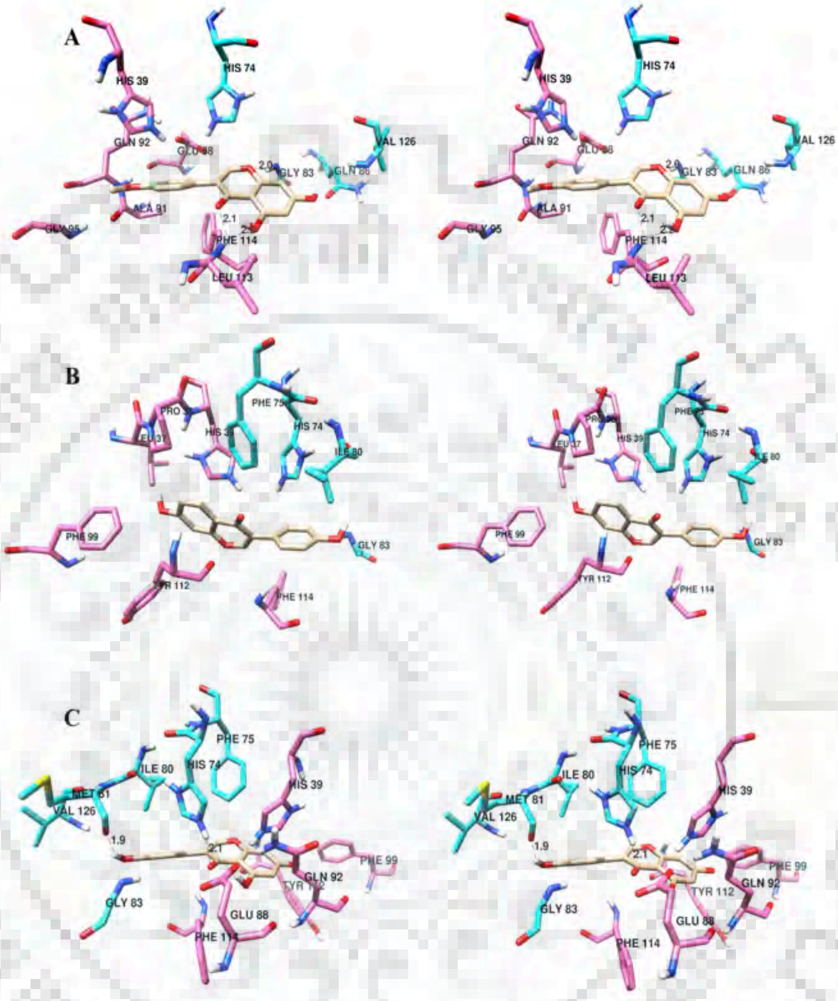
A
HIS 39
HIS 74
GLN 92
GLU 88
VAL 126
2.0
GLY 83
GLN 86
ALA 91
2.1
2.1
GLN 95
PHE 114
LEU 113
B
PHE 75
PRO 38
HIS 39
LEU 37
HIS 74
ILE 80
PHE 99
GLY 83
TYR 112
PHE 114
C
PHE 75
ILE 80
HIS 74
HIS 39
MET 81
VAL 126
1.9
2.1
PHE 99
GLN 92
TYR 112
GLY 83
GLU 88
PHE 114

Figure 3.19. Molecular docking based studies.

Stereo images showing the interactions of biochanin A (A), daidzein (B), genistein (C), juglone (D), quercetin (E) and catechin gallate (F) with McFabZ. Interacting residues of both chains are shown as sticks and colored as cyan (chain A) and hot pink (chain B). Hydrogen bonds are labeled and shown as black dash lines. Docked inhibitors are shown in tan color.

3.3.9.2 ***Genistein docking Study.*** The predicted binding location of genistein is similar to that of biochanin A but in opposite orientation of the benzene ring. It’s found in the substrate-binding tunnel interacting with catalytic residues. Genistein has a hydroxyl benzyl moiety instead of methoxy benzyl, which makes this molecule more polar than biochaninA. The hydroxyl benzene moiety is interacting with His74, Pro82, Gly83, Met81 and Glu88. Polar and nonpolar interaction involved in the binding of genistein. Residues which are interacting with genistein hydrophobic-ally includes Met81, Pro82, Gly83, Ile80, Phe75, His74, Glu88*, Ala91*, His39*, Leu37*, Phe99*, Gly95* and Tyr112*. Oxo group of pyran ring making hydrogen bond with NH group of catalytic residue His74. Other Hydrogen bonding involved between the carboxyl group of Met81 with hydroxyl benzene moiety. The Predicted binding energy and affinity of genistein is -6.67 kcal mol^{-1} and 12.96 µM respectively.

3.3.9.3 ***Daidzein docking Study.*** The binding of daidzein to McFabZ is similar to that of genistein and largely dominated by hydrophobic interactions. Benzene rings of daidzein are buried inside the hydrophobic pocket of active site. Only one polar interaction involved between hydroxyl benzene moiety of daidzein with carboxyl group of Met81. Residues involved in non-polar interaction includes Met81, Pro82, Ile80, Gly 83, Phe 75, His74, His39*, Pro38*, Leu37*, Gly95*, Phe99*, Try112* and Phe114*. The predicted binding energy and affinity of daidzein is -6.98 kcal mol^{-1} and 7.61 µM respectively.

3.3.9.4 ***Juglone docking Study.*** Juglone is binding to the active site of McFabZ via polar and non-polar interactions. In the docked pose, juglone is making interactions with key residues. Two Oxo groups of the naphthalene ring are involved in hydrogen bonding interactions with His74 and Tyr112*. One polar interaction is present between the OH group with a carboxyl group of Glu88* residue. Other residues involved in hydrophobic interaction include His74, Phe75, Leu111*, His39*, Tyr112*, Glu88*, Ala91* and Gln92*. The predicted binding energy of juglone is -6.92 kcal mol^{-1}.

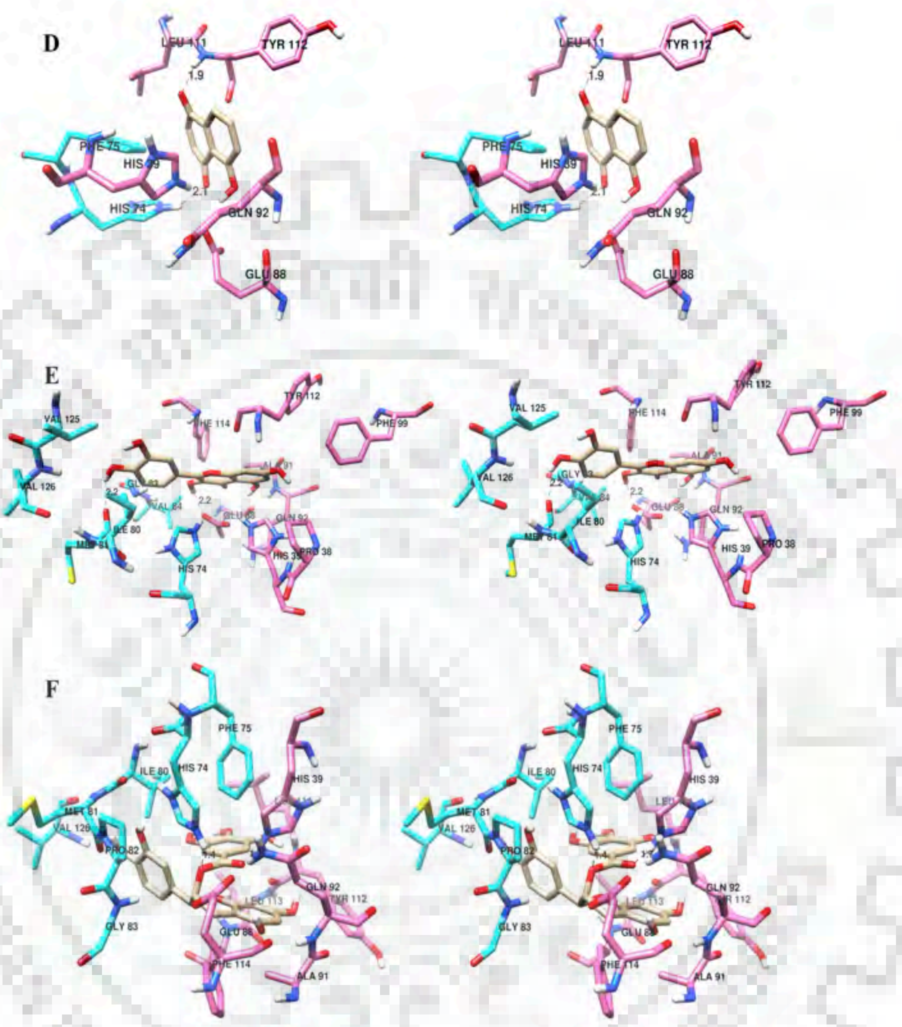
D
LEU 111
TYR 112
1.9
PHE 75
HIS 39
2.1
HIS 74
GLN 92
GLU 88
E
VAL 125
VAL 126
PHE 114
TYR 112
PHE 99
ALA 91
GLY 83
VAL 84
2.2
ILE 80
GLU 88
GLN 92
MET 81
HIS 74
HIS 39
PRO 38
F
PHE 75
ILE 80
HIS 74
HIS 39
MET 81
VAL 126
PRO 82
GLN 92
TYR 112
LEU 113
GLY 83
GLU 88
PHE 114
ALA 91

Figure 3.19. Molecular docking based studies (continued).

Besides this, the binding energy of other inhibitors (catechin gallate, quercetin, fisetin and myricetin) as given in Table 3.5 has values higher than above-mentioned inhibitors. Figure 3.19 shows the interactions of these different inhibitors with McFabZ.

Table 3.5 Binding energy and Binding constant calculated via auto dock

Compound Name	Binding energy (kcal/mol)	Binding constant (μM)
Genistein	-6.67	12.96
Myricetin	-3.94	1300
Biochanin A	-7.49	3.24
Daidzein	-6.98	7.61
Juglone	-6.92	8.4
Quercetin	-4.75	329
Catechin gallate	4.68	ND
Fisetin	-5.99	40.73

3.3.10. Molecular dynamics based simulation studies

The analysis of structural stability of three complexes of McFabZ with biochanin A, daidzein and genistein were provided by the assessment of the RMSD of Cα atoms during the MD simulation. The comparative RMSD plot of all complexes shown in Figure 3.20. Although, throughout the duration of MD simulations, the RMSD of all the complexes appeared to be stable, but genistein and daidzein complexes achieved the equilibrium early in comparison to biochanin A part. Also, for whole duration the RMSD for genistein and daidzein remain in range of 2.5 Å. The RMSD for biochanin A fluctuated at ~8 ns to 3.5 Å and then stabilized. The RMSD for genistein and daidzein were following the similar trend for most of the duration; however at 18 ns, the RMSD of daidzein jumped to 3 Å and stabilized. The RMSD for genistein was highly stable throughout the duration and exhibited highest structural stability among all three complexes.

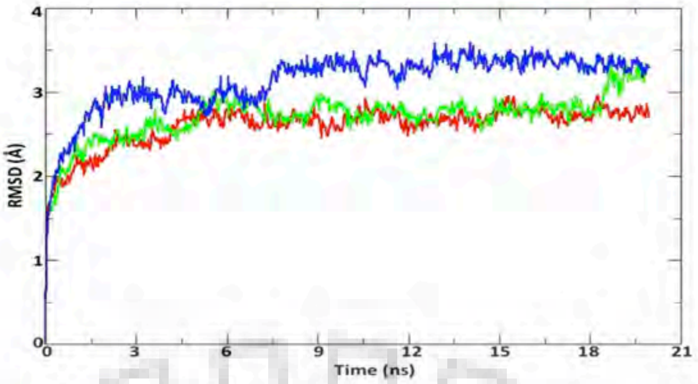

Figure 3.20 MD simulation studies.

RMSD values of the three inhibitors (genistein in red, daidzein in green and biochanin A in blue) in MD simulation.

3.3.11. Antibacterial activity assay

To assess the *in vivo* inhibitory efficacy of daidzein, genistein, biochaninA and juglone, growth inhibition assay (MIC) has been performed against *Moraxella catarrhalis, Bacillus subtilis and Pseudomonas sp.* microorganisms. MIC test was set up using a broth microdilution method in 96 wells microtiter plate. A MIC value for daidzein, genistein, biochanin A and juglone were determined and has been given in Table 3.6.

Table 3.6 Minimum inhibitory concentration (MIC) values of inhibitors tested against *M. catarrhalis, B. subtilis and Pseudomonas sp.*

Compounds	***M. catarrhalis***	***B. subtilis***	***Pseudomonas sp***
Biochanin A	32-50 µg/ml	16-32 µg/ml	8-16 µg/ml
Daidzein	16-20 µg/ml	20-30 µg/ml	16-32 µg/ml
Genistein	20-30 µg/ml	32-64 µg/ml	32-50 µg/ml
Juglone	16-32 µg/ml	8-16 µg/ml	4-8 µg/ml

3.4. Discussion

The emergence of drug resistance in bacterial pathogens ensures that there is a need to identify new chemical scaffolds that targets cellular processes. The type II FAS pathway will remain an important part of drug discovery because it's an essential pathway, and chances of cross-resistance to existing drugs, which target other pathways, will be minimum [80,94,96]. Natural compounds have been known to inhibit fatty acid biosynthesis pathway [190–192]. Till date, FabZ inhibitors for *Helicobacter pylori*[186,228], *Psueodomonas aeroginosa* [233], *Plasmodium falciparum* [104,189] and *Yersinia pestis* [106] have been known. In this study, FabZ from *Moraxella catarrhalis* pathogen has been characterized by biochemical, biophysical and *in silico* based studies. Based on inhibitory efficacy, we report three compounds biochanin A, daidzein and genistein belong to the class of flavonoids as inhibitors against FabZ.

3.4.1 Biochemical and stability aspects of McFabZ

Biochemical studies have demonstrated that activity of McFabZ is higher than other reported homologs. The k_{cat} was determined to 1.663 ± 0.06 S^{-1} for McFabZ while other homologs fall in the range of 0.013 to 1.45 S^{-1}. The reason for this discrepancy is not apparent, but it has been found that the high salt concentration (500 µM) in assay buffer inhibits the FabZ activity [145]. Gel filtration chromatography has shown that McFabZ is dimeric in solution. The most stable form of FabZ is hexameric assembley. In PfFabZ, hexameric state is more active than dimeric form. The transition from hexameric to dimeric form is triggered by low pH [183]. In McFabZ, a low pH leads to the conversion of an active dimeric state (at pH 6.0 – 8.0) to an inactive monomeric form. The gel filtration results are in agreement with biochemical findings where McFabZ is found to be catalytically inactive at pH 3.0. As the pH decreases two histidine residues (His74, His39*) in the active site of McFabZ become more positive which leads to the electrostatic repulsion between resulting in the expulsion from the active site. Glu88, in the active site becomes protonated and lesser negative, which will further contribute towards electrostatic repulsion. These changes further lead to disturbance in hydrogen bonding and hydrophobic interactions between the monomers, which will further lead to subunits dissociation. A lower activity at a higher salt concentration has also explained the same as higher salt leads to disturbance in hydrophobic interactions.

Thermal sensitivity of McFabZ is explained using CD analysis as melting temperature (T_M) was determined to be 42.5 ^{0}C and CD spectra of native protein changed with temperature. The characteristic broad minimum band, which represents the integrity of helical content, was present up to 40 ^{0}C but significant loss was observed beyond 40 ^{0}C. The biochemical experiments have also shown that around 50% loss in activity was observed at 40 ^{0}C. At 90 ^{0}C, it becomes completely inactive. The existence of the dimeric form in solution rather than stable hexameric form might be one more reason for its temperature sensitivity. Temperature stable hexameric HpFabZ [185] protein has higher T_M value and even showing 50% activity at 90 ^{0}C. The hexameric assembly in HpFabZ where three dimers interacts through hydrogen bonding and hydrophobic interactions, provide thermal stability to HpFabZ, while in McFabZ extent of H- bonds and hydrophobic interactions would be much lower than hexameric HpFabZ.

3.4.2 Inhibition mechanism and Structure activity relationship

Biochemical assay indicates that out of the eight compounds tested against McFabZ, biochanin A, daidzein, genisetin and juglone have good a IC_{50} range from 6.8 µM to 32.4 µM and the kinetic inhibition constant (K_i) value lie between 4.3 µM to 15.48 µM. Based upon the analysis of double reciprocal plots, inhibition mechanism of daidzein, biochanin A and genistein is found to be competitive suggesting that these compounds may interfere with the binding of substrate crotonyl-CoA, while juglone exhibited a mixed type of inhibition suggesting that it can bind either to the substrate binding site or interfere with the enzyme substrate complex. The inhibition study suggested that the binding affinity of daidzein (11.83 ± 1.99) is close to biochanin A (16.83 ± 3.59) while genistein (4.3 ± 0.62) has a strong affinity over these compounds. ITC provide valuable information on macromolecule- ligand interactions. ITC measures the heat change, i.e. heat absorbed or released (ΔH) when ligand bind to macromolecule. From the ITC data Table 3.4, it is evident that biochanin A and daidzein have a strong binding affinity as compare to other compounds. Both daidzein and biochanin A have comparable binding affinities for McFabZ but have different enthalpies and entropies suggesting different binding mechanisms. Binding signature plots of daidzein, biochanin A and genistein have been shown in Figure 3.21.

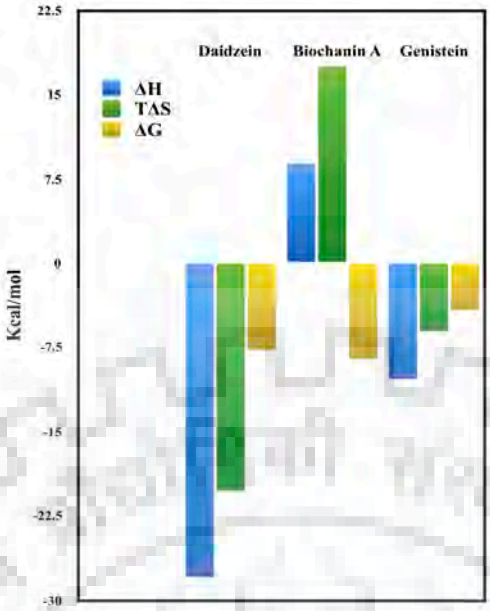

Figure 3.21 Thermodynamic Signatures.

Thermodynamic profile of the binding of daidzein, biochanin A and genistein with McFabZ based on ITC measurements. The measured parameters include the Gibbs free energy of binding (ΔG), the enthalpy change (ΔH) and the temperature dependent entropy change (TΔS).

As evident from docking positions, the presence of the methoxy group on benzene ring makes biochanin A more hydrophobic than daidzein and genistein. This makes binding of biochanin A to McFabZ is an endothermic process, while binding with others is an exothermic process. It shows that hydrophobic interaction plays a major role in binding of biochanin A to McFabZ, while with other compounds polar interactions are the main contributing factor.

CD studies have shown how binding of these inhibitors is affecting the stability and active conformation of McFabZ protein. The far-UV CD spectrum has become more distorted upon inhibitors binding. Overall significant changes in broad minimum (210-220 nm) and maximum bands (195 nm) have been observed. Loss of helical contents as evident by diminished ellipticity at 208 nm, 222 nm and 195 nm peaks (signature peaks of alpha helix). Similarly, the beta sheet content is also reduced as shown in Table 3.2. Significant changes in the near-UV CD spectra of McFabZ have been observed upon ligand binding. Lower substrate concentration (10 µM -100 µM) increases the flexibility of Tyr and Phe residues as evidenced by a decrease in MRE towards negative values at 262nm and 280nm respectively, while higher substrate (200 μM) leads to a reduction in the flexibility of these residues as evident by the increase in MRE towards positive values. Similarly, changes in tertiary structure upon inhibitors binding were also observed. An overall decrease in MRE at 262 nm, 280 nm and 290 nm towards negative values has been observed. This leads to increase in the flexibility of Phe, Tyr and Trp residues.

Based on these findings, it can be assumed that central alpha helix α3 participate in ligand binding and possesses structural plasticity. The ligand binding may be accompanied by the uncoiling or disordering of helix α3. This may also be the indicative of intermediate state of ligand bound enzyme with the secondary structural reorganization of central helix α3 and nearby sheets. These conformational changes observed in McFabZ secondary structure elements upon binding of these compounds influences its active site and physiological functions, making McFabZ catalytically inactive. Fluorescence spectroscopy complemented the outcomes observed via CD spectroscopy. Blue shift in λ_{max} value is observed in the binding of crotonyl-CoA, daidzein and juglone to McFabZ protein. These three ligands have changed the conformation of McFabZ and aromatic amino acids buried more towards hydrophobic pockets. While the red shift is observed upon the binding of biochanin A and genistein, which exposed the aromatic residues towards the polar environment. As the concentration of ligands increases, more loss of fluorescence intensity was observed, which shows the unfolding of protein takes place. Similarly, CD studies have shown as higher concentrations of ligands uncoiling of helices and sheet to random coils takes place.

The plausible interactions involved in the binding of inhibitors with McFabZ have been assessed using molecular docking based investigation. These inhibitors are channel blocker as they are found near the active site and making contacts with catalytic residues as shown in Figure 3.17. When we compared the binding poses of these four inhibitors with an emodin bound crystal structure of HpFabZ [228], biochanin A is sandwiched between two gatekeeper residues (Val125 and Leu113*) and Phe114. Emodin is sacked between Tyr100 and Pro112* in HpFabZ. Similarly, we compared the binding poses with other inhibitors. Genistein is interacting with tunnel residues linearly through hydrophobic interactions and residues involved are Phe99, Tyr112, Ile80*. So based upon comparison of binding poses, critical residues which are important for binding include gatekeeper residues (Val125 and Leu 113*), exist residues (Phe99 and Tyr112) and other tunnel residues (Phe114, Ile80* and Gly83*).

The structure of all these compounds suggests that the hydroxylation pattern of flavonoids may play an important role in the recognition process. Flavonoids have backbone consists of 2-phenyl-1,4-benzopyrone (flavone) and isoflavonoids are derived from 3-phenyl-1,4-benzopyrone (isoflavone) backbone. The difference in the hydroxyl group's position in backbone and number of hydroxyl groups affects the efficacy and affinity of these compounds. BiochaninA, diadzein and genistein are isoflavonoids with 2 to 3 OH groups on isoflavone backbone. These compounds have a strong affinity and good IC_{50} values over other flavonoids in consideration. Highly hydroxylated compounds like quercetin, myricetin, fisetin, epicatechin gallate (Figure 3.1) show the McFabZ inhibition but with lesser affinity. Genistein and daidzein have better K_i (4.3 μM and 11.83 μM respectively) and IC_{50} (6.85 μM and 7.48 μM respectively) values over biochainA (K_i: 16.83μM, IC_{50}: 29.7 μM), while biochanin A has good K_D value (0.5 μM) over genistein (71.0 μM) and daidzein (2.5 μM). The MD based simulations clearly indicate that the binding of biochanin A with McFabZ resulted in most conformational perturbations followed by daidzein and genistein. The MD simulation results are in agreement with the kinetic data, which favors genistein as best inhibitor candidate followed by daidzein and biochanin A. If we look at the structure of these three compounds (Figure 3.1), methoxy moiety makes biochanin A is more hydrophobic over daidzein and genistein, and this further helps in stabilizing the interactions further leads to good binding. Besides these flavonoids, Juglone which is 5-hydroxy-1,4-naphthalenedione has shown inhibition with IC_{50} value of 32.4 μM and good affinity with a dissociation constant (K_D) 85.0 μM. The binding energy and binding constant calculations of these polyphenols using Autodock is in agreement with the biochemical and the ITC data. Biochanin A, daidzein, genistein and juglone have a binding energy of -7.49 kcal mol^{-1}, -6.98 kcal mol^{-1}, -6.67 kcal mol^{-1} and -6.92 kcal mol^{-1} respectively, which is lesser than other compounds.

Since FabZ shares the similar active site architecture with its isoforms, it may be postulated that these inhibitors will show similar binding with them. To validate this assumption, we performed docking studies of FabA from *Pseudomonas aeruginsoa* [192] (PDB id: 5B0J) with three isoflavones (biochaninA, daidzein and genistein). As expected, these compounds exhibit the similar mode of binding with comparable binding affinities as in case of McFabZ. BiochaninA, daidzein and genistein have a binding energy of -8.25 kcal mol^{-1}, -8.79 kcal mol^{-1} and -7.99 kcal mol^{-1} respectively against FabA. These results indicate the possibility of these inhibitors to act as broad-spectrum antimicrobial agents. Here, we can say that among the class of polyphenols, compounds with isoflavone backbone and a less number of hydroxyl groups will give good inhibition, high affinity and selectivity. Taken together, this data explains that scaffolds of daidzein, biochanin A, genistein and juglone all are good starting points for inhibitor design against FabZ variants.

3.5. Conclusion

In summary, we have presented the biochemical and biophysical characterization of FabZ from *Moraxella catarrhalis*. Additionally, we have reported three isoflavonoids (daidzein, biochaninA and genistein) as novel potent inhibitors against FabZ. In general isoflaovonids show less toxicity towards humans and can accumulate in human plasma up to 8μM concentration [234]. Based upon this study, these compounds represent class of plant secondary metabolites with potent antibacterial activity via inhibiting FASII pathway. Altogether we can say that these compounds represent an interesting class of chemical scaffolds, which needs further development to improve the pharmacokinetic profiles and selectivity against bacterial pathogens. Lastly, comparing the strength of different FabZ inhibitors, we have categorized the more selective and potent inhibitor scaffold. In total we expect this study will help in the development of more potent FabZ inhibitors in the future.

3.6 Future prospects

In this study, we have shown the scaffold of biochanin A, genistein, daidzein and juglone are potent inhibitors of McFabZ. In order to develop the potent inhibitors of FabZ with binding of nanomolar range, different derivatives of these four compounds can be made in future and compared with the parent scaffold. Also, effect of these compounds on human cell lines can also be explored to further develop the lead candidates based upon these compounds.

भारतीय प्रौद्योगिकी संस्थान रुड़की
INDIAN INSTITUTE OF TECHNOLOGY ROORKEE

Chapter 4

Biochemical, Biophysical and structural characterization of FabD from *Moraxella catarrhalis*

Chapter 4

4.1 Introduction

Fatty acids, being essential components of cell membrane and possess vital biological functions, are synthesized by a complex, elegant and essential biosynthetic machinery. The biosynthesis of fatty acid is an important pathway for the survival of living beings. In nature, fatty acid biosynthesis (FAS) is evolved into two types, type I (FAS I) and type II (FAS II). The type I system exists in mammals, where all the reactions are carried out at active sites situated on the single polypeptide chain with eight distinct domains[79,80,94]. Bacteria and plants synthesize fatty acids via type II system, where the group of structurally dissociated enzymes carries out the reactions. Due to the large differences in the subcellular organization of the components of both systems, the type II fatty acid biosynthetic pathway has been considered an attractive target for the development of novel antibacterial agents. Additionally, the higher level of conservation among the different enzymes involved in FAS II pathway makes it a suitable pathway for the development of broad-spectrum antibiotics[75,105,235].

Malonyl-CoA:acyl carrier protein transacylase (FabD) is an important enzyme in type II FAS pathway and performs the initiation reaction, which involves the transfer of malonyl moiety from malonyl-CoA to holo-ACP forming malonyl-ACP, which is the key building element in FAS II pathway[75,235,236]. Additionally, FabD plays a vital role in the synthesis of aromatic polyketides [236]. The research has shown that FabD is an important enzyme for the synthesis of fatty acids and inhibition or genetic inactivation of FabD gene is lethal in microbes[81,236–240]. Therefore, it has become a good promising target for the development of antibiotics. However, it has been argued earlier[241] and also a recent report on *Staphylococcus aureus* has suggested that this bacteria can become resistant to FAS II inhibitors in presence of exogenous fatty acids with a high frequency of mutation in FabD gene[242,243]. But such kind of resistance against FAS II inhibitors for other pathogens has been remained elusive, which holds the possibility of developing new antibiotics by targeting FAS II pathway.

To date, FabD enzyme has been characterized from several species such as *E.coli*[244] (EcFabD), *Streptomyces coelicolor*[245] (ScFabD), *Staphylococcus aureus*[237] (SaFabD), *Plasmodium falciparum*[246] (PfFabD), *Helicobacter* *pylori*[97,235] (HpFabD) and *Mycobacterium tuberculosis*[247] (MtFabD). The solved crystal structures include EcFabD (1MLA[248]), ScFabD (1NM2[249]), HpFabD (2H1Y[235]), SaFabD (3IM9[237])and MtFabD (2QC3[236]). Overall, FabD shares similar architecture and composed of two subdomains. One domain consists of 12 helices and four-stranded parallel β- sheets, while another domain has two helices and four-stranded antiparallel β- sheets. It has been found that FabD performs malonyl transfer via a ping-pong mechanism with His and Ser at the catalytic site. Such kind of mechanism is commonly found in serine dependent acyl hydrolases[249]. In *Mycobacterium tuberculosis*, mechanism of FabD reaction differs from the other homologs as there is a difference in the orientation of Ser residue of active site which leads to overall changes in the active site[236]. The FabD protein has two motifs related to its biological activity. One is the catalytic site, which is located in the deep between two subdomains, while the second motif is ACP binding site, which is present on the surface of FabD enzyme. The interaction of FabD with ACP has been demonstrated computationally in *H. pylori*[235]. Till now, one natural inhibitor corytuberine has been discovered to inhibit HpFabD[97] with IC_{50} value 33.1± 3.29 μM. Aporphine alkaloids are naturally occurring chemical compounds found in plants and known to exhibit various biological activities as antioxidant, antiviral, anticancer, analgesic, diuretic etc. The activities and chemical nature of these alkaloids are structure dependent and governed by the degree of hydroxylation, presence of different constituents, groups, etc [250,251].

In this study, we have characterized FabD from drug-resistant gram-negative pathogen *Moraxella catarrhalis*, which is a most common bacterial pathogen of respiratory tract after *Streptococcus pneumoniae* and *Haemophilis infuenzae*[171,252]. Additionally, we have checked the binding of McFabD with the compounds from the class of aporphine alkaloids and inhibitor (Iodoacetamide)[88,253]. Biohemical characterization of McFabD and inhibitory activities of these alkaloids against McFabD have been determined using spectrophotometric based biochemical assays. Binding studies have been performed using spectroscopic methods (circular dichroism, fluorescence, and UV-visible) and thermodynamic (ITC) based assays. These are widely accepted and scientifically validated techniques used to probe the protein-ligand interactions and to explore the qualitative and quantitative measures of molecular binding. Molecular modeling and docking studies have been performed to see how these compounds are interacting with McFabD protein. The growth inhibition assay has been performed to calculate the minimum inhibitory concentration (MIC). Therefore, the current study suggests that aporphine alkaloids can act as potential antibacterial agents targeting FabD and could be helpful for the development of new chemical scaffolds against bacterial pathogens.

4.2. Experimental

4.2.1 Materials

Moraxella catarrhalis strain MTCC No.445 (equivalent to ATCC 8176) was procured from the Microbial Type Culture Collection, Chandigarh. All enzymes used in molecular cloning were purchased from New England Bio Labs. Plasmid isolation, purification of PCR products and gel extraction procedures were carried out using Qiagen kits. All nucleic acid operations were carried out using standard protocols[152]. *Escherichia coli* strains (DH5α and Rosetta) were obtained from Novagen. The oligo primers purchasing and DNA sequencing was done from Eurofins (India). All other chemicals, antibiotics, and reagents were purchased from Sigma. Media components and supplements were purchased from Merck Millipore. Aporphine alkaloids (apomorphine, boldine, and magnoflorine), malonyl-CoA and iodoacetamide were purchased from Sigma.

4.2.2. Methods

4.2.2.1. Cloning of McFabD gene from *Moraxella catarrhalis*

McFabD gene was amplified from *M. catarrhalis* (ATCC No. 8176) genomic DNA using Forward (5’-GAATCCATATGACAGAAGCCAACAGCGGTATGACAAAG-3’) and reverse (5’-GAGGACTCGTGTCATACCAAATTCTCCAATTTTTCTAGGCGTGC- 3’) primers, which were designed on the basis of genomic sequences of *Moraxella catarrhalis* strain RH4 (Genbank Accession No. EKF83038). 957 bp fragment coding McFabD gene was PCR amplified from *M. catarrhalis* genomic DNA. The amplified PCR product was purified and digested with NdeI and XhoI restriction enzymes. The digested product was then ligated into similarly treated pET28c expression vector using T4 DNA ligase. The ligated product was then transformed into cloning host DH5α (*E. coli*) cells. The recombinant clone confirmation was accomplished using restriction digestion and subsequently by DNA sequencing.

4.2.2.2. Expression and purification of McFabD

The Plasmid carrying the desired gene (pET28c-McFabD) was transformed into Rosetta strain of *E.coli* cells growing in the LB broth supplemented with kanamycin (50 µg/ml) and chloramphenicol (35 µg/ml) at 37 ^{0}C. When OD_{600} reached to 0.6 - 0.8, the culture was induced with 0.4 mM IPTG and incubated at 30 ^{0}C for 6-8 hrs. After the incubation, cells were pelleted by centrifugation at 6000 rpm for 15 min. The supernatant was decanted and cell pellets were kept at -80 ^{0}C. For purification, cell pellets were resuspended in lysis buffer (25 mM Tris-HCl pH 7.8, 200 mM NaCl, 10 % glycerol, 10 mM imidazole and 1mM PMSF). The lysozyme was added to final concentration 0.25 mg/ml, and then cells disruption was carried out using a high-pressure French press. The soluble supernatant obtained by centrifuging at 12000 rpm for 80 min and then applied to pre-equilibrated Ni-NTA affinity column. The contaminants were removed by washing the column with wash buffer (25 mM Tris-HCl pH 7.8, 500 mM NaCl, 10 % glycerol and 20 mM imidazole) for 10 bed volumes and the desired protein was then eluted using elution buffer (25 mM Tris-HCl pH 7.8, 200 mM NaCl, 10 % glycerol and 200 mM imidazole). The fractions containing the purified protein were merged and dialyzed against 2 litres of 25 mM Tris HCl buffer (pH 7.8) for 8-10 hrs. The purified protein was concentrated up to 5 mg/ml using a 10 kDa cutoff concentrator (Amicon Ultra-15).

4.2.2.3. Oligomeric characterization of McFabD

The oligomeric state of McFabD was determined using size exclusion chromatography. The purified McFabD protein (5 mg/ml) was loaded onto HiLoad 16/600 superdex 75 gel filtration column, which was pre-equilibrated with buffer A (25 mM Tris-HCl pH 7.8, 100 mM NaCl and 5% glycerol). The flow rate was maintained at 0.5 ml/min. Elution was performed with buffer A. Fractions were collected and analyzed using SDS-PAGE analysis. The apparent molecular weight of McFabD was determined by interpolation using standard calibration curve. Five globular proteins with known molecular weight have been used to calibrate the column and plot standard curve.

4.2.2.4 Biochemical characterization of McFabD

The biochemical assay of McFabD is performed using spectrophotometric assay. A standard reaction mixture consists of 50 µg of McFabD, 25 µM Malonyl-CoA and 10 µM of Pantethine, 25 mM Sodium Phosphate buffer pH 7.8, 1.0 mM EDTA and 1.0 mm DTT in a total reaction volume of 200 µL. After 10 min incubation at 25 ^{o}C, reaction was stopped using 1 M HCl and then 50 µL of Aldrithiol – 4 reagent has been added which reacts with CoA and forms an adduct which absorbs specifically at 324 nm. Standard curve is plotted using varying amount of CoA and used for quantification of liberated CoA. Kinetic parameters (K_m, k_{cat}, V_{max} and k_{cat}/K_m) have been determined by varying malonyl – CoA (5-150 µM) and keeping pantethine constant (20 µM).

4.2.2.5 Kinetic inhibition studies

Inhibitory activity of aporphine alkaloids (apomorphine, boldine and magnoflorine) against McFabD is determined using above-mentioned spectrophotometric assay. IC_{50} was calculated by fitting the data in the dose response curve using graphpad prism. Kinetic inhibition constant is determined by varying substrate (10-150 µM) and alkaloids (0-100 µM) and in consideration for steady state kinetics. Inhibitors were incubated with McFabD for 30 min at 4 ^{o}C and then the reaction was initiated by adding malonyl- CoA. The data were fitted using graph-pad prism.

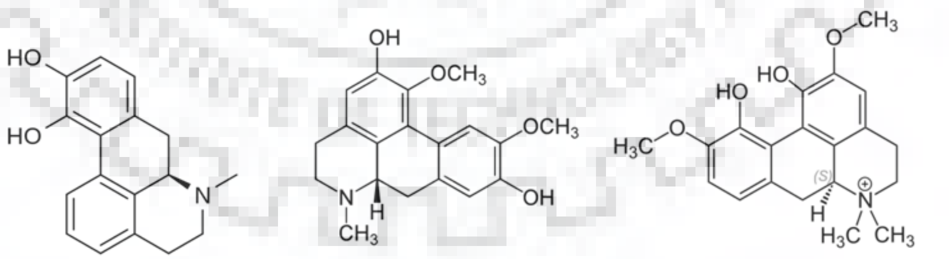

Apomorphine (AMF) **Boldine (BLD)** **Magnoflorine (MNG)**

Figure 4.1 Chemical structures of aporphine alkaloids.

4.2.2.6 Circular dichroism studies

All the CD measurements of McFabD were performed using spectrophotometer model J -1500 (JASCO) equipped with Peltier thermostat under continuous nitrogen flow. McFabD concentration was kept to 0.2 mg/ml in buffer B (25 mM sodium phosphate buffer pH 7.8, 100 mM NaCl, 2 % glycerol and 0.5 mM TECP). All spectral measurements were carried out at 25 ^{0}C using quartz cuvette of 0.1 cm path length. All scans were recorded with a scan speed of 50 nm/min. The far-UV and near-UV CD spectra were taken to observe the changes in secondary and tertiary structure respectively. Effect of pH on the conformation of McFabD was studied using different buffer systems (citrate buffer for pH 3.0-5.0, phosphate buffer for 6.0 - 8.0). Effect of temperature on the McFabD was studied by observing thermal spectra at different temperature intervals (20 to 90 ^{0}C). The Temperature induced unfolding study of McFabD was carried out by observing the ellipticity change at 222 nm and was recorded at the scan speed of 1^{0}C/min from 20 to 90 ^{0}C. The melting temperature of McFabD was calculated by the following equation:

$$[\theta]_t = \alpha([\theta]_F - [\theta]_U) + [\theta]_U$$

T_M is the temperature where $\alpha = 0.5$, θ_t is the ellipticity observed at any temperature, θ_F is the ellipticity of the fully folded protein and θ_U is the ellipticity of the unfolded form[194]. All spectral scans have been taken in triplicates and final spectra obtained by averaging them. All CD analysis was performed using Dicroweb server[195]. All results were expressed in molar ellipticity ($\Delta\varepsilon$) in deg cm^{2} dmol^{-1}, which is defined as per following equation:

$$\Delta\varepsilon = \frac{\theta\text{ (mdeg)} \times 0.1 \times \text{MRW}}{P \times C \times 3298}$$

Where MRW is mean residue weight (Molecular weight of protein / no. of residues - 1), P is path length in cm, C is molar concentration of McFabD protein and 3298 is the constant path[216].

4.2.2.7. Fluorescence spectroscopy

All fluorescence measurements were performed at 25 ^{0}C using Horba Fluro Log Spectrofluorometer using 1.0 cm path length cell with emission slits at 5 nm. The excitation wavelength was kept at 295 nm to excite Trp residue from McFabD protein. The final concentration of McFabD was kept at 2.0 - 4.0 µM in buffer C (20 mM sodium phosphate buffer pH 7.8, 100 mM NaCl, 2 % glycerol and 0.5mM TECP. Emission spectra were recorded in the range of 300-500 nm and three parallel scans have been taken for each reaction. Fluorescence quenching experiments were performed with five ligands (malonyl-CoA, apomorphine, boldine, magnoflorine, and iodoacetamide). In quenching experiments the fixed amount of protein (2.0 µM) was kept in the cuvette and manually titrated with successive addition of ligands (1.0-20 µM). Aporphine alkaloids (Figure 1) were dissolved in DMSO (100%) and added to the reaction mixture with final concentration ≤ 1% DMSO. Malonyl-CoA (M-CoA) and iodoacetamide (IDA) were dissolved in buffer C.

4.2.2.8. UV-Visible spectroscopy studies

All UV-Visible spectroscopy based experiments were performed using Carry 300 UV-Visible spectrophotometer. All measurements were carried out by keeping McFabD concentration constant (20 µM) in buffer D (20 mM Tris-HCl pH 7.8, 100 mM NaCl and 0.5 mM TCEP). McFabD protein was incubated with the different amount (5 µM to 100 µM) of ligands (malonyl-CoA, iodoacetamide, apomorphine, magnoflorine, and boldine). All samples were kept for 10 min at room temperature and the spectra were recorded in the range of 200- 350 nm.

4.2.2.9 Binding studies using Isothermal titration calorimetry based assays

Binding of different ligands with McFabD was performed using microcal ITC200 (GE healthcare). All reactions were performed at 25 ^{0}C. McFabD protein was extensively dialyzed against buffer E (20 mM Tris-HCl pH 7.8, 100 mM NaCl, 2% glycerol and 0.5 mM TECP). In order to remove buffer-buffer mismatch, a corresponding amount of DMSO (1%) was added to the protein solution during the titration reaction of alkaloids. A typical titration reaction consists of McFabD protein (50-100 µM) in the sample cell and ligands (0.5 - 1.5 mM) in the syringe. The stirring speed was kept at 800 rpm and initial delay of 60 sec. After the initial injection (0.5 µl, not used in data fitting), 15-20 injections (2.0 µl each) were performed with 150 seconds gap between each injection, and heat changes were subsequently monitored. The reference cell was kept at 8.0 µW. ITC data were analyzed using one site model of Origin 7.0 software. The free energy of reaction (ΔG) was calculated by the following equation:

$$\Delta G = \Delta H - T\,\Delta S$$

where ΔG is the Gibbs free energy change, ΔH is the enthalpy change, ΔS is the entropy change and T is the temperature (298K).

4.2.2.10 Molecular modeling

A suitable template for modeling McFabD protein was searched in the PDB database using pBLAST to find out the homologous structures[254]. Template structure showing high sequence identity has been selected to model McFabD using Modeller 9.17[255] and Swiss-Model programs[256]. The best 3D model of McFabD was selected on the basis of energy minimization based upon DOPE score value. Model validation for their stereochemical quality and accuracy was assessed using PROCHECK analysis[222], ERRAT[225], Verify3D[224], ProQ[201] and ProSA[202]. Structural studies and model figures were generated by Chimera tool[204].

4.2.2.11. Molecular Docking

The docking study of McFabD with different ligands was carried out using Autodock 4.2[163] form ADT tools. Grids maps were prepared using 60×60×60 grid points with 0.2 Å spacing in the x, y and z directions centered at the active site of McFabD. Autogrid4 and aurodock4 programs were used for calculating energy maps and docking of ligands, respectively. One hundred docked structure, i.e. 100 runs were generated using Lamarchian Genetic Algorithm. Docked conformations were converted into the pdbqt format and analyzed. Chimera tool[204] was used for visualization and figures generation.

4.2.2.12. Minimum inhibitory concentration determination

MIC of apomorphine, boldine, and magnoflorine against *Moraxella catarrhalis* has been determined using a broth microdilution method [166,212]. A concentration gradient (0.5 µg/ml – 256 µg/ml) of inhibitors was tested. A single colony of *Moraxella catarrhalis* strain MTCC No. 445 was used to inoculate the nutrient broth medium. Correlation between OD_{600} and colony forming units (cfu) has been determined using serial dilution technique. Bacterial suspension adjusted to 2.0×10^6 cfu per ml was used to inoculate 96 well microtiter plates. The different dilutions of inhibitors were prepared in sterile broth. 100 µl of broth solution was added to all wells. 50 µl of inhibitor solution was used in each well, except growth control (broth and inoculum) and sterility control (broth only) wells. 50 µl of bacterial suspension adjusted to 2.0 × 10^6 cfu per ml has been used which gives final inoculum 5×10^5 cfu per ml. The microtiter plate was then incubated at 37 ^{0}C for 16-20 h.

4.3. Results

4.3.1. Purification and oligomeric characterization of McFabD

McFabD gene was successfully cloned into a pET28c expression vector (Figure 4.2) and expressed in *E. coli* Rosetta cells at 30 ^{0}C by inducing with 0.4 mM IPTG.

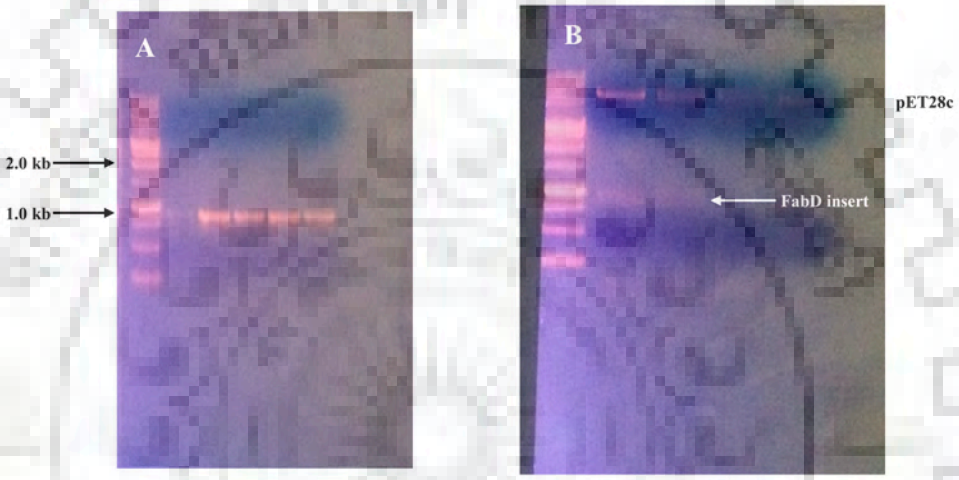

Figure 4.2 Molecular cloning of McFabD gene.

(A) PCR amplification of McFabD gene (B) Clone confirmation using restriction digestion experiment. 957 bp McFabD gene fragment was amplified and cloned into pET28c expression vector.

The Ni-NTA affinity-based chromatography was used to purify the McFabD protein. A single band of ~35.09 kDa size McFabD protein was obtained as visualized in 12 % SDS-PAGE gel (Figure 4.3A).

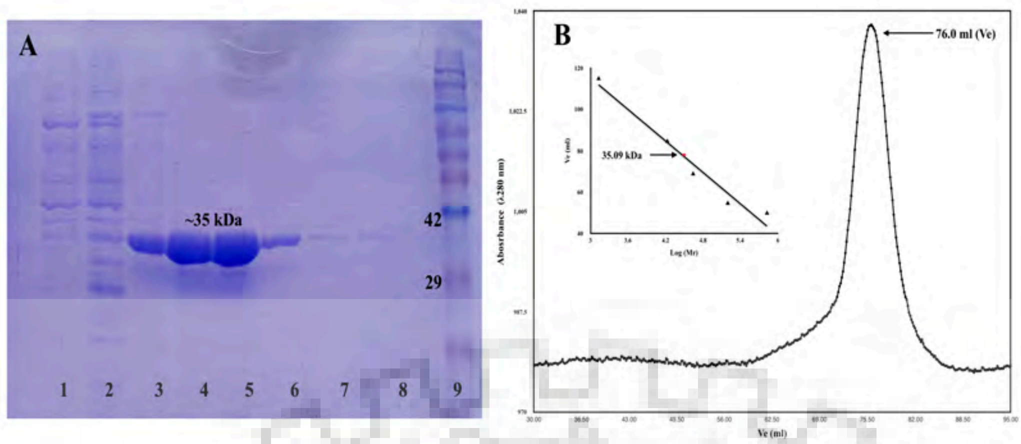

Figure 4.3 Purification and oligomeric state characterization of McFabD.
(A) 12% SDS-PAGE gel showing purified McFabD protein as a single band. Lane 1-2, wash 1 and wash 2; Lane 3-8, McFabD protein (35.09 kDa) fractions eluted at 100-200 mM imidazole; Lane 9 Protein ladder (Abcam), (B inset) Standard curve of Log of Molecular weight versus elution volume (Ve) was derived from the elution profile of standard proteins run on superdex G75 gel filtration column. Standards used were as follows: 1. Thyroglobulin (670 kDa) 2. Aldolase (158 kDa) 3. Ovalbumin (44 kDa) 4. Myoglobin (17 kDa) 5.Vitamin-B12 (1.35 kDa), (B) Chromatogram of McFabD protein observed under native conditions.

The oligomeric state of McFabD was determined using size exclusion chromatography. The standard curve of Log of molecular mass versus Ve was derived from the elution profile of standard proteins. The apparent molecular weight of McFabD was then estimated by interpolation using standard calibration curve (Figure 4.3B inset). McFabD was eluted at 76.0 ml elution volume using buffer A. A single peak of 76.0 ml (Figure 4.3B), which corresponds to ~ 35 kDa size was observed and purity of McFabD was confirmed by SDS-PAGE analysis. This shows that in solution, McFabD exists in monomeric form, which was consistent with other characterized FabD homologs[236,248,249].

4.3.2 Kinetic characterization and inhibition studies

The enzymatic assay of McFabD is performed using spectrophotometric assay where free CoA reacts with Aldrithiol-4 led to the formation of adduct which absorbs at 324 nm. McFabD is found to be active with K_m 114.3 ± 13.6 μM for malonyl-CoA and V_{max} 13.54 ± 0.764 μM /min respectively. The Michaelis Menten and double reciprocal plot of McFabD has shown in Figure 4.4A & 4.4B. The enzymatic characterization of FabD has been reported from several homologs with K_m of 21.03 ± 2.3 µM (HpFabZ)[97], 12.6 µM (MtFabD)[247], 25 µM (EcFabD)[244], and 60.0 µM (ScFabD)[257]. The k_{cat} and k_{cat}/K_m were determined to 0.677 ± 0.038 S^{-1} and 5.9×10^3 $M^{-1}S^{-1}$ respectively. The higher value of K_m of McFabD for malonyl-CoA as compared to other reported homologs might be due to transfer of malonyl group to panethine instead of ACP which is its natural substrate along with Malonyl-CoA.

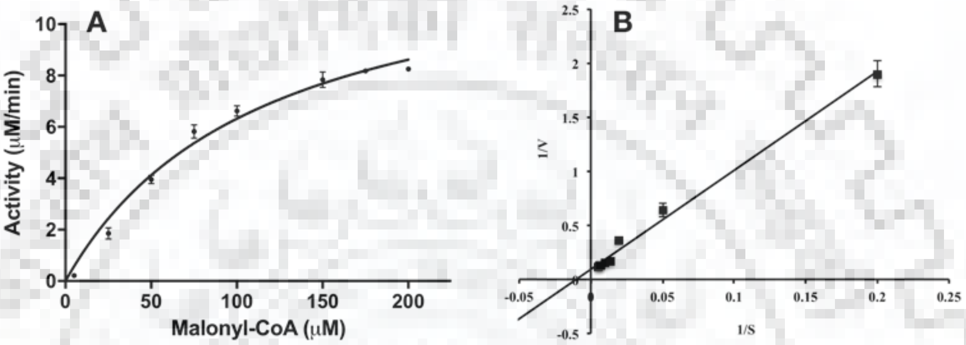

Figure 4.4. Kinetic characterization of McFabD.
(A) Michaelis Menten plot of McFabD for malonyl-CoA substrate (B) Double reciprocal plot.

Inhibitory activities of aporphine alkaloids against McFabD have been determined using a same spectrophotometric assay and kinetic inhibition parameters (K_i and IC_{50}) have been calculated. Table 4.1 shows the K_i and IC_{50} values determined for apomorphine, magnoflorine and boldine against McFabD. Based upon the *Ki* values AMF and MNG have inhibited the McFabD with stronger affinity as compared to boldine. Mode of inhibition of these compounds was further analyzed via plotting double recriprocal plots as shown in Figure 4.5. All three inhibitors have inhibited the McFabD via non-competitive mode (mixed), which means these compounds can bind to enzyme as well as with enzyme substrate (ES) complex.

Table 4.1 Inhibitory activities of aporphine alkaloids against McFabD

Alkaloids	IC_{50} (µM)	K_i (µM)
Apomorphine	16.7 ± 3.1	27.3 ± 2.45

Magnoflorine	19.2 ± 1.56	23.2 ± 3.2
Boldine	32.9 ± 2.67	35.2 ± 3.77

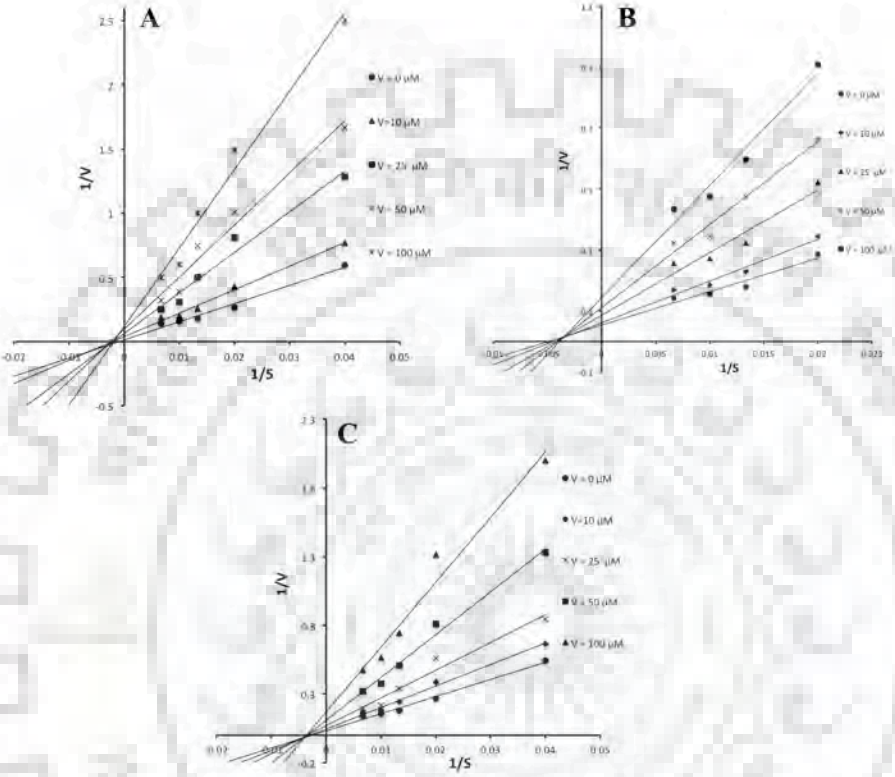

Figure 4.5 Analysis of the mode of inhibition of aporphine alkaloids.

Double reciprocal plots of apormorphine (A), boldine (B) and magnoflorine (C) for for McFabD. All three inhibitors were found to be inhibiting the McFabD via non-competitive (mixed) mode of inhibition.

4.3.3 Circular dichroism based studies

CD spectroscopy has been proven to be a valuable tool, which provides information related to the conformation and stability aspects of protein under different environmental conditions as well as in the presence of ligands (substrates, inhibitors, small molecules etc.) The far-UV CD is mainly used to monitor the changes in the secondary structure elements, while near-UV CD helps in understanding the tertiary structure of proteins[105,196,216].

The far-UV CD spectra of McFabD (Figure 4.6A) under native conditions (20 mM sodium phosphate pH 7.8, 25 ^{0}C) shows two minima bands at 209 nm and 222 nm wavelength which is characteristic to α- helices. The presence of one positive maxima band at 197 nm and broad minima at 210-220 nm ranges depicts the presence of β-sheets in McFabD protein. Secondary structure content of McFabD has been calculated by SELCON[258] method using dichroweb web server for CD analysis. For McFabD protein under native condition, helical, sheets, turns and coils contents were found to be 41.7 %, 14.0 %, 21.7 % and 27.0 %, respectively. The near-UV CD spectrum (260 – 320 nm) arises due to aromatic amino acids. The near-UV CD spectra of McFabD (Figure 4.6B) show two minima in the region of phenylalanine (255-270nm) and tryptophan (290-305 nm), while maxima in tyrosine (275-282 nm) region.

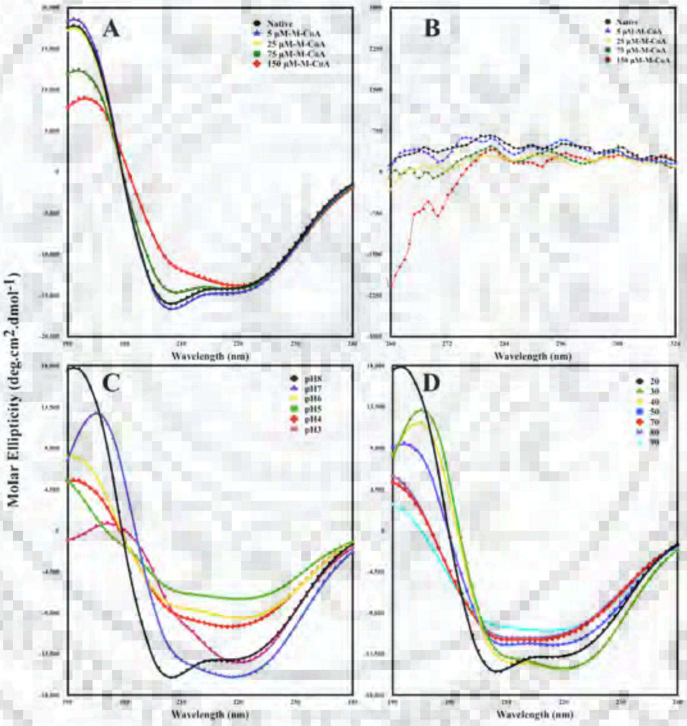

Figure 4.6. Circular dichroism based studies.

(A) & (B) The far-UV and the near-UV CD spectra of McFabD under native conditions as well as under different amounts of substrate (Malonyl-CoA). (C) Effect of pH on the far-UV CD spectra of McFabD. At lower pH, loss of ellipticity at 209 nm and 222 nm was observed. (D) Effect of temperature upon far-UV CD spectra of McFabD. At the higher temperature loss of helical and sheet content has been observed.

4.3.3.1 Effect of Substrate (Malonyl-CoA)

It has been clearly observed that as the substrate binding has caused the decrease in the ellipticity at 209 nm and 222 nm, and positive ellipticity at 197 nm. Higher substrate concentration (100 µM -200 µM) has produced more effect on the conformation of McFabD protein (Figure 4.6A). At 200 µM substrate concentration, helical, sheets, turns, and random coils contents were found to be 32.9 %, 17.2 %, 20.6% and 32.9 % respectively. This shows that helical content has been decreased while sheets content has been increased in McFabD upon substrate binding. In near-UV spectra (Figure 4.6B), we have observed a decrease in MRE (Mean residue ellipticity) towards negative values in all three regions of the spectra. The region of Phe (260 nm to 275 nm) has been affected more at a higher amount of substrate as compared to Tyr and Trp regions of near-UV spectra, which might be resulted in the substantial change in the tertiary structure of McFabD upon malonyl- CoA binding.

4.3.3.2 Effect of pH and Temperature

Effect of pH on the Far-UV CD spectra on McFabD has been studied by using different buffer systems. Figure 4.6C shows the Far-UV CD spectra of McFAbD at different pH. A gradual decrease in the ellipticity at 209 nm and 222 nm was observed. Helical content has been reduced, while sheets content has been increased at lower pH. At pH 3.0, the helical and sheet contents were 24.3 % and 21.2 % respectively. To study the effect of temperature on McFabD stability, thermal-induced unfolding was conducted. Melting temperature (T_M) was determined to 50.14 ^{0}C. As shown in Figure 4.6D McFabD started to lose secondary elements above 45 ^{0}C and lost completely above 60 ^{0}C. At the higher temperature, considerable loss of helical and sheet contents was observed evident by the loss of ellipticity at 208 nm, 222 nm and 195 nm. At 90 ^{0}C, helical and sheet content was found to be 22.3 % and 17.8 % respectively.

To understand the temperature based unfolding process, thermodynamic parameters were quantitatively calculated. The thermodynamic based unfolding curve as shown in Figure 4.7A follows a typical two-state pattern and sigmoidal in nature. The apparent activation energy (E_a) of temperature-induced shift could be determined using following equation [194]:

$$\ln(\ln 1/F_{app}) = E_a/R(1/T_M - 1/T)$$

where F_{app} is a fraction of native protein at the corresponding temperature. F_{app} is equal to the $(\theta-\theta_U)/(\theta_F - \theta_U)$. T_M is the temperature where the maximum heat change happened.

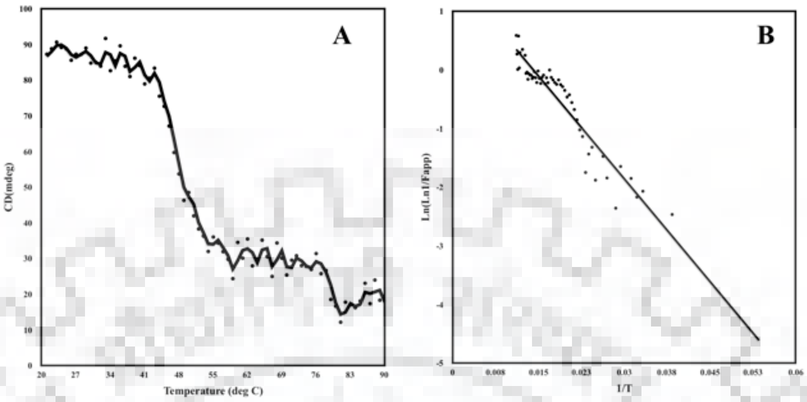

Figure 4.7 Melting curve of McFabD.

(A) Melting temperature was determined to 50.14 ^{o}C for McFabD. Melting curve is sigmoidal and has two state transition pattern. (B) Linear relationship between L_n ($L_n(1/F_{app})$) Vs 1/T. The apparent activation energy of thermal transition can be calculated from the slope of this curve.

The apparent activation energy of McFabD transition was estimated to 970.57 ± 0.12 Joules/mol. The melting temperature and activation energy for temperature induced unfolding process for McFabD is found to be lesser than the HpFabD (T_M = 65.5, E_a = 160 kJ/mol) which shows that McFabD is thermally less stable than HpFaD enzyme[97].

4.3.3.4. Effect of different ligands

Effects of different ligands on the conformation of McFabD have been studied by observing the far-UV and near-UV spectra. Different concentration range (5-250 µM) of ligands has been used. Figure 4.8 & 4.9, shows the far-UV and near-UV spectra of McFabD in presence of different ligands.

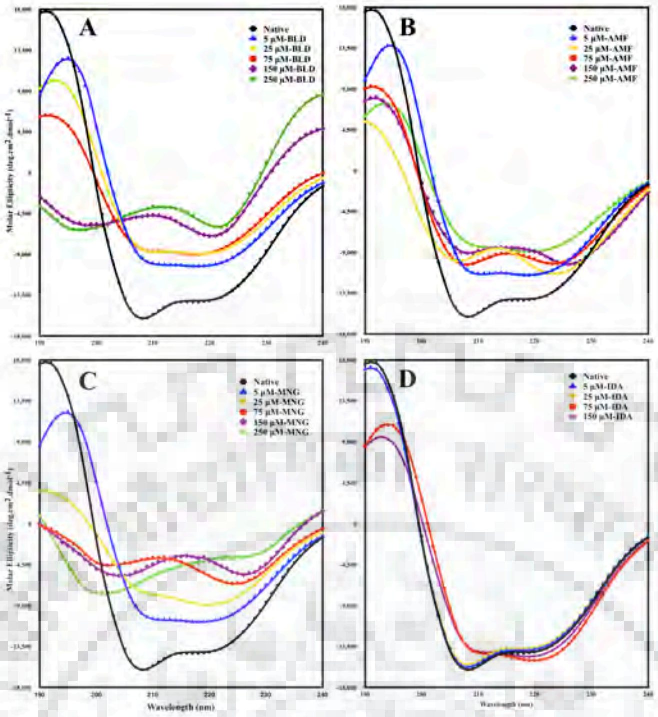

Figure 4.8 Effect of (A) Boldine, (B) Apomorphine, (C) Magnoflorine and (D) Iodoacetamide upon Far-UV CD spectra of McFabD.

Loss of ellipticity at 222 nm, 209 nm, and 197 nm was observed upon the binding of different ligands. Effect of BLD (A) and MNG (C) upon the McFabD secondary structure was more prominent as compared to AMF (B). IDA (D) binding has produced a similar effect, but with lesser extent as compared to other ligands.

The ligands binding have brought some striking changes in the far-UV spectra (Figure 4.8A-4.8D) of McFabD and common observation was loss of helical content evident by the ellipticity loss at 209, 222 and 197 nm. Although changes in sheet content were observed, but the extent of variation was much lesser than the helical part. β-sheets contents have been increased upon the binding of ligands. Figure 4.9E-4.9H, shows the changes in the secondary structure elements upon the binding of different amount of substrate and aporphine alkaloids. Overall with increasing concentration of ligands, degree of randomness (random coils %) has been increased.

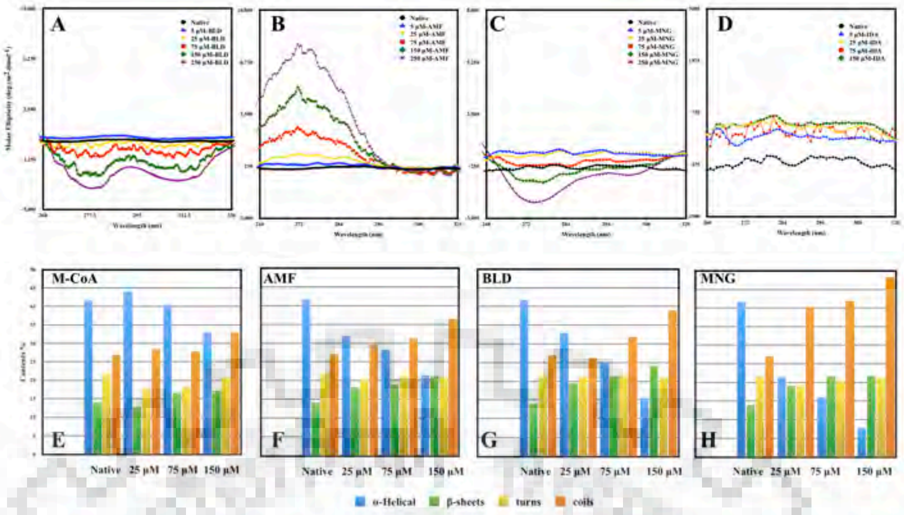

Figure 4.9 The near-UV CD spectra of McFabD in presence of (A) Boldine, (B) Aporphine, (C) Magnoflorine and (D) Iodoacetamide. Changes in the tertiary structure of McFabD were observed upon binding. Aporphine alkaloids (A-C) have shown more effect on the tertiary structure as compared to IDA (D). E-H, bar diagrams showing the changes observed in the secondary structure elements of McFabD upon the binding of Malonyl-CoA (E), apomorphine (F), Boldine (G) and Magnoflorine (H). Helical content has been decreased, while sheets content has been increased.

Effect on the tertiary structure of McFabD was studied by observing the near-UV CD spectra in the presence of different concentration of ligands. Overall all three aporphine alkaloids binding lead to the changes in the tertiary structure of McFabD as shown in Figure 4.9A-4.9D. BLD binding resulted in the increase in MRE values towards negative. Phe and Trp regions of near-UV spectra have been affected more as compare to Tyr regions. AMF binding to McFabD has shown opposite effect on near-UV spectra as compare to BLD. In this case, an increase in MRE towards positive values has been observed. Phe and Tyr regions were more affected as compared to Trp region. Magnoflorine binding has shown mixed kind of effect. In this case, at a lower amount of MNG (<100 µM) resulted in the MRE increase towards positive, while higher conc. (>100 µM) lead to increase in MRE towards negative values with more profound effect in the region of Phe. Overall, we can say that substantial changes in the tertiary structure of McFabD were observed upon the binding of aporphine alkaloids.

4.3.4 Fluorescence analysis

Fluorescence based titration studies have been widely used to investigate the interaction of protein with ligands (drugs, inhibitors etc). Tryptophan residues in the proteins have properties of intrinsic fluorescence and are commonly used in spectral studies[231,259–261]. McFabD protein has three tryptophan residues, and therefore fluorescence-quenching experiments were conducted to study the ligand-protein interactions. Binding of different ligands leads to the decrease in the fluorescence intensity of McFabD protein, indicating the change in the structure of McFabD upon ligands binding.

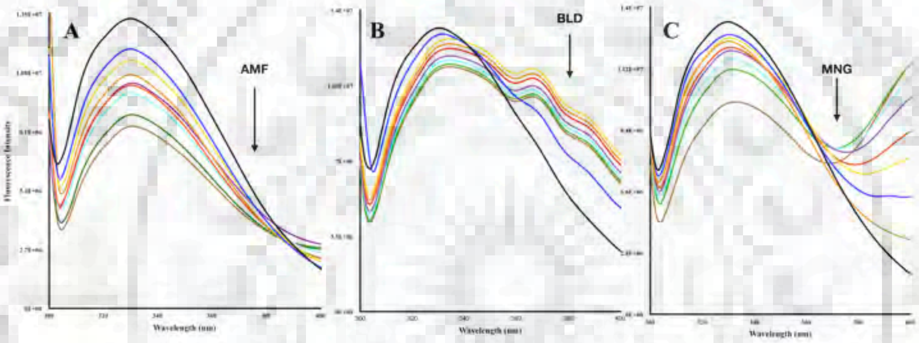

Figure 4.10 McFabD fluorescence quenching studies.

Fluorescence emission spectra of McFabD in the presence of different amount of apomorphine (A), boldine (B) and magnoflorine (C). Overall, a decrease in the fluorescence intensity was observed upon the binding of these three ligands.

The results have shown that McFabD has an intrinsic fluorescence emission band at 330 nm when excited at 295 nm, which shows that Trp residues in McFabD were exposed in the hydrophobic environment. Binding of the substrate (Malonyl-CoA) and different ligands (IDA, BLD, AMF, and MNG) to McFabD has resulted in a gradual decrease in the fluorescence intensity. Binding of Malonyl- CoA leads to decrease in the fluorescent intensity with a blue shift of of 1.0 nm. Binding of BLD to McFabD resulted in a red shift of 4.0 nm, while binding of AMF, MNG, and IDA has resulted in a red shift of 1.0, 2.0 and 1.0 nm respectively. These results have shown that binding of the substrate have made Trp environment more hydrophobic, while others ligands have exposed Trp towards the hydrophilic environment. The extent of red shift was more observed in BLD binding when compared to other ligands. Figure 4.10A-4.10C shows the McFabD fluorescence emission spectra in presence of aporphine alkaloids, while emission spectra of McFabD with the substrate (M-CoA) and inhibitor (IDA) have been given in Figure 4.12.

4.3.4.1 Quenching mechanism

In general, quenching mechanism can be classified into dynamic or static quenching or by mixed pattern. The mechanism of quenching is distinguished by variation in temperature and viscosities[259,262]. In dynamic quenching, the quenching constant increases with temperature rise, while reverse trend observed in static quenching. In order to determine the possible mechanism, the Stern-Volmer equation was used:

$$F_0/F = 1 + K_{sv}[Q] = 1 + K_q\,\tau_o\,[Q]$$

Where F_0 and F are the fluorescence intensities in absence and presence of quencher (Q), K_{sv} is the quenching constant, K_q is the bimolecular quenching rate constant and τ_o is the fluorescence lifetime without a quencher. For proteins, the value of τ_o is 10^{-8} sec[259,263]. A linear plot of F_0/F vs [Q] indicates that quenching is either static or dynamic, while non-linear implies to mixed pattern of quenching[259]. Figure (4.11A-4.11C) shows the Stern-Volmer plots of McFabD with AMF, BLD, and MNG.

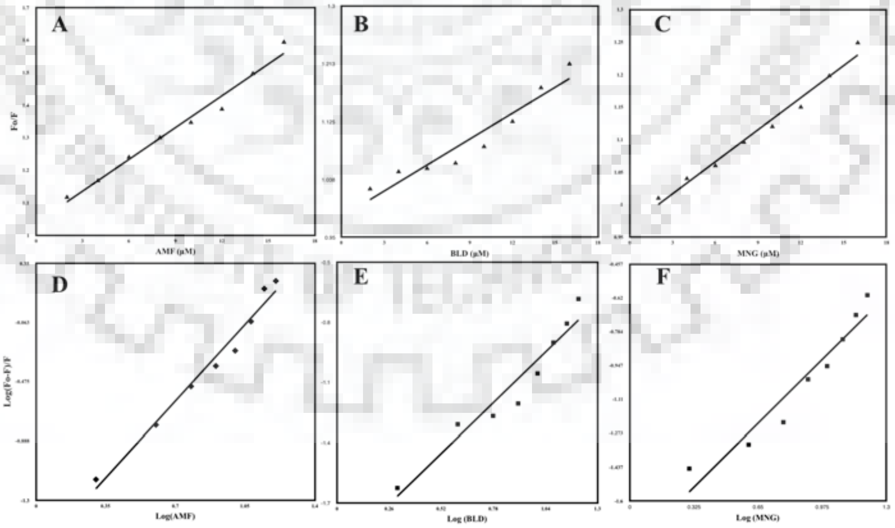

Figure 4.11 Stern-Volmer plots of McFabD quenching studies with apomorphine (A), boldine (B) and magnoflorine (C).

The mechanism of fluorescence quenching was found to be static for all ligands which depcits the ground state complex formation upon ligand binding. The modified Stern-Volmer plots for apomorphine (D), boldine (E) and magnoflorine (F). Binding constant (K_b) and N (no. of binding sites) are calculated from this plot.

We have determined the quenching mechanism by calculating K_q value ($K_q = K_{sv}/\tau_o$). For dynamic quenching K_q found to be less than 10^{10} while for static quenching K_q value found to be higher than this value. In this study, K_q values for all ligand-protein interaction were found to more than 10^{10}, which show that the possible mechanism of quenching is static and the formation of the ground state protein-ligand complexes. Table 4.2 gives the value of K_{sv}, K_q, and R^2 (goodness of fit).

Table 4.2 The quenching constants of McFabD interactions with different ligands determined by Stern- Volmer plots:

Ligand	K_{sv} (10^4 M^{-1})	K_q (10^{12} M^{-1} S^{-1})	R^2
Malonyl- CoA	1.37	1.37	0.97
Boldine	1.31	1.31	0.94
Apomorphine	3.26	3.26	0.98
Magnoflorine	1.64	1.64	0.98
Iodoacetamide	1.07	1.07	0.99

4.3.4.2. Binding equilibrium analysis

For the static quenching model, the equilibrium binding constant (K_b) and a number of binding sites have been calculated by the following equation:

$$\text{Log } (F_0\text{-}F)/F = \log K_b + N \log (Q)$$

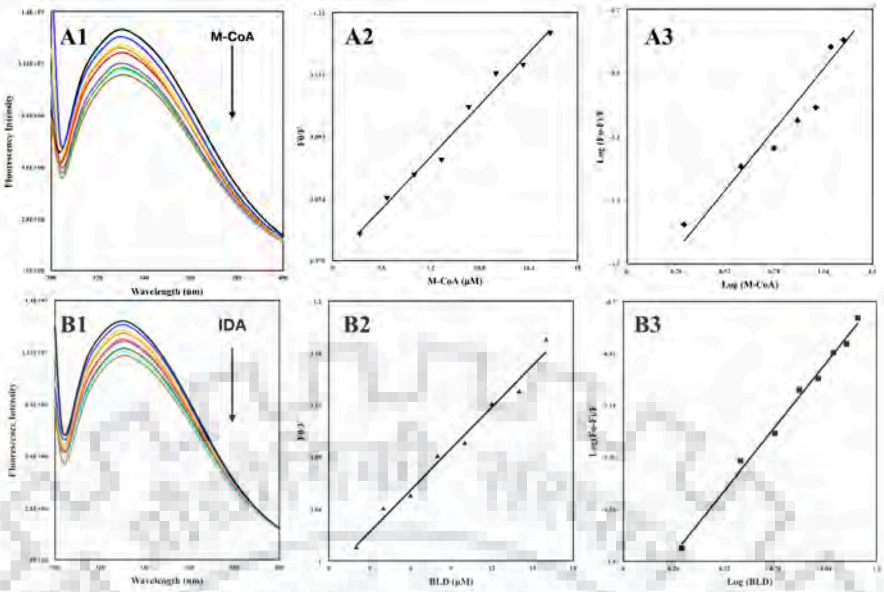

Figure 4.12. Fluorescence quenching of malonyl-CoA and iodoacedamide.

Fluorescence emission spectra of McFabD in presence of M-CoA (A1) and IDA (B1). Stern-Volmer plots and modified Stern-Volmer plots of McFabD quenching with M-CoA (A2,A3) and IDA (B2,B3) respectively.

Where K_b is the equilibrium binding constant and N is the no of binding sites. Both parameters can be easily calculated by intercept and slope of the curve. Figure 4.11D-4.11F shows the fitted curves for the calculation of binding parameters. The values of K_b and N, for all the ligands to McFabD interactions, have been given in Table 4.3.

Table 4.3 Binding constant and number of binding sites

Ligand	K_b (10^4 M^{-1})	N	R^2
Malonyl- CoA	1.67	1.39	0.97
Boldine	1.95	1.03	0.99
Apomorphine	2.90	1.31	0.97
Magnoflorine	1.84	0.94	0.92
Iodoacetamide	1.23	1.16	0.98

4.3.5 UV-Visible spectroscopic studies

UV- visible absorption spectroscopy is a simple and valuable tool for exploring structural changes and understanding the protein-ligand complex formation. Figure 58 shows the absorption spectra of McFabD in native condition and with different ligands. Absorption spectra of McFabD show absorption maxima at 280 nm which arises due to the presence of aromatic amino acids (Tyr, Trp, and Phe) in protein[264]. Upon ligand addition, changes in the spectra observed, which depicts the conformational changes as well as complex formation during binding. Absorption spectra were recorded in different concentration of ligands (5 µM - 100 µM).

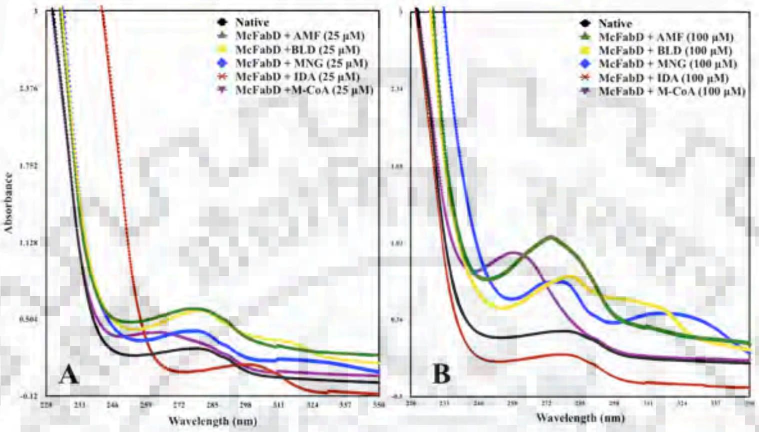

Figure 4.13 UV-Visible spectra of McFabD under native conditions and in the presence of different ligands. Spectra obtained at 25 µM (A) and 100 µM (B) concentration of ligands have been shown here.

Upon substrate binding (Figure 4.13), an increase in the absorption intensity with absorption maxima shifted towards lower absorption maxima (280 nm to 258 nm) was observed. Binding of BLD, AMF, and MNG to McFabD resulted in the increase in absorption intensity (hyperchromic shift) and absorption maxima also shifted towards lower wavelength, blue shift (Figure 4.13). In case of IDA, decrease in the absorption intensity (hypochromic effect) was observed. The extent of the absorption maxima shift (Blue shift) was more prominent in the case of M-CoA and AMF binding as compared to BLD, MNG, and IDA. Altogether, these results have shown that there is a complex formation and a conformation change upon binding of these ligands to McFabD.

4.3.6 Isothermal Titration Calorimetry (ITC) based studies

Interaction of McFabD with different ligands was further explored through isothermal titration calorimetry, which determines the binding parameters including affinity, thermodynamic parameters (ΔH, TΔS, and ΔG) and stoichiometry in a single reaction. A typical 1:1 stoichiometric binding was observed in all reaction. Binding isotherms and fitted curves of binding of McFabD with Malonyl-CoA, BLD, AMF, IDA, and MNG have been shown in Figure 4.14.

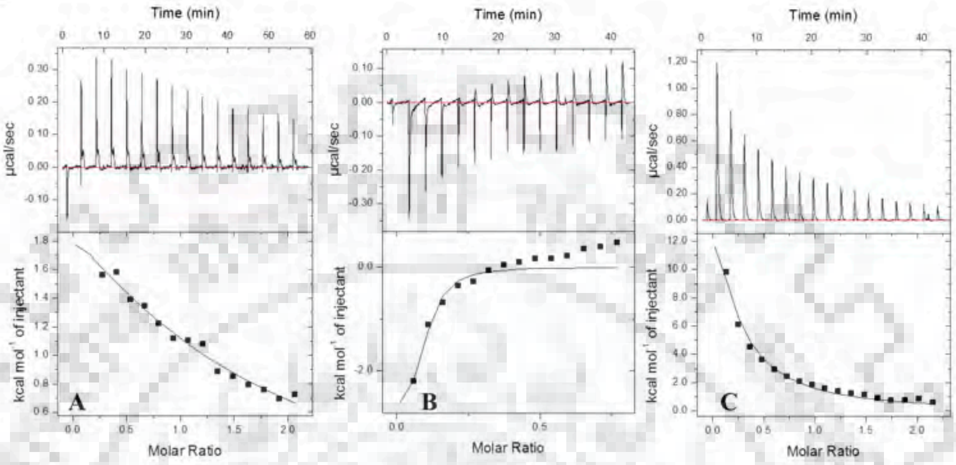

Figure 4.14 ITC based binding assay.

ITC titration data describing the binding of boldine (A), apomorphine (B), malonyl-CoA (C), Iodoacetamide (D) and magnoflorine (E) with McFabD. Data is fitted using one site model analysis of Origin 7.0. The upper part of each panel shows the thermogram (thermal power Vs time) after baseline correction while the lower part of each panel is binding isotherm (normalized heat vs molar ratio of reactants). Binding of BLD (A) and M-CoA (C) to McFabD is an endothermic reaction, driven by entropy while binding of AMF (B), IDA (D) and MNG (E) to McFabD is an enthalpy driven exothermic reaction.

Upward trends in the binding isotherms as obtained during the reaction of McFabD with M-CoA and BLD represent the endothermic nature of the reaction, while downward trends as observed in AMF, MNG And IDA reactions depict the exothermic nature of the reactions. This shows that binding of BLD and M-CoA to McFabD was driven by entropy change (ΔS > 0), while binding reactions of AMF, IDA and MNG were driven by the enthalpy change (ΔH <0). All reactions were spontaneous as evidenced by the negative value of free energy change (ΔG <0). All data have been fitted using one site model analysis program of Origin 7. Table 4.4 shows the thermodynamics and binding parameters of all the reactions.

Table 4.4 Thermodynamic parameters

Ligand	K_D (µM)	ΔH (cal/mol)	ΔS (cal/mol/deg)	ΔG (cal/mol)	N
M-CoA	25.83	2.9×10^6	9.81×10^3	$- 2.3 \times 10^3$	0.81 ± 0.05
Boldine	7.19	4572	32.1	-5.02×10^3	1.3 ± 0.11
Apomorphine	4.87	-3285	13.3	-7.248×10^3	0.64 ± 0.09
Magnoflorine	11.7	-6858	0.799	-7.096×10^3	0.79 ± 0.21
IDA	16.5	-9924	-11.4	-6.5×10^3	1.12 ± 0.02

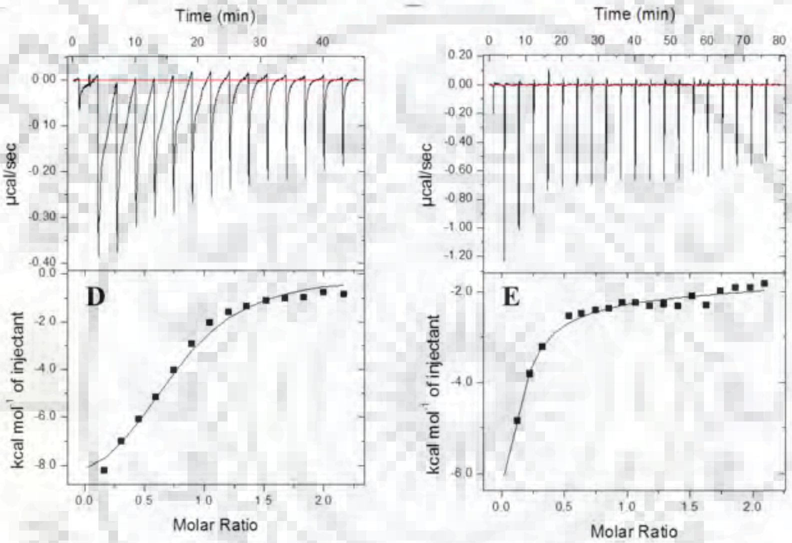

Figure 4.14 ITC based binding assay (continued).

Binding of BLD (K_D = 7.19 µM) and apomorphine (K_D = 4.87 µM) to McFabD was more favorable as compared to other ligands. Based upon the dissociation constant values as given in Table 4.4 we can say that McFabD has a strong binding affinity for BLD and apomorphine with K_D values of 7.19 µM and 4.87 µM respectively.

4.3.7 Molecular Modelling of McFabD

As the crystal structure of McFabD is not available, a suitable template (PDB Id: 3HJV, sequence Identity 46%) was chosen to build the 3D model of McFabD using pBLAST analysis. The predicted 3D model was further validated for stereochemical quality using PROCHECK server. The PROCHECK analysis revealed that 99.3 % residues were within allowed regions. Various validation tools have been used to assess the quality of predicted models of McFabD. Table 4.5 shows the assessment of a built 3D model using various validation tools. ERRAT analysis gave an overall quality score of 98.63, where good resolution structures have a score of 95% or more. Verify- 3D server analysis has shown that 99.67% residues had an averaged 3D-1D score >= 0.2. ProSa server gives the Z score of -9.16, which lies within the range of structure determined using NMR and X-ray crystallography. The overall quality was further checked using ProQ server. All of these validation servers suggested that built 3D model of McFabD (Figure 4.15A) could be accepted with high confidence.

Table 4.5 The quality assessment of predicted 3D model of McFabD

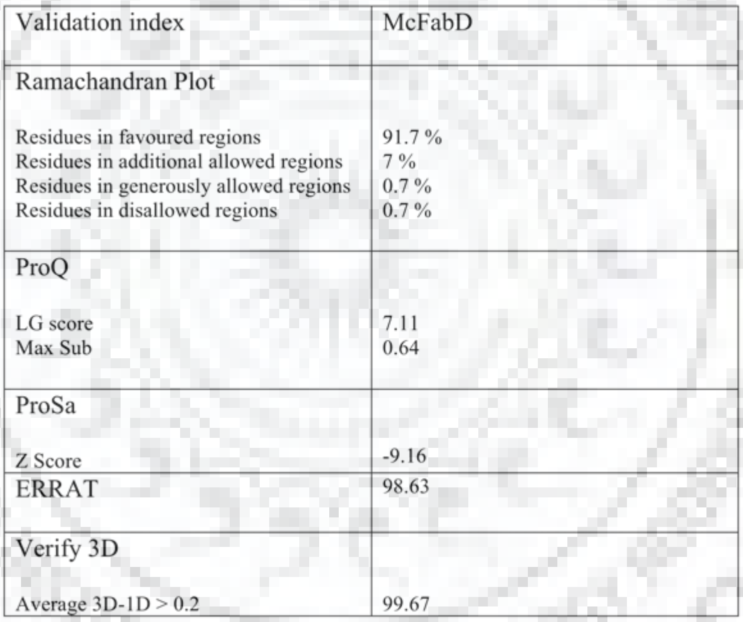

Validation index	McFabD
Ramachandran Plot	
Residues in favoured regions Residues in additional allowed regions Residues in generously allowed regions Residues in disallowed regions	91.7 % 7 % 0.7 % 0.7 %
ProQ	
LG score Max Sub	7.11 0.64
ProSa	
Z Score	-9.16
ERRAT	98.63
Verify 3D	
Average 3D-1D > 0.2	99.67

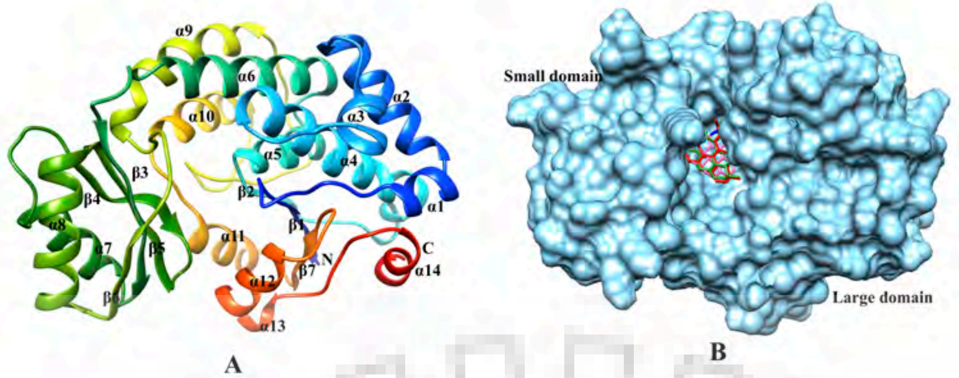

Figure 4.15 Predicted 3D model (A) and binding pocket of McFabD (B). (A) Cartoon diagram of McFabD predicted 3D model. McFabD is colored blue to red from its N terminus to C terminus. Secondary structure elements are labeled. (B) Surface diagram of McFabD with its binding pocket. Docked ligands are shown in different color.

4.3.7.1 Sequence and phylogenetic analysis

Multiple sequence alignment of McFabD protein with other homologs has been performed using T coffee server[199]. Figure 4.16 shows the MSA profile of McFabD with HpFabD, MtFabD, PfFabD, ScFabD, and EcFabD. McFabD shared 46.73 % sequence identity with EcFabD. Additionally, two highly conserved motifs (GHSXGE and PGQGXQ) and other conserved regions have been observed. Phylogenetic analysis of McFabD has been performed using phyml server[265]. McFabD gene is found to be closely related to EcFabD, VcFabD, and StFabD gene family (Figure 4.17). As per the reported literature, FabD protein was considered to have two active sites, the malonyl-CoA binding site, and holo-ACP binding sites. It has been found that these two highly conserved motifs and conserved residues might play important role in the formation of active sites[97].

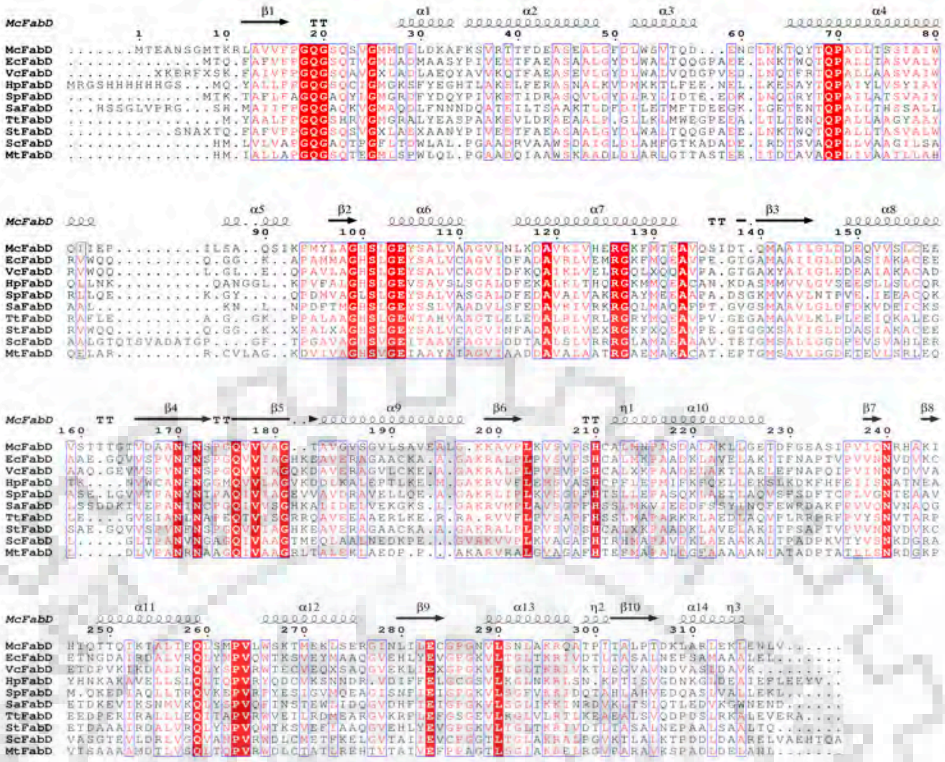

Figure 4.16 Multiple sequence analysis.

Sequence analysis of McFabD with different homologs. FabD gene was found to be highly conserved among these homologs. The conserved regions have been shown in red blocks. The predicted secondary structure elements were also shown here. The alignment was performed using ESPript 3 software.

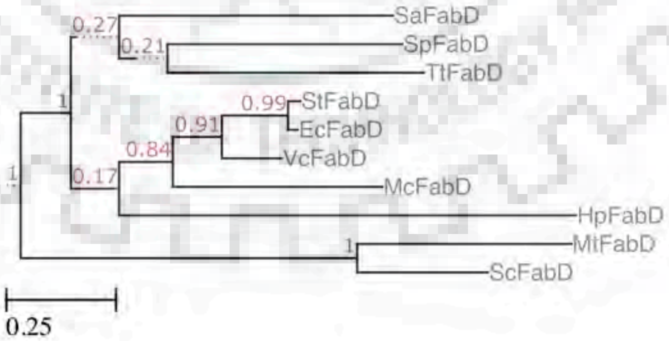
0.27
SaFabD
0.21
SpFabD
TtFabD
1
0.99
StFabD
0.91
EcFabD
0.84
VcFabD
1
0.17
McFabD
HpFabD
1
MtFabD
ScFabD
0.25

Figure 4.17. Phylogenetic analysis of McFabD gene.

4.3.8 Docking studies

In order to get more information regarding the binding mode of different ligands to McFabD, docking based investigations were carried out using Auto Dock[163]. Binding pocket of these ligands has been shown in Figure 4.15B. BLD, AMF, and MNG were interacting with McFabD in a similar way as malonyl moiety of M-CoA. These ligands were interacting with active site residues through polar and non-polar interactions. Binding energy and binding constant values of AMF, BLD, IDA, MNG, M-CoA, corytuberine, and juglone have been given in Table 4.6.

Table 4.6 Binding parameters of different ligands determined using Autodock

Ligands	Binding energy (kcal/mol)	Binding constant (µM)
Malonyl-CoA	-7.56	2.89
Apomorphine	-7.18	5.45
Boldine	-5.49	95.33
Magnoflorine	-5.39	111.42
Iodoacetamide	-3.62	2210
Corytuberine	-6.31	23.57
Juglone	-6.18	29.51

Binding modes of all these ligands to McFabD have been shown in Figure 4.18. BLD interacts with McFabD through polar and non-polar interactions. Ser 209 and Arg 106 residues are involved in hydrogen bonds with BLD. Met141 and His100 are making polar interactions with BLD, while residues Val 170, Gly 18, Met141, His100, Asn 170, Ser 209, Thr 65, Met 130, Gln 19, Ser 101, Leu 102 and Gln 69 are involved in non-polar interactions.

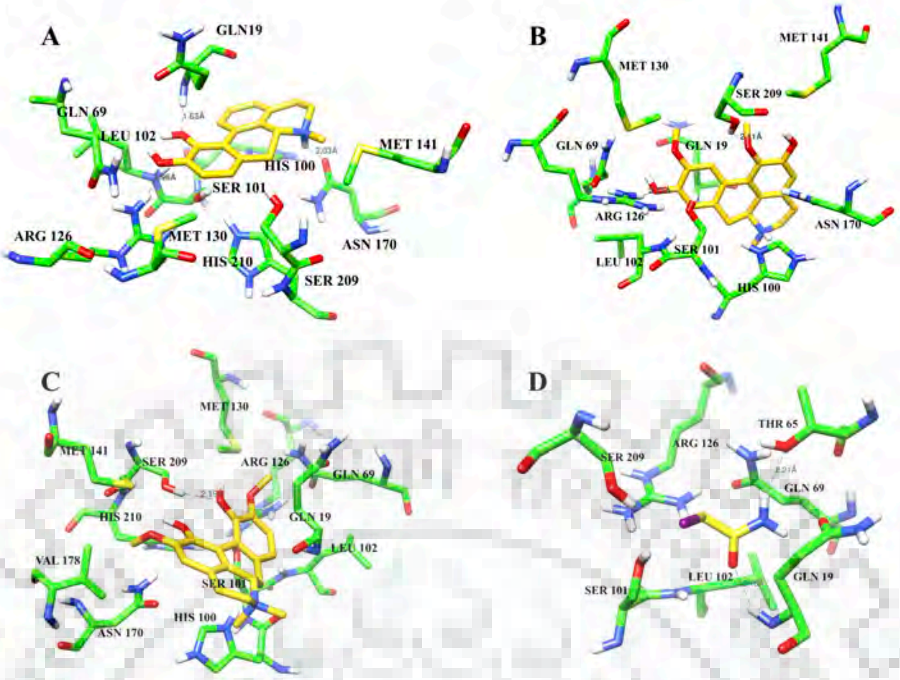
A
GLN19
GLN 69
LEU 102
1.83Å
HIS 100
2.03Å
MET 141
SER 101
ARG 126
MET 130
HIS 210
ASN 170
SER 209
B
MET 141
MET 130
SER 209
GLN 69
GLN 19
ARG 126
ASN 170
LEU 102
SER 101
HIS 100
C
MET 130
MET 141
SER 209
ARG 126
GLN 69
HIS 210
GLN 19
LEU 102
VAL 178
SER 101
HIS 100
ASN 170
D
THR 65
SER 209
ARG 126
2.01Å
GLN 69
SER 101
LEU 102
GLN 19

Figure 4.18 Molecular docking based studies.

Predicted binding mode of AMF (A), BLD (B), MNG (C) and IDA (D) with McFabD. Interacting residues are shown in green color. Ligands are shown in yellow. Hydrogen bonds are labeled and shown as black dash lines.

Binding mode of AMF to McFabD is similar to BLD binding. Both polar and non-polar indications play important role in binding. AMF forms three hydrogen bonds with Gln 19, Arg 126 and Asn 170 residues. Residues involved in hydrophobic interactions include Gly 18, His 100, Ser 209, Asn 170, Met 130, Met 141, Arg 126, Gln 69, Leu 102, Ser 101 and Gln 19. The predicted binding energy of AMF is found to be -7.18 kcal/mol, which is lower than the other ligands used in the current study. Other ligands MNG and IDA are interacting in a similar fashion as BLD and AMF. Table 4.7 shows the list of interacting residues and different interactions involved in binding.

Table 4.7 Predicted binding interactions of McFaBD with different ligands.

Ligand	Hydrogen bonded interactions	Polar interactions (Except hydrogen bonding)	Non-polar interactions
M-CoA	Glu283, Ser21 and Asn63	Not found	Lys64, Gln19, Ser21, Val289, Leu290, Glu283, Thr65, Pro17, Gly18, Leu102, Gln69, Ser206, Val207, Met130, Arg126, Ser200, His210, Asn170, Asn172, His100, Ser101
AMF	Gln19, Asn170, and Arg126	Not found	Gly18, His100, Ser209, Asn170, Met130, Met141, Arg126, Gln69, Leu102, Ser101 and Gln19
BLD	Ser209 and Arg106	Met141 and His100	Val170, Gly18, Met141, His100, Asn 170, Ser209, Thr65, Met130, Gln19, Ser101, Leu102, and Gln69
MNG	Ser209	Not found	Met141, Val178, Asn170, His210, Gly18, His100, Gln19, Leu102, Ser101, Met130, Thr65, Gln69, Ser209 and His210
IDA	Gln19 and Thr65	Not found	Gln19, Gln69, Leu102, Arg126, Ser101, Thr65, Met30

4.3.9 Growth inhibition assay

To assess the *in vivo* efficacy of BLD, AMF, and MNG growth inhibition assay (MIC) has been performed against *Moraxalla caterrhalis* using the broth microdilution method. Apomorphine has inhibited the growth of *Moraxalla* sp. with a MIC value of 4-8 µg/ml, while MIC values of BLD and MNG were determined to 8-16 µg/ml and 32-64 µg/ml respectively.

4.4. Discussion

The emerging resistance in bacterial pathogens against current antibiotics is a pressing concern for human health in all over the world. Therefore, it has become more important to develop new chemical scaffolds to combat the drug resistance related problems. Natural products and their molecular designs offer medicinal chemists a wide range of chemical scaffolds for the development of new drugs and chemical probes[110,111,266]. In this study, we have explored the natural products for their antibacterial effects from the class of aporphine alkaloids. Among aporphine alkaloids, Magnoflorine is known to exhibit antiplasmodial, antiamoebic effects[251] and anti-viral effects against HSV-1 virus[267]. Boldine has shown chemotheraputic effects upon breast cancer with dosage toleration of 100 mg/kg body weight in rats [268] and also known to be a potent anticancer agent at non-toxic concentations[269]. Apomorphine being a dopaminergic agonist have been used in the treatment of Parkinson’s disease and erectile dysfunction [270–272].Till date, one natural inhibitor (corytuberine) from the quinolone alkaloid’s class has been discovered against HpFabD[97]. In this study, FabD from *Moraxella catarrhalis* has been characterized using biochemical, biophysical and *in silico* based studies. The detailed binding studies of aporphine alkaloids with McFabD have been performed.

Biochemical inhibition assay has shown that among these alkaloids MNG have inhibited FabD with K_i and IC_{50} values of 23.2 µM and 19.2 µM respectively which are comparable to AMF kinetic inhibition parameters (K_i = 27.3 µM; IC_{50} = 16.7 µM). Both AMF and MNG have inhibited FabD with stronger affinity as compared to BLD. Also, mode of inhibition of these compunds was found to be non-competitive. However, if compared with corytuberine (IC_{50} = 33.1 ± 3.29 µM), which is known natural inhibitor of FabD (*Helicobacter pylori*), AMF and MNG have better IC_{50} values while BLD have comparable IC_{50} value. One major differences lie in the mode of inhibition, where corytuberine has shown uncompetitive mode for HpFabD while in our case all these aporphine alkaloids have shown non-competitive mode of inhibition.

Fluorescence quenching experiments were carried out to determine the various binding parameters. The binding of all ligands resulted in the loss of fluorescence intensity of McFabD, which lead to the formation of the ligand-protein complex. Based upon the binding parameters determined using fluorescence quenching studies (Table 4.3), it has been found that apomorphine has a stronger binding affinity (2.90×10^4 M^{-1}) as compared to other ligands. Binding affinities of boldine, magnoflorine and M-CoA were comparable to each other. K_b values for all ligands were in 10^4 range which shows the moderate level of binding affinity of McFabD to these ligands. All ligands were binding to McFabD with a stoichiometry of 1:1 ratio. Binding studies were further explored in terms of thermodynamic properties using ITC based titration studies. ITC measures the heat absorbed or released during the binding of a ligand to the macromolecule. Binding reactions of all these ligands to McFabD were spontaneous in nature with a negative value of ΔG. Based on the K_D values we can say that apomorphine and boldine have stronger binding affinities to McFabD as compared to other ligands. Both AMF and BLD have comparable binding affinities, but have different enthalpies and entropies, suggesting a different binding mechanism. Binding signature plots of AMF, BLD, MNG, and IDA have been shown in Figure 4.19.

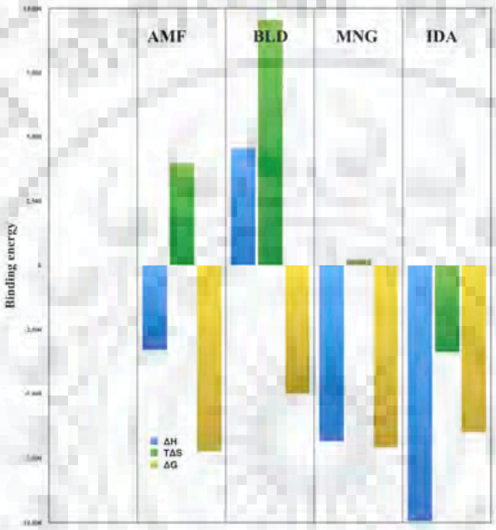

Figure 4.19 Thermodynamic signatures of Binding.

Thermodynamic profile of AMF, BLD, MNG, and IDA binding with McFabD based upon ITC data. The measured parameters include the Gibbs free energy change (ΔG), the enthalpy change (ΔH) and the temperature dependent entropy change (TΔS).

Binding of M-CoA and BLD to McFabD were entropy driven reactions (ΔS>0), where hydrophobic interactions play a main role in the binding while in case of AMF, MNG and IDA binding reactions were enthalpy driven (ΔH<0) where polar interactions were the major contributing factor.

Further, conformational changes observed during the binding of McFabD with these different ligands were monitored using circular dichroism based studies. The far-UV CD studies have shown that upon ligand binding to McFabD, loss of ellipticity at 209 nm, 222 nm and 197 nm were observed, which corresponds to the loss of helical content while sheets content has been increased. This effect was more prominent in the case of BLD and Magnoflorine as compared to other compounds used in this study. Based upon the analysis of near-UV spectra of McFabD in presence of different ligands, it has been found that substantial changes in the tertiary structure of McFabD take place upon ligand binding. Binding of BLD, MNG, and M-CoA have resulted in the MRE increase towards more negative values, which is responsible for increasing the flexibility of aromatic amino acids. MNG and M-CoA have resulted in the increased Phe residues flexibility, while BLD binding has affected Phe and Trp residues. AMF binding has increased the MRE towards positive values with prominent effect in the Phe and Tyr regions. This increase in MRE resulted in the reduced flexibility of Phe and Tyr residues. Based upon these finding it may be assumed that structural rearrangement in the region of α6, α5, and α4 helices might have taken place. Ligand binding may be accompanied by the uncoiling or disordering of α4, α5, and α6 helices. This may be indicative of the intermediate ligand-bound state of McFabD with the structural reorganization of these three helices (α4, α5 and α6) and nearby sheets (β2 and β4). Fluorescence and UV-visible measurements have shown that there was a formation of complex upon ligand binding and changes in the conformation evident by changes in the microenvironment of aromatic amino acids were observed.

The plausible interactions involved during the binding of these ligands to McFabD were studied using molecular docking based investigations. The binding poses of docked compounds were compared with malonate bound (PDB ID: 2G2Y) and M-CoA bound (2G2Z) crystal structures of EcFabD[273]. Binding locations of AMF, BLD, MNG, and IDA were found to be similar to that of malonate bound EcFabD (Figure 4.20).

Malonate has interacted with His201, Ser92, Arg117, Gln11 and Leu93 residues from the active site of EcFabD. Similarly, AMF was interacting with His210, Ser101, Arg126, His100, Asn170, Leu102 and Gln19 residues of McFabD. BLD, MNG, and IDA were also binding to McFabD in a similar fashion as AMF.

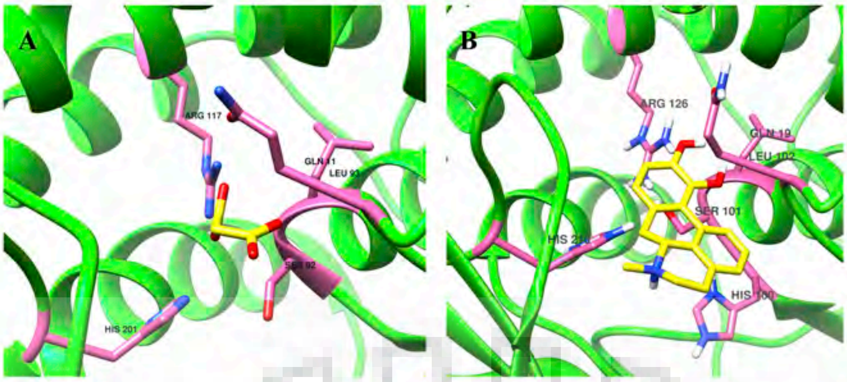

Figure 4.20 Structural comparison of binding poses.

Binding location of malonate bound in the crystal structure of EcFabD (A) and predicted binding location of apomorphine in 3D model of McFabD (B). Interacting residues are shown in hot pink color and ligands are shown in yellow color. From the analysis of binding poses it has been found that aporphine alkaloids are interacting with McFabD in a similar fashion as malonate was interacting with EcFabD in crystal structure. The critical residues that might play important role in the binding of aporphine alkaloids to McFabD are Arg126, Ser101, His209, His100, Leu102, and Gln19.

These observations have shown that these compounds were interacting with active site residues including catalytic residues (Ser and His) in a similar fashion as found in the malonate bound crystal structure of close homologs[273]. So based upon docking poses we can say that critical residues involved in binding include His 210, Leu102, Gln19, Ser 101 and Arg 126. As mentioned in the table 4.6 predicted binding energy of M-CoA (-7.56 kcal/mol) and AMF (-7.18 kcal/mol) was found to be lesser than BLD, MNG and IDA. If we see the chemical structure of aporphine alkaloids as shown in Figure 4.1, differences in hydroxylation patterns and methoxy group patterns resulted in the variation in the binding energy and dissociation constant values. Presence of methoxy groups on boldine and magnoflorine, made these compounds more hydrophobic. As we have observed through binding signatures of these compounds shown in Figure 4.19, binding of apomorphine was favored by both enthalpy change ($\Delta H < 0$) and entropy change ($\Delta S > 0$), while in case of boldine, the reaction was driven mainly by entropy factor, which makes reaction of the boldine is an endothermic process. Reactions of magnoflorine and iodoacetamide were enthalpy driven reactions. Based on the K_D values we can say that AMF scaffold is more appropriate among these compounds, and it has inhibited the *Moraxalla caterrhalis growth in vivo* level at 4-8 µg/mg concentrations. To further validate our study, we have performed docking investigation on McFabD with corytuberine, a natural inhibitor of HpFabD[97] and juglone, a multitargeted inhibitor of HpFabD and HpFabZ[274]. It has been found that corytuberine and juglone occupied similar binding locations in the active site of McFabD as with aporphine alkaloids.

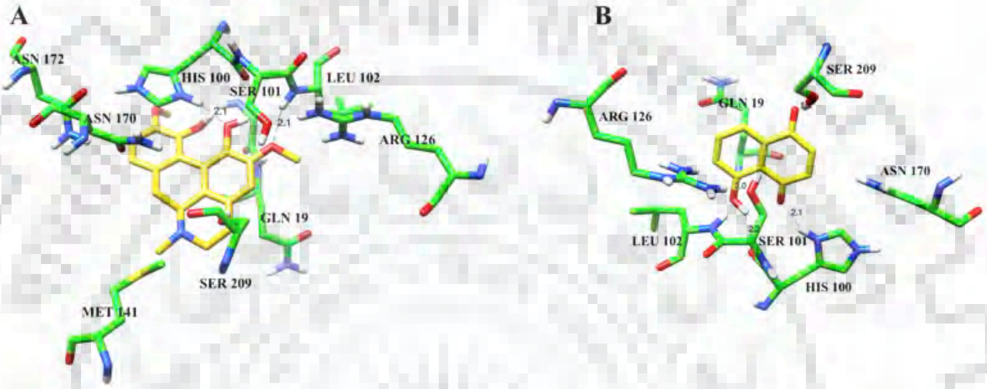

Figure 4.21 Molecular docking of known inhibitor corytuberine (A) and juglone (B) with McFabD. Predicted binding mode of corytuberine (A) and juglone (B)with McFabD. Interacting residues are shown in green color. Ligands are shown in yellow. Hydrogen bonds are labeled and shown as black dash lines.

The predicted binding energy and binding constant of corytuberine and juglone have been given in table (4.6). The predicted binding modes of aporphine alkaloids are similar with corytuberine and juglone binding modes (Figure 4.21) but mode of inhibition were found to different. Also, apomorphine has shown better binding energy (-7.18 kcal/mol) than corytuberine (-6.31 kcal/mol) and juglone (-6.18 kcal/mol) based upon docking calculations. This study suggests that aporphine alkaloids can act as antibacterial agents by targeting FabD enzyme form FAS II pathway. Taken together, all this study explains that amomg these alkaloids, AMF scaffold could be good starting points for the development of lead antibacterial compounds targeting FabD.

4.5. Conclusion

In the current study, biochemical, biophysical and *in silico* characterizations of FabD from *Moraxella catarrhalis* pathogen has been presented. This is the first report where binding studies of aporphine alkaloids to FabD has performed. Aporphine alkaloids had been known to exhibit various biological important activities. In this study, antibacterial actions of apomorphine, boldine, and magnoflorine have been studied. Based on this study, we can say that aporphine alkaloids can act as antibacterial agents by targeting FabD from FAS II pathway. Among these compounds, apomorphine and boldine have a stronger binding affinity to McFabD over other compounds. Based upon the findings of CD and fluorescence studies, substantial changes in the secondary and tertiary structure of McFabD were observed. Among these compounds, apomorphine has shown better binding and in vivo inhibition, as compared to other compounds. In total, we expect this study will help in the development of potent antibacterial agents targeting FabD enzyme.

4.6 Future prospects

In this study, we report the antibacterial action of aporphine alkaloids against *Moraxella catarrhalis* and possible target of these compounds could be FabD enzyme from FAS II pathway. Among these alkaloids, apomorphine has shown good binding and in vivo inhibition as compared to other compounds. To further develop more potent inhibitors, potency and efficacy of these compounds should be increased, and possible way is to make derivatives of apomorphine with different polarity and inhibitory potential must be checked and compared against FabD enzyme.

Chapter 5

Identification and characterization of dual inhibitors against FabD and FabZ using biochemical, biophysical and in silico approaches

Chapter 5

5.1 Introduction

The emergence of drug resistance in bacterial pathogens is pressing concerns in health sector all over the world. It has become more important to develop new approaches to overcome drug resistance[20,32,43,105,266]. Since the bacterial pathogens have developed the resistance against the antibiotics which targeted the essential pathways like cell wall synthesis, DNA (or RNA) replication, protein synthesis, and folate biosynthesis pathways it has become more important to discover antibacterial agents targeting other vital pathways or processes of bacteria. Other essential pathways of bacteria that have been validated for drug development are shikimate pathway, fatty acid biosynthesis, lipid polysaccharide synthesis, cell division, two-component regulatory system, and bacterial efflux pumps[6,8,32].

Being an essential pathway, and minimum chances of cross-resistance to existing drugs targeting other pathways, the type II fatty acid biosynthesis pathway provide excellent opportunity to develop lead compounds against bacteria[79,80,105]. This pathway is validated by the use of potent antibacterials like cerulenin and thiolactomycin, and other empirically selected inhibitors (diazaborines, isoniazid, and triclosan), which specifically inhibit the enzymes from FAS II pathway [77,80]. Also, the higher level of conservation among the different enzymes of FAS II pathway gives the possibility to develop broad-spectrum antibiotics. The substantial differences in the organization of different components of FAS pathway in bacteria (Type II) and mammals (Type II) make effective antibacterials specific to respective targets[75,79,80,94,105,241].

Naturals products and their elaborated molecular frameworks offer medicinal chemist a wide range of chemotypes for the discovery of drugs and chemical probes. Naturals compounds always have biologically relevant scaffolds and pharmacophore patterns with ligand-protein binding motifs [6,110,111]. Naphthoquinones and their derivatives have been known to exhibit various pharmacological properties like antibacterial, anticancer, antiviral, antifungal, etc [275].

In this study, we have shown the inhibitory action of Naphthoquinones (1,4-naphthoquinone) and aporphine alkaloids on two enzymes (FabD and FabZ) of type II Fatty acid biosynthesis pathway from drug resistant *Moraxella catarrhalis*. *Moraxella* *catarrhalis* is a Gram-negative pathogen, which causes infections in respiratory tracts. In immune compromised host, it can cause a number of infections including pneumonia, endocarditis, septicemia, and meningitis[105,171,252].

FabD (Malonyl-CoA: acyl carrier protein transacylase) is an essential enzyme of type II FAS pathway and performs initiation reaction where malonyl moiety is transferred to holo-ACP. Genetic inactivation of FabD gene is lethal in microbes and hence FabD regarded as an attractive drug target for developing broad-spectrum drugs[236,237,273]. FabZ (β-hydroxyacyl-acyl carrier protein dehydratase) is a dehydratase and ubiquitously expressed in type II FAS systems. It is an important enzyme and has uniform distribution in bacteria, which makes FabZ excellent target for drugs development [105,106,186,233].

This chapter has divided into two parts, first part report the 1,4-naphthoquinone (NPQ) as a multi-targeted inhibitor against two key enzymes FAS II pathway from *Moraxella catarrhalis* (McFabZ and McFabD). The structural changes observed upon the binding of NPQ to McFabD and McFabZ, is monitored by using Spectroscopy (Circular dichroism and fluorescence) based techniques. Thermodynamic parameters of binding are determined using ITC technique. Molecular docking was further conducted to predict the binding modes and analyze the interactions. The growth inhibition assay is performed to calculate the MIC value of NPQ against *Moraxella catarrhalis*. In the second part of this chapter, we have shown the inhibitory actions of aporphine alkaloids against McFabZ using biochemical, biophysical and *in silico* based studies. Therefore, this study suggests that a single compound can inhibit the both FabD and FabZ enzymes. NPQ and aporphine alkaloids (AMF, BLD, and MNG) have inhibited the both enzymes and could be exploited as multi-targeted inhibitors against the FAS II pathway for the development of potent antibacterial agents.

5.2 1,4- Naphthoquinone as multi-targeted dual inhibitor of FAS II pathway.

5.2.1 Materials and Methods

5.2.1.1 Materials

1,4-Naphthoquinone is purchased from Sigma. Media components procured from Himedia India or Merck. All other chemicals used were purchased from Sigma and of analytical grade. All molecular biology kits (Genomic DNA isolation, Plasmid isolation, PCR purification and gel extraction) were procured from Qiagen. DNA polymerase, restriction enzymes and T4-DNA ligase were obtained from New England Biolabs. All molecular cloning procedures were performed using standard methods[152]. Purification columns (Ni-NTA and gel filtration) were purchased from GE healthcare. *Moraxella catarrhalis* (MTCC No.445) is obtained from MTCC, Chandigarh. *E.coli* strains (DH5α, BL21 (DE3) and Rosetta) were purchased from Novagen. Primer procurement and DNA sequencing were performed from Eurofins (India).

5.2.1.2 Methods

5.2.1.2.1 Expression and Purification of McFabZ

The cloning, expression and purification of McFabZ is done as previously described [105]. Briefly, McFabZ was cloned in a pET28c expression vector using Nde I and XhoI restriction sites and expressed in *E.coli* Rosetta cells at 20 ^{o}C by inducing with 0.5 mM IPTG. Purification of McFabZ was achieved using Ni-NTA affinity chromatography using imidazole as eluent followed by size exclusion chromatography using Buffer A (25 mM Tris-HCl, 100 mM NaCl and 5 %Glycerol) as elution buffer.

5.2.1.2.2 Expression and purification of McFabD

McFabD was cloned expressed and purified in a similar way as McFabZ. 957 bp McFabD gene was PCR amplified and digested using NdeI and XhoI restriction enzymes followed by ligation into pET28c expression vector using T4 DNA ligase. Correct clones were screened and identified using restriction digestion followed by DNA sequencing. McFabD was expressed in *E.coli* Rosetta cells at 30 ^{o}C with induction of 0.4 mM IPTG. Cell pellets were suspended in lysis buffer (25 mM Tris-HCl pH 7.8, 200 mM NaCl, 5% glycerol & 1 mM PMSF) and disrupted using French Press followed by high-speed centrifugation to give a clear supernatant. Ni-NTA affinity-based chromatography used to purify the protein using imidazole as eluent. Fractions containing the purified McFabD protein were pooled together and dialyzed against Buffer B (25 mM Tris-HCl pH 7.8, 100 mM NaCl, 2 % glycerol and 0.5 mM TCEP).

5.2.1.2.3 McFabZ inhibition assay

The inhibitory activity of NPQ against McFabZ is monitored using reported spectrophotometric method [104–106,186]. NPQ has been dissolved in DMSO (100 %) and added to the reaction mixture at conc. ≤ 1 % of DMSO. A standard reaction mixture consists of 20 μg McFabZ, 20 mM Tris-HCl (pH 7.8), 100 mM NaCl, 2% glycerol and 1% DMSO in the total volume of 200 μL. IC_{50} was determined by fitting the data in dose response curve using Graph pad prism[193]. Reaction mechanism was studied by varying inhibitor concentration (0-100 μM) and in consideration of steady-state kinetics. McFabZ was incubated with the inhibitor for 30 min at 4 ^{o}C, and reaction was started by adding the substrate crotonyl-CoA (10-200 μM). Data was fitted using graph pad prism software.

5.2.1.2.4 McFabD inhibition assay

The inhibitory activity of NPQ against McFabD is determined using spectrophotometric assay mentioned in section 4.2.2.4. IC_{50} was calculated by fitting the data in the dose response curve using Graphpad prism. Kinetic inhibition constant (K_i) is determined by the varying substrate (10-150 μM) and NPQ (0-100 μM) and in consideration for steady state kinetics. NPQ was incubated with McFabD for 30 min at 4 ^{o}C and then the reaction was initiated by adding malonyl- CoA. The Data was fitted using Graph-pad prism.

5.2.1.2.5 Circular dichroism based studies

The far-UV and near-UV CD spectra were recorded using J-Model-1500 spectrophotometer (JASCO) equipped with temperature control system. McFabD and McFabZ concentrations were kept at 0.2 mg/ml in buffer C (20 mM Sodium phosphate pH 7.8, 100 mM NaCl, 2 % glycerol and 0.5 mM TECP). Both proteins

(McFabZ and McFabD) were incubated with varying conc. of NPQ for 15 min and then CD spectra were recorded at 25 ^{o}C. All data analysis was performed by Dichroweb server[195]. All data expressed in molar ellipticity -Δε (deg cm^{2} dmol^{-1}).

5.2.1.2.6 Fluorescence quenching based binding studies

Binding investigations of NPQ with McFabZ and McFabD were studied using fluorescence quenching based experiments. Fluorescence spectra were recorded at 25 ^{o}C using Horba Fluro Log spectrofluorometer using 1.0 cm path length cell with emission slits at 5 nm. The excitation wavelength was kept at 295 nm in order to excite tryptophan residues in McFabZ and McFabD proteins. Both proteins conc. were kept around 2-5 μM in buffer C. The emission was recorded in the range of 300-500 nm ranges. In quenching experiment, a fixed amount of protein (3 μM) was kept in the cuvette and manually titrated with successive addition of NPQ (1-20 μM). The data were fitted using a non-linear regression using one site binding analysis using equation $Y = B_{max}.X/(K_{d(app)} + X)$, where B_{max} is maximum extent of quenching and $K_{d(app)}$ is apparent dissociation constant[276]. Three parallel scans have been taken for each respective reaction.

5.2.1.2.7 Binding studies using ITC

Thermodynamic parameters of binding of NPQ with McFabZ and McFabD were determined using ITC based binding assays. All reactions were performed at 25 ^{o}C using microcal ITC200 (GE Health care). Both proteins were dialyzed using Buffer D (Tris-HCl pH 7.8, 100 mM NaCl, 2 % glycerol and 0.5 mM TCEP). The corresponding amount of DMSO (1%) was added to protein solution to avoid the buffer-buffer mismatch. A typical titration reaction consists of protein in the sample cell (50- 100 μM) and NPQ in the syringe (1-2 mM) with stirring speed of 1000 rpm. The initial delay was kept at 60 s. After the initial injection (0.5 μl, not used in data fitting), 15-20 injections (2.0 μl each) were performed with 150 seconds gap between each injection, and heat changes were subsequently monitored. The reference cell was kept at 8.0 μW. ITC data were analyzed using one site model of Origin 7.0 software.

5.2.1.2.8 Molecular docking

The possible binding mode of NPQ with McFabZ and McFabD was predicted using molecular docking based studies. 3D models of McFabZ and McFabD were made using Modeller[277] and Swiss model[197] based upon homology. Best 3D models for respective proteins have been selected on the basis of energy minimization. The docking study of McFabZ and McFabD with NPQ were carried out using Autodock 4.2[163] form ADT tools. Grids maps were prepared using 60×60×60 grid points with 0.2 Å spacing in the x, y and z directions centered at the active site of McFabZ and McFabD respectively. Autogrid4 and aurodock4 programs were used for calculating energy maps and docking of ligands, respectively. One hundred docked structure, i.e. 100 runs were generated using Lamarchian Genetic Algorithm. Docked conformations were converted into the pdbqt format and analyzed. Chimera tool[204] was used for visualization and figures generation.

5.2.1.2.9 Growth inhibition assay

MIC of 1,4-Naphthoquinone against *Moraxella catarrhalis* has been determined using a broth micro dilution method [105,166,278]. A concentration gradient (0.5 µg/ml – 256 µg/ml) of inhibitors was tested. A single colony of *Moraxella catarrhalis* strain MTCC No. 445 was used to inoculate the nutrient broth medium. Correlation between OD_{600} and colony forming units (cfu) has been determined using serial dilution technique. Bacterial suspension adjusted to 2.0×10^6 cfu per ml was used to inoculate 96 well microtiter plates. 100 µl of broth solution was added to all wells. 50 µl of inhibitor solution was used in each well, except growth control (broth and inoculum) and sterility control (broth only) wells. 50 µl of bacterial suspension adjusted to 2.0×10^6 cfu per ml has been used which gives final inoculum 5×10^5 cfu per ml. The microtiter plate was then incubated at 37 ^{o}C for 16-20 h.

5.2.2. Results

5.2.2.1 Kinetic inhibition of McFabZ and McFabD

Inhibitory activities of NPQ against McFabZ and McFabD have been determined using biochemical assays. The kinetic inhibition parameters (K_i and IC_{50}) have been determined and given in Table 5.1. NPQ has inhibited the McFabZ with K_i of 21.86 ± 3.08 µM and IC_{50} of 26.67 ± 1.34 µM, and McFabD with K_i 19.36 ± 4.64 µM of and IC_{50} of 23.18 ± 2.48 µM respectively.

Mode of inhibition of NPQ has been analyzed by plotting double reciprocal plots (LB plots) as shown in Figure 5.1. Based on the analysis of LB plots, NPQ was found to be a non-competitive inhibitor of McFabZ and McFabD.

Table 5.1 Kinetic inhibition parameters of NPQ against McFabD and McFabZ

Enzyme	***K*$_i$ (μM)**	**IC$_{50}$ (μM)**
McFabZ	21.86 ± 3.08	26.67 ± 1.34
McFabD	19.36 ± 4.64	23.18 ± 2.48

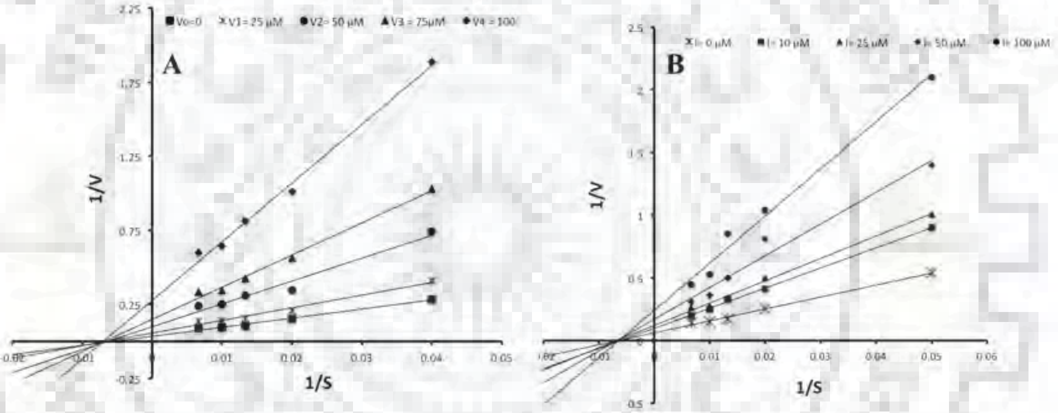

Figure 5.1 Kinetic inhibition of McFabZ and McFabD by NPQ.

Double reciprocal plots of kinetic inhibition of McFabZ (A) and McFabD (B) by NPQ. Mode of inhibition is determined to be a non-competitive or mixed type.

5.2.2.2 Monitoring changes in secondary and tertiary structures upon the binding of NPQ

Circular dichroism is a useful technique to study the changes observed in the conformation of proteins upon ligand binding. The far-UV CD spectra give information about the secondary structure elements while near-UV CD measurements are useful in depicting the changes observed in the tertiary structure[194,216,279]. The Far-UV CD spectra of McFabD and McFabZ in native conditions are shown in

Figure 5.2. For native McFabD protein, there is a presence of characteristic minima at 209 nm and 223 nm and maxima at 197 nm, which shows the presence of helical content in protein. Broad minima in the range of 210-220 depict the presence of b-sheets contents. The helical, sheets and coils content for a native protein was found to be 41.7 %, 14.0 %, and 21.7 % respectively. Similarly for McFabZ protein characteristic negative peaks at 208 nm and 222 nm, and positive peaks in the range of 190-195 nm were observed. Broad minima in the range of 210-220 show the presence of β- sheets content. For a native McFabZ, there is the presence of 20.5 %, 38.6 % and 16.5 % helical, sheets and coils contents. Upon the binding of NPQ to both proteins, changes in the secondary structure elements have been observed.

5.2.2.2.1 Monitoring structural changes in McFabD

It is clearly shown in the far-UV spectra (Figure 5.2A), with increasing inhibitor (NPQ amount) there is a loss of ellipticity at the characteristic peaks (209 nm, 223 nm, and 197 nm). The common observation was the loss of helical and sheet contents with increasing inhibitor amount when compared with native spectra. At higher NPQ Concentration (150 μM), unfolding of McFabD took place with helical and sheets contents of McFabD were found to be 13.8 % and 11.5 % respectively.

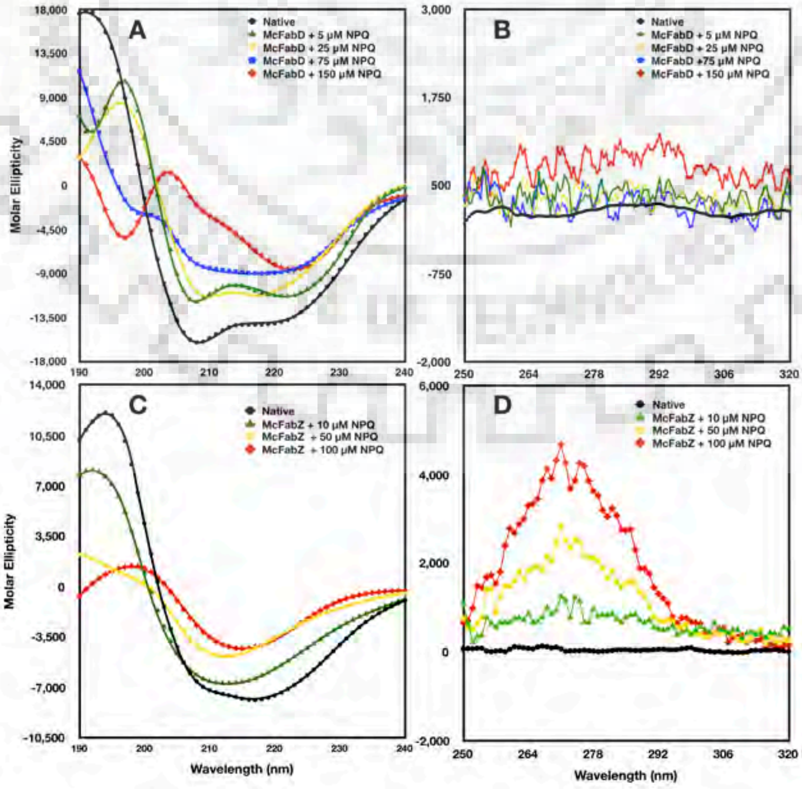

Figure 5.2 The far-UV and near-UV CD spectra of McFabD and McFabZ upon the binding of NPQ. Loss of helical content was observed in both cases.

The near-UV CD spectra arise due to the presence of aromatic amino acids. The near-UV CD spectrum of McFabD in native condition shows negative peaks in the region of Phe (255 nm-270 nm) and Trp (290 nm-305 nm), while the positive peak in the region of Tyr (275 nm-282 nm). Upon the addition of NPQ, changes observed in the near-UV CD spectra. There is an increase in the ellipticity towards positive values with increasing concentrations of NPQ. Effect becomes more evident at the higher concentration as shown in Figure 5.2B.

5.2.2.2.2. Monitoring structural changes in McFabZ

From the Far-UV CD spectra of McFabZ (Figure 5.2C) under different amounts of NPQ, we have observed the loss of helical and sheet contents in McFabZ as evidenced by the diminished ellipticty at characteristic peaks of alpha helices (222 nm, 208 nm) and b sheets (210-220 nm). At higher concentration of NPQ (100 µM), helical and sheet contents were found to be 10.2 % and 23.2 % respectively. Effect on the near-UV spectra has been shown in Figure 5.2D. The native McFabZ protein shows positive peaks in the region of Tyr and Phe regions, while negative peak in Trp region. Upon ligand binding, increase in MRE towards negative has been observed with more effect in the region of Phe (255 nm-270 nm).

5.2.2.3 Binding studies using Fluorescence quenching

Fluorescence spectroscopy is the widely used technique to study the ligand-protein interactions[105,259,280–282]. In this study, tryptophan based fluorescence quenching experiments were conducted to study the binding of NPQ to McFabZ and McFabD proteins. Under native conditions (buffer C & 5 µM protein concentration), McFabZ and McFabD both show emission spectra (λmax) at 351 nm and 330 nm respectively. It means for McFabZ, single tryptophan residue is exposed in the polar environment while for McFabD tryptophan residues (Trp53, Trp80 and Trp266) are exposed in the hydrophobic region comparatively.

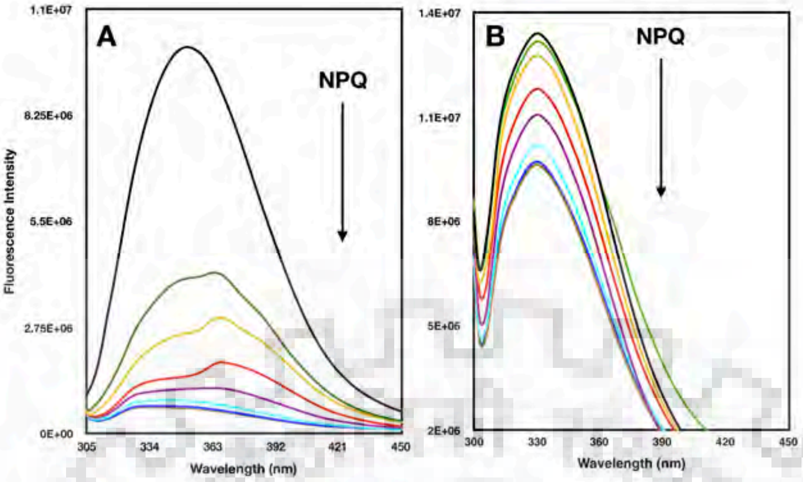

Figure 5.3 Fluorescence emission spectra of McFabZ (A) and McFabD (B) in presence of NPQ.

Upon the addition of NPQ, there is a decrease in the fluorescence intensity in both cases. With the increasing amount of NPQ, emission spectra of McFabZ shifted towards higher wavelength (Red shift), which means Trp residue got more exposed towards the polar environment. For McFabD, there is not much change in the λmax upon the interaction with NPQ. Mechanism of fluorescence quenching was determined using Stern-Volmer equation as follows:

$F_0/F = 1 + K_{sv} [Q] = 1 + K_q \tau_O [Q]$

Where F_0 and F are the fluorescence intensities in the absence and presence of quencher (Q), K_{sv} is the quenching constant, K_q is the bimolecular quenching rate constant and τ_O is the fluorescence lifetime without quencher. For proteins, the value of τ_O is 10^{-8} sec. Values of K_{sv} and K_q have been calculated for both proteins and given in Table 5.2. The K_q values for McFabZ and McFabD were determined to be the range of 10^{14} and 10^{12} respectively, which depicts the static quenching mechanism and ground state complex formation.

Table 5.2 Fluorescence quenching parameters

Enzyme	K_{sv} (M^{-1})	K_q ($M^{-1}S^{-1}$)	R^2
McFabZ	1.14×10^6	1.14×10^{14}	98.8

McFabD	3.16×10^4	3.16×10^{12}	97.7

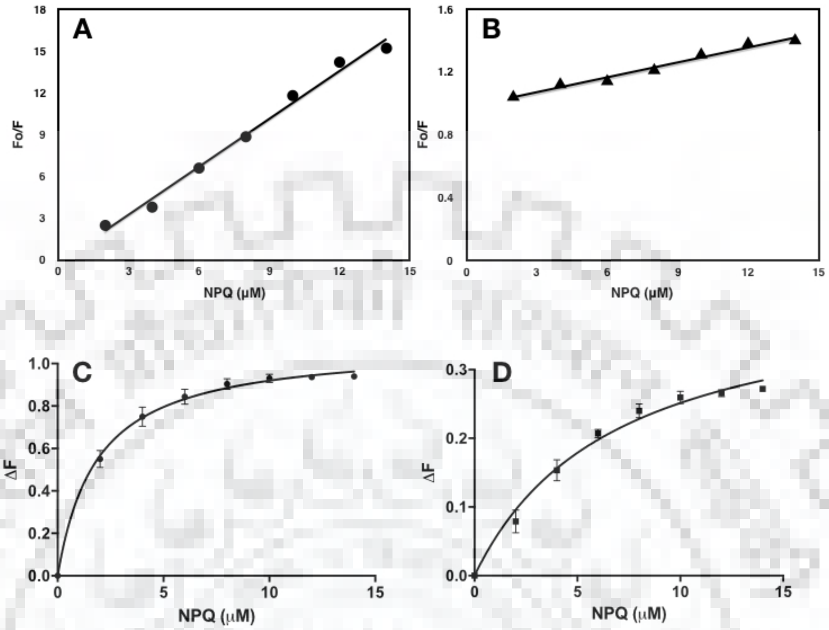

Figure 5.4 Stern-Volmer plots and fluorescence quenching based binding studies. Stern-Volmer plots of McFabZ (A) and McFabD (B) quenching with NPQ. Mechanism of quenching was found to be static in both cases. Binding saturation curves of McFabZ (C) and McFabD (D). $\Delta F = F_0 - F/F_0$, where F_0 and F are the fluorescence intensity in absence and presence of quencher (NPQ).

The binding constant (K_d) for both proteins were calculated as per the equation mentioned in methods and data were fitted in using non-linear regression analysis. Binding saturation curves for both proteins have been shown in Figure 5.4C & 5.4D. Based upon the fluorescence binding kinetics, McFabZ has shown a stronger affinity ($K_d = 1.85 \pm 0.13$) for NPQ as compared to McFabD ($K_d = 12.74 \pm 1.67$).

5.2.2.4 Thermodynamic studies of Binding interactions

Isothermal thermal titration calorimetry (ITC) based binding assays were performed to determine the thermodynamics of NPQ interactions with McFabZ and McFabD. Thermodynamic parameters, which include enthalpy change (ΔH), entropy change (ΔS), equilibrium dissociation constant (K_D), free energy change (ΔG & binding sites

(N) have been evaluated and shown in Table 5.3. Binding isotherms and fitted curves for both proteins have been shown in Figure 5.5.

Downward trends in binding isotherms have shown that reactions of NPQ with McFabZ and McFabD were exothermic in nature, which were driven by enthalpy change ($\Delta H < 0$). Both proteins are binding to NPQ in 1:1 stoichiometric ratio as indicated by N values. Based on the K_D values we can say that McFabZ (K_D = 12.5 µM) has a stronger affinity for NPQ as compared to McFabD (K_D = 18.56 µM).

Table 5.3 Thermodynamic parameters of binding of NPQ with McFabZ and McFabD

Protein-ligand	Enthalpy change, ΔH (cal/mol)	Entropy change, ΔS cal/mol/degree	Free energy change, ΔG (cal/mol)	Dissociation constant, K_D (µM)	N (Binding sites)
McFabZ-NPQ	-4.70×10^5	-1.56×10^3	-5.5×10^3	12.5	0.39 ± 0.12
McFabD-NPQ	-1.23×10^5	-393	-5.8×10^3	18.56	0.43 ± 0.04

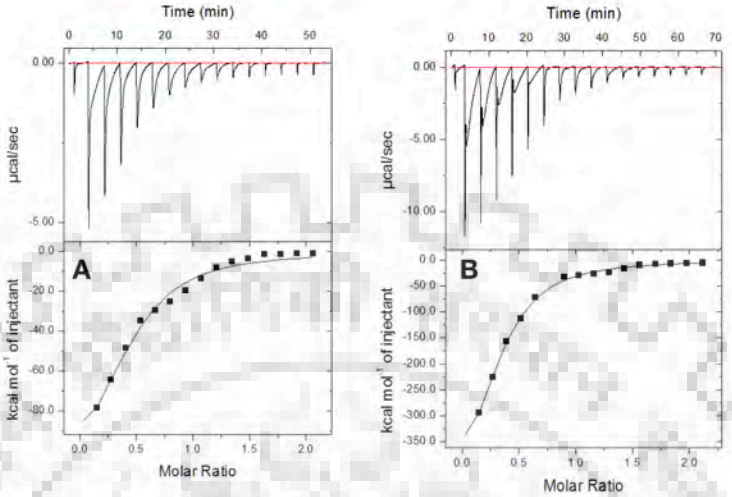

Figure 5.5 Binding studies using ITC based assay.

Thermograms and fitted curves for the binding of NPQ with McFabD (A) and McFabZ (B). Reactions of NPQ with McFabD and McFabZ are accompanied by enthalpy changes (ΔH<0) and exothermic in nature.

5.2.2.5 Predicting binding modes using molecular docking based studies

The possible interactions involved during the binding of NPQ to McFabZ and McFabD have been predicted by performing docking studies using Autodock4.2. 3D structural model of both proteins was built based upon homology. The suitable templates (3HJV for McFabD and 5bux for McFabZ) have been used to build the 3D model. The predicted 3D models were further validated using different validations tools[201,202,222,225]. The binding constant and binding energy of NPQ for McFabZ and McFabD were given in Table 5.4. Figure 5.6 shows the binding mode of NPQ with McFabZ and McFabD respectively.

5.2.2.5.1 McFabZ-NPQ docking study

Based on the docking studies, NPQ is interacting with the active site of mcFabZ through polar and non-polar interactions. NH group of Tyr112 residue is involved in the hydrogen bonding with the Oxo group (O1) of naphthalene ring. Other residues are interacting through hydrophobic interactions. These are Glu88, Ala91, Gln92, Gly75, Phe99, Leu37, Pro38, His39, Phe114, Tyr112, Leu111, His74*, and Phe75* (* indicating the residue from opposite monomer). The predicting binding energy and affinity of NPQ for McFabZ were - 6.71 kcal/mol and 12.12 μM respectively. Figure 5.6B shows the binding mode and interactions of NPQ with McFabZ.

Table 5.4 Binding parameters and predicted binding interactions

Complexes	**Binding constant (μM)**	**Binding energy (kcal/mol)**	**Hydrogen bonded interactions**	**Hydrophobic interactions**
McFabZ-NPQ	12.12	- 6.71	Tyr112	Glu88, Ala91, Gln92, Gly75, Phe99, Leu37, Pro38, His39, Phe114, Tyr112, Leu111, His74*, and Phe75*
McFabD-NPQ	63.63	- 5.72	Ser209, Gln19, and Leu102	His210, Ser209, Met130, Arg126, Asn170, His100, Ser101, Leu102, Gly103, Gln19, and Gly18

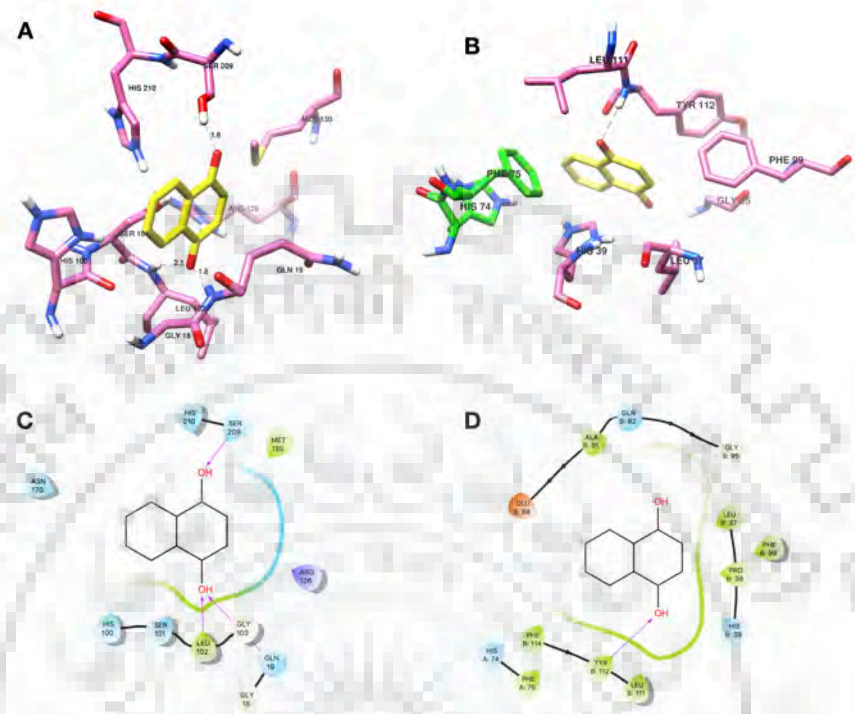
A
B
C
D
HIS 210
SER 209
MET 130
ARG 126
GLN 19
LEU 102
GLY 18
HIS 100
LEU 111
TYR 112
PHE 99
PHE 75
HIS 74
HIS 39
OH
OH

Figure 5.6 Docking studies of McFabZ and mcFabD with NPQ.

Binding mode of NPQ with McFabD (A) and McFabZ (B). Different chains of McFabZ are colored cyan and hot pink. Ligands have been shown in tan color. H-bonds are shown as dashed lines. Interactions of NPQ with McFabD (C) and McFabZ (D).

5.2.2.5.2 McFabD-NPQ docking study

Docking study suggested that binding of NPQ to McFabD involves both polar as well as non-polar interactions. Ser209, Gln19, and Leu102 residues were interacting with Oxo groups through hydrogen bonding. Residues His210, Ser209, Met130, Arg126, Asn170, His100, Ser101, Leu102, Gly103, Gln19, and Gly18 were interacting through hydrophobic interactions. Three hydrogen bonds were formed as follows: 1) NH-group of Gln19 with O2 (Oxo group) of NPQ, 2) OH-group of Ser209 with O1 (Oxo group) of NPQ, and 3) NH- group of Leu102 with O2 (Oxo group) of NPQ. The predicted binding energy and affinity of NPQ for McFabD were -5.72 kcal/mol and 63.63 µM respectively.

5.2.3 Discussion

Natural-products based synthetic compounds can provide the innovative and probable solutions to address the critical and continuing drug design challenges. Being an essential pathway, the type II FAS pathway will remain important part for the development of broad-spectrum antibacterial agents[78–80,105]. In the current study, we are reporting 1,4 Naphthoquinone as a multi-targeted inhibitor of FAS II pathway targeting FabD and FabZ enzymes. Biochemical based enzymatic assays have shown that NPQ has inhibited both FabD and FabZ enzymes with K_i values of 32.46 µM and 35.86 µM respectively. Mode of inhibition of NPQ has been analyzed by plotting a double reciprocal plot (Figure 5.1) and it was found that NPQ was inhibiting both enzymes through non-competitive or mixed mode. Structural changes in McFabD and McFabZ enzymes upon the binding of NPQ were monitored using circular dichroism based studies. In both cases, the loss of ellipticity was observed at the characteristic bands of alpha helices and beta sheets in the Far-UV CD spectra which led to the loss of helices and sheets contents upon the binding of NPQ. In near-UV CD studies, binding of NPQ to McFabD led to the increase in the MRE values towards positive which depicts the reduction in the flexibility of aromatic residues with profound effect on Phe and Tyr regions. In McFabZ, there is an increase in the MRE towards negative values with increasing amount of NPQ that led to the increase in the flexibility of aromatic amino acids. Fluorescence quenching based studies have shown that there is a loss of fluorescence intensity in McFabD and McFabZ upon the addition of NPQ and possible mechanism of quenching is found to be static in both cases with the formation of ground state complexes. Binding studies were further evaluated using ITC based titration assays to determine the thermodynamics of interactions. In both cases, reactions of NPQ with McFabZ and McFabD were spontaneous in nature as evidenced by negative free energy values ($\Delta G < 0$). Both reactions were enthalpy driven, which shows that polar interactions were the major contributing towards binding. NPQ has a better binding affinity for McFabZ as compared to McFabD based upon the K_D values which are in agreement with binding constant data obtained by fluorescence quenching based binding studies.

The plausible interactions involved during the binding of NPQ to McFabZ and McFabD were predicted using molecular docking based studies. Binding poses of McFabZ-NPQ complex were compared with the emodin bound HpFabZ[228] for comparative analysis. NPQ is binding deep inside the active site pocket and interacting with key residues His39, His74*, Tyr112, Phe99, Phe75*, Leu37 and Leu111. While in case of HpFabZ, emodin is sandwiched between Tyr100 and Pro112* residues. In case of McFabD, we have compared the docking poses with the malonate bound crystal structure of EcFabD[273]. NPQ is interacting with McFabD in a similar fashion as malonate interacted with EcFabD. Critical residues that might play important role in NPQ-McFabD binding are Arg126, Gln19, Leu102, His100, and Ser210 while in EcFabD-malonate case these residues are Arg117, Gln11, Leu93, Ser92, and His201. The predicted binding energy of McFabZ-NPQ complex (-6.71 kcal/mol) is lesser than the McFabD-NPQ complex (- 5.72 kcal/mol), which shows NPQ has a stronger binding affinity for FabZ as compared to FaD which is agreement with ITC and fluorescence binding data. However, biochemical data suggests that NPQ has similar binding affinity for both McFabZ and McFabD in respect to Kinetic inhibition (K_i) values while NPQ has comparatively better IC_{50} values for FabZ over FabD enzyme. Growth inhibition assay on *Moraxella catarrhalis* we have found that NPQ has shown growth inhibition at 8-16 µg/ml MIC value. To further validate NPQ as a multi-targeted inhibitor of type II FAS pathway, we have tried in silico based docking studies with EcFabI enzyme (PDB: 1QG6) from the same pathway. NPQ has shown binding to EcFabI with binding constant and binding energy of 20.08 µM and -6.41 kcal/mol respectively. Docking poses of docked EcFabI-NPQ complex has been compared with Triclosan bound crystal of EcFabI complex[283] and its found that NPQ is binding in the same pocket in similar fashion and interacting with Tyr156 through H- Bonds. Therefore, current study suggests that NPQ can act as multi-targeted inhibitors of FAS II pathway, and biochemical and biophysical studies have shown that it is inhibiting McFabZ and FabD enzymes. Our *In silico* based docking studies have shown the possibility that NPQ can also bind to FabI enzyme along with FabZ and FabD enzymes rendering its applicability towards multi-targeted inhibitors. We expect the current study will help further in the development of potent inhibitors of FAS II pathway with improved potency and efficacy and NPQ scaffold might be useful for developing lead compounds targeting multiple targets from the FAS II pathway.

5.3 Characterization of aporphine alkaloids as inhibitors of McFabZ

5.3.1 Kinetic inhibition of McFabZ by aporphine alkaloids

The biochemical inhibition assay of McFabZ for aporphine alkaloids has been performed in the similar way as described in 5.2.1.2.3 section. BLD, MNG, and AMF have been dissolved in the DMSO and added to the reaction mixture with ≤ 1% of DMSO. Kinetic inhibition parameters (Ki and IC50) have been determined.

Based upon the inhibition assay it has been found that among these alkaloids BLD has better K_i value (12.14 ± 2.42 µM) as compared to MNG (K_i = 50.01 ± 7.033 µM) and AMF (K_i = 62.06 ± 6.57 µM). IC_{50} values of BLD, AMF, and MNG against McFabZ were determined to be 20.56 ± 1.23 µM, 76.56 ± 4.6 µM and 41.88 ± 6.7 µM respectively.

Mode of inhibition of these inhibitors has been determined via plotting double reciprocal plots as shown in Figure 5.7. All these inhibitors (AMF, BLD, and MNG) have inhibited the McFabZ enzyme via non-competitive (mixed kind) mode of inhibition.

5.3.2 Binding studies using Fluorescence bases quenching

Binding of FabZ with AMF, MNG, and BLD have been performed using fluorescence quenching. Fluorescence quenching experiments have been conducted in the similar way as mentioned in section 5.2.1.2.6. Native spectra of McFabZ shows emission maxima (λ_{max}) at 351 nm which depicts that tryptophan residue in McFabZ is exposed in the surface region.

Binding of AMF and MNG to McfabZ led to the loss of fluorescence quenching while BLD resulted in the fluorescence enhancement in titration experiments as shown in Figure 5.8. In MNG and AMF, the blue shift was observed in the λ_{max} emission while in case of boldine large red shift was observed.

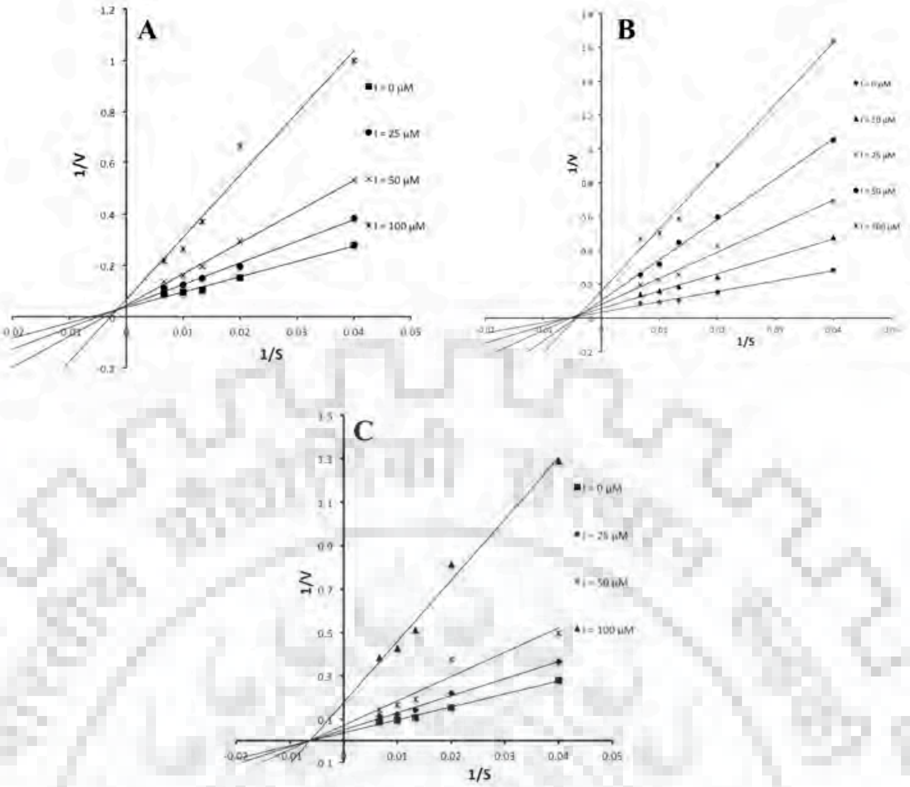

Figure 5.7. Kinetic inhibition of McFabZ by aporphine alkaloids.

Double reciprocal plots of inhibition of McFabZ by AMF (A), BLD (B) and MNG (C).

Binding constant (K_d) is calculated as per the equation mentioned in section 5.2.1.2.6. Binding constant (K_d) values for AMF, BLD and MNG were determined to 12.28 ± 3.1 µM, 21.76 ± 4.7 µM, and 15.4 ± 1.9 µM respectively. Binding of AMF and MNG have a comparative similar binding affinity for McFabZ as compared to BLD. Figure 5.9 shows the binding of these aporphine alkaloids to McFabZ.

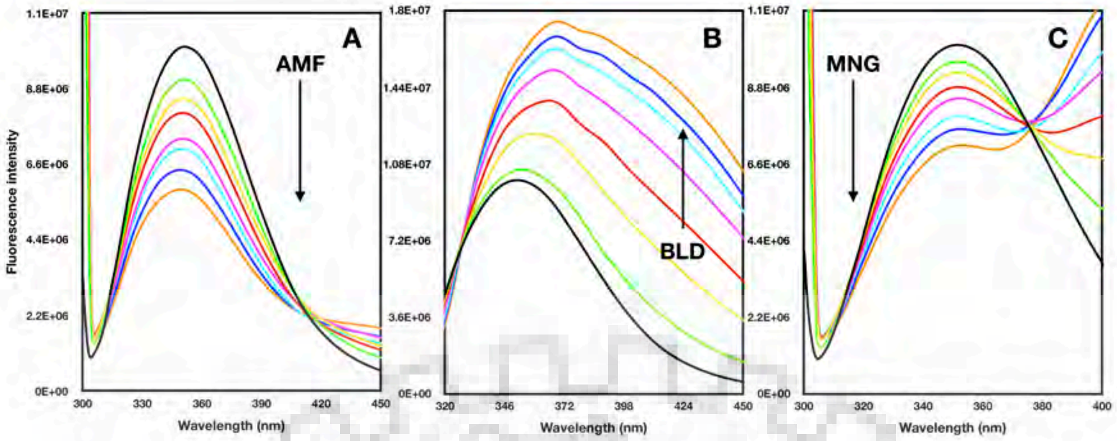

Figure 5.8. Fluorescence emission spectra of McFabZ in presence of AMF (A), BLD (B) and MNG (C). Binding of AMF and MNG to led to the decrease in the fluorescence intensity while BLD led to fluorescence enhancement.

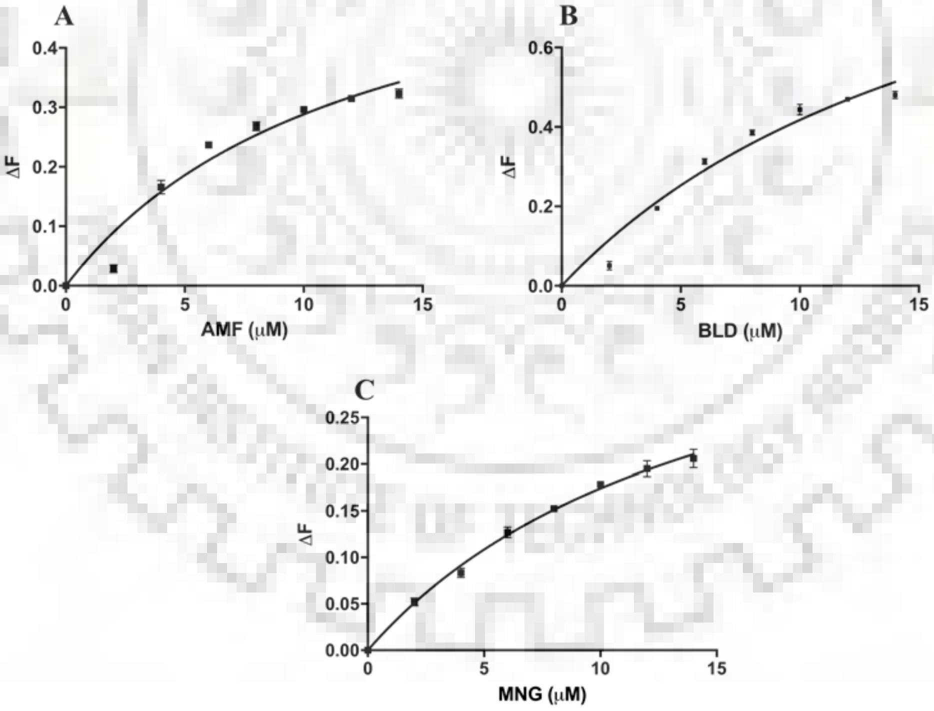

Figure 5.9 Fluorescence based binding studies of AMF (A), BLD (B), and MNG (C) with McFabZ.

5.3.3 Molecular docking studies

Molecular docking based binding studies were further performed to decipher the binding mode of aporphine alkaloids with McFabZ. These three alkaloids are interacting in a similar fashion with McFabZ and interacting with active site key residues and tunnel residues through polar as well as non-polar interactions. Table 5.5 shows the interacting residues and docking parameters for AMF, BLD, and MNG. Based upon the docking studies, MNG has shown a stronger binding affinity for McFabZ with a binding energy of -9.06 kcal/mol followed by BLD (-8.91 kcal/mol) and then AMF (-8.6 kcal/mol). Figure 5.10 shows the docking poses of these alkaloids and their possible interactions with the McFabZ active site.

Table 5.5 Docking results summary

Ligands	**Binding energy (kcal/mol)**	**Binding constant ((μM))**	**Polar interactions (H-bonding)**	**Hydrophobic intercations**
Apomorphine	- 8.6	0.4935	Tyr112	Leu111, Phe99, Tyr112, Phe114, Gln92, Glu88, His39, Val84*, Gly83*, Phe95*, His74*
Magnoflorine	- 9.06	0.2295	Gly83*, Glu88	Glu88, Phe114, Leu113, Gly75, Tyr112, His39, Leu111, Phe95*, His74*, Ile80*, Pro82*, Gly83*, Val84*
Boldine	- 8.91	0.293	Tyr112, Glu88	Leu111, Leu113, Phe114, Tyr112, Ala91, Gln92, Glu88, His39, Gly83*, His74*, Phe75*, Ile80*, Val125*

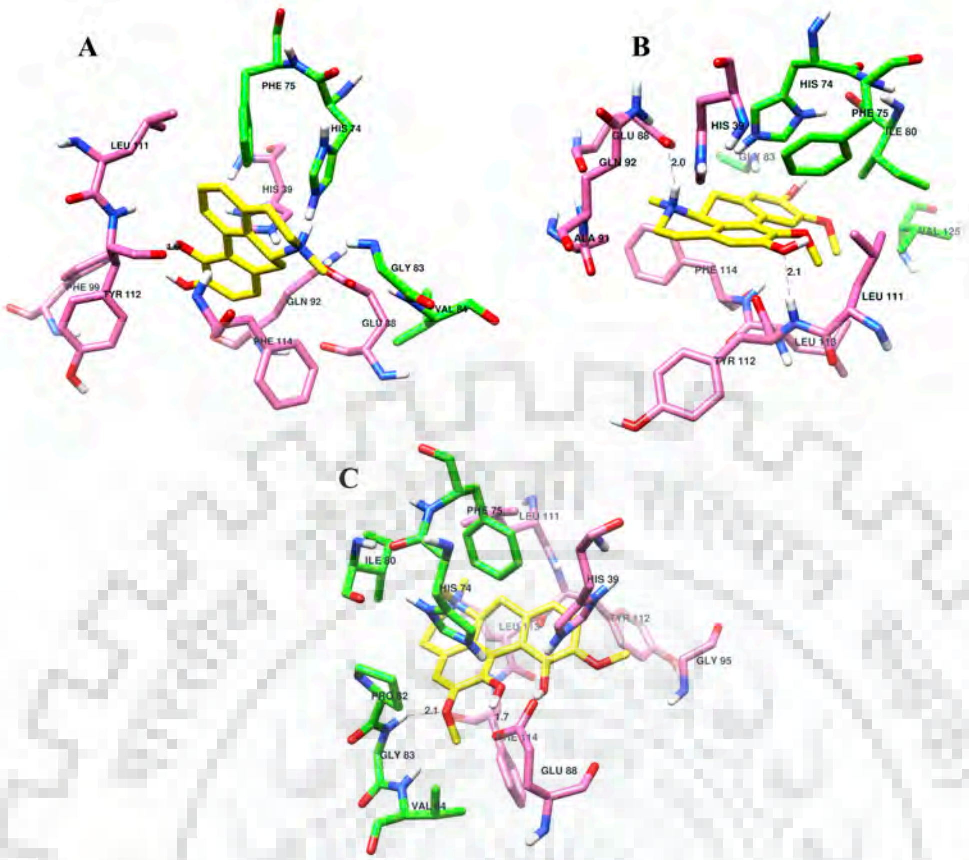
A
PHE 75
HIS 74
LEU 111
HIS 39
GLY 83
VAL 84
PHE 99
TYR 112
GLN 92
GLU 88
PHE 114
B
HIS 74
PHE 75
ILE 80
GLU 88
HIS 39
GLN 92
GLY 83
2.0
ALA 91
VAL 125
PHE 114
2.1
LEU 111
LEU 110
TYR 112
C
PHE 75
LEU 111
ILE 80
HIS 74
HIS 39
TYR 112
LEU 113
GLY 95
PRO 82
2.1
1.7
GLY 83
PHE 114
GLU 88
VAL 84

Figure 5.10 Molecular docking of McFabZ with AMF (A), BLD (B) and MNG (C). Binding mode of Aporphine alkaloids with McFabZ. Both chains of McFabZ are shown as green and hot pink color. Ligands are shown in yellow color and H- bonds as black dashed lines.

5.4. Conclusion and future prospects

In this study, we have shown the inhibitory action of NPQ against FabD and FabZ enzymes. Also, aporphine alkaloids have shown the inhibitory potential against FabZ along with FabD. This study explores the possibility of these compounds to act as dual inhibitors of these two enzymes. NPQ have shown binding with both FabD and FabZ at micromolar scale. Different derivatives of NPQ can be made and analyzed against these two enzymes to further develop more potent inhibitors. Also, the binding characterization of aporphine alkaloids against FabZ can be explored to further validate these alkaloids as multi-targeted inhibitors of FAS II pathway.

Bibliography

[1] K. Bush, The coming of age of antibiotics: Discovery and therapeutic value, Ann. N. Y. Acad. Sci. 1213 (2010) 1–4. doi:10.1111/j.1749-6632.2010.05872.x.

[2] S.A. Waksman, H.B. Woodruff, Selective Antibiotic Action of Various Substances of Microbial Origin, J. Bacteriol. 44 (1942) 373–384. http://www.ncbi.nlm.nih.gov/pmc/articles/PMC373686/.

[3] A. Fleming, On the antibacterial action of cultures of a penicillium, with special reference to their use in the isolation of B. influenzae. 1929., Bull. World Health Organ. 79 (2001) 780–790. http://www.ncbi.nlm.nih.gov/pmc/articles/PMC2566493/.

[4] A. Fleming, On the Antibacterial Action of Cultures of a Penicillium, with Special Reference to their Use in the Isolation of B. influenzæ, Br. J. Exp. Pathol. 10 (1929) 226–236. http://www.ncbi.nlm.nih.gov/pmc/articles/PMC2048009/.

[5] B.L. Ligon, Penicillin: its discovery and early development, Semin. Pediatr. Infect. Dis. 15 (2004) 52–57. doi:https://doi.org/10.1053/j.spid.2004.02.001.

[6] S.E. Rossiter, M.H. Fletcher, W.M. Wuest, Natural Products as Platforms to Overcome Antibiotic Resistance, Chem. Rev. 117 (2017) 12415–12474. doi:10.1021/acs.chemrev.7b00283.

[7] R. Laxminarayan, R.R. Chaudhury, Antibiotic Resistance in India: Drivers and Opportunities for Action, PLoS Med. 13 (2016) 1–7. doi:10.1371/journal.pmed.1001974.

[8] A. Petchiappan, D. Chatterji, Antibiotic Resistance: Current Perspectives, ACS Omega. 2 (2017) 7400–7409. doi:10.1021/acsomega.7b01368.

[9] M.N. Gwynn, A. Portnoy, S.F. Rittenhouse, D.J. Payne, Challenges of antibacterial discovery revisited, Ann. N. Y. Acad. Sci. 1213 (2010) 5–19. doi:10.1111/j.1749-6632.2010.05828.x.

[10] E.D. Brown, G.D. Wright, Antibacterial drug discovery in the resistance era, Nature. 529 (2016) 336–343. doi:10.1038/nature17042.

[11] H. Von Döhren, Antibiotics: Actions, origins, resistance, by C. Walsh. 2003. Washington, DC: ASM Press. 345 pp. $99.95 (hardcover)., Protein Sci. 13

(2004) 3059–3060. doi:10.1110/ps.041032204.

[12] C.R. Bourne, Utility of the Biosynthetic Folate Pathway for Targets in Antimicrobial Discovery, Antibiotics. 3 (2014) 1–28. doi:10.3390/antibiotics3010001.

[13] D. LA, D. TS, Mechanisms of bacterial resistance to antibiotics, Arch. Intern. Med. 151 (1991) 886–895. http://dx.doi.org/10.1001/archinte.1991.00400050040010.

[14] T.S. Crofts, A.J. Gasparrini, G. Dantas, Next-generation approaches to understand and combat the antibiotic resistome, Nat. Rev. Microbiol. 15 (2017) 422–434. doi:10.1038/nrmicro.2017.28.

[15] J.M.A. Blair, M.A. Webber, A.J. Baylay, D.O. Ogbolu, L.J. V Piddock, Molecular mechanisms of antibiotic resistance, Nat. Rev. Microbiol. 13 (2014) 42. http://dx.doi.org/10.1038/nrmicro3380.

[16] K.P. Langton, P.J.F. Henderson, R.B. Herbert, Antibiotic resistance: multidrug efflux proteins, a common transport mechanism?, Nat. Prod. Rep. 22 (2005) 439–451. doi:10.1039/b413734p.

[17] J.M. Munita, C.A. Arias, A.R. Unit, A. De Santiago, HHS Public Access, Mech. Antibiot. Resist. 4 (2016) 1–37. doi:10.1128/microbiolspec.VMBF-0016-2015.Mechanisms.

[18] H. Nikaido, Multidrug Resistance in Bacteria, Annu. Rev. Biochem. 78 (2009) 119–146. doi:10.1146/annurev.biochem.78.082907.145923.

[19] P.K. Thakur, J. Kumar, D. Ray, F. Anjum, M.I. Hassan, Search of potential inhibitor against New Delhi metallo-beta-lactamase 1 from a series of antibacterial natural compounds., J. Nat. Sci. Biol. Med. 4 (2013) 51–6. doi:10.4103/0976-9668.107260.

[20] G.D. Wright, A.D. Sutherland, New strategies for combating multidrug-resistant bacteria, Trends Mol. Med. 13 (2007) 260–267. doi:10.1016/j.molmed.2007.04.004.

[21] A. Balasubramanian, T. Teramoto, A.A. Kulkarni, A.K. Bhattacharjee, R. Padmanabhan, Antiviral activities of selected antimalarials against dengue virus type 2 and Zika virus, Antiviral Res. 137 (2017) 141–150. doi:10.1016/j.antiviral.2016.11.015.

[22] H.W. Boucher, G.H. Talbot, J.S. Bradley, J.E. Edwards, D. Gilbert, L.B. Rice, M. Scheld, B. Spellberg, J. Bartlett, Bad Bugs, No Drugs: No ESKAPE! An

Update from the Infectious Diseases Society of America, Clin. Infect. Dis. 48 (2009) 1–12. doi:10.1086/595011.

[23] S. Santajit, N. Indrawattana, Mechanisms of Antimicrobial Resistance in ESKAPE Pathogens, Biomed Res. Int. 2016 (2016). doi:10.1155/2016/2475067.

[24] S. Verma, S. Kumar, V.P. Gupta, S. Gourinath, S. Bhatnagar, R. Bhatnagar, Structural basis of Bacillus anthracis MoxXT disruption and the modulation of MoxT ribonuclease activity by rationally designed peptides, J. Biomol. Struct. Dyn. 33 (2015) 606–624. doi:10.1080/07391102.2014.899924.

[25] H.K. Dkhar, A. Gopalsamy, S. Loharch, A. Kaur, I. Bhutani, K. Saminathan, E. Bhagyaraj, V. Chandra, K. Swaminathan, P. Agrawal, R. Parkesh, P. Gupta, Discovery of Mycobacterium tuberculosis ??-1,4-glucan branching enzyme (GlgB) inhibitors by structure- And ligand-based virtual screening, J. Biol. Chem. 290 (2015) 76–89. doi:10.1074/jbc.M114.589200.

[26] S.A. Bhat, N. Singh, A. Trivedi, P. Kansal, P. Gupta, A. Kumar, The mechanism of redox sensing in Mycobacterium tuberculosis, Free Radic. Biol. Med. 53 (2012) 1625–1641. doi:10.1016/j.freeradbiomed.2012.08.008.

[27] J. Drebes, M. Künz, B. Windshügel, A.G. Kikhney, I.B. Müller, R.J. Eberle, D. Oberthür, H. Cang, D.I. Svergun, M. Perbandt, C. Betzel, C. Wrenger, Structure of ThiM from Vitamin B1 biosynthetic pathway of Staphylococcus aureus – Insights into a novel pro-drug approach addressing MRSA infections, Sci. Rep. 6 (2016) 22871. doi:10.1038/srep22871.

[28] C.F.M. Bowden, A.C.K. Chan, E.J.W. Li, A.L. Arrieta, L.D. Eltis, M.E.P. Murphy, Structure-function analyses reveal key features in Staphylococcus aureus IsdB-associated unfolding of the heme-binding pocket of human hemoglobin, J. Biol. Chem. (2017) jbc.M117.806562. doi:10.1074/jbc.M117.806562.

[29] M. Seo, J. Do Kim, D. Neau, I. Sehgal, Y.H. Lee, Structure-based development of small molecule PFKFB3 inhibitors: A framework for potential cancer therapeutic agents targeting the Warburg effect, PLoS One. 6 (2011). doi:10.1371/journal.pone.0024179.

[30] F. Liu, J. Xiong, S. Kumar, C. Yang, S. Ge, S. Li, N. Xia, K. Swaminathan, Structural and biophysical characterization of Mycobacterium tuberculosis dodecin Rv1498A, J. Struct. Biol. 175 (2011) 31–38.

doi:10.1016/j.jsb.2011.04.013.

[31] T. Kashav, R. Nitharwal, S.A. Abdulrehman, A. Gabdoulkhakov, W. Saenger, S.K. Dhar, S. Gourinath, Three-dimensional structure of N-terminal domain of DnaB helicase and helicase-primase interactions in Helicobacter pylori, PLoS One. 4 (2009). doi:10.1371/journal.pone.0007515.

[32] D.J. Payne, M.N. Gwynn, D.J. Holmes, D.L. Pompliano, Drugs for bad bugs: confronting the challenges of antibacterial discovery, Nat. Rev. Drug Discov. 6 (2007) 29–40. doi:10.1038/nrd2201.

[33] S. Agarwal, N.K. Mishra, S. Bhatnagar, R. Bhatnagar, PemK toxin of Bacillus anthracis is a ribonuclease: An insight into its active site, structure, and function, J. Biol. Chem. 285 (2010) 7254–7270. doi:10.1074/jbc.M109.073387.

[34] A. Dhiman, S. Bhatnagar, P. Kulshreshtha, R. Bhatnagar, Functional characterization of WalRK: A two-component signal transduction system from Bacillus anthracis, FEBS Open Bio. 4 (2014) 65–76. doi:10.1016/j.fob.2013.12.005.

[35] A. Sinha, F. Ahmad, M. Imtaiyaz Hassan, I. Hassan, Structure Based Functional Annotation of Putative Conserved Proteins from Treponema pallidum : Search for a Potential Drug Target, Lett. Drug Des. Discov. 12 (2015) 46–59. http://www.ingentaconnect.com/content/ben/lddd/2014/00000012/00000001/art00008.

[36] I. Nagpal, I. Raj, N. Subbarao, S. Gourinath, Virtual screening, identification and in vitro testing of novel inhibitors of O-acetyl-L-serine sulfhydrylase of Entamoeba histolytica, PLoS One. 7 (2012) 1–7. doi:10.1371/journal.pone.0030305.

[37] H.K. Dkhar, R. Nanduri, S. Mahajan, S. Dave, A. Saini, A.K. Somavarapu, A. Arora, R. Parkesh, K.G. Thakur, S. Mayilraj, P. Gupta, Mycobacterium tuberculosis Keto-Mycolic Acid and Macrophage Nuclear Receptor TR4 Modulate Foamy Biogenesis in Granulomas: A Case of a Heterologous and Noncanonical Ligand-Receptor Pair, J. Immunol. 193 (2014) 295–305. doi:10.4049/jimmunol.1400092.

[38] U. Das, V. Pogenberg, U.K.T. Subhramanyam, M. Wilmanns, S. Gourinath, A. Srinivasan, Crystal structure of the VapBc-15 complex from mycobacterium tuberculosis reveals a two-metal ion dependent pin-domain ribonuclease and a

variable mode of toxin-antitoxin assembly, J. Struct. Biol. 188 (2014) 249–258. doi:10.1016/j.jsb.2014.10.002.

[39] D. Oberthür, J. Achenbach, A. Gabdulkhakov, K. Buchner, C. Maasch, S. Falke, D. Rehders, S. Klussmann, C. Betzel, Crystal structure of a mirror-image L-RNA aptamer (Spiegelmer) in complex with the natural L-protein target CCL2, Nat. Commun. 6 (2015) 6923. doi:10.1038/ncomms7923.

[40] M. Perbandt, C. Burmeister, R.D. Walter, C. Betzel, E. Liebau, Native and Inhibited Structure of a Mu class-related Glutathione S-transferase from Plasmodium falciparum, J. Biol. Chem. 279 (2004) 1336–1342. doi:10.1074/jbc.M309663200.

[41] A.M. Crowe, I. Casabon, K.L. Brown, J. Liu, J. Lian, J.C. Rogalski, T.E. Hurst, V. Snieckus, L.J. Foster, L.D. Eltis, Catabolism of the Last Two Steroid Rings in *Mycobacterium tuberculosis* and Other Bacteria, MBio. 8 (2017) e00321-17. doi:10.1128/mBio.00321-17.

[42] M.A. Silvers, S. Pakhomova, D.B. Neau, W.C. Silvers, N. Anzalone, C.M. Taylor, G.L. Waldrop, Crystal Structure of Carboxyltransferase from Staphylococcus aureus Bound to the Antibacterial Agent Moiramide B, Biochemistry. 55 (2016) 4666–4674. doi:10.1021/acs.biochem.6b00641.

[43] D.A. Rasko, V. Sperandio, Anti-virulence strategies to combat bacteria-mediated disease, Nat. Rev. Drug Discov. 9 (2010) 117–128. doi:10.1038/nrd3013.

[44] P. Pandey, V. Verma, G. Gautam, N. Kumari, S.K. Dhar, S. Gourinath, Targeting the β-clamp in Helicobacter pylori with FDA-approved drugs reveals micromolar inhibition by diflunisal, FEBS Lett. 591 (2017) 2311–2322. doi:10.1002/1873-3468.12734.

[45] J.K. Capyk, I. Casabon, R. Gruninger, N.C. Strynadka, L.D. Eltis, Activity of 3-ketosteroid 9??-hydroxylase (KshAB) indicates cholesterol side chain and ring degradation occur simultaneously in Mycobacterium tuberculosis, J. Biol. Chem. 286 (2011) 40717–40724. doi:10.1074/jbc.M111.289975.

[46] R. Sharma, R. Kothapalli, A.M.J. van Dongen, K. Swaminathan, Chemoinformatic identification of novel inhibitors against Mycobacterium tuberculosis l-aspartate α-decarboxylase, PLoS One. 7 (2012). doi:10.1371/journal.pone.0033521.

[47] A. Deepthi, C.W. Liew, Z.X. Liang, K. Swaminathan, J. Lescar, Structure of a

diguanylate cyclase from thermotoga maritima: Insights into activation, feedback inhibition and thermostability, PLoS One. 9 (2014) 1–9. doi:10.1371/journal.pone.0110912.

[48] V.K. Srivastava, S. Srivastava, A. Arora, J.V. Pratap, Structural Insights into Putative Molybdenum Cofactor Biosynthesis Protein C (MoaC2) from Mycobacterium tuberculosis H37Rv, PLoS One. 8 (2013). doi:10.1371/journal.pone.0058333.

[49] S. Joon, M. Gopalani, A. Rahi, P. Kulshreshtha, H. Gogoi, S. Bhatnagar, R. Bhatnagar, Biochemical characterization of the GTP-sensing protein, CodY of Bacillus anthracis, Pathog. Dis. 75 (2017) ftx048-ftx048. http://dx.doi.org/10.1093/femspd/ftx048.

[50] J.P. Hughes, S.S. Rees, S.B. Kalindjian, K.L. Philpott, Principles of early drug discovery, Br. J. Pharmacol. 162 (2011) 1239–1249. doi:10.1111/j.1476-5381.2010.01127.x.

[51] M. Shahbaaz, K. Bisetty, F. Ahmad, M.I. Hassan, Towards New Drug Targets? Function Prediction of Putative Proteins of Neisseria meningitidis MC58 and Their Virulence Characterization., OMICS. 19 (2015) 416–34. doi:10.1089/omi.2015.0032.

[52] I. Bhutani, S. Loharch, P. Gupta, R. Madathil, R. Parkesh, Structure, dynamics, and interaction of Mycobacterium tuberculosis (Mtb) DprE1 and DprE2 examined by molecular modeling, simulation, and electrostatic studies, PLoS One. 10 (2015) 1–31. doi:10.1371/journal.pone.0119771.

[53] H. Lai, D. Dou, S. Aravapalli, T. Teramoto, G.H. Lushington, T.M. Mwania, K.R. Alliston, D.M. Eichhorn, R. Padmanabhan, W.C. Groutas, Design, synthesis and characterization of novel 1,2-benzisothiazol-3(2H)- one and 1,3,4-oxadiazole hybrid derivatives: Potent inhibitors of Dengue and West Nile virus NS2B/NS3 proteases, Bioorganic Med. Chem. 21 (2013) 102–113. doi:10.1016/j.bmc.2012.10.058.

[54] S. Bhatnagar, G.S. Rao, T.P. Singh, The role of dehydro-Alanine in the design of peptides, BioSystems. 34 (1995) 143–148. doi:10.1016/0303-2647(94)01445-D.

[55] V. Tzin, G. Galili, A. Aharoni, Shikimate Pathway and Aromatic Amino Acid Biosynthesis, eLS. (2012). doi:10.1002/9780470015902.a0001315.pub2.

[56] C.W. Roberts, F. Roberts, R.E. Lyons, M.J. Kirisits, E.J. Mui, J. Finnerty, J.J.

Johnson, D.J.P. Ferguson, J.R. Coggins, T. Krell, G.H. Coombs, W.K. Milhous, D.E. Kyle, S. Tzipori, J. Barnwell, J.B. Dame, J. Carlton, R. McLeod, The shikimate pathway and its branches in apicomplexan parasites., J. Infect. Dis. 185 Suppl (2002) S25-36. doi:10.1086/338004.

[57] K.M. Herrmann, The Shikimate Pathway: Early Steps in the Biosynthesis of Aromatic Compounds, Plant Cell Online. 7 (1995) 907–919. doi:10.1105/tpc.7.7.907.

[58] E. Lilly, Regulation Biosynthesis of Aromatic in Bacillus Amino subtilis Acid, (1974) 4467–4473.

[59] K.M. Herrmann, L.M. Weaver, the Shikimate Pathway, Annu. Rev. Plant Physiol. Plant Mol. Biol. 50 (1999) 473–503. doi:10.1146/annurev.arplant.50.1.473.

[60] R. Mir, S. Jallu, T.P. Singh, The shikimate pathway: Review of amino acid sequence, function and three-dimensional structures of the enzymes, Crit. Rev. Microbiol. 41 (2015) 172–189. doi:10.3109/1040841X.2013.813901.

[61] A. Dev, S. Tapas, S. Pratap, P. Kumar, Structure and function of enzymes of shikimate pathway, Curr. Bioinform. 7 (2012) 374–391. doi:10.2174/157489312803900983.

[62] C.M. Stephens, R. Bauerle, Analysis of the metal requirement of 3-deoxy-D-arabino-heptulosonate- 7-phosphate synthase from Escherichia coli, J. Biol. Chem. 266 (1991) 20810–20817.

[63] C.J. Webby, H.M. Baker, J.S. Lott, E.N. Baker, E.J. Parker, The Structure of 3-deoxy-D-arabino-heptulosonate 7-phosphate synthase from Mycobacterium tuberculosis reveals a common catalytic scaffold and ancestry for type I and type II enzymes, J. Mol. Biol. 354 (2005) 927–939. doi:10.1016/j.jmb.2005.09.093.

[64] C. Furdui, L. Zhou, R.W. Woodard, K.S. Anderson, Insights into the mechanism of 3-deoxy-D-arabino-heptulosonate 7-phosphate synthase (Phe) from Escherichia coli using a transient kinetic analysis, J. Biol. Chem. 279 (2004) 45618–45625. doi:10.1074/jbc.M404753200.

[65] I.A. Shumilin, R.H. Kretsinger, R.H. Bauerle, Crystal structure of phenylalanine-regulated 3-deoxy-D-arabino-heptulosonate-7-phosphate synthase from Escherichia coli, Structure. 7 (1999) 865–875. doi:https://doi.org/10.1016/S0969-2126(99)80109-9.

[66] J.M. Lambert, M.R. Boocock, J.R. Coggins, The 3-dehydroquinate synthase activity of the pentafunctional arom enzyme complex of Neurospora crassa is Zn2+-dependent., Biochem. J. 226 (1985) 817–829. http://www.ncbi.nlm.nih.gov/pmc/articles/PMC1144782/.

[67] A.R. Hawkins, H.K. Lamb, The Molecular Biology of Multidomain Proteins Selected Examples, Eur. J. Biochem. 232 (1995) 7–18. doi:10.1111/j.1432-1033.1995.tb20775.x.

[68] E.P. Carpenter, A.R. Hawkins, J.W. Frost, K.A. Brown, Structure of dehydroquinate synthase reveals an active site capable of multistep catalysis, Nature. 394 (1998) 299–302. doi:10.1038/28431.

[69] E. Haslam, 1 - The Shikimate Pathway: Biosynthesis of the Aromatic Amino Acids BT - The Shikimate Pathway, in: Biosynth. Nat. Prod. Ser., Butterworth-Heinemann, 1974: pp. 3–48. doi:https://doi.org/10.1016/B978-0-408-70569-1.50008-2.

[70] J.R. Coggins, A.R. Hawkins, C. Abell, A. Shneier, J. Harris, C. Iueanthous, Evidence Reactions for Opposite Catalysed Courses for the By Type I and Type Ii Dehydroquinases, (1993) 1399–1402.

[71] G. Michel, A.W. Roszak, V. Sauvé, J. Maclean, A. Matte, J.R. Coggins, M. Cygler, A.J. Lapthorn, Structures of shikimate dehydrogenase AroE and its paralog YdiB: A common structural framework for different activities, J. Biol. Chem. 278 (2003) 19463–19472. doi:10.1074/jbc.M300794200.

[72] M.J. Romanowski, S.K. Burley, Crystal structure of the Escherichia coli shikimate kinase I (AroK) that confers sensitivity to mecillinam, Proteins Struct. Funct. Genet. 47 (2002) 558–562. doi:10.1002/prot.10099.

[73] E. Schönbrunn, S. Eschenburg, W.A. Shuttleworth, J. V Schloss, N. Amrhein, J.N.S. Evans, W. Kabsch, Interaction of the herbicide glyphosate with its target enzyme 5-enolpyruvylshikimate 3-phosphate synthase in atomic detail, Proc. Natl. Acad. Sci. U. S. A. 98 (2001) 1376–1380. http://www.ncbi.nlm.nih.gov/pmc/articles/PMC29264/.

[74] P.J. White, G. Millar, J.R. Coggins, The overexpression, purification and complete amino acid sequence of chorismate synthase from Escherichia coli K12 and its comparison with the enzyme from Neurospora crassa, Biochem. J. 251 (1988) 313–322. doi:10.1042/bj2510313.

[75] J. Beld, D.J. Lee, M.D. Burkart, Fatty acid biosynthesis revisited: structure

elucidation and metabolic engineering, Mol. BioSyst. 11 (2015) 38–59. doi:10.1039/C4MB00443D.

[76] Y.-M. Zhang, C.O. Rock, Membrane lipid homeostasis in bacteria, Nat. Rev. Microbiol. 6 (2008) 222. http://dx.doi.org/10.1038/nrmicro1839.

[77] S.W. White, J. Zheng, Y. Zhang, C.O. Rock, F Atty a Cid B Iosynthesis, Rev. Lit. Arts Am. 1 (2005) 791–831. doi:10.1146/annurev.biochem.74.082803.133524.

[78] D.J. Payne, P. V. Warren, D.J. Holmes, Y. Ji, J.T. Lonsdale, Bacterial fatty-acid biosynthesis: A genomics-driven target for antibacterial drug discovery, Drug Discov. Today. 6 (2001) 537–544. doi:10.1016/S1359-6446(01)01774-3.

[79] C.O. Rock, S. Jackowski, Forty Years of Bacterial Fatty Acid Synthesis, Biochem. Biophys. Res. Commun. 292 (2002) 1155–1166. doi:10.1006/bbrc.2001.2022.

[80] H.T. Wright, K.A. Reynolds, Antibacterial targets in fatty acid biosynthesis, Curr. Opin. Microbiol. 10 (2007) 447–453. doi:10.1016/j.mib.2007.07.001.

[81] J.W. Campbell, J.E. Cronan, Bacterial Fatty Acid Biosynthesis: Targets for Antibacterial Drug Discovery, Annu. Rev. Microbiol. 55 (2001) 305–332. doi:10.1146/annurev.micro.55.1.305.

[82] D. McDevitt, M. Rosenberg, Exploiting genomics to discover new antibiotics, Trends Microbiol. 9 (2001) 611–617. doi:10.1016/S0966-842X(01)02235-1.

[83] C.O. Rock, J.E. Cronan, Escherichia coli as a model for the regulation of dissociable (type II) fatty acid biosynthesis, Biochim. Biophys. Acta - Lipids Lipid Metab. 1302 (1996) 1–16. doi:https://doi.org/10.1016/0005-2760(96)00056-2.

[84] R.J. Heath, S. Jackowski, C.O.B.T.-N.C.B. Rock, Chapter 3 Fatty acid and phospholipid metabolism in prokaryotes, in: Biochem. Lipids, Lipoproteins Membr. 4th Ed., Elsevier, 2002: pp. 55–92. doi:https://doi.org/10.1016/S0167-7306(02)36005-8.

[85] J.E. Cronan, G.L. Waldrop, Multi-subunit acetyl-CoA carboxylases, Prog. Lipid Res. 41 (2002) 407–435. doi:https://doi.org/10.1016/S0163-7827(02)00007-3.

[86] T.C. Broussard, S. Pakhomova, D.B. Neau, R. Bonnot, G.L. Waldrop, Structural Analysis of Substrate, Reaction Intermediate, and Product Binding in Haemophilus influenzae Biotin Carboxylase, Biochemistry. 54 (2015) 3860–

3870. doi:10.1021/acs.biochem.5b00340.

[87] T.C. Broussard, M.J. Kobe, S. Pakhomova, D.B. Neau, A.E. Price, T.S. Champion, G.L. Waldrop, The three-dimensional structure of the biotin carboxylase-biotin carboxyl carrier protein complex of E. coli acetyl-CoA carboxylase, Structure. 21 (2013) 650–657. doi:10.1016/j.str.2013.02.001.

[88] F.E. Ruch, P.R. Vagelos, The Isolation and General Properties of Coenzyme A-Acyl Carrier Protein Transacylase, J. Biol. Chem. 248 (1973) 8086–8094. papers2://publication/uuid/626CD889-574C-4E08-9759-9A1DD6B232CA.

[89] S. Jackowski, C.O. Rock, Acetoacetyl-acyl carrier protein synthase, a potential regulator of fatty acid biosynthesis in bacteria., J. Biol. Chem. 262 (1987) 7927–7931.

[90] L. Zhang, J. Xiao, J. Xu, T. Fu, Z. Cao, L. Zhu, H.-Z. Chen, X. Shen, H. Jiang, L. Zhang, Crystal structure of FabZ-ACP complex reveals a dynamic seesaw-like catalytic mechanism of dehydratase in fatty acid biosynthesis, Cell Res. 26 (2016) 1330–1344. doi:10.1038/cr.2016.136.

[91] A.C. Price, Y.-M. Zhang, C.O. Rock, S.W. White, Structure of β-Ketoacyl-[acyl carrier protein] Reductase from Escherichia coli: Negative Cooperativity and Its Structural Basis, Biochemistry. 40 (2001) 12772–12781. doi:10.1021/bi010737g.

[92] M.S. Kimber, F. Martin, Y. Lu, S. Houston, M. Vedadi, A. Dharamsi, K.M. Fiebig, M. Schmid, C.O. Rock, The structure of (3R)-hydroxyacyl-acyl carrier protein dehydratase (FabZ) from Pseudomonas aeruginosa, J. Biol. Chem. 279 (2004) 52593–52602. doi:10.1074/jbc.M408105200.

[93] E. Kasner, C.A. Hunter, D. Ph, K. Kariko, D. Ph, NIH Public Access, 70 (2013) 646–656. doi:10.1002/ana.22528.Toll-like.

[94] Y.M. Zhang, S.W. White, C.O. Rock, Inhibiting bacterial fatty acid synthesis, J. Biol. Chem. 281 (2006) 17541–17544. doi:10.1074/jbc.R600004200.

[95] J. Yao, C.O. Rock, Bacterial fatty acid metabolism in modern antibiotic discovery, Biochim. Biophys. Acta - Mol. Cell Biol. Lipids. 1862 (2017) 1300–1309. doi:10.1016/j.bbalip.2016.09.014.

[96] S.W. White, J. Zheng, Y.-M. Zhang, C.O. Rock, the Structural Biology of Type Ii Fatty Acid Biosynthesis, Annu. Rev. Biochem. 74 (2005) 791–831. doi:10.1146/annurev.biochem.74.082803.133524.

[97] W. Liu, C. Han, L. Hu, K. Chen, X. Shen, H. Jiang, Characterization and

inhibitor discovery of one novel malonyl-CoA: Acyl carrier protein transacylase (MCAT) from Helicobacter pylori, FEBS Lett. 580 (2006) 697–702. doi:10.1016/j.febslet.2005.12.085.

[98] X. He, A.M. Reeve, U.R. Desai, G.E. Kellogg, K.A. Reynolds, 1,2-Dithiole-3-Ones as Potent Inhibitors of the Bacterial 3-Ketoacyl Acyl Carrier Protein Synthase III (FabH), Antimicrob. Agents Chemother. 48 (2004) 3093–3102. doi:10.1128/AAC.48.8.3093-3102.2004.

[99] S. Kodali, A. Galgoci, K. Young, R. Painter, L.L. Silver, K.B. Herath, S.B. Singh, D. Cully, J.F. Barrett, D. Schmatz, J. Wang, Determination of selectivity and efficacy of fatty acid synthesis inhibitors, J. Biol. Chem. 280 (2005) 1669–1677. doi:10.1074/jbc.M406848200.

[100] A. Banerjee, E. Dubnau, A. Quemard, V. Balasubramanian, K.S. Um, T. Wilson, D. Collins, G. de Lisle, W.R. Jacobs, inhA, a gene encoding a target for isoniazid and ethionamide in Mycobacterium tuberculosis, Science (80-.). 263 (1994) 227 LP-230. http://science.sciencemag.org/content/263/5144/227.abstract.

[101] C.W. Levy, A. Roujeinikova, S. Sedelnikova, P.J. Baker, A.R. Stuitje, A.R. Slabas, D.W. Rice, J.B. Rafferty, Molecular basis of triclosan activity, Nature. 398 (1999) 383. http://dx.doi.org/10.1038/18803.

[102] J. Round, R. Roccor, S.-N. Li, L.D. Eltis, A fatty acyl-CoA reductase promotes wax ester accumulation in *Rhodococcus jostii* RHA1, Appl. Environ. Microbiol. 83 (2017) AEM.00902-17. doi:10.1128/AEM.00902-17.

[103] Y.M. Zhang, C.O. Rock, Evaluation of epigallocatechin gallate and related plant polyphenols as inhibitors of the FabG and FabI reductases of bacterial type II fatty-acid synthase, J. Biol. Chem. 279 (2004) 30994–31001. doi:10.1074/jbc.M403697200.

[104] S.K. Sharma, M. Kapoor, T.N.C. Ramya, S. Kumar, G. Kumar, R. Modak, S. Sharma, N. Surolia, A. Surolia, Identification, Characterization, and Inhibition of Plasmodium falciparum β-Hydroxyacyl-Acyl Carrier Protein Dehydratase (FabZ), J. Biol. Chem. 278 (2003) 45661–45671. doi:10.1074/jbc.M304283200.

[105] V. Kumar, A. Sharma, S. Pratap, P. Kumar, Characterization of isoflavonoids as inhibitors of β-hydroxyacyl-acyl carrier protein dehydratase (FabZ) from Moraxella catarrhalis: Kinetics, spectroscopic, thermodynamics and in silico

studies, Biochim. Biophys. Acta - Gen. Subj. (2017). doi:https://doi.org/10.1016/j.bbagen.2017.10.017.

[106] B.E. McGillick, D. Kumaran, C. Vieni, S. Swaminathan, β-Hydroxyacyl-acyl Carrier Protein Dehydratase (FabZ) from Francisella tularensis and Yersinia pestis: Structure Determination, Enzymatic Characterization, and Cross-Inhibition Studies, Biochemistry. 55 (2016) 1091–1099. doi:10.1021/acs.biochem.5b00832.

[107] L. He, L. Zhang, X. Liu, X. Li, M. Zheng, H. Li, K. Yu, K. Chen, X. Shen, H. Jiang, H. Liu, Discovering potent inhibitors against the beta-hydroxyacyl-acyl carrier protein dehydratase (FabZ) of Helicobacter pylori: structure-based design, synthesis, bioassay, and crystal structure determination., J. Med. Chem. 52 (2009) 2465–81. doi:10.1021/jm8015602.

[108] M. Chu, R. Mierzwa, L. Xu, S.-W. Yang, L. He, M. Patel, J. Stafford, D. Macinga, T. Black, T.-M. Chan, V. Gullo, Structure elucidation of Sch 538415, a novel acyl carrier protein synthase inhibitor from a microorganism, Bioorg. Med. Chem. Lett. 13 (2003) 3827–3829. doi:https://doi.org/10.1016/j.bmcl.2003.07.011.

[109] S.Y. Gerdes, M.D. Scholle, M. D'Souza, A. Bernal, M. V Baev, M. Farrell, O. V Kurnasov, M.D. Daugherty, F. Mseeh, B.M. Polanuyer, J.W. Campbell, S. Anantha, K.Y. Shatalin, S.A.K. Chowdhury, M.Y. Fonstein, A.L. Osterman, From Genetic Footprinting to Antimicrobial Drug Targets: Examples in Cofactor Biosynthetic Pathways, J. Bacteriol. 184 (2002) 4555–4572. doi:10.1128/JB.184.16.4555-4572.2002.

[110] G.M. Cragg, D.J. Newman, Natural products: A continuing source of novel drug leads, Biochim. Biophys. Acta - Gen. Subj. 1830 (2013) 3670–3695. doi:https://doi.org/10.1016/j.bbagen.2013.02.008.

[111] T. Rodrigues, D. Reker, P. Schneider, G. Schneider, Counting on natural products for drug design, Nat. Chem. 8 (2016) 531–541. doi:10.1038/nchem.2479.

[112] C.W. Murray, D.C. Rees, The rise of fragment-based drug discovery, Nat. Chem. 1 (2009) 187. http://dx.doi.org/10.1038/nchem.217.

[113] E.I. Parkinson, J.S. Bair, B.A. Nakamura, H.Y. Lee, H.I. Kuttab, E.H. Southgate, S. Lezmi, G.W. Lau, P.J. Hergenrother, Deoxynybomycins inhibit mutant DNA gyrase and rescue mice infected with fluoroquinolone-resistant

bacteria, Nat. Commun. 6 (2015) 6947. http://dx.doi.org/10.1038/ncomms7947.

[114] C.A. Lipinski, Drug-like properties and the causes of poor solubility and poor permeability, J. Pharmacol. Toxicol. Methods. 44 (2000) 235–249. doi:10.1016/S1056-8719(00)00107-6.

[115] M. Congreve, R. Carr, C. Murray, H. Jhoti, A “Rule of Three” for fragment-based lead discovery?, Drug Discov. Today. 8 (2003) 876–877. doi:https://doi.org/10.1016/S1359-6446(03)02831-9.

[116] R.J. Quinn, A.R. Carroll, N.B. Pham, P. Baron, M.E. Palframan, L. Suraweera, G.K. Pierens, S. Muresan, Developing a Drug-like Natural Product Library, J. Nat. Prod. 71 (2008) 464–468. doi:10.1021/np070526y.

[117] J. Nickel, B.O. Gohlke, J. Erehman, P. Banerjee, W.W. Rong, A. Goede, M. Dunkel, R. Preissner, SuperPred: Update on drug classification and target prediction, Nucleic Acids Res. 42 (2014) 26–31. doi:10.1093/nar/gku477.

[118] A. Lagunin, A. Stepanchikova, D. Filimonov, V. Poroikov, PASS: Prediction of activity spectra for biologically active substances, Bioinformatics. 16 (2000) 747–748. doi:10.1093/bioinformatics/16.8.747.

[119] Y. Yamanishi, Chemogenomic Approaches to Infer Drug–Target Interaction Networks BT - Data Mining for Systems Biology: Methods and Protocols, in: H. Mamitsuka, C. DeLisi, M. Kanehisa (Eds.), Humana Press, Totowa, NJ, 2013: pp. 97–113. doi:10.1007/978-1-62703-107-3_9.

[120] N.H. Mueller, N. Pattabiraman, C. Ansarah-Sobrinho, P. Viswanathan, T.C. Pierson, R. Padmanabhan, Identification and biochemical characterization of small-molecule inhibitors of west nile virus serine protease by a high-throughput screen, Antimicrob. Agents Chemother. 52 (2008) 3385–3393. doi:10.1128/AAC.01508-07.

[121] D. Reker, T. Rodrigues, P. Schneider, G. Schneider, Identifying the macromolecular targets of de novo-designed chemical entities through self-organizing map consensus, Proc. Natl. Acad. Sci. 111 (2014) 4067–4072. doi:10.1073/pnas.1320001111.

[122] R. Bentley, E. Haslam, The Shikimate Pathway — A Metabolic Tree with Many Branche, Crit. Rev. Biochem. Mol. Biol. 25 (1990) 307–384. doi:10.3109/10409239009090615.

[123] R.G. Ducati, L.A.B. and D.S. Santos, Mycobacterial Shikimate Pathway Enzymes as Targets for Drug Design, Curr. Drug Targets. 8 (2007) 423–435.

doi:http://dx.doi.org/10.2174/138945007780059004.

[124] H. Maeda, N. Dudareva, The Shikimate Pathway and Aromatic Amino Acid Biosynthesis in Plants, Annu. Rev. Plant Biol. 63 (2012) 73–105. doi:10.1146/annurev-arplant-042811-105439.

[125] P.J. Cross, A.L. Pietersma, T.M. Allison, S.M. Wilson-Coutts, F.C. Cochrane, E.J. Parker, Neisseria meningitidis expresses a single 3-deoxy-D-arabino-heptulosonate 7-phosphate synthase that is inhibited primarily by phenylalanine, Protein Sci. 22 (2013) 1087–1099. doi:10.1002/pro.2293.

[126] P.J. Cross, R.C.J. Dobson, M.L. Patchett, E.J. Parker, Tyrosine latching of a regulatory gate affords allosteric control of aromatic amino acid biosynthesis, J. Biol. Chem. 286 (2011) 10216–10224. doi:10.1074/jbc.M110.209924.

[127] C.J. Webby, W. Jiao, R.D. Hutton, N.J. Blackmore, H.M. Baker, E.N. Baker, G.B. Jameson, E.J. Parker, Synergistic allostery, a sophisticated regulatory network for the control of aromatic amino acid biosynthesis in Mycobacterium tuberculosis, J. Biol. Chem. 285 (2010) 30567–30576. doi:10.1074/jbc.M110.111856.

[128] I.A. Shumilin, C. Zhao, R. Bauerle, R.H. Kretsinger, Allosteric inhibition of 3-deoxy-D-arabino-heptulosonate-7-phosphate synthase alters the coordination of both substrates, J. Mol. Biol. 320 (2002) 1147–1156. doi:10.1016/S0022-2836(02)00545-4.

[129] P.J. Cross, E.J. Parker, Allosteric inhibitor specificity of Thermotoga maritima 3-deoxy-d-arabino-heptulosonate 7-phosphate synthase, FEBS Lett. 587 (2013) 3063–3068. doi:https://doi.org/10.1016/j.febslet.2013.07.044.

[130] L.R. Schofield, B.F. Anderson, M.L. Patchett, G.E. Norris, G.B. Jameson, E.J. Parker, Substrate Ambiguity and Crystal Structure of Pyrococcus furiosus 3-Deoxy-d-arabino-heptulosonate-7-phosphate Synthase: An Ancestral 3-Deoxyald-2-ulosonate-phosphate Synthase?, Biochemistry. 44 (2005) 11950–11962. doi:10.1021/bi050577z.

[131] S.H. Light, A.S. Halavaty, G. Minasov, L. Shuvalova, W.F. Anderson, Structural analysis of a 3-deoxy-D-arabino-heptulosonate 7-phosphate synthase with an N-terminal chorismate mutase-like regulatory domain, Protein Sci. 21 (2012) 887–895. doi:10.1002/pro.2075.

[132] C.J. Webby, M.L. Patchett, E.J. Parker, Characterization of a recombinant type II 3-deoxy-D-arabino-heptulosonate-7-phosphate synthase from Helicobacter

pylori, Biochem. J. 390 (2005) 223–230. doi:10.1042/BJ20050259.

[133] L. Zhou, J. Wu, V. Janakiraman, I.A. Shumilin, R. Bauerle, R.H. Kretsinger, R.W. Woodard, Structure and characterization of the 3-deoxy-d-arabino-heptulosonate 7-phosphate synthase from Aeropyrum pernix, Bioorg. Chem. 40 (2012) 79–86. doi:https://doi.org/10.1016/j.bioorg.2011.09.002.

[134] S. Sasso, M. Ökvist, K. Roderer, M. Gamper, G. Codoni, U. Krengel, P. Kast, Structure and function of a complex between chorismate mutase and DAHP synthase: efficiency boost for the junior partner, EMBO J. 28 (2009) 2128–2142. doi:10.1038/emboj.2009.165.

[135] G. Gosset, C.A. Bonner, R.A. Jensen, Microbial Origin of Plant-Type 2-Keto-3-Deoxy-d-arabino-Heptulosonate 7-Phosphate Synthases, Exemplified by the Chorismate- and Tryptophan-Regulated Enzyme from Xanthomonas campestris, J. Bacteriol. 183 (2001) 4061–4070. doi:10.1128/JB.183.13.4061-4070.2001.

[136] R.A. Jensen, G. Xie, D.H. Calhoun, C.A. Bonner, The Correct Phylogenetic Relationship of KdsA (3-Deoxy-D-manno-octulosonate 8-Phosphate Synthase) with One of Two Independently Evolved Classes of AroA (3-Deoxy-D-arabino-heptulosonate 7-Phosphate Synthase), J. Mol. Evol. 54 (2002) 416–423. doi:10.1007/s00239-001-0031-z.

[137] J. Wu, R.W. Woodard, New insights into the evolutionary links relating to the 3-deoxy-D-arabino-heptulosonate 7-phosphate synthase subfamilies, J. Biol. Chem. 281 (2006) 4042–4048. doi:10.1074/jbc.M512223200.

[138] C.H. Doy, K.D. Brown, Control of aromatic biosynthesis: The multiplicity of 7-phospho-2-oxo-3-deoxy-d-arabino-heptonate d-erythrose-4-phosphate-lyase (pyruvate-phosphorylating) in Eschetichia coli W, Biochim. Biophys. Acta - Gen. Subj. 104 (1965) 377–389. doi:https://doi.org/10.1016/0304-4165(65)90343-0.

[139] N.J. Blackmore, A.R. Nazmi, R.D. Hutton, M.N. Webby, E.N. Baker, G.B. Jameson, E.J. Parker, Complex Formation between Two Biosynthetic Enzymes Modifies the Allosteric Regulatory Properties of Both: AN EXAMPLE OF MOLECULAR SYMBIOSIS, J. Biol. Chem. 290 (2015) 18187–18198. doi:10.1074/jbc.M115.638700.

[140] J. Wu, D.L. Howe, R.W. Woodard, Thermotoga maritima 3-deoxy-d-arabino-heptulosonate 7-phosphate (DAHP) synthase: The ancestral eubacterial DAHP

synthase?, J. Biol. Chem. 278 (2003) 27525–27531. doi:10.1074/jbc.M304631200.

[141] I.A. Shumilin, R. Bauerle, J. Wu, R.W. Woodard, R.H. Kretsinger, Crystal structure of the reaction complex of 3-Deoxy-D-arabino- heptulosonate-7-phosphate synthase from Thermotoga maritima refines the catalytic mechanism and indicates a new mechanism of allosteric regulation, J. Mol. Biol. 341 (2004) 455–466. doi:10.1016/j.jmb.2004.05.077.

[142] T.J.P. Hubbard, B. Ailey, S.E. Brenner, A.G. Murzin, C. Chothia, SCOP: A structural classification of proteins database, Nucleic Acids Res. 27 (1999) 254–256. doi:10.1093/nar/27.1.254.

[143] J. Stewart, D.B. Wilson, B. Ganem, A genetically engineered monofunctional chorismate mutase, J. Am. Chem. Soc. 112 (1990) 4582–4584. doi:10.1021/ja00167a088.

[144] A.Y. Lee, P.A. Karplus, B. Ganem, J. Clardy, Atomic-Structure of the Buried Catalytic Pocket of Escherichia-Coli Chorismate Mutase, J. Am. Chem. Soc. 117 (1995) 3627–3628. doi:Doi 10.1021/Ja00117a038.

[145] A.R. Nazmi, E.J.M. Lang, Y. Bai, T.M. Allison, M.H. Othman, S. Panjikar, V.L. Arcus, E.J. Parker, Interdomain conformational changes provide allosteric regulation en route to chorismate, J. Biol. Chem. 291 (2016) 21836–21847. doi:10.1074/jbc.M116.741637.

[146] E.W. Nester, J.H. Lorence, D.S. Nasser, An Enzyme Aggregate Involved in the Biosynthesis of Aromatic Amino Acids in Bacillus subtilis. Its Possible Function in Feedback Regulation*, Biochemistry. 6 (1967) 1553–1563. doi:10.1021/bi00857a042.

[147] J. V Gray, D. Eren, J.R. Knowles, Monofunctional chorismate mutase from Bacillus subtilis: kinetic and carbon-13 NMR studies on the interactions of the enzyme with its ligands, Biochemistry. 29 (1990) 8872–8878. doi:10.1021/bi00489a051.

[148] J. Wu, G.Y. Sheflyan, R.W. Woodard, Bacillus subtilis 3-deoxy-D-arabino-heptulosonate 7-phosphate synthase revisited: resolution of two long-standing enigmas, Biochem. J. 390 (2005) 583–590. doi:10.1042/BJ20050294.

[149] A. Roy, W. Eugene, Regulatory Enzymes of Aromatic Amino Acid Biosynthesis in Bacillus subtilis, 241 (1966) 3365–3372.

[150] R.M. TAMIMI, P. LAGIOU, H.-O. ADAMI, D. TRICHOPOULOS, Prospects

for chemoprevention of cancer, J. Intern. Med. 251 (2002) 286–300. doi:10.1046/j.1365-2796.2002.00969.x.

[151] X. Zhu, H. Zhang, R. Lo, Phenolic Compounds from the Leaf Extract of Artichoke (Cynara scolymus L.) and Their Antimicrobial Activities, J. Agric. Food Chem. 52 (2004) 7272–7278. doi:10.1021/jf0490192.

[152] J. Sambrook, Molecular cloning : a laboratory manual, Third edition. Cold Spring Harbor, N.Y. : Cold Spring Harbor Laboratory Press, [2001] ©2001, n.d. https://search.library.wisc.edu/catalog/999897924602121.

[153] Z. Otwinowski, W. Minor, Processing of X-ray diffraction data collected in oscillation mode, Methods Enzymol. 276 (1997) 307–326. doi:10.1016/S0076-6879(97)76066-X.

[154] P.D. Adams, P. V Afonine, G. Bunkóczi, V.B. Chen, I.W. Davis, N. Echols, J.J. Headd, L.-W. Hung, G.J. Kapral, R.W. Grosse-Kunstleve, A.J. McCoy, N.W. Moriarty, R. Oeffner, R.J. Read, D.C. Richardson, J.S. Richardson, T.C. Terwilliger, P.H. Zwart, {\it PHENIX}: a comprehensive Python-based system for macromolecular structure solution, Acta Crystallogr. Sect. D. 66 (2010) 213–221. doi:10.1107/S0907444909052925.

[155] M.D. Winn, C.C. Ballard, K.D. Cowtan, E.J. Dodson, P. Emsley, P.R. Evans, R.M. Keegan, E.B. Krissinel, A.G.W. Leslie, A. McCoy, S.J. McNicholas, G.N. Murshudov, N.S. Pannu, E.A. Potterton, H.R. Powell, R.J. Read, A. Vagin, K.S. Wilson, Overview of the CCP4 suite and current developments, Acta Crystallogr. Sect. D Biol. Crystallogr. 67 (2011) 235–242. doi:10.1107/S0907444910045749.

[156] A. Vagin, A. Teplyakov, *MOLREP* : an Automated Program for Molecular Replacement, J. Appl. Crystallogr. 30 (1997) 1022–1025. doi:10.1107/S0021889897006766.

[157] A.A. Vagin, R.A. Steiner, A.A. Lebedev, L. Potterton, S. McNicholas, F. Long, G.N. Murshudov, {\it REFMAC}5 dictionary: organization of prior chemical knowledge and guidelines for its use, Acta Crystallogr. Sect. D. 60 (2004) 2184–2195. doi:10.1107/S0907444904023510.

[158] P. Emsley, K. Cowtan, {\it Coot}: model-building tools for molecular graphics, Acta Crystallogr. Sect. D. 60 (2004) 2126–2132. doi:10.1107/S0907444904019158.

[159] V.B. Chen, W.B. Arendall, J.J. Headd, D.A. Keedy, R.M. Immormino, G.J.

Kapral, L.W. Murray, J.S. Richardson, D.C. Richardson, MolProbity: all-atom structure validation for macromolecular crystallography, Acta Crystallogr. Sect. D Biol. Crystallogr. 66 (2010) 12–21. doi:10.1107/S0907444909042073.

[160] E. Krissinel, Crystal contacts as nature's docking solutions, J. Comput. Chem. 31 (2010) 133–143. doi:10.1002/jcc.21303.

[161] pymol, (n.d.).

[162] B.R. Brooks, C.L. Brooks, A.D. MacKerell, L. Nilsson, R.J. Petrella, B. Roux, Y. Won, G. Archontis, C. Bartels, S. Boresch, A. Caflisch, L. Caves, Q. Cui, A.R. Dinner, M. Feig, S. Fischer, J. Gao, M. Hodoscek, W. Im, K. Kuczera, T. Lazaridis, J. Ma, V. Ovchinnikov, E. Paci, R.W. Pastor, C.B. Post, J.Z. Pu, M. Schaefer, B. Tidor, R.M. Venable, H.L. Woodcock, X. Wu, W. Yang, D.M. York, M. Karplus, CHARMM: The Biomolecular Simulation Program, J. Comput. Chem. 30 (2009) 1545–1614. doi:10.1002/jcc.21287.

[163] G.M. Morris, R. Huey, W. Lindstrom, M.F. Sanner, R.K. Belew, D.S. Goodsell, A.J. Olson, AutoDock4 and AutoDockTools4: Automated Docking with Selective Receptor Flexibility, J. Comput. Chem. 30 (2009) 2785–2791. doi:10.1002/jcc.21256.

[164] Y.M. Chook, H. Ke, W.N. Lipscomb, Crystal structures of the monofunctional chorismate mutase from Bacillus subtilis and its complex with a transition state analog., Proc. Natl. Acad. Sci. U. S. A. 90 (1993) 8600–8603. http://www.ncbi.nlm.nih.gov/pmc/articles/PMC47405/.

[165] B.E. Davidson, G.S.B.T.-M. in E. Hudson, [53] Chorismate mutase-prephenate dehydrogenase from Escherichia coli, in: Metab. Aromat. Amin. Acids Amin., Academic Press, 1987: pp. 440–450. doi:https://doi.org/10.1016/S0076-6879(87)42055-7.

[166] I. Wiegand, K. Hilpert, R.E.W. Hancock, Agar and broth dilution methods to determine the minimal inhibitory concentration (MIC) of antimicrobial substances, Nat. Protoc. 3 (2008) 163–175. http://dx.doi.org/10.1038/nprot.2007.521.

[167] E. Krissinel, K. Henrick, Inference of Macromolecular Assemblies from Crystalline State, J. Mol. Biol. 372 (2007) 774–797. doi:https://doi.org/10.1016/j.jmb.2007.05.022.

[168] S.K. Kim, S.K. Reddy, B.C. Nelson, H. Robinson, P.T. Reddy, J.E. Ladner, A comparative biochemical and structural analysis of the intracellular chorismate

mutase (Rv0948c) from Mycobacterium tuberculosis H37R v and the secreted chorismate mutase (y2828) from Yersinia pestis, FEBS J. 275 (2008) 4824–4835. doi:10.1111/j.1742-4658.2008.06621.x.

[169] K. Anita, T.S. Faseela, Y.K. Rai, S. Chaithra, M.S. Mallya, Moraxella catarrhalis: An often overlooked pathogen of the respiratory tract, J. Clin. Diagnostic Res. 5 (2011) 495–497.

[170] C.M. Verduin, C. Hol, H. Van Dijk, A. Van Belkum, Moraxella catarrhalis:, Society. 15 (2002) 125–144. doi:10.1128/CMR.15.1.125.

[171] T.F. Murphy, G.I. Parameswaran, *Moraxella catarrhalis*, a Human Respiratory Tract Pathogen, Clin. Infect. Dis. 49 (2009) 124–131. doi:10.1086/599375.

[172] S. Pratap, M. Katiki, P. Gill, P. Kumar, D. Golemi-Kotra, Active-site plasticity is essential to carbapenem hydrolysis by OXA-58 class D β-lactamase of Acinetobacter baumannii, Antimicrob. Agents Chemother. 60 (2016) 75–86. doi:10.1128/AAC.01393-15.

[173] M.H. RICHMOND, R.B. SYKES, The β-lactamases of Gram-negative bacteria and their possible physiological role., Adv. Microb. Physiol. 9 (1973) 31–88.

[174] A.C. Palmer, R. Kishony, Understanding, predicting and manipulating the genotypic evolution of antibiotic resistance, Nat. Rev. Genet. 14 (2013) 243–248. doi:10.1038/nrg3351.

[175] C.T. Keith, A.A. Borisy, B.R. Stockwell, Multicomponent therapeutics for networked systems, Nat. Rev. Drug Discov. 4 (2005) 71. http://dx.doi.org/10.1038/nrd1609.

[176] C.O.R. J.E. Cronan, Escherichia coli and Salmonella : cellular and molecular biology, American Society for Microbiology, Washington, 1996.

[177] L.R. Kass, K. Bloch, On the enzymatic synthesis of unsaturated fatty acids in Escherichia coli., Proc. Natl. Acad. Sci. U. S. A. 58 (1967) 1168–1173. http://www.ncbi.nlm.nih.gov/pmc/articles/PMC335764/.

[178] D.F. Silbert, P.R. Vagelos, Fatty acid mutant of E. coli lacking a beta-hydroxydecanoyl thioester dehydrase., Proc. Natl. Acad. Sci. U. S. A. 58 (1967) 1579–1586. http://www.ncbi.nlm.nih.gov/pmc/articles/PMC223964/.

[179] I.S. Rosenfeld, G. D'Agnolo, P.R. Vagelos, Synthesis of Unsaturated Fatty Acids and the Lesion in fab B Mutants, J. Biol. Chem. . 248 (1973) 2452–2460. http://www.jbc.org/content/248/7/2452.abstract.

[180] S. Mohan, T.M. Kelly, S.S. Eveland, C.R. Raetz, M.S. Anderson, An

Escherichia coli gene (FabZ) encoding (3R)-hydroxymyristoyl acyl carrier protein dehydrase. Relation to fabA and suppression of mutations in lipid A biosynthesis., J. Biol. Chem. . 269 (1994) 32896–32903. http://www.jbc.org/content/269/52/32896.abstract.

[181] H. Wang, J.E. Cronan, Functional Replacement of the FabA and FabB Proteins of Escherichia coli Fatty Acid Synthesis by Enterococcus faecalis FabZ and FabF Homologues, J. Biol. Chem. . 279 (2004) 34489–34495. doi:10.1074/jbc.M403874200.

[182] R.J. Heath, C.O. Rock, Roles of the FabA and FabZ β-Hydroxyacyl-Acyl Carrier Protein Dehydratases in Escherichia coli Fatty Acid Biosynthesis, J. Biol. Chem. . 271 (1996) 27795–27801. doi:10.1074/jbc.271.44.27795.

[183] P.L. Swarnamukhi, S.K. Sharma, P. Bajaj, N. Surolia, A. Surolia, K. Suguna, Crystal structure of dimeric FabZ of Plasmodium falciparum reveals conformational switching to active hexamers by peptide flips, FEBS Lett. 580 (2006) 2653–2660. doi:10.1016/j.febslet.2006.04.014.

[184] D. Kostrewa, F.K. Winkler, G. Folkers, L. Scapozza, R. Perozzo, The crystal structure of PfFabZ, the unique β-hydroxyacyl-ACP dehydratase involved in fatty acid biosynthesis of Plasmodium falciparum, Protein Sci. 14 (2005) 1570–1580. doi:10.1110/ps.051373005.

[185] W. Liu, C. Luo, C. Han, S. Peng, Y. Yang, J. Yue, X. Shen, H. Jiang, A new β-hydroxyacyl-acyl carrier protein dehydratase (FabZ) from Helicobacter pylori: Molecular cloning, enzymatic characterization, and structural modeling, Biochem. Biophys. Res. Commun. 333 (2005) 1078–1086. doi:10.1016/j.bbrc.2005.05.197.

[186] L. Zhang, W. Liu, T. Hu, L. Du, C. Luo, K. Chen, X. Shen, H. Jiang, Structural basis for catalytic and inhibitory mechanisms of ??-hydroxyacyl-acyl carrier protein dehydratase (FabZ), J. Biol. Chem. 283 (2008) 5370–5379. doi:10.1074/jbc.M705566200.

[187] C.M. Bryan, J. Bhandari, A.J. Napuli, D.J. Leibly, R. Choi, A. Kelley, W.C. Van Voorhis, T.E. Edwards, L.J. Stewart, High-throughput protein production and purification at the Seattle Structural Genomics Center for Infectious Disease, Acta Crystallogr. Sect. F Struct. Biol. Cryst. Commun. 67 (2011) 1010–1014. doi:10.1107/S1744309111018367.

[188] A.S. Kirkpatrick, T. Yokoyama, K.-J. Choi, H.-J. Yeo, Campylobacter jejuni

fatty acid synthase II: Structural and functional analysis of β-hydroxyacyl-ACP dehydratase (FabZ), Biochem. Biophys. Res. Commun. 380 (2009) 407–412. doi:10.1016/j.bbrc.2009.01.115.

[189] K. Maity, B.S. Venkata, N. Kapoor, N. Surolia, A. Surolia, K. Suguna, Structural basis for the functional and inhibitory mechanisms of β-hydroxyacyl-acyl carrier protein dehydratase (FabZ) of Plasmodium falciparum, J. Struct. Biol. 176 (2011) 238–249. doi:10.1016/j.jsb.2011.07.018.

[190] S.K. and A. Pandey, Chemistry and Biological Activities of Flavonoids: An Overview, Sci. J. 2013 (2013). doi:http://dx.doi.org/10.1155/2013/162750.

[191] J. Robak, R.J. Gryglewski, Bioactivity of flavonoids, Pol. J. Pharmacol. 48 (1996) 555–564. http://europepmc.org/abstract/MED/9112694.

[192] J.B. Harborne, C.A. Williams, Advances in flavonoid research since 1992, Phytochemistry. 55 (2000) 481–504. doi:https://doi.org/10.1016/S0031-9422(00)00235-1.

[193] N.H.G. Holford, 2. Fitting models to biological data using linear and non-linear regression: a practical guide to curve fitting. Harvey Motulsky and Arthur Christopoulos, Oxford University Press, Oxford, 2004. No. of pages: 352. Price: £19.99, $29.29 (paperback); £40.00, Stat. Med. 24 (2005) 2745–2746. doi:10.1002/sim.2181.

[194] N.J. Greenfield, Using circular dichroism collected as a funcion of temperature to determine the thermodynamics of protein unfolding and binding interactions, Nat. Protoc. 1 (2009) 2527–2535. doi:10.1038/nprot.2006.204.Using.

[195] L. Whitmore, B.A. Wallace, DICHROWEB, an online server for protein secondary structure analyses from circular dichroism spectroscopic data, Nucleic Acids Res. 32 (2004) W668–W673. doi:10.1093/nar/gkh371.

[196] N. Bijari, S. Ghobadi, H. Mahdiuni, R. Khodarahmi, S.A. Ghadami, Spectroscopic and molecular modeling studies on binding of dorzolamide to bovine and human carbonic anhydrase II, Int. J. Biol. Macromol. 80 (2015) 189–199. doi:10.1016/j.ijbiomac.2015.06.028.

[197] M. Biasini, S. Bienert, A. Waterhouse, K. Arnold, G. Studer, T. Schmidt, F. Kiefer, T.G. Cassarino, M. Bertoni, L. Bordoli, T. Schwede, SWISS-MODEL: modelling protein tertiary and quaternary structure using evolutionary information, Nucleic Acids Res. 42 (2014) W252–W258. doi:10.1093/nar/gku340.

[198] B. Webb, A. Sali, Comparative Protein Structure Modeling Using MODELLER, in: Curr. Protoc. Bioinforma., John Wiley & Sons, Inc., 2002. doi:10.1002/0471250953.bi0506s47.

[199] C. Notredame, D.G. Higgins, J. Heringa, T-coffee: a novel method for fast and accurate multiple sequence alignment11Edited by J. Thornton, J. Mol. Biol. 302 (2000) 205–217. doi:https://doi.org/10.1006/jmbi.2000.4042.

[200] S. Cristobal, A. Zemla, D. Fischer, L. Rychlewski, A. Elofsson, A study of quality measures for protein threading models, BMC Bioinformatics. 2 (2001) 5. doi:10.1186/1471-2105-2-5.

[201] B. Wallner, A. Elofsson, Can correct protein models be identified?, Protein Sci. 12 (2003) 1073–1086. http://www.ncbi.nlm.nih.gov/pmc/articles/PMC2323877/.

[202] M. Wiederstein, M.J. Sippl, ProSA-web: interactive web service for the recognition of errors in three-dimensional structures of proteins, Nucleic Acids Res. 35 (2007) W407–W410. http://dx.doi.org/10.1093/nar/gkm290.

[203] Y. Zhang, J. Skolnick, TM-align: a protein structure alignment algorithm based on the TM-score, Nucleic Acids Res. 33 (2005) 2302–2309. doi:10.1093/nar/gki524.

[204] E.F. Pettersen, T.D. Goddard, C.C. Huang, G.S. Couch, D.M. Greenblatt, E.C. Meng, T.E. Ferrin, UCSF Chimera—A visualization system for exploratory research and analysis, J. Comput. Chem. 25 (2004) 1605–1612. doi:10.1002/jcc.20084.

[205] D.A. Case, T. Darden, T.E.C. Iii, C. Simmerling, S. Brook, A. Roitberg, J. Wang, U.T. Southwestern, R.E. Duke, U. Hill, R. Luo, U.C. Irvine, D.R. Roe, R.C. Walker, S. Legrand, J. Swails, D. Cerutti, J. Kaus, R. Betz, R.M. Wolf, K.M. Merz, M. State, G. Seabra, P. Janowski, F. Paesani, J. Liu, X. Wu, T. Steinbrecher, H. Gohlke, N. Homeyer, Q. Cai, U.C. Irvine, W. Smith, U.C. Irvine, D. Mathews, R. Salomon-ferrer, C. Sagui, N.C. State, V. Babin, N.C. State, T. Luchko, S. Gusarov, A. Kovalenko, J. Berryman, P.A. Kollman, U.C.S. Francisco, Amber 14, 2014.

[206] G. M. J. Frisch, G. W. Trucks, H. B. Schlegel, G. E. Scuseria, M. A. Robb, J. R. Cheeseman, G. Scalmani, V. Barone, G. A. Petersson, H. Nakatsuji, X. Li, M. Caricato, A. V. Marenich, J. Bloino, B. G. Janesko, R. Gomperts, B. Mennucci, H. P. Hratchian, J. V., Gaussian 16, Revision A.03, Wallingford CT.

(2016).

[207] J. Wang, W. Wang, P.A. Kollman, D.A. Case, Automatic atom type and bond type perception in molecular mechanical calculations, J. Mol. Graph. Model. 25 (2006) 247–260. doi:https://doi.org/10.1016/j.jmgm.2005.12.005.

[208] S. Miyamoto, P.A. Kollman, Settle: An analytical version of the SHAKE and RATTLE algorithm for rigid water models, J. Comput. Chem. 13 (1992) 952–962. doi:10.1002/jcc.540130805.

[209] M.J. Abraham, J.E. Gready, Optimization of parameters for molecular dynamics simulation using smooth particle-mesh Ewald in GROMACS 4.5, J. Comput. Chem. 32 (2011) 2031–2040. doi:10.1002/jcc.21773.

[210] H.J.C. Berendsen, J.P.M. Postma, W.F. van Gunsteren, A. DiNola, J.R. Haak, Molecular dynamics with coupling to an external bath, J. Chem. Phys. 81 (1984) 3684–3690. doi:10.1063/1.448118.

[211] W. Humphrey, A. Dalke, K. Schulten, VMD: Visual molecular dynamics, J. Mol. Graph. 14 (1996) 33–38. doi:https://doi.org/10.1016/0263-7855(96)00018-5.

[212] S. Pratap, A. Dev, V. Kumar, R. Yadav, M. Narwal, S. Tomar, P. Kumar, Structure of Chorismate Mutase-like Domain of DAHPS from Bacillus subtilis Complexed with Novel Inhibitor Reveals Conformational Plasticity of Active Site, Sci. Rep. 7 (2017) 6364. doi:10.1038/s41598-017-06578-1.

[213] J.B. Baell, G.A. Holloway, New Substructure Filters for Removal of Pan Assay Interference Compounds (PAINS) from Screening Libraries and for Their Exclusion in Bioassays, J. Med. Chem. 53 (2010) 2719–2740. doi:10.1021/jm901137j.

[214] D. Lagorce, O. Sperandio, J.B. Baell, M.A. Miteva, B.O. Villoutreix, FAF-Drugs3: a web server for compound property calculation and chemical library design, Nucleic Acids Res. 43 (2015) W200–W207. doi:10.1093/nar/gkv353.

[215] A. Sharma, V. Kumar, A. Chatrath, A. Dev, R. Prasad, A.K. Sharma, S. Tomar, P. Kumar, In vitro metal catalyzed oxidative stress in DAH7PS: Methionine modification leads to structure destabilization and induce amorphous aggregation, Int. J. Biol. Macromol. 106 (2018) 1089–1106. doi:10.1016/j.ijbiomac.2017.08.105.

[216] S.M. Kelly, T.J. Jess, N.C. Price, How to study proteins by circular dichroism, Biochim. Biophys. Acta - Proteins Proteomics. 1751 (2005) 119–139.

doi:10.1016/j.bbapap.2005.06.005.

[217] B. Ahmad, G. Muteeb, P. Alam, A. Varshney, N. Zaidi, M. Ishtikhar, G. Badr, M.H. Mahmoud, R.H. Khan, Thermal induced unfolding of human serum albumin isomers: Assigning residual α helices to domain II, Int. J. Biol. Macromol. 75 (2015) 447–452. doi:10.1016/j.ijbiomac.2015.02.003.

[218] G. Siligardi, R. Hussain, S.G. Patching, M.K. Phillips-Jones, Ligand- and drug-binding studies of membrane proteins revealed through circular dichroism spectroscopy, Biochim. Biophys. Acta - Biomembr. 1838 (2014) 34–42. doi:10.1016/j.bbamem.2013.06.019.

[219] H. Ojha, K. Mishra, M.I. Hassan, N.K. Chaudhury, Spectroscopic and isothermal titration calorimetry studies of binding interaction of ferulic acid with bovine serum albumin, Thermochim. Acta. 548 (2012) 56–64. doi:10.1016/j.tca.2012.08.016.

[220] I.H.M. van Stokkum, H.J.W. Spoelder, M. Bloemendal, R. van Grondelle, F.C.A. Groen, Estimation of protein secondary structure and error analysis from circular dichroism spectra, Anal. Biochem. 191 (1990) 110–118. doi:https://doi.org/10.1016/0003-2697(90)90396-Q.

[221] D.T. Jones, Protein secondary structure prediction based on position-specific scoring matrices11Edited by G. Von Heijne, J. Mol. Biol. 292 (1999) 195–202. doi:https://doi.org/10.1006/jmbi.1999.3091.

[222] R.A. Laskowski, M.W. MacArthur, D.S. Moss, J.M. Thornton, {\it PROCHECK}: a program to check the stereochemical quality of protein structures, J. Appl. Crystallogr. 26 (1993) 283–291. doi:10.1107/S0021889892009944.

[223] G.N. Ramachandran, C. Ramakrishnan, V. Sasisekharan, Stereochemistry of polypeptide chain configurations, J. Mol. Biol. 7 (1963) 95–99. doi:https://doi.org/10.1016/S0022-2836(63)80023-6.

[224] R. Luthy, J.U. Bowie, D. Eisenberg, Assessment of protein models with three-dimensional profiles, Nature. 356 (1992) 83–85. http://dx.doi.org/10.1038/356083a0.

[225] C. Colovos, T.O. Yeates, Verification of protein structures: patterns of nonbonded atomic interactions., Protein Sci. 2 (1993) 1511–1519. http://www.ncbi.nlm.nih.gov/pmc/articles/PMC2142462/.

[226] M. Leesong, B.S. Henderson, J.R. Gillig, J.M. Schwab, J.L. Smith, Structure of

a dehydratase–isomerase from the bacterial pathway for biosynthesis of unsaturated fatty acids: two catalytic activities in one active site, Structure. 4 (1996) 253–264. doi:https://doi.org/10.1016/S0969-2126(96)00030-5.

[227] A. Dereeper, V. Guignon, G. Blanc, S. Audic, S. Buffet, F. Chevenet, J.-F. Dufayard, S. Guindon, V. Lefort, M. Lescot, J.-M. Claverie, O. Gascuel, Phylogeny.fr: robust phylogenetic analysis for the non-specialist, Nucleic Acids Res. 36 (2008) W465–W469. doi:10.1093/nar/gkn180.

[228] J. Chen, L. Zhang, Y. Zhang, H. Zhang, J. Du, J. Ding, Y. Guo, H. Jiang, X. Shen, Emodin targets the β-hydroxyacyl-acyl carrier protein dehydratase from Helicobacter pylori: enzymatic inhibition assay with crystal structural and thermodynamic characterization, BMC Microbiol. 9 (2009) 91. doi:10.1186/1471-2180-9-91.

[229] C.S. Hughes, E. Longo, M.K. Phillips-Jones, R. Hussain, Characterisation of the selective binding of antibiotics vancomycin and teicoplanin by the VanS receptor regulating type A vancomycin resistance in the enterococci, Biochim. Biophys. Acta - Gen. Subj. 1861 (2017) 1951–1959. doi:10.1016/j.bbagen.2017.05.011.

[230] A. Kumar, M. Rao, A novel bifunctional peptidic aspartic protease inhibitor inhibits chitinase A from Serratia marcescens: Kinetic analysis of inhibition and binding affinity, Biochim. Biophys. Acta - Gen. Subj. 1800 (2010) 526–536. doi:10.1016/j.bbagen.2010.01.014.

[231] M.S. Borana, P. Mishra, R.R.S. Pissurlenkar, R. V. Hosur, B. Ahmad, Curcumin and kaempferol prevent lysozyme fibril formation by modulating aggregation kinetic parameters, Biochim. Biophys. Acta - Proteins Proteomics. 1844 (2014) 670–680. doi:10.1016/j.bbapap.2014.01.009.

[232] A. Naiyer, M.I. Hassan, A. Islam, M. Sundd, F. Ahmad, Structural characterization of MG and pre-MG states of proteins by MD simulations, NMR, and other techniques, J. Biomol. Struct. Dyn. 33 (2015) 2267–2284. doi:10.1080/07391102.2014.999354.

[233] L. Moynié, S.M. Leckie, S.A. McMahon, F.G. Duthie, A. Koehnke, J.W. Taylor, M.S. Alphey, R. Brenk, A.D. Smith, J.H. Naismith, Structural insights into the mechanism and inhibition of the β-hydroxydecanoyl-acyl carrier protein dehydratase from Pseudomonas aeruginosa, J. Mol. Biol. 425 (2013) 365–377. doi:10.1016/j.jmb.2012.11.017.

[234] C. Manach, G. Williamson, C. Morand, A. Scalbert, C. Remesy, Bioavailability and bioefficacy of polyphenols in human, Am J Clin Nutr. 81 (suppl) (2005) 230S–242S. doi:81/1/230S [pii].

[235] L. Zhang, W. Liu, J. Xiao, T. Hu, J. Chen, K. Chen, H. Jiang, X. Shen, Malonyl-CoA: acyl carrier protein transacylase from Helicobacter pylori: Crystal structure and its interaction with acyl carrier protein, Protein Sci. 16 (2007) 1184–1192. doi:10.1110/ps.072757307.1184.

[236] Z. Li, Y. Huang, J. Ge, H. Fan, X. Zhou, S. Li, M. Bartlam, H. Wang, Z. Rao, The Crystal Structure of MCAT from Mycobacterium tuberculosis Reveals Three New Catalytic Models, J. Mol. Biol. 371 (2007) 1075–1083. doi:10.1016/j.jmb.2007.06.004.

[237] S.K. Hong, K.H. Kim, J.K. Park, K.W. Jeong, Y. Kim, E.E.K. Kim, New design platform for malonyl-CoA-acyl carrier protein transacylase, FEBS Lett. 584 (2010) 1240–1244. doi:10.1016/j.febslet.2010.02.038.

[238] L. Miesel, J. Greene, T.A. Black, Genetic strategies for antibacterial drug discovery, Nat. Rev. Genet. 4 (2003) 442. http://dx.doi.org/10.1038/nrg1086.

[239] A.J. Kutchma, T.T. Hoang, H.P. Schweizer, Characterization of a *Pseudomonas aeruginosa* fatty acid biosynthetic gene cluster: Purification of acyl carrier protein (ACP) and malonyl-coenzyme A:ACP transacylase (FabD), J. Bacteriol. 181 (1999) 5498–5504. http://jb.asm.org/content/181/17/5498.short%5Cnhttp://jb.asm.org/content/181/17/5498.full.

[240] S. Natarajan, J.K. Kim, T.K. Jung, T.T.N. Doan, H.P.T. Ngo, M.K. Hong, S. Kim, V.P. Tan, S.J. Ahn, S.H. Lee, Y. Han, Y.J. Ahn, L.W. Kang, Crystal structure of malonyl CoA-acyl carrier protein transacylase from Xanthomanous oryzae pv. oryzae and its proposed binding with ACP, Mol. Cells. 33 (2012) 19–25. doi:10.1007/s10059-012-2155-y.

[241] J.B. Parsons, C.O. Rock, Is bacterial fatty acid synthesis a valid target for antibacterial drug discovery?, Curr. Opin. Microbiol. 14 (2011) 544–549. doi:10.1016/j.mib.2011.07.029.

[242] C. Morvan, D. Halpern, G. Kénanian, C. Hays, J. Anba-Mondoloni, S. Brinster, S. Kennedy, P. Trieu-Cuot, C. Poyart, G. Lamberet, K. Gloux, A. Gruss, Environmental fatty acids enable emergence of infectious Staphylococcus aureus resistant to FASII-targeted antimicrobials, Nat. Commun. 7 (2016).

doi:10.1038/ncomms12944.

[243] K. Gloux, C. Soler, C. Morvan, D. Halpern, C. Pourcel, H.V. Thien, G. Lamberet, A. Gruss, crossm Clinical Relevance of Type II Fatty Acid, 61 (2017) 1–10.

[244] J. Molnos, R. Gardiner, G.E. Dale, R. Lange, A continuous coupled enzyme assay for bacterial malonyl-CoA:acyl carrier protein transacylase (FabD), Anal. Biochem. 319 (2003) 171–176. doi:10.1016/S0003-2697(03)00327-0.

[245] C.J. Arthur, C. Williams, K. Pottage, E. Płoskoń, S.C. Findlow, S.G. Burston, T.J. Simpson, M.P. Crump, J. Crosby, Structure and malonyl CoA-ACP transacylase binding of Streptomyces coelicolor fatty acid synthase acyl carrier protein, ACS Chem. Biol. 4 (2009) 625–636. doi:10.1021/cb900099e.

[246] S.T. Prigge, X. He, L. Gerena, N.C. Waters, K.A. Reynolds, The initiating steps of a type II fatty acid synthase in Plasmodium falciparum are catalyzed by pfACP, pfMCAT, and pfKASIII, Biochemistry. 42 (2003) 1160–1169. doi:10.1021/bi026847k.

[247] L. Kremer, K.M. Nampoothiri, S. Lesjean, L.G. Dover, S. Graham, J. Betts, P.J. Brennan, D.E. Minnikin, C. Locht, G.S. Besra, Biochemical Characterization of Acyl Carrier Protein (AcpM) and Malonyl-CoA:AcpM Transacylase (mtFabD), Two Major Components of Mycobacterium tuberculosis Fatty Acid Synthase II, J. Biol. Chem. 276 (2001) 27967–27974. doi:10.1074/jbc.M103687200.

[248] L. Serre, E.C. Verbree, Z. Dauter, a R. Stuitje, Z.S. Derewenda, The Escherichia coli malonyl-CoA:acyl carrier protein transacylase at 1.5-A resolution. Crystal structure of a fatty acid synthase component., J. Biol. Chem. 270 (1995) 12961–12964. doi:10.1074/jbc.270.22.12961.

[249] A.T. Keatinge-Clay, A.A. Shelat, D.F. Savage, S.C. Tsai, L.J.W. Miercke, J.D. O’Connell, C. Khosla, R.M. Stroud, Catalysis, specificity, and ACP docking site of Streptomyces coelicolor malonyl-CoA:ACP Transacylase, Structure. 11 (2003) 147–154. doi:10.1016/S0969-2126(03)00004-2.

[250] G.A. Cordell, M. Lou Quinn-Beattie, N.R. Farnsworth, The potential of alkaloids in drug discovery, Phyther. Res. 15 (2001) 183–205. doi:10.1002/ptr.890.

[251] C.W. Wright, S.J. Marshall, P.F. Russell, M.M. Anderson, J.D. Phillipson, G.C. Kirby, D.C. Warhurst, P.L. Schiff, In Vitro Antiplasmodial, Antiamoebic, and

Cytotoxic Activities of Some Monomeric Isoquinoline Alkaloids, J. Nat. Prod. 63 (2000) 1638–1640. doi:10.1021/np000144r.

[252] H. Prashanth, R.D. Saldanha, S. Shenoy, Moraxella catarrhalis - A Rediscovered Pathogen, Int. J. Biol. Med. Res. 2 (2011) 979–981. http://www.biomedscidirect.com/333/moraxella_catarrhalis_a_rediscovered_pathogen/articlescategories.

[253] S.J. Barnes, E. M. & Wakil, Studies on the mechanism of fatty acid synthesis, J. Biol. Chem. 243 (1968) 2955–2962.

[254] S.F. Altschul, W. Gish, W. Miller, E.W. Myers, D.J. Lipman, Basic local alignment search tool, J. Mol. Biol. 215 (1990) 403–410. doi:https://doi.org/10.1016/S0022-2836(05)80360-2.

[255] A. Šali, T.L. Blundell, Comparative Protein Modelling by Satisfaction of Spatial Restraints, J. Mol. Biol. 234 (1993) 779–815. doi:https://doi.org/10.1006/jmbi.1993.1626.

[256] M. Biasini, S. Bienert, A. Waterhouse, K. Arnold, G. Studer, T. Schmidt, F. Kiefer, T.G. Cassarino, M. Bertoni, L. Bordoli, T. Schwede, SWISS-MODEL: modelling protein tertiary and quaternary structure using evolutionary information, Nucleic Acids Res. 42 (2014) W252–W258. http://dx.doi.org/10.1093/nar/gku340.

[257] A.E. Szafranska, T.S. Hitchman, R.J. Cox, J. Crosby, T.J. Simpson, Kinetic and mechanistic analysis of the malonyl CoA:ACP transacylase from Streptomyces coelicolor indicates a single catalytically competent serine nucleophile at the active site, Biochemistry. 41 (2002) 1421–1427. doi:10.1021/bi012001p.

[258] N. Sreerama, S.Y. Venyaminov, R.W. Woody, Estimation of the number of alpha-helical and beta-strand segments in proteins using circular dichroism spectroscopy., Protein Sci. 8 (1999) 370–380. http://www.ncbi.nlm.nih.gov/pmc/articles/PMC2144265/.

[259] C. Li, Y. Liu, Y. Fu, T. Huang, L. Kang, C. Li, The antiproliferative activity of di-2-pyridylketone dithiocarbamate is partly attributed to catalase inhibition: detailing the interaction by spectroscopic methods, Mol. BioSyst. 51 (2017) 2778–2786. doi:10.1039/C7MB00032D.

[260] A. Sharma, V. Kumar, A. Chatrath, A. Dev, R. Prasad, A. Kumar Sharma, S. Tomar, P. Kumar, ARTICLE IN PRESS G Model In vitro metal catalyzed oxidative stress in DAH7PS: Methionine modification leads to structure

destabilization and induce amorphous aggregation, Int. J. Biol. Macromol. Int. J. Biol. Macromol. Int. J. Biol. Macromol. (2017). doi:10.1016/j.ijbiomac.2017.08.105.

[261] P. Agnihotri, A.K. Mishra, S. Mishra, V.K. Sirohi, A.A. Sahasrabuddhe, J.V. Pratap, Identification of Novel Inhibitors of Leishmania donovani γ-Glutamylcysteine Synthetase Using Structure-Based Virtual Screening, Docking, Molecular Dynamics Simulation, and in Vitro Studies, J. Chem. Inf. Model. 57 (2017) 815–825. doi:10.1021/acs.jcim.6b00642.

[262] N. Ali Mohammed Sultan, R. Nagender Rao, S.K. Nadimpalli, M.J. Swamy, Tryptophan environment, secondary structure and thermal unfolding of the galactose-specific seed lectin from Dolichos lablab: Fluorescence and circular dichroism spectroscopic studies, Biochim. Biophys. Acta - Gen. Subj. 1760 (2006) 1001–1008. doi:10.1016/j.bbagen.2006.03.016.

[263] P. Sen, S. Fatima, B. Ahmad, R.H. Khan, Interactions of thioflavin T with serum albumins: Spectroscopic analyses, Spectrochim. Acta - Part A Mol. Biomol. Spectrosc. 74 (2009) 94–99. doi:10.1016/j.saa.2009.05.010.

[264] N. Shahabadi, S. Hadidi, F. Feizi, Study on the interaction of antiviral drug “Tenofovir” with human serum albumin by spectral and molecular modeling methods, 138 (2015) 169–175. doi:10.1016/j.saa.2014.10.070.

[265] S. Guindon, J.-F. Dufayard, V. Lefort, M. Anisimova, W. Hordijk, O. Gascuel, New Algorithms and Methods to Estimate Maximum-Likelihood Phylogenies: Assessing the Performance of PhyML 3.0, Syst. Biol. 59 (2010) 307–321. http://dx.doi.org/10.1093/sysbio/syq010.

[266] A. Coates, Y. Hu, R. Bax, C. Page, The future challenges facing the development of new antimicrobial drugs, Nat. Rev. Drug Discov. 1 (2002) 895–910. doi:10.1038/nrd940.

[267] S.M. Mohamed, E.M. Hassan, N.A. Ibrahim, Cytotoxic and antiviral activities of aporphine alkaloids of Magnolia grandiflora L ., 6419 (2017). doi:10.1080/14786410902906959.

[268] M. Paydar, B. Kamalidehghan, Y.L. Wong, W.F. Wong, C.Y. Looi, M.R. Mustafa, Evaluation of cytotoxic and chemotherapeutic properties of boldine in breast cancer using in vitro and in vivo models, Drug Des. Devel. Ther. 8 (2014) 719–733. doi:10.2147/DDDT.S58178.

[269] S.K. Noureini, F. Tanavar, Chemico-Biological Interactions Boldine , a natural

aporphine alkaloid , inhibits telomerase at non-toxic concentrations, Chem. Biol. Interact. 231 (2015) 27–34. doi:10.1016/j.cbi.2015.02.020.

[270] K. Matsumoto, M. Yoshida, K.-E. Andersson, P. Hedlund, Effects in vitro and in vivo by apomorphine in the rat corpus cavernosum, Br. J. Pharmacol. 146 (2005) 259–267. doi:10.1038/sj.bjp.0706317.

[271] G.U. Corsini, M.D. Zompo, G.L. Gessa, A. Mangoni, THERAPEUTIC EFFICACY OF APOMORPHINE COMBINED WITH AN EXTRACEREBRAL INHIBITOR OF DOPAMINE RECEPTORS IN PARKINSON'S DISEASE, Lancet. 313 (1979) 954–956. doi:https://doi.org/10.1016/S0140-6736(79)91725-2.

[272] C.G. C., P.P. S., F. Clas, K. Barry, M. Ismael, Similarities between Neurologic Effects of L-Dopa and of Apomorphine, N. Engl. J. Med. 282 (1970) 31–33. doi:10.1056/NEJM197001012820107.

[273] C. Oefner, H. Schulz, A. D'Arcy, G.E. Dale, Mapping the active site of {\it Escherichia coli} malonyl-CoA{--}acyl carrier protein transacylase (FabD) by protein crystallography, Acta Crystallogr. Sect. D. 62 (2006) 613–618. doi:10.1107/S0907444906009474.

[274] Y.H. Kong, L. Zhang, Z.Y. Yang, C. Han, L.H. Hu, H.L. Jiang, X. Shen, Natural product juglone targets three key enzymes from Helicobacter pylori: Inhibition assay with crystal structure characterization, Acta Pharmacol. Sin. 29 (2008) 870–876. doi:10.1111/j.1745-7254.2008.00808.x.

[275] P. Babula, V. Adam, L. Havel, R. Kizek, Noteworthy Secondary Metabolites Naphthoquinones – their Occurrence, Pharmacological Properties and Analysis, Curr. Pharm. Anal. 5 (2009) 47–68. doi:10.2174/157341209787314936.

[276] M.F. Ahmad, I. Alam, S.E. Huff, J. Pink, S.A. Flanagan, D. Shewach, T.A. Misko, N.L. Oleinick, W.E. Harte, R. Viswanathan, M.E. Harris, C.G. Dealwis, Potent competitive inhibition of human ribonucleotide reductase by a nonnucleoside small molecule, Proc. Natl. Acad. Sci. 114 (2017) 8241–8246. doi:10.1073/pnas.1620220114.

[277] Comparative Protein Modelling by Satisfaction of Spatial Restraints, J. Mol. Biol. 234 (1993) 779–815. doi:10.1006/JMBI.1993.1626.

[278] S. Pratap, A. Dev, V. Kumar, R. Yadav, M. Narwal, S. Tomar, P. Kumar, Structure of Chorismate Mutase- like Domain of DAHPS from Bacillus subtilis Complexed with Novel Inhibitor Reveals Conformational Plasticity of Active

Site, (n.d.). doi:10.1038/s41598-017-06578-1.

[279] N.C. Garbett, P.A. Ragazzon, J.B. Chaires, Circular dichroism to determine binding mode and affinity of ligand–DNA interactions, Nat. Protoc. 2 (2007) 3166–3172. doi:10.1038/nprot.2007.475.

[280] Protein Fluorescence, Princ. Fluoresc. Spectrosc. (2006) 529–575. doi:10.1007/978-0-387-46312-4_16.

[281] M.F. Ahmad, S.E. Huff, J. Pink, I. Alam, A. Zhang, K. Perry, M.E. Harris, T. Misko, S.K. Porwal, N.L. Oleinick, M. Miyagi, R. Viswanathan, C.G. Dealwis, Identification of Non-nucleoside Human Ribonucleotide Reductase Modulators, J. Med. Chem. 58 (2015) 9498–9509. doi:10.1021/acs.jmedchem.5b00929.

[282] P. Agnihotri, P. Vishwakarma, T.K. Chaitanya, P. Kancharla, T. Khaliq, N. Tadigoppula, Synthesis, Structure − Activity Relationships, and Biological Studies of Chromenochalcones as Potential Antileishmanial Agents, (2014). doi:10.1021/jm401893j.

[283] W.H.J. Ward, G.A. Holdgate, S. Rowsell, E.G. McLean, R.A. Pauptit, E. Clayton, W.W. Nichols, J.G. Colls, C.A. Minshull, D.A. Jude, A. Mistry, D. Timms, R. Camble, N.J. Hales, C.J. Britton, I.W.F. Taylor, Kinetic and structural characteristics of the inhibition of enoyl (acyl carrier protein) reductase by triclosan, Biochemistry. 38 (1999) 12514–12525. doi:10.1021/bi9907779.